



Swansea University  
Prifysgol Abertawe



## Swansea University E-Theses

---

# Impact of ventricular assist devices on the activity of white blood cells and the implications for device design testing

Radley, Gemma

### How to cite:

---

Radley, Gemma (2018) *Impact of ventricular assist devices on the activity of white blood cells and the implications for device design testing*. Doctoral thesis, Swansea University.

<http://cronfa.swan.ac.uk/Record/cronfa40670>

### Use policy:

---

This item is brought to you by Swansea University. Any person downloading material is agreeing to abide by the terms of the repository licence: copies of full text items may be used or reproduced in any format or medium, without prior permission for personal research or study, educational or non-commercial purposes only. The copyright for any work remains with the original author unless otherwise specified. The full-text must not be sold in any format or medium without the formal permission of the copyright holder. Permission for multiple reproductions should be obtained from the original author.

Authors are personally responsible for adhering to copyright and publisher restrictions when uploading content to the repository.

Please link to the metadata record in the Swansea University repository, Cronfa (link given in the citation reference above.)

<http://www.swansea.ac.uk/library/researchsupport/ris-support/>

# **Impact of ventricular assist devices on the activity of white blood cells and the implications for device design testing**

**Gemma Radley BSc (Hons)**

*Submitted to Swansea University in fulfilment of the  
requirements for the Degree of Doctor of Philosophy*



**Swansea University  
Prifysgol Abertawe**

2018



## Abstract

Ventricular assist devices (VADs) offer long term therapy to chronic heart failure patients who are ineligible for transplant. However, complications such as infection and thrombosis remain characteristic of VAD therapy.

Leukocytes contribute to both infection and thrombosis, but research on the effect VADs have on these cells is limited. Through observing the impact of biomaterial choice, level of shear stress, and overall VAD design on leukocytes, this research has demonstrated the importance of incorporating leukocyte analysis into VAD testing to better understand and reduce complications.

Leukocyte response to VAD-candidate biomaterials (titanium alloy (Ti), diamond-like carbon (DLC), single crystal sapphire (Sap), silicon nitride (SiN), and zirconia toughened alumina (ZTA)) revealed that monocytes become activated in the presence of DLC, Sap and SiN. The addition of shear stress on these biomaterials revealed an immunosuppressive effect by Sap and Ti through attenuated phagocytic function of neutrophils, and an inhibition of cytokine production in response to pathogenic stimuli. This is relevant in that VAD-patients are susceptible to recurrent infections around the driveline.

Pro-inflammatory and pro-thrombogenic leukocyte microparticles (LMPs) are produced due to damage or stress. To measure the effect of shear stress on their formation, a mock circulatory loop with the CentriMag™ operated at different conditions was used. The high-speed condition generated the most LMPs that also expressed the activation marker CD11b whereas the standard condition generated the most LMPs expressing HLA-DR. This suggested that operating condition differentially affects leukocyte subsets.

To compare the effect of overall VAD design on leukocytes, mock circulatory loops were used to compare the Calon MiniVAD™ with competitor devices. The MiniVAD produced fewer LMPs in comparison to the HVAD™ and HeartMate II™ as well as lower haemolysis and lower platelet activation.

This research has shown that material choice, operating condition, and overall VAD design can significantly impact leukocyte activation and functionality. Interestingly, the widely accepted biocompatible material (Ti) utilised in many types of devices, has an immunosuppressive capacity when combined with shear. These findings provide novel insight into why some VAD-patients suffer recurrent infections and sepsis.

## DECLARATION

This work has not previously been accepted in substance for any degree and is not being concurrently submitted in candidature for any degree.

Signed ..  (candidate)

Date .....10<sup>th</sup> May 2018

## STATEMENT 1

This thesis is the result of my own investigations, except where otherwise stated. Where correction services have been used, the extent and nature of the correction is clearly marked in a footnote(s).

Other sources are acknowledged by footnotes giving explicit references. A bibliography is appended.

Signed ..  (candidate)

Date .....10<sup>th</sup> May 2018

## STATEMENT 2

I hereby give consent for my thesis, if accepted, to be available for photocopying and for inter-library loan, **after expiry of a bar on access** approved by Swansea University.

Signed ..  (candidate)

Date .....10<sup>th</sup> May 2018

## **Acknowledgements**

Firstly, I would like to express my sincere gratitude to my supervisor, Prof. Cathy Thornton. Her continued support, immense knowledge, and careful guidance of this research is at the core of this thesis. I could not have wished for a better mentor and consider her a role-model to aspire to.

None of this work could have been accomplished without the contribution Dr Ina Laura Pieper made to this research. She has become another role-model to myself through her careful attention to detail, incredible knowledge, and motivation. I would like to thank her immeasurably.

My thanks also go to my supervisor Dr Karl Hawkins and his team of rheologists, Dr Bethan Thomas and Dr Nafiseh Badiei, who aided the shear stress aspect of this research – which was the most challenging to complete!

To everyone at Calon, both past and present, I would like to thank for answering my questions relating to engineering, supporting me through this PhD, and including me in an environment that feels like a second family. I would like to thank Dr Graham Foster for his substantial efforts towards both my research and Calon.

Finally, a special thanks to my fantastic friends (you know who you are), Mum, Laura, and Ron who have helped me immensely throughout these years. I cannot convey how grateful I am to you all for getting me through some difficult personal trials on top of the challenges of being a PhD student.

# Contents

<b>Chapter 1</b>	<b>Introduction .....</b>	<b>1-1</b>
1.1	Anatomy of the heart .....	1-1
1.2	Heart failure .....	1-3
1.2.1	Classes of heart failure .....	1-3
1.2.2	Drug therapy.....	1-6
1.2.3	Heart transplant .....	1-6
1.2.4	Current medical need .....	1-7
1.3	Ventricular assist devices (VADs) .....	1-9
1.3.1	Pulsatile .....	1-9
1.3.2	Continuous .....	1-9
1.3.3	Extracorporeal devices .....	1-10
1.3.4	Intracorporeal devices .....	1-12
1.4	Calon Cardio – Technology Ltd. ....	1-15
1.5	MiniVAD™.....	1-16
1.6	Blood .....	1-17
1.6.1	Erythrocytes .....	1-17
1.6.2	Leukocytes .....	1-19
1.6.3	The immune response.....	1-21
1.6.4	Haemostasis.....	1-28
1.7	Interactions of leukocytes with implantable continuous-flow LVADs... ..	1-32
1.8	Complications of VADs .....	1-33
1.8.1	Thrombosis.....	1-33
1.8.2	Infection .....	1-35
1.8.3	Bleeding .....	1-36

1.8.4	Chronic right heart failure .....	1–37
1.8.5	Aortic insufficiency.....	1–37
1.8.6	Known complications in current VADs.....	1–37
1.9	Objectives .....	1–38
<b>Chapter 2</b>	<b>Enabling technologies .....</b>	<b>2–39</b>
2.1	Introduction .....	2–39
2.1.1	DNA Dyes and absolute count beads.....	2–39
2.1.2	Blood preservation .....	2–41
2.2	Objectives .....	2–43
2.3	Methods .....	2–44
2.3.1	Blood collection ethics .....	2–44
2.3.2	Viability Counting Protocol .....	2–44
2.3.3	Preservation of whole blood with Streck Cell Preservative in vitro	2–46
2.3.4	Haematology .....	2–46
2.3.5	Flow cytometry .....	2–46
2.3.6	Data analysis .....	2–46
2.3.7	Statistical analysis .....	2–46
2.4	Results .....	2–48
2.4.1	CyTRAK Orange selectively stains leukocytes .....	2–48
2.4.2	Spectral properties of DRAQ7 versus conventional viability dyes .	2–50
2.4.3	Counting bead usability and repeatability .....	2–52
2.4.4	Viability counts using CyTRAK Orange, DRAQ7, and absolute counting beads.....	2–54
2.4.5	Efficiency of viability protocol in human, bovine, and ovine.....	2–56
2.4.6	Streck Cell Preservative in vitro .....	2–60
2.5	Discussion .....	2–67



2.6	Conclusion .....	2-69
<b>Chapter 3</b>	<b>Biomaterials: Foreign surface blood interactions .....</b>	<b>3-70</b>
3.1	Introduction .....	3-70
3.1.1	Definition of a biomaterial .....	3-70
3.1.2	History of biomaterials .....	3-70
3.1.3	Biomaterial applications .....	3-71
3.1.4	Foreign body reaction to biomaterials .....	3-72
3.1.5	Progressing biocompatibility .....	3-73
3.2	Objectives .....	3-75
3.3	Methods .....	3-76
3.3.1	Ethics .....	3-76
3.3.2	Biomaterial discs .....	3-76
3.3.3	Biomaterial- induced contact activation .....	3-79
3.3.4	Biomaterial-induced cell activation .....	3-80
3.3.5	Haemolysis .....	3-80
3.3.6	Haematology .....	3-80
3.3.7	Flow cytometry .....	3-81
3.3.8	Cell culture supernatants and plasma processing .....	3-82
3.3.9	Microscopy .....	3-83
3.3.10	Data and statistical analysis .....	3-84
3.4	Results .....	3-85
3.4.1	Endotoxin .....	3-85
3.4.2	The effect of biomaterials on erythrocytes .....	3-85
3.4.3	The effect of biomaterials on the coagulation cascade .....	3-87
3.4.4	The effect of biomaterials on platelets .....	3-90
3.4.5	The effect of biomaterials on leukocytes .....	3-92

3.5	Discussion .....	3-108
3.6	Conclusion.....	3-111
<b>Chapter 4</b>	<b>Shear stress cell activation and damage.....</b>	<b>4-112</b>
4.1	Introduction .....	4-112
4.1.1	Definition of shear.....	4-112
4.1.2	Physiological shear stress.....	4-114
4.1.3	Shear stress on blood components .....	4-114
4.1.4	Medical device shear stress.....	4-117
4.2	Objectives .....	4-118
4.3	Methods .....	4-119
4.3.1	CentriMag™ at different operating conditions .....	4-119
4.3.2	Rheometry .....	4-120
4.3.3	Flow Cytometry .....	4-122
4.3.4	Cytokine analysis .....	4-124
4.3.5	Data and statistical analysis .....	4-125
4.4	Results .....	4-126
4.4.1	The effect of different CentriMag operating conditions on ovine blood 4-126	
4.4.2	The effect of biomaterials and shear on leukocyte counts, activation, and death 4-134	
4.4.3	The effect of biomaterials and shear on leukocyte functionality ... 4-138	
4.5	Discussion .....	4-147
4.6	Conclusion.....	4-152
<b>Chapter 5</b>	<b>VADs: From bench to bedside .....</b>	<b>5-153</b>
5.1	Introduction .....	5-153
5.1.1	In vitro testing .....	5-154

5.1.2	Preclinical testing .....	5-157
5.1.3	Clinical testing.....	5-159
5.2	Objectives .....	5-161
5.3	Methods .....	5-162
5.3.1	In vitro testing .....	5-162
5.3.2	In vivo testing.....	5-164
5.3.3	Data and statistical analysis.....	5-166
5.4	Results .....	5-167
5.4.1	Benchmarking study.....	5-167
5.4.2	Pre-clinical trials – leukocyte microparticles .....	5-179
5.4.3	Pre-clinical trials – clot structure .....	5-184
5.4.4	Non-Calton explanted VAD .....	5-189
5.5	Discussion.....	5-193
5.6	Conclusion.....	5-201
<b>Chapter 6</b>	<b>General discussion.....</b>	<b>6-203</b>
6.1	Biomaterials.....	6-204
6.2	Shear stress .....	6-206
6.1	Ventricular assist device testing .....	6-209
6.2	Limitations.....	6-213
6.2.1	Enabling Technologies .....	6-213
6.2.2	Biomaterials: Foreign surface interactions.....	6-213
6.2.3	Shear stress cell activation and damage .....	6-213
6.2.4	VADs: From bench to bedside .....	6-213
6.3	Future work.....	6-215
6.3.1	Heart failure, CPB, and paediatric blood .....	6-215
6.3.2	LVAD patient blood.....	6-215

6.3.3	Antibody development .....	6–215
6.3.4	Creating thrombus in vitro .....	6–216
6.3.5	Clinical trials .....	6–216
6.4	Conclusion.....	6–217
<b>Chapter 7</b>	<b>Bibliography .....</b>	<b>7–218</b>
<b>Chapter 8</b>	<b>Appendix.....</b>	<b>8–251</b>
8.1	Supplementary figures.....	8–251
8.1.1	Time-course data.....	8–251
8.1.2	Human inflammatory multiplex panel .....	8–253
8.1.3	Leukocyte activation in response to biomaterials and shear .....	8–254
8.1.4	Leukocyte microparticles gating strategy .....	8–255
8.1.5	Microparticle differentiation .....	8–256
8.1.6	Optimisation of phagocytosis assay .....	8–257
8.2	Publications and conferences .....	8–258
8.2.1	Publications .....	8–258
8.2.2	Conference posters .....	8–259
8.2.3	Conference presentations .....	8–259

## List of Figures

Figure 1.1: Anatomy of the human heart. ....	1-1
Figure 1.2: INTERMACS classification system. ....	1-5
Figure 1.3: Section view of the MiniVAD.....	1-16
Figure 1.4: Cells of the blood.....	1-17
Figure 1.5: Erythropoiesis.....	1-18
Figure 1.6: Haemolysed blood.....	1-19
Figure 1.7: The lymphatic system. ....	1-23
Figure 1.8: The blood cells of the immune system derived from haematopoietic stem cells within the bone marrow. ....	1-24
Figure 1.9: Inflammatory response. ....	1-25
Figure 1.10: The complement pathway.....	1-26
Figure 1.11: The coagulation cascade and the points at which anticoagulants block the pathway. ....	1-29
Figure 1.12: Thrombus formation in the HeartMate II.....	1-34
Figure 1.13: Driveline infection.....	1-35
Figure 2.1: DRAQ7 outcompetes CyTRAK Orange in cells with a compromised membrane.....	2-40
Figure 2.2: Comparison of CD45+ staining and CyTRAK Orange staining in three species. ....	2-48
Figure 2.3: CyTRAK Orange negative events are platelets. ....	2-49
Figure 2.4: Staining of human blood with DRAQ7. ....	2-50
Figure 2.5: DRAQ7 emission profile compared to 7AAD and PI. ....	2-51
Figure 2.6: Scatter and emission profile of various counting bead standards.....	2-53
Figure 2.7: CyTRAK Orange and DRAQ7 gating strategy. ....	2-55
Figure 2.8: Absolute counting beads versus haematology analyser for human, bovine, and ovine. ....	2-56

Figure 2.9: Live cell count correlation between single- and double-stained blood for each bead/species. ....	2–58
Figure 2.10: Dead cell count correlation between single- and double-stained blood for each bead/species. ....	2–59
Figure 2.11: Erythrocyte, leukocyte, and platelet count .....	2–61
Figure 2.12: Leukocyte differential cell counts. ....	2–63
Figure 2.13: Forward- vs side-scatter of CyTRAK Orange positive leukocytes over time in Streck and Control ovine blood. ....	2–65
Figure 2.14: Change in forward and side scatter of granulocytes for each species over time.....	2–66
Figure 3.1: Types of medical implant .....	3–71
Figure 3.2: Biomaterial set-up.....	3–78
Figure 3.3: Endotoxin levels. ....	3–85
Figure 3.4: The effects of various biomaterials on erythrocyte counts and haemolysis. ....	3–86
Figure 3.5: The effects of various biomaterials on clotting time. ....	3–87
Figure 3.6: The effects of various biomaterials on peptidase activity. ....	3–88
Figure 3.7: The effects of various biomaterials on thrombin activity.....	3–89
Figure 3.8: The effects of various biomaterials on platelet counts and activation status .....	3–90
Figure 3.9: Gating strategy for leukocyte-platelet aggregates. ....	3–91
Figure 3.10: The effects of biomaterials on neutrophil-platelet and monocyte-platelet aggregates.....	3–92
Figure 3.11: The effects of various biomaterials on total leukocyte and subset counts. ....	3–93
Figure 3.12: Gating strategy for leukocyte activation and death. ....	3–95
Figure 3.13: The effect of various biomaterials on neutrophil and monocyte activation and death. ....	3–96

Figure 3.14: The effect of various biomaterials on lymphocyte activation and death. .....	3-99
Figure 3.15: The effects of various biomaterials on soluble CD62L. ....	3-100
Figure 3.16: The effects of biomaterials on cytokine response in both LPS-stimulated and unstimulated blood .....	3-102
Figure 3.17: Confocal microscope images of leukocytes present on rough titanium. 3- 104	
Figure 3.18: CyTRAK Orange positive leukocytes present on the biomaterial discs 3- 106	
Figure 3.19: ImageJ analysis and leukocyte counts on biomaterials .....	3-107
Figure 4.1: The mock circulatory loop.....	4-119
Figure 4.2: Rheometer model.....	4-121
Figure 4.3: Computational fluid dynamic results of shear in the CentriMag™... 4-127	
Figure 4.4 Haematological analysis of blood run in the CentriMag™ loop under different operating conditions .....	4-128
Figure 4.5 Haemolysis in the CentriMag™ at different operating conditions.....	4-129
Figure 4.6: Leukocyte-derived microparticles and necrotic cells .....	4-130
Figure 4.7: Scatter profiles for each antibody at each time point for the high speed condition.....	4-131
Figure 4.8: CD11b and HLA-DR expression on LMPs .....	4-133
Figure 4.9: Complete cell counts before and after shear on different biomaterials ... 4- 135	
Figure 4.10: Leukocyte activation and death before and after shear on different biomaterials .....	4-136
Figure 4.11: Leukocyte microparticle generation before and after shear on different biomaterials. ....	4-138
Figure 4.12: Gating strategy for phagocytosis. ....	4-139

Figure 4.13: Phagocytic ability of neutrophils and monocytes before and after shear on different biomaterials .....	4–140
Figure 4.14: ROS production before and after shear on different biomaterials...	4–142
Figure 4.15: Proteome profile. ....	4–144
Figure 4.16: IL-1 $\alpha$ and MIF expression before and after shear on different biomaterials .....	4–146
Figure 5.1: The devices used in the Benchmarking study .....	5–167
Figure 5.2: Haemolysis .....	5–168
Figure 5.3: Haematology.....	5–170
Figure 5.4: Gating strategy for measuring platelet activation.....	5–172
Figure 5.5: Platelet activation .....	5–173
Figure 5.6: Leukocyte microparticles gating strategy for benchmarking study...	5–175
Figure 5.7: Leukocyte microparticles and necrotic leukocytes.....	5–176
Figure 5.8: Parentage of activated leukocyte microparticles .....	5–177
Figure 5.9. Activated leukocyte microparticles. ....	5–178
Figure 5.10: Preclinical activated leukocyte microparticles .....	5–181
Figure 5.11: Leukocyte- derived microparticles in blood taken from VAD-implanted sheep into Cyto-Chex-BCT tubes. ....	5–182
Figure 5.12: Leukocyte-derived microparticles from blood taken from VAD-implanted sheep and mixed with Streck Cell Preservative. ....	5–183
Figure 5.13: Sample from on top of the rotor stained with CyTRAK Orange.....	5–187
Figure 5.14: SEM of biological matter found on KULOV-07 MiniVAD rotor...	5–188
Figure 5.15: Confocal image of HA-5 outflow stained with CyTRAK Orange..	5–192
Figure 8.1: Time-course data for platelet activation, platelet aggregation, and leukocyte-platelet aggregation .....	8–251
Figure 8.2: Time-course data for CD62L expression, CD11b expression, and death	8–252



Figure 8.3: Cytokine expression in cell culture supernatants measured using the LEGENDplex kit.....	8–253
Figure 8.4: Leukocyte activation in response to biomaterials and shear .....	8–254
Figure 8.5: Gating strategy for leukocyte microparticles.....	8–255
Figure 8.6: Differentiating leukocyte-derived and platelet-derived microparticles... 8–	256
Figure 8.7: Optimisation of phagocytosis assay.....	8–257

### **List of Tables**

Table 1.1: Classes of heart failure .....	1–4
Table 1.2: Examples of extracorporeal devices .....	1–11
Table 1.3: Examples of intracorporeal devices approved in Europe .....	1–13
Table 2.1: Coefficient of variance (%CV) for different cell counting bead types and species. ....	2–52
Table 3.1: Biomaterial specifications .....	3–77
Table 4.1: CentriMag operating conditions.....	4–126
Table 5.1: Specifications for the MiniVAD .....	5–153
Table 5.2: Summary of practice from ASTM F1841-97.....	5–155
Table 5.3: Good laboratory practice specifications.....	5–158
Table 5.4: Antibodies for pre-clinical samples .....	5–164
Table 5.5: Histological staining of samples obtained from the pump implanted into KULOV-08.....	5–185
Table 5.6: Samples from the HA-5 stained using the Carstairs’ method.....	5–190

## Abbreviations

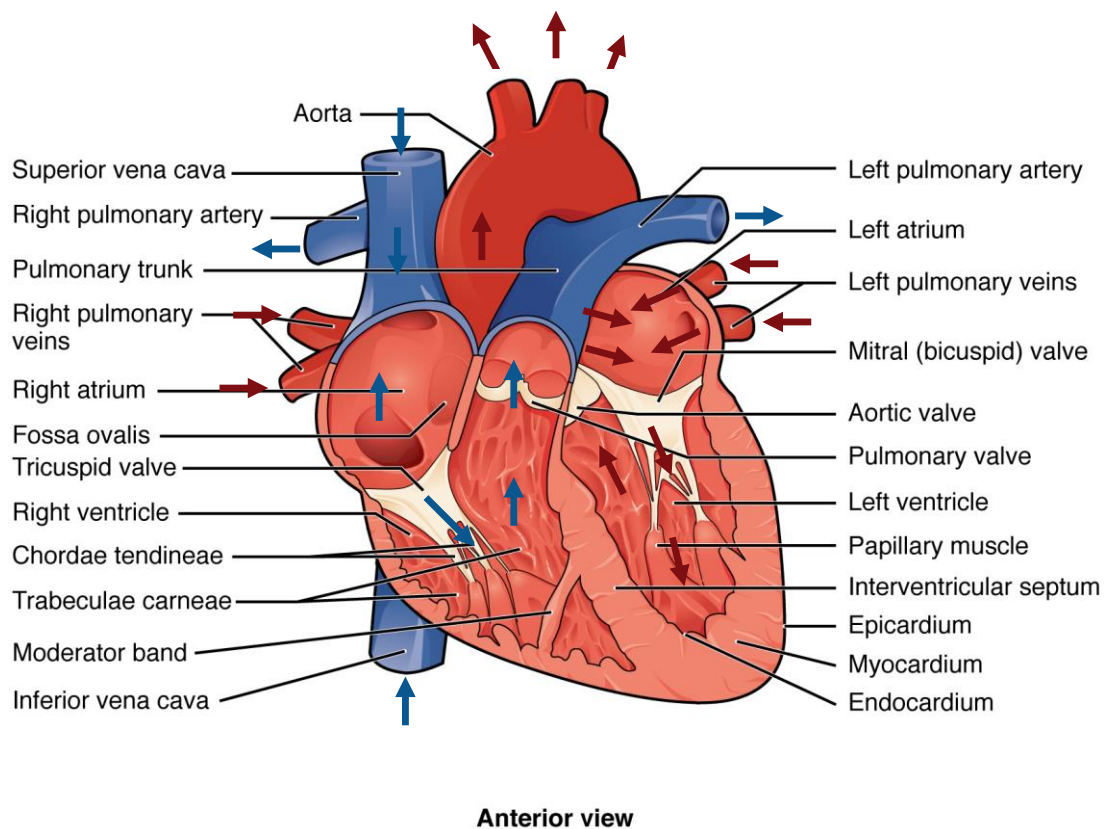
APC	Antigen presenting cell
ATP	Adenosine triphosphate
AVWS	Acquired von Willebrand syndrome
BMI	Body mass index
BSA	Bovine serum albumin
CD	Cluster of differentiation
CEO	Chief Executive Officer
CHF	Chronic heart failure
CRP	C-reactive protein
CTO	Chief Technology Officer
DLC	Diamond-like carbon
dPBS	Dulbecco's phosphate buffered saline
dsRNA	Double stranded RNA
EDTA	Ethylenediaminetetraacetic acid
ELISA	Enzyme-linked immunosorbent assay
FBGC	Foreign body giant cell
FBS	Fetal bovine serum
FACS	Flow assisted cell sorting
HF	Heart failure
HIV	Human immunodeficiency virus
HUVECs	Human umbilical cord endothelial cells
IFN	Interferon
IHC	Immunohistochemistry
IL-	Interleukin-

LDH	Lactate dehydrogenase
LPS	Lipopolysaccharide
MCP-1	Monocyte chemotactic protein-1
MI	Myocardial infarction
MMP	Matrix metalloproteinase
mtDNA	Mitochondrial DNA
NETs	Neutrophil extracellular traps
NIH	Normalised index of haemolysis
PB	Peripheral blood
PBS	Phosphate buffered saline
PBMC	Peripheral blood mononuclear cell
pfHB	Plasma free haemoglobin
PMA	Phorbol 12-myristate 13-acetate
PMNC	Polymorphonuclear cell
RBC	Red blood cell
RIPA	Radio-immunoprecipitation assay
ROS	Reactive oxygen species
ssRNA	Single stranded RNA
TBS	Tris-buffered saline
TF	Tissue factor
TNF- $\alpha$	Tumour necrosis factor alpha
VAD	Ventricular assist device
vWF	von Willebrand factor
WBC	White blood cell
WHO	World Health Organisation

# Chapter 1 Introduction

## 1.1 Anatomy of the heart

The heart (Figure 1.1) is within the thoracic cavity, protected by the ribcage. It has four chambers, two reservoirs (left and right atria) and two pumping chambers (left and right ventricles).



**Figure 1.1: Anatomy of the human heart.**

Creative Commons Attribution 3.0 Unported license. Original image source: Anatomy & Physiology, Connexions Web site. <http://cnx.org/content/col11496/1.6/> Jun 19, 2013

The function of the heart is to pump blood through the circulatory system to supply the tissues with oxygen and essential nutrients whilst also gathering waste for disposal. The heart itself is supplied with blood via the coronary arteries, the right coronary and the left main artery. The adult human heart weighs around 200-425 g, has a stroke

volume of around 70 mL and pumps 5L/min during rest (1). The tissue type that allows the heart to pump blood is the thick muscular layer of the cardiac tissue known as the myocardium, the only muscle of its type in the body.

## 1.2 Heart failure

Heart failure (HF) is both acute (sudden onset) and chronic (2). It occurs when cardiac structure or function becomes abnormal leading to failure of the heart to deliver oxygen at a rate proportionate with the requirements of the metabolising tissues, despite normal filling pressures (3). Diagnosis of heart failure is a difficult process as many of the symptoms (e.g. breathlessness, fatigue, ankle-swelling) are non-discriminating and the diagnostic tests such as chest x-rays, and electro-, and echocardiographs are not always conclusive (4, 5).

There are three main types of heart failure: Left ventricular systolic dysfunction (LVSD) due to weakening of the left ventricle (heart failure with reduced ejection fraction (HFrEF,  $< 40\%$ ); heart failure with preserved ejection fraction (HFpEF,  $\geq 50\%$ ) due to stiffening of the left ventricle and delayed early relaxation (6); and heart failure due to valve disease (7). More recently a new category, heart failure with mid-range ejection fraction (HFmrEF,  $40 - 49\%$ ), has been established to encourage research into these patients who have differing symptoms to HFrEF and HFpEF (8).

Heart failure is the result of stress to the heart due to a number of causative factors such as coronary artery disease, high blood pressure, arrhythmias, diabetes, obesity, and age (8). The strongest predictor of HFrEF is a myocardial infarction (MI) (5). Activation of the immune system and release of inflammatory cytokines in the early stages helps maintain ventricular function (9) and is necessary to initiate repair of the myocytes (10). During repair, the ventricle is remodelled which modifies size, shape, and contractility of the cardiac tissue cells (11, 12). Excessive inflammation detrimentally affects repair of the heart and can culminate in cell damage and death leading to functional impairment of the myocardium through fibrosis and hypertrophy (10, 13, 14). Hypertension rather than MI is thought to be an important contributor to the slow progression of HFpEF (15).

### *1.2.1 Classes of heart failure*

Traditionally, the New York Heart Association classification system which classifies HF into stages I to IV has been used (16): it was introduced in 1928 and has been revised several times. Similarly, the American College of Cardiology/ American Heart

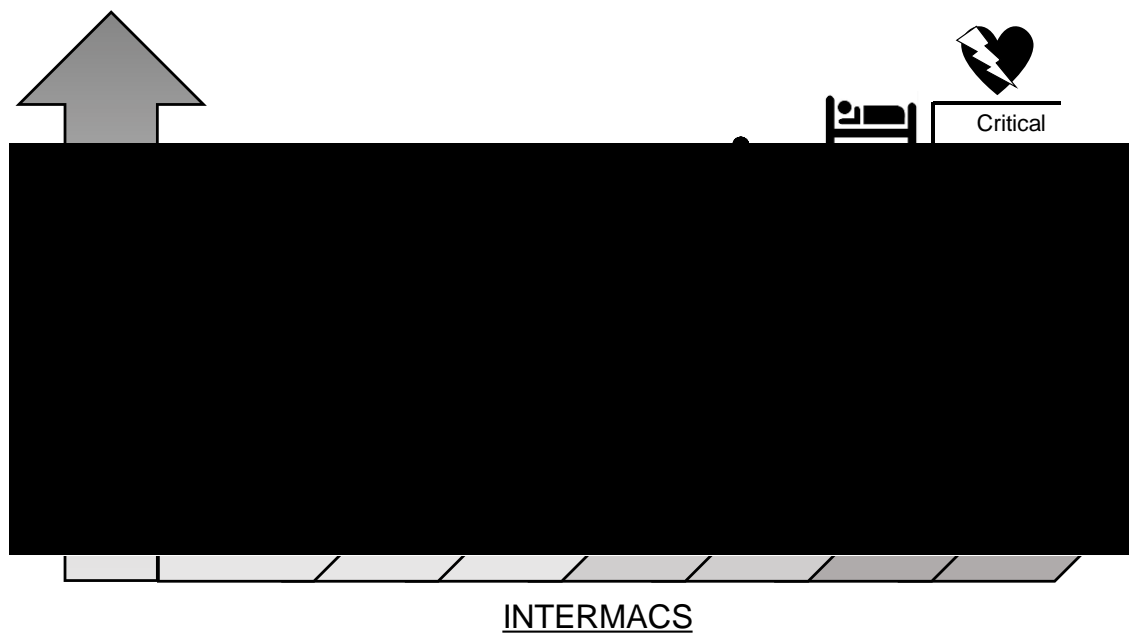
Association (ACC/AHA) have classified HF into 4 stages based on disease progression (17) (Table 1.1).

**Table 1.1: Classes of heart failure**

<b>ACC/AHA Heart Failure Stage</b>	<b>NYHA Functional Class</b>
<b>A.</b> At risk for heart failure but without structural heart disease or symptoms	None
<b>B.</b> Structural heart disease but without heart failure	<b>I.</b> Asymptomatic
<b>C.</b> Structural heart disease with prior or current heart failure symptoms	<b>II.</b> Symptomatic with moderate exertion <b>III.</b> Symptomatic with minimal exertion
<b>D.</b> Refractory heart failure requiring specialised interventions	<b>IV.</b> Symptomatic at rest

In stage A, patients are asymptomatic for HF but are at high risk of developing HF due to the presence of strongly associated conditions such as diabetes, coronary artery disease, hypertension, obesity, or a history of familial cardiomyopathies. These patients possess no structural or functional abnormality of the heart and treatment focuses on slowing the progression into later stages of HF (9). Progression into stage B occurs when the heart shows evidence of structural remodelling, particularly in the left ventricle and a lowered ejection fraction (EF).

At stage C, patients have current or prior symptoms of HF, such as breathlessness or fatigue, associated with underlying structural heart disease (17). During this stage, the ventricular function is maintained by adrenergic stimulation, activation of renin-angiotensin-aldosterone, and other neurohumoral and cytokine systems (9). As HF progresses further, these compensatory mechanisms become less effective, the cardiac function deteriorates to the point where patients have marked symptoms at rest. This is stage D and these patients require specialised therapy such as continuous inotropic support, heart transplant, mechanical circulatory support, or hospital care (17).



**Figure 1.2: INTERMACS classification system.**

Heart failure disease progression per the New York Heart Association (NYHA) classification and Interagency Registry for Mechanically Assisted Circulatory Support (INTERMACS) profile for determination of patient treatment with mechanical circulatory devices (MCS). Adapted from (18-20).

Throughout stages C & D (III & IV), patients can be sub-divided through the INTERMACS (Interagency Registry for Mechanically Assisted Circulatory Support) classification system (Figure 1.2) to better inform treatment decisions. Profiles 7 through to 1 define the decline in patient health from those who live reasonably comfortably (profiles 7 to 5) to those who are in urgent need of intervention through the use of circulatory support (profiles 2 and 1) within days or even hours (21).

Chronic heart failure (CHF), stage D/class IV HF, is increasing in prevalence along with an ageing population and an increase in lifestyle diseases such as obesity and type 2 diabetes (7). At the beginning of the 21<sup>st</sup> Century, 6.5 million people in Europe (22), 5.3 million in the USA (9), and 2.4 million in Japan (22) suffered from CHF every year and the prevalence is ever increasing. Surveys in UK primary care suggest a CHF prevalence of 8-16 cases per 1000 increasing to 40-60 cases per 1000 among those aged 70 and over (22). The suggested prevalence of CHF for the global population is approximately 1-2% and >10% in those aged  $\geq 65$  years (5, 23). The quality of life (QoL) for those with severe CHF is poor and deemed to have a greater negative impact



on QoL than diabetes, arthritis, or hypertension (5). The long-term prognosis associated with CHF is also poor: half of all patients will die within 4 years of diagnosis (5). Those with end-stage failure have the worst survival rate of 75% mortality in 2 years with heart transplant being the only effective therapy. Hospitalisation is the highest costing event in CHF and accounts for ~2% of UK NHS expenditure (24).

### *1.2.2 Drug therapy*

The European Society of Cardiology guidelines recommend the use of angiotensin-converting enzyme (ACE) inhibitors in combination with diuretics, beta-blockers, and aldosterone antagonists (3). Angiotensin II receptor antagonists are recommended for those who do not respond well to ACE-inhibitors. These drugs have shown evidence of prolonging survival, reducing hospitalisations, and delaying disease progression, improving quality of life, and increasing exercise capacity in symptomatic HF patients and even advanced stage HF patients (5).

Patients also undergo anticoagulation/anti-platelet therapy through taking aspirin, warfarin, and clopidogrel bisulphate (25).

### *1.2.3 Heart transplant*

The first human heart transplant was performed by Dr Christiaan Barnard on a patient with end-stage heart failure in 1967 (26). The patient survived for 18 days but it was the beginning of an era in which patients with end-stage heart failure could be saved. A heart transplant is considered when a patient's heart failure is severe to the point of no longer responding to medication, they are predicted to die within the year, and they fit the eligibility criteria. In the UK, adult patients on the heart transplant waiting list has increased each year from 72 in 2007 to 207 in 2016, with an increase in patients urgently requiring transplantation too (27). Non-urgent patients can expect to wait 3 years for a heart with only 21% transplanted, 37% moved to the urgent list, and 27% removed due to being too ill or deceased (27). When a heart becomes available, from a recently deceased or brain-dead donor it is taken immediately to the operating theatre for inspection. The recipient patient is brought to the theatre having been evaluated both physically and mentally before taking pre-surgical and immunosuppressant medication.

Once the patient is under general anaesthesia, two types of procedures can take place, orthotopic or heterotopic. Orthotopic procedures involve opening the chest, opening the pericardium and dissecting the great vessels (28). The patient is attached to cardiopulmonary bypass whilst the donor heart is injected with cardioplegia solution which stops it beating. The donor heart is put on ice for up to 4 hours, or more recently, transported using a TransMedics™ Organ Care System (OCS) which maintains the donor heart in a warm, functioning state for normothermic reperfusion. The patients' pulmonary veins are left on a circular portion of the left atrium allowing the donor heart to be trimmed to fit and sutured into place. The heart is restarted, the patient weaned off bypass and the chest cavity closed. Heterotopic procedures are conducted when the donor heart is sub-optimal, or the recipient suffers pulmonary hypertension. In this type of procedure, the patient's heart is left in place and the donor heart connected to essentially give a 'double heart' so that the patient heart can recover or in case the donor heart is rejected (29).

Post-operation, the patient is taken to intensive care. Time in hospital depends on recovery but is usually 2-4 weeks with regular check-ups and rehabilitation. The patient continues taking immunosuppressants for the rest of their life to prevent rejection. Complications of this procedure includes infection, sepsis, rejection, and the problems associated with immunosuppression. However, the survival rates are: 1 year, males (88%) and females (86.2%); 3 years, males (79.3%) and females (77.2%); and 5 years (males (73.1%) and females (69%)) (30). However, the supply of donor hearts does not meet the growing demand with as few as 2449 in the USA, 1468 in Europe, and 279 in other countries transplanted in 2012 (31).

#### *1.2.4 Current medical need*

In 2014/2015, there were 181 heart transplants in seven hospitals in the UK (32). Not all patients are eligible for transplant, including those with kidney, lung, or liver disease, diabetes mellitus, life-threatening diseases unrelated to heart failure, vascular diseases of neck and leg arteries, recent thromboembolism, substance abuse, morbid obesity, and being over 65 years old (centre dependent) (33). Due to the lack of donor hearts for those with advanced stage HF and the number of patients ineligible for transplant, an artificial alternative has been developed. Mechanical circulatory support

(MCS) includes a wide-variety of devices that can provide short term support for ventricular recovery in the acute stages, or long-term support for those whose only option is transplant. Ventricular Assist Devices (VADs) have three main clinical applications, bridge-to-transplant (BTT), bridge-to-recovery (BTR), and destination therapy (DT) which is used for those who are ineligible for transplant.

## 1.3 Ventricular assist devices (VADs)

### *1.3.1 Pulsatile*

First generation VADs contained artificial heart valves and ejected blood at rates typically between 80 and 100 times per minute in a pulsatile fashion using air or electricity (34). Pulsatile VADs mimic the natural pulsing action of the heart and are positive displacement pumps. The volume occupied by blood varies during the pumping cycle, and if the pump is contained inside the body then a vent tube to the outside air may be required. Thoratec have many VADs on the market, their pulsatile VADs include the PVAD™, IVAD™, and HeartMate XVE™. The PVAD is a pneumatically driven, pulsatile pump which consists of a rigid plastic housing chamber and a blood pumping sac fitted externally against the chest wall (paracorporeal). The need for an intracorporeal (pump housed inside the patient body) VAD led to the development of the IVAD. It is the only intracorporeal device capable of biventricular support. The HeartMate XVE is an intracorporeal VAD which is electrically driven by a motor located in the pump housing. This motor is separated from the blood-pumping sac by a diaphragm that divides the pump into two chambers. Blood is pushed through the device using a pusher plate and negative pressure created by the diaphragm recoil (9, 35).

### *1.3.2 Continuous*

Continuous flow VADs use either axial flow or centrifugal pumps, and are smaller and more durable than pulsatile VADs (36, 37). Both types have a central rotor containing permanent magnets controlled using electric currents which apply forces to the magnets making the rotor spin. In centrifugal pumps, the rotors are shaped to accelerate the blood circumferentially and thereby cause it to move toward the outer rim of the pump. The axial flow pumps have rotor's that are roughly cylindrical with helical blades causing blood to be accelerated in the direction of the rotors axis (38). Early versions of the continuous pumps used solid bearings, however, newer pumps use either electromagnetic suspension ('maglev'), hydrodynamic suspension, or a combination of both (39).


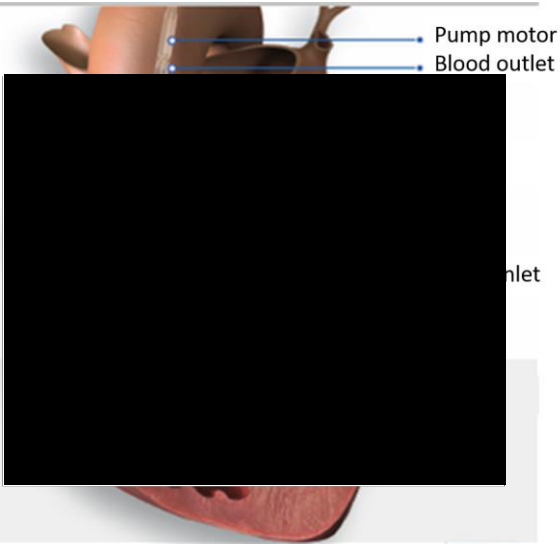
Blood flow through continuous-flow pumps is directly proportional to pump speed and inversely related to the pressure difference across the inlet (LV pressure) and outlet

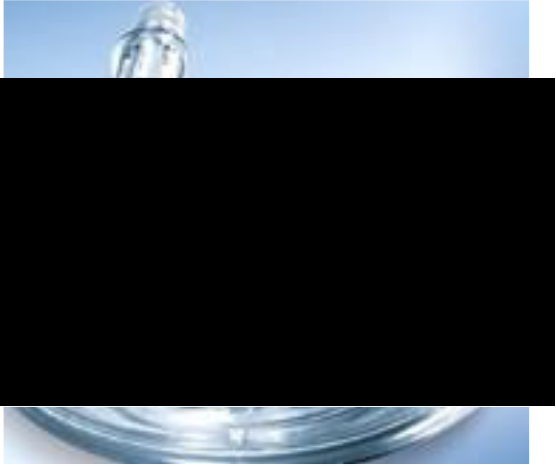
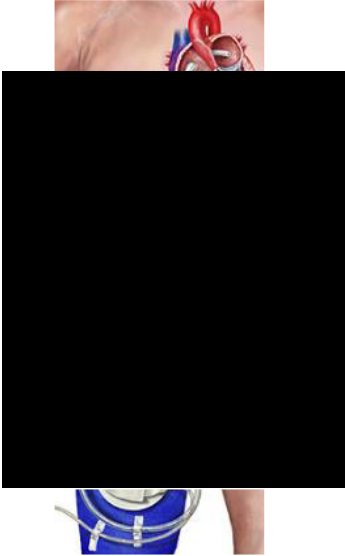
(aortic pressure) (40). Interactions between heart contraction and the hydrodynamic properties of the pump means that flow through the LVAD is sensitive to pressure changes. During systole, the pressure gradient across the pump is less, resulting in more flow and more work by the pump (41). During diastole, the pressure gradient across the pump is greatest, resulting in less flow (40). This is the basis for the pulsatility index (PI), as referred to in the HMII user's guide, and is affected by state of hydration, contractility, right ventricular function, and exercise (41). It is important to remember this when considering the blood-handling capabilities of various pumps.

### *1.3.3 Extracorporeal devices*

Extracorporeal devices (Table 1.2) circulate blood using a pump that is outside the body and attached to the patient via tubing. Such devices are used for patients of all ages, including neonates, who suffer from acute HF. The purpose of these pumps is to stabilise the patient's systemic circulation and heart function after cardiogenic shock with the aim to eventually remove the device. If recovery is unlikely, the patient is referred to ventricular assist system (VAS) programs (42).

**Table 1.2: Examples of extracorporeal devices**

<p><b>CentriMag™ (Thoratec® Co.)</b></p>	
 <p>(43)</p>	<ul style="list-style-type: none"> <li>• Continuous-flow, centrifugal, extracorporeal device.</li> <li>• Magnetically-levitated pump impeller.</li> <li>• High blood flows up to 9.9 rpm.</li> <li>• Approved for short-term use (14 days) for patients with cardiogenic shock.</li> </ul>
<p><b>Impella® devices, Abiomed Inc.</b></p>	
 <p>(44)</p>	<ul style="list-style-type: none"> <li>• Device types: Impella 2.5 L/min, Cardiac Power, and Impella 5.0 L/min.</li> <li>• Intracardiac pumps.</li> <li>• Inserted via the femoral artery.</li> <li>• Non-pulsatile, axial flow.</li> <li>• Pump blood from the left ventricle to the ascending aorta.</li> <li>• Short term use (<math>\leq 4</math> days) for cardiogenic shock (45).</li> </ul>

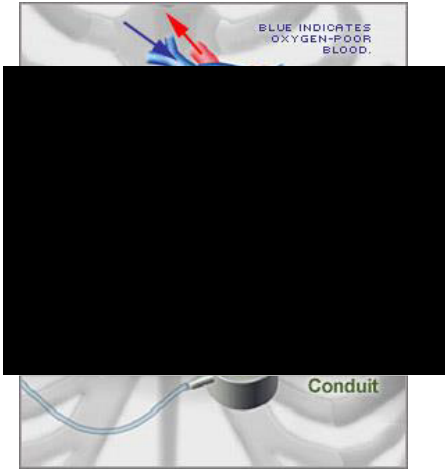

<b>ROTAFLOW™ Centrifugal Pump (Maquet Holding B.V. &amp; Co. KG)</b>	
 <p>(46)</p>	<ul style="list-style-type: none"> <li>• Continuous-flow, centrifugal, extracorporeal device.</li> <li>• Peg-top, one-point sapphire bearing, housing made from polycarbonate.</li> <li>• Can be used for cardiogenic shock patients awaiting bridge-to-decision/recovery for 30 days (47).</li> </ul>
<b>TandemHeart® (CardiacAssist Inc.)</b>	
 <p>(48)</p>	<ul style="list-style-type: none"> <li>• Continuous-flow, centrifugal, extracorporeal device.</li> <li>• Transseptal cannula withdraws oxygenated blood from the left atrium into the aorta.</li> <li>• Blood flow rates of 3.5 – 5.0 L/min.</li> <li>• Short term use from hours to 14 days (45).</li> </ul>

*1.3.4 Intracorporeal devices*

Intracorporeal devices (Table 1.3) are those that are implanted intrapericardially with an inflow cannula into the left ventricle and operate using a portable battery pack which can be worn on the body. These devices can be used as bridge-to-recovery,

bridge-to-transplant, and as destination therapy in certain countries like the USA. Some examples of intracorporeal devices are:

**Table 1.3: Examples of intracorporeal devices approved in Europe**

<p><b>DuraHeart™ (Terumo)</b></p>	
 <p>The diagram shows a cross-section of the DuraHeart™ device. At the top, a legend states 'BLUE INDICATES OXYGEN-POOR BLOOD.' Below this, blue arrows indicate the flow of oxygen-poor blood. A central impeller is shown, which is magnetically levitated. The impeller is surrounded by a chamber with wide gaps (250 microns) to improve washing. A conduit is shown at the bottom, labeled 'Conduit'.</p> <p>(49)</p>	<ul style="list-style-type: none"> <li>• Centrifugal flow.</li> <li>• Magnetically-levitated impeller.</li> <li>• Wide gaps (250 micron) between impeller and chamber to improve washing.</li> <li>• Heparin covalently bound to surfaces.</li> </ul>
<p><b>HeartAssist5™ (HA-5, ReliantHeart)</b></p>	
 <p>The image shows the HeartAssist5™ device, which is a small, cylindrical pump. It is shown in a perspective view, highlighting its compact design and the various ports and connectors on its surface.</p> <p>(50)</p>	<ul style="list-style-type: none"> <li>• Weighs 95 g</li> <li>• Axial flow impeller with ceramic (silicon carbide) conical bearing, hybrid contact hydrodynamic bearing (51).</li> <li>• Operates at 4 L/min, 100 mmHg pressure gradient across the HA-5 at 12500 rpm (51) with a power of 10 Watts at 6 L/min during clinical study (52).</li> </ul>



**HeartMate II™ (Thoratec® Co.)**



(53)


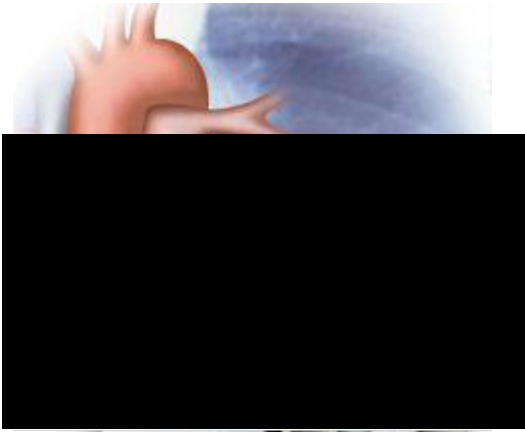
- Weighs 281.3 g
- Axial flow impeller with ceramic ball and cup bearings at both ends.
- Operates at < 10 Watts power.
- Provides 5 L/min flow against pressure of 100 mmHg at 11000 rpm.

**HeartMate III™ (St. Jude Medical (formerly Thoratec® Co.))**



(54)

- Based on the CentriMag™
- Fully magnetically-levitated impeller.
- Can provide 2.5 to 10 L/min.
- Artificial pulse technology (54).

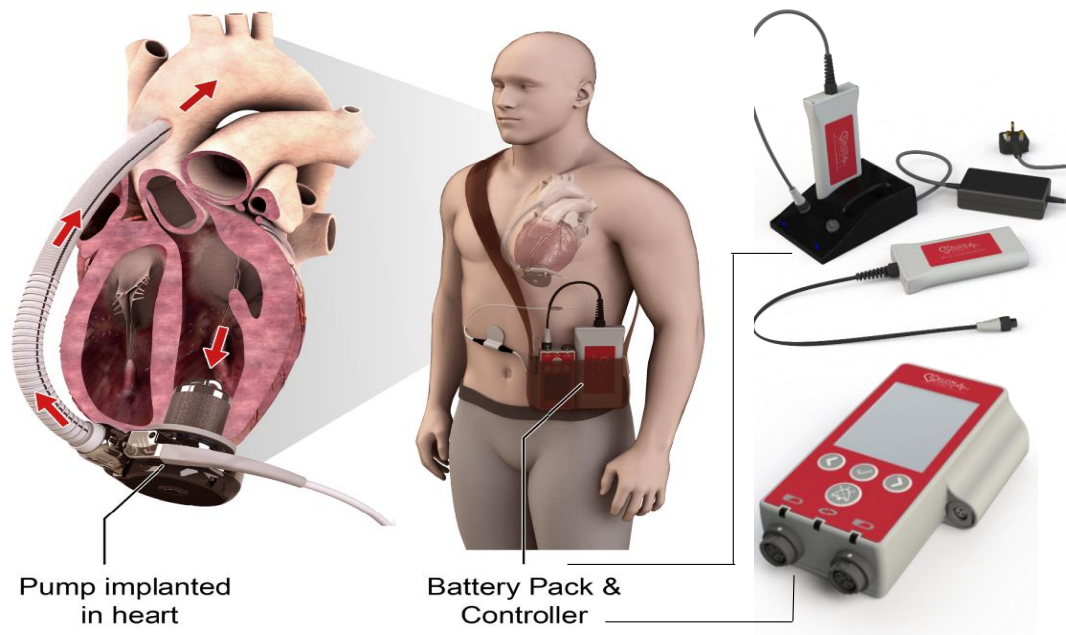
<b>HVAD™ (HeartWare)</b>	
 <p>(55)</p>	<ul style="list-style-type: none"> <li>• Weighs 145 g</li> <li>• Radial flow impeller with radial passive magnetic bearing and hydrodynamic bearing.</li> <li>• Average power consumption is approximately <math>4.5 \pm 0.5</math> Watts at a performance of 5 L/min, 100 mmHg at 3000 rpm (56).</li> </ul>
<b>Jarvik 2000™ (Jarvik Heart)</b>	
 <p>(57)</p>	<ul style="list-style-type: none"> <li>• Weighs 90 g</li> <li>• Axial flow impeller with ceramic (silicon carbide) conical bearing, hybrid contact hydrodynamic bearing (58).</li> <li>• Operates at 12.5 Watts at a speed of 10000 rpm</li> <li>• Designed to perform at 5 L/min, 100 mmHg pressure at 13250 rpm</li> </ul>

#### 1.4 Calon Cardio – Technology Ltd.

Calon Cardio – Technology Ltd. (Calon) is a commercial company developing an implantable left ventricular assist device (LVAD) and accompanying system. It was established at Swansea University in 2007 under the clinical expertise of Professor Stephen Westaby and entrepreneurial guidance of Professor Marc Clement. Calon, under Chief Technology Officer Dr Graham Foster, Chief Executive Officer Stuart McConchie, along with Swansea University, has sponsored this research into the biocompatibility of the ventricular assist devices.

## 1.5 MiniVAD™

The device under current development by Calon is the MiniVAD™ system. The MiniVAD consists of an implantable left ventricular assist device pump connected to an external controller via a percutaneous driveline. Two rechargeable batteries are attached to the controller and worn by the patient (Figure 1.3).



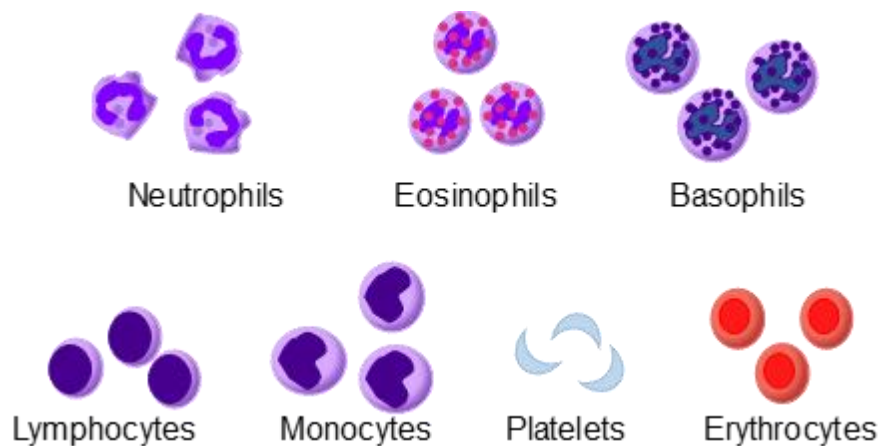
**Figure 1.3: Section view of the MiniVAD**

The inflow cannula of the pump is inserted into the left ventricular apex of the heart with outflow graft attached to ascending aorta. Battery pack and controller is worn externally with driveline inserted under ribcage. Image supplied by Calon.

The MiniVAD system is intended for use as destination therapy. So far, Calon has successfully completed an acute animal study involving implantation into sheep for 30 days with minimal complications associated with the pump. One of the key differences between Calon and other VAD developers is the focus on developing *in vitro* assays to refine the design of the pump prior to implantation in animals and humans.

## 1.6 Blood

Current VADs have benefited many patients although the introduction of a foreign material and high shear stresses by the VAD causes blood trauma. Reported blood trauma includes haemolysis, platelet activation, alterations in the coagulation cascade, degradation of proteins, and damage to leukocytes. These blood components are vital to the normal functioning of haemostasis (stopping of bleeding (59)) and the immune system. Trauma to the blood is causative of VAD complications detailed later in this chapter (1.8 Complications of VADs).



**Figure 1.4: Cells of the blood**

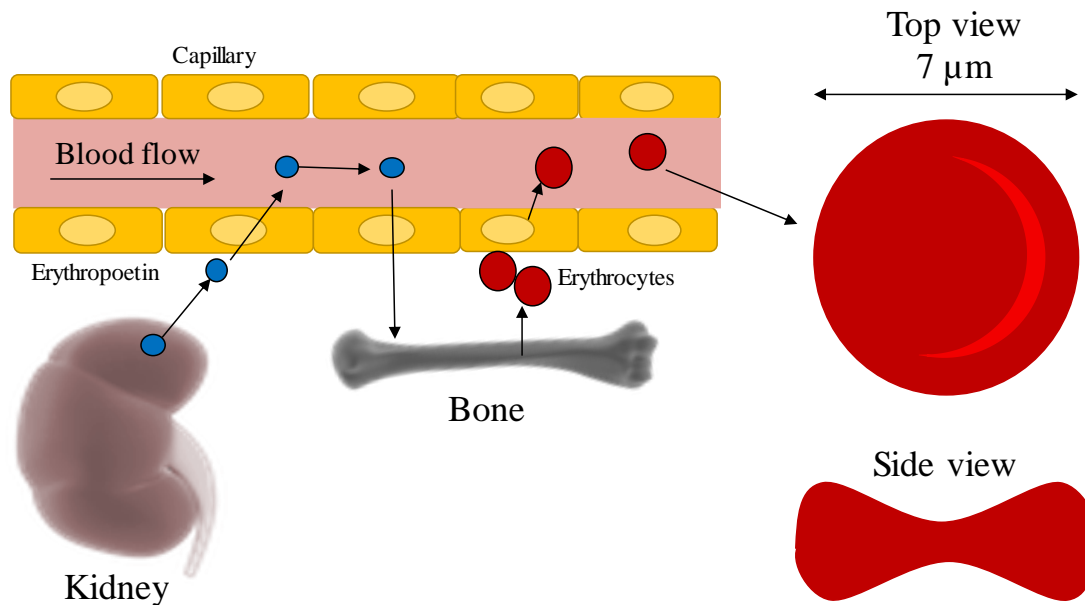
### 1.6.1 Erythrocytes

#### 1.6.1.1 Red Blood Cells

Red blood cells (RBCs) or erythrocytes (from the Greek ‘*erythos*’ meaning red and ‘*cyte*’ meaning cell) are the most abundant type of blood cell in vertebrates and their function is to transport oxygen in the blood. RBCs are adapted to their function through being bi-concave discs which increases the surface area-to-volume ratio of the cell. This increases the diffusion efficiency of oxygen and carbon dioxide in and out of the cell. RBCs also have a flexible plasma membrane, allowing the 7  $\mu\text{m}$  wide cells to squeeze through capillaries as small as 3  $\mu\text{m}$  wide (60). The lack of a nucleus and other organelles seen in other cell types allows more room for the oxygen binding protein haemoglobin. However, this lack of organelles means that RBCs cannot repair themselves when damaged so have a lifespan of approximately 120 days (61). 2-3

million RBCs die every second and are removed via the spleen. For every RBC death, another is produced through a process called erythropoiesis.

### 1.6.1.2 Erythropoiesis



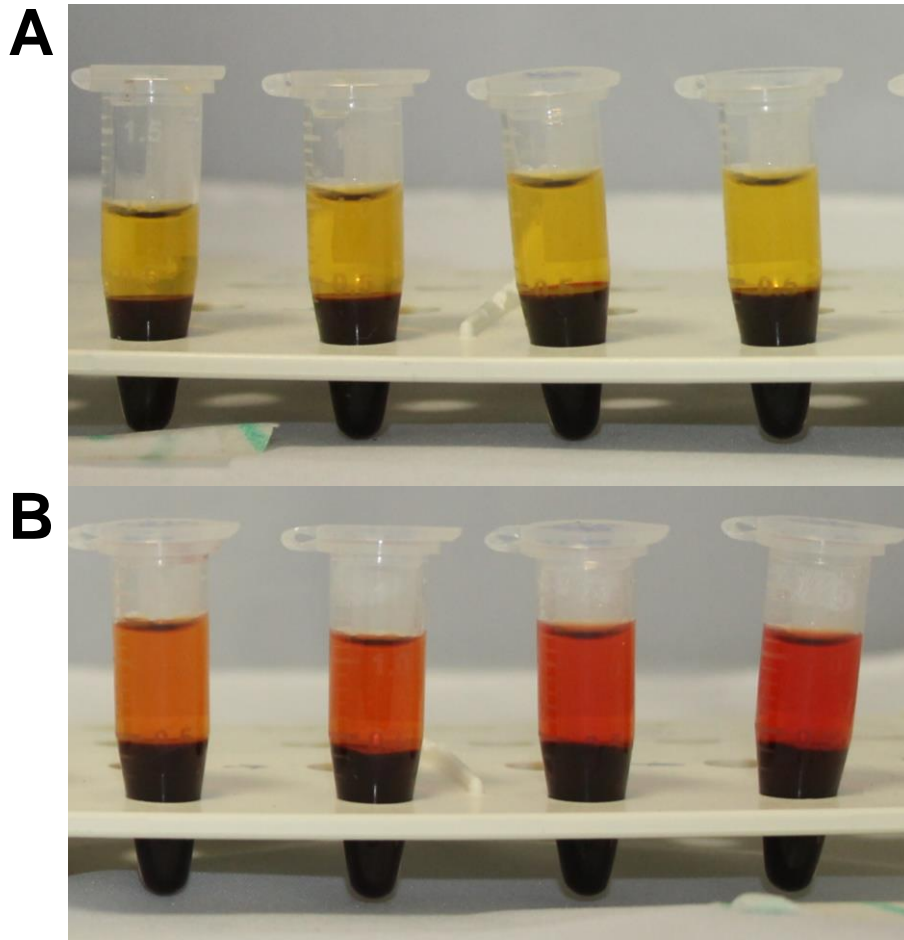
**Figure 1.5: Erythropoiesis**

Low oxygen levels lead to the production of erythropoietin (EPO) by the kidney (blue circles). EPO enters the bloodstream and stimulates EPO receptors on red bone marrow cells. Erythrocytes are then produced (red circles) which increases the oxygen concentration, signalling the kidney to reduce EPO production.

RBCs must be produced at the rate that matches the body's needs. This is achieved through erythropoiesis which is regulated by the kidney (Figure 1.5). If oxygen levels are low, then the kidney produces erythropoietin (EPO) which enters the blood stream to eventually act on EPO receptor bearing precursor cells within the red bone marrow (Figure 1.5). This stimulates the production of erythrocytes from the bone marrow which then enter the blood stream. As the population increases, so too does the oxygen concentration, thus signalling to the kidney to reduce production of EPO (62).

### 1.6.1.3 Plasma-Free Haemoglobin

As RBCs are unable to repair themselves, damaged RBCs can leak haemoglobin causing the plasma to appear red when centrifuged (Figure 1.6). This damage is referred to as haemolysis and can be measured through several different methods.



**Figure 1.6: Haemolysed blood**

Comparison of **A)** healthy blood plasma with no haemolysis and **B)** haemolysed blood.

Damage to RBCs can occur due to bacteria such as *Streptococcus*, *Enterococcus*, and *Staphylococcus* which produce haemolysins to form pores or cleave the RBC membrane, or due to mechanical influences outside of the body such as excessive suction through hypodermic needles. Shear stress induced by medical devices is also a cause of haemolysis and testing for this is a key regulatory standard. Therefore, such devices must be below a normalised index of haemolysis of 0.01 g/L (63) before approval (64).

### 1.6.2 Leukocytes

White blood cells (WBCs) or leukocytes (from the Greek '*leuko*' meaning white) are the cells of the immune system involved in protection of the host against foreign bodies and pathogens (60).

### *1.6.2.1 Polymorphonuclear Cells*

Polymorphonuclear (PMN) leukocytes comprise neutrophils, eosinophils, and basophils that are all rich in intracellular granules containing enzymes that are released during the immune response.

Neutrophils are the most abundant (50-60%) blood leukocyte in humans and are continuously generated in the bone marrow. They are well recognised as the first leukocytes to be recruited into an inflammatory site during an innate immune response where they survive in tissues for 1-2 days. The major role of neutrophils is to eliminate pathogens through phagocytosis whereby pathogens are engulfed and killed using reactive-oxygen species (ROS) or antibacterial proteins (cathepsins, defensins, lactoferrin, and lysozyme) contained within the granules (65). These antibacterial proteins can also be released from the cell into the area of invasion (degranulation). Highly activated neutrophils undergo a process called NETosis where neutrophils release neutrophil extracellular traps (NETs), a combination of histones, proteins, and enzymes from the granules to immobilise pathogens to prevent the spread of infection (66).

Eosinophils have a high affinity for coal tar dyes (eosin), the granules turning brick red when stained with such. They are 12-17  $\mu\text{m}$  in diameter and account for approximately 1-6% of the WBC population in the blood. Eosinophils have a bi-lobed nucleus and granules containing toxic eosinophil peroxidase and other proteins. They play an important role in parasitic and allergic diseases (67).

Basophils so named for being 'base-loving' as they stain well with basic dyes. They are the least common of the granulocytes, representing approximately 0.01% to 0.3% of circulating WBCs. Large granules within the cytoplasm contain heparin to prevent rapid blood clotting and histamine which promotes blood flow to tissues released upon binding with IgE to surface receptors (60).

### *1.6.2.2 Mononuclear Cells*

Mononuclear cells – monocytes and lymphocytes – are those blood cells with an essentially round uni-lobed nucleus and agranular cytoplasm. Monocytes are the largest leukocyte at 15-30  $\mu\text{m}$  accounting for 2 – 10% of all blood leukocytes. They are round-shaped with agranulated cytoplasm and a unilobed, kidney-shaped nucleus.

Monocytes circulate in the blood for 1-3 days and migrate quickly to infiltrate infected tissues after neutrophils have already arrived. Within these tissues, monocytes differentiate into macrophages which are responsible for protecting tissues from foreign substances through three main functions: phagocytosis, antigen presentation, and cytokine production. Macrophages are long-lived and can perform phagocytosis of pathogens and dying neutrophils as well as functioning as antigen-presenting cells (APCs) as part of the adaptive immune system (67).

Lymphocytes divided into T-, B-, and NK cells. T-cells (thymus-derived cells) and B-cells (bone marrow-derived cells) are components of the adaptive immune response and provide the antigen-specific response to ‘non-self’ antigens initiated via antigen presentation by dendritic cells (67). T cells are critical in cell-mediated immunity and there are several different subsets such as helper, memory, and cytotoxic T cells. These subsets have different roles including production of cytokines to direct the type of response, provide antigen-specific immunological memory, or kill infected cells, respectively. B cells are responsible for humoral immunity through producing antigen-specific antibodies to combat non-self entities such as foreign bodies and pathogens.

NK (natural killer) cells play a role in defending the host from transformed cells that might form tumours and virally infected cells through interacting with altered Major Histocompatibility Complex (MHC) class I and various inhibitory and activating receptors. They are typically activated by a family of cytokines called interferons and proceed to release cytotoxic granules which destroy altered host cells (68).

### *1.6.3 The immune response*

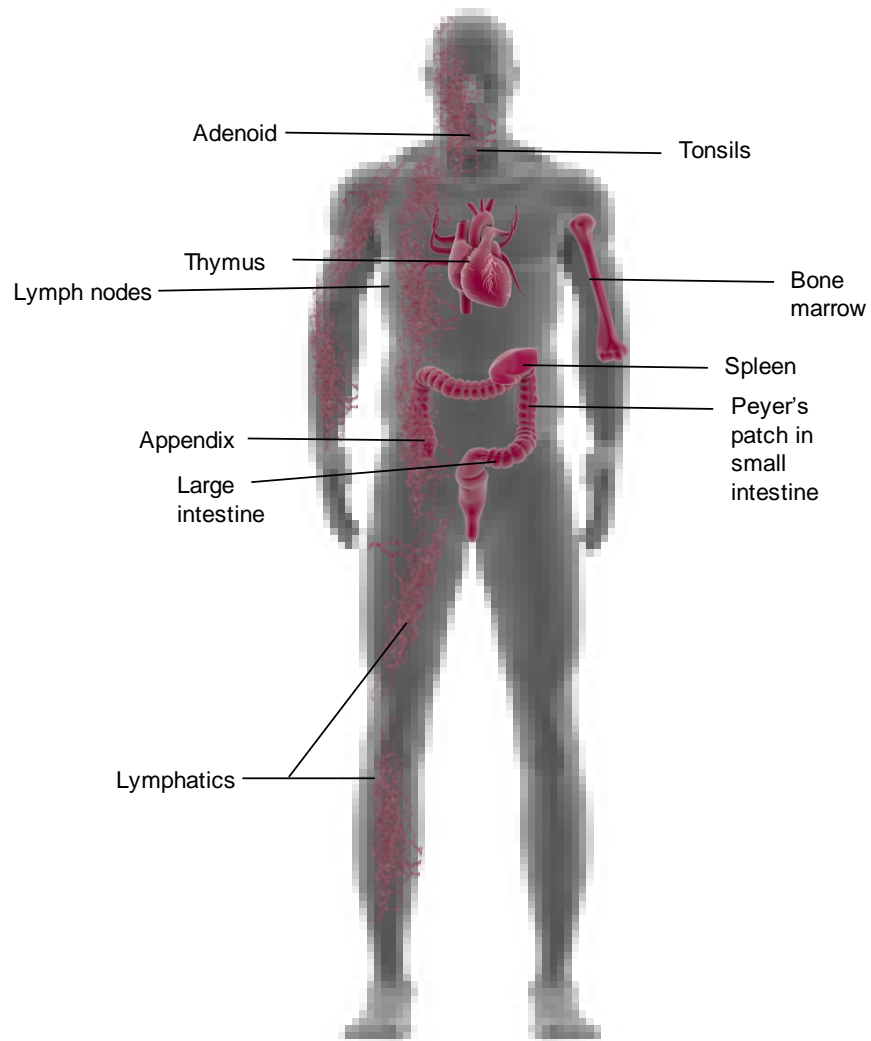
The immune response is a cascade of interconnected responses to trauma and infection which detects and eliminates substances dangerous to the host. The response in healthy individuals spans 10-14 days and takes place in the secondary lymphoid organs and at sites of inflammation. Factors that determine the nature of the immune responses include whether the triggering danger is intracellular or extracellular, the exposure time and dose, and the location of infection (69). The immune response can be divided into three main lines of defence: barrier immunity, innate immunity, and adaptive immunity. These overlap and aid each other in the removal of infection.



Barrier immunity is the first line of defence against invading pathogens and other dangers. It is non-specific and designed to provide a barrier in areas that are vulnerable such as in the gastrointestinal (GI) tract and external orifices. Barrier function is provided by epithelial cells, various enzymes and other bioactive secretions, and other physiological and anatomical features such as cilia, sweat, tears, and mucus. Epithelial barriers can rapidly and effectively discriminate toxic entities and repair the damaged barrier to avoid trauma (70). These layers also consist of lysozymes, secretory immunoglobulin A (sIgA), high concentrations of white blood cells, destructive pHs, and commensal bacteria that all work to prevent entry into the body.

The outer most barriers of the body are also patrolled by leukocytes, especially dendritic cells and macrophages: if a barrier is breached then innate immunity mediated by these cells kicks in. This response is broad and non-specific, is evolutionary ancient, and present in all creatures from birth. Pathogens express pathogen-associated molecular patterns (PAMPs) that are recognised by germ-line encoded pathogen recognition receptors (PRR) expressed on epithelial and immune cells. Binding to PRRs stimulates inflammation through the secretion of chemokines which forms a chemical gradient attracting neutrophils and monocytes from the blood to the site of inflammation (71). The main purpose of this response is to enable phagocytosis and pathogen destruction to ideally resolve the situation quickly.

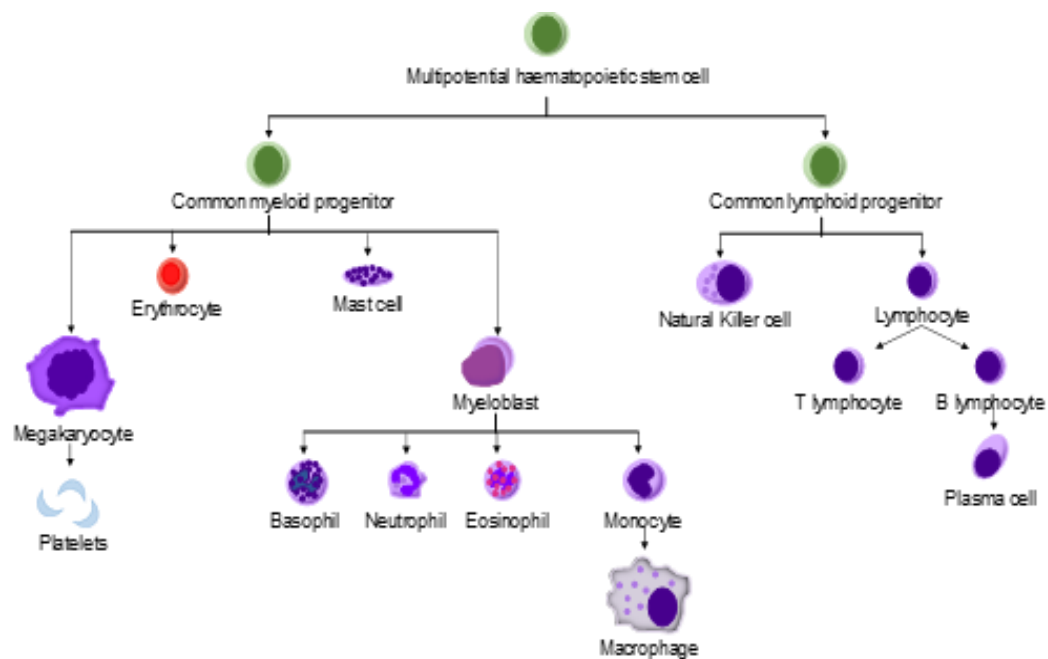
If the innate immune response is ineffective, adaptive immunity responds to generate an antibody-specific attack with features of immunological memory. This response only occurs in vertebrates and is key to the development of vaccines. It involves the process of developing antigen-specific antibodies and memory cells via the T and B lymphocytes. Adaptive immunity relies on the sampling of the environment by dendritic cells (DCs) and presentation of antigen peptides on the surface using the (MHC). The peptide-MHC is then recognised by lymphocytes which undergo clonal selection, expansion, and differentiation (Figure 1.7) to elicit a directed response against the pathogen and more effective removal (69).



**Figure 1.7: The lymphatic system.**

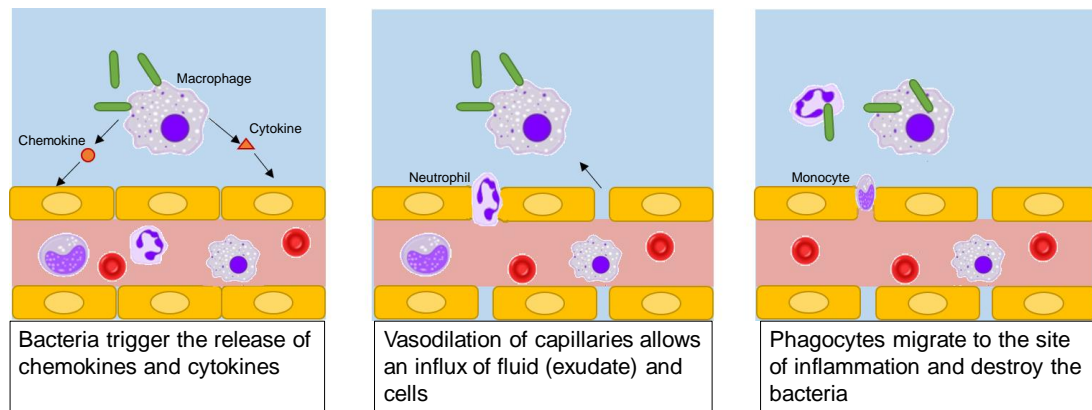
Primary lymphoid organs such as bone marrow and thymus are responsible for the production and maturation of lymphocytes. Secondary lymphoid organs such as the spleen and lymph nodes are sites of initiation of the adaptive immune response.

### 1.6.3.1 Innate Immunity



**Figure 1.8: The blood cells of the immune system derived from haematopoietic stem cells within the bone marrow.**

The common myeloid progenitor cell (Figure 1.8) is the precursor to granulocytes, monocytes, and dendritic cells of the innate immune system (69). It is also the precursor to red blood cells and platelets. Tissue resident and activated macrophages are derived from circulating monocytes either in the steady state or upon an inflammation trigger, respectively. Macrophages scavenge cell debris, dead cells and phagocytose and kill invading pathogens. They also dispose of infected cells targeted by the adaptive immune response. Additional to this, macrophages help induce inflammation and secrete signalling proteins to activate other immune cells and recruit them to the site of infection (Figure 1.9).



**Figure 1.9: Inflammatory response.**

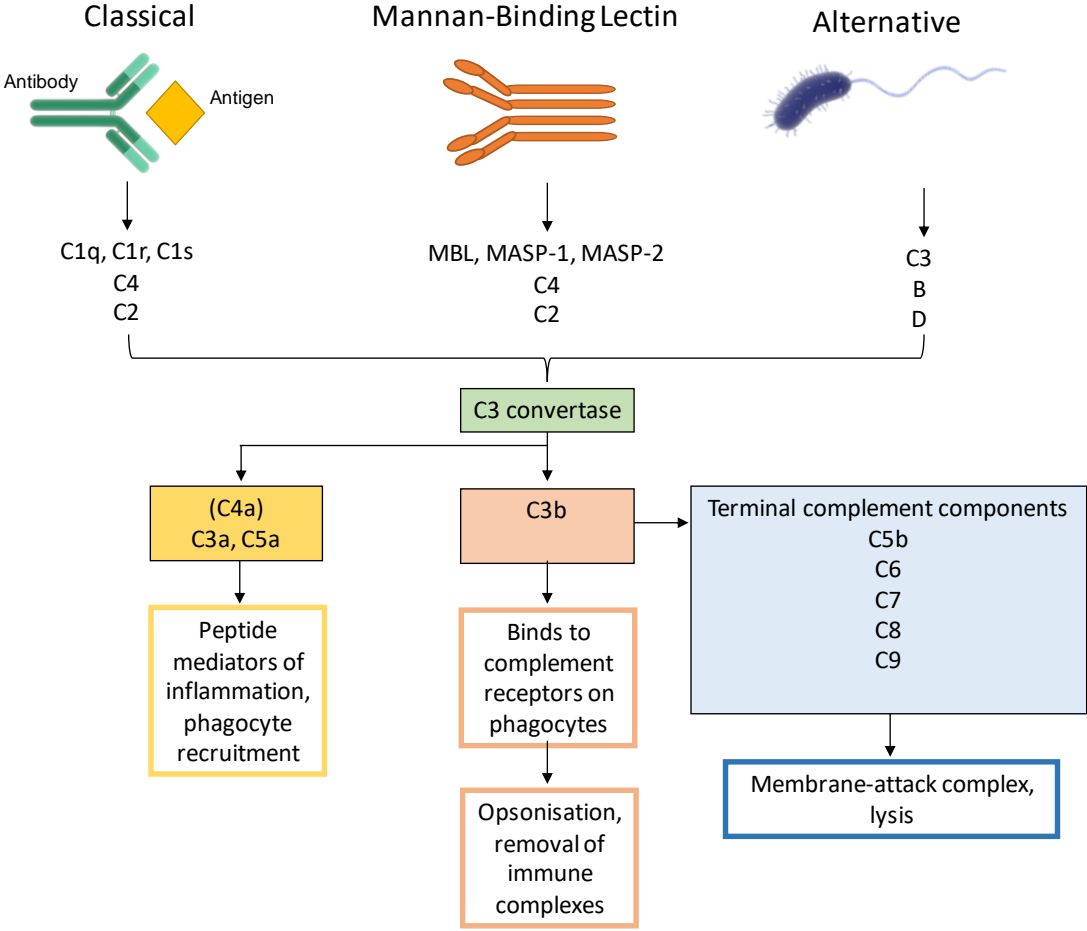
Bacteria trigger macrophages to release cytokines which increase the permeability of blood vessels to allow fluid and proteins to pass into the tissue. Chemokines attract neutrophils and monocytes to the site. This accumulation of fluid and cells to the site causes pain, swelling, heat, and redness – the signs of inflammation.

Dendritic cells are also found within tissue sites and form a network of cells constantly surveying the tissues for damage and danger. Their key function is to take up and process the agent of danger/damage and present it in the context of MHC class I and II molecules to initiate antigen-specific responses by CD8<sup>+</sup> and CD4<sup>+</sup> T cells, respectively. The different molecules expressed on the surface of DCs and the cytokines they secrete direct the type of adaptive immune response that is made, i.e. if a fungus is the trigger than an appropriate anti-fungal response is favoured. DCs, therefore, provide a crucial link between the innate and the adaptive immune response (69).

#### 1.6.3.2 Complement

Complement is so named because it ‘complements’ the innate immune system. It is made up of large and small plasma proteins which interact with one another to opsonise pathogens and induce a series of inflammatory responses. The precursor enzymes, or zymogens, are widely distributed throughout bodily fluids and tissues. When the complement system becomes activated, an active complement protease cleaves inactive zymogens to their active enzyme form in a cascade-like manner (69). Complement is activated in three pathways (Figure 1.10) dependent on the surface of the pathogen. These pathways converge to generate the same set of effector complement proteins. These effector proteins aid the immune response in three ways:

covalent binding to pathogens thus opsonising them for engulfing by phagocytes carrying complement receptors; small fragments acting as chemoattractants to attract and activate more phagocytes; and thirdly, to create pores in bacterial membranes (69).



**Figure 1.10: The complement pathway.**

The classical, lectin, and alternative pathway all eventually converge into the formation of C3 convertase which becomes C3a and C3b to activate certain functions.

The classical pathway is activated through the binding of C1q to the pathogen surface. It can bind in three ways: directly to surface components of bacteria; binding to C-reactive protein; binding to antigen: antibody complexes therefore linking the innate and adaptive immune response. The lectin pathway is activated by the binding of carbohydrate-binding proteins to arrays of carbohydrates on the surface of the pathogen. The alternative pathway is initiated by the binding of spontaneously activated complement component C3 in plasma to the surface of the pathogen. The three pathways all proceed to form C3 convertase at the binding site on the pathogen

(69, 72). Here, C3 convertase cleaves C3 into C3a, a peptide mediator of inflammation, and C3b, the main effector molecule. C3b opsonises pathogens and binds with C3 convertase to form C5 convertase. C5 convertase produces the most potent complement peptide, C5a, as well as C5b which initiates the late events of the pathway. These comprise a series of polymerisation reactions in which terminal complement components interact to form membrane-attack complexes which create pores in the cell membranes of certain pathogens (72).

#### *1.6.3.3 Cytokines and Chemokines*

Cytokines are small proteins that are released from various cells to enable communication between cells through binding to specific receptors. They can act in an autocrine (on the cell they've been released from), a paracrine (on cells adjacent to them), or an endocrine (on distant cells) manner (67).

Chemokines are a subset of cytokines that control the migration of immune cells. A relevant example is IL-8 that mediates the transmigration of neutrophils from the circulation into the inflamed tissue. The effects of IL-8 include regulation of leukocyte interactions with the endothelial cells lining blood vessels: encouraging leukocytes to roll along endothelial cells at the site of inflammation, and converting this rolling phenotype to stable binding by triggering adhesion molecules to change conformation allowing the leukocytes to migrate through the blood vessel walls (71). Chemokines also direct the migration of leukocytes by binding to the extracellular matrix and surfaces of endothelial cells at the inflammatory site to create a gradient that can be followed by the responsive cells. Bacteria also make peptides that act as neutrophil chemoattractants. An example of this is the formyl-methionyl-leucyl-phenylalanine (fMLP) peptide that binds to the G-coupled fMLP receptor on neutrophils (71).

#### *1.6.3.4 Adaptive Immunity*

The key features of the adaptive immune response are memory, specificity, and diversity. Memory allows for the immune system to remember pathogens it has 'seen' before and elicit a specific, quicker response to that pathogen if it invades again. However, the specificity of the adaptive response means that a single change in pathogen can mean a new response is needed, for example such as in different strains of the flu virus. The diversity of the adaptive response means that responses can be made to a multitude of different organisms.

Antigen-laden DCs move from the tissue into the lymphoid tissue and come into intimate contact with lymphocytes. Here, the DCs present the peptide MHC to the T cell receptor (TCR) and 'show' the T lymphocytes (also known as T cell) the antigen in a process known as clonal selection. Each T lymphocyte has a receptor unique to itself called the T Cell Receptor (TCR) which will recognise the antigen bound to the MHC. Once the correct T cell has been found, the binding of the MHC-antigen-TCR is referred to as signal 1, and requires a further signal 2 which requires adhesion molecules to bind the cells together to prolong exposure (73). This process is called co-stimulation and uses various types of adhesion molecules such as CD28, CD80, CD86, CD40, and CD40L (74).

There are several subsets of T cells, and they all have different functions. T helper cells ( $T_h$  or CD4+ cells) recognise MHC class II molecules and when activated help the immune response through stimulation of B cells to produce antibodies. T cytotoxic cells ( $T_c$  or CD8+ cells) recognise MHC class I molecules and when activated move to kill infected cells. When the T cells have recognised the antigen, they will multiply in a process called clonal expansion to provide a more direct, specific response to the invading pathogen (75).

Once the pathogen has been cleared, the immune response needs to return to a resting state. This is a complex process but put simply, a subset of T cells, called T regulatory cells ( $T_{reg}$ ) aid in this process through producing anti-inflammatory cytokines and prevent excessive damage caused by an over active system (76).

#### *1.6.4 Haemostasis*

Haemostasis is the process whereby a vascular injury is stopped and repaired. It depends on the interaction between the vessel wall, platelets, and coagulation factors. Various inhibitors of coagulation and the fibrinolytic system ensure that healthy coagulation only occurs at the site of injury.

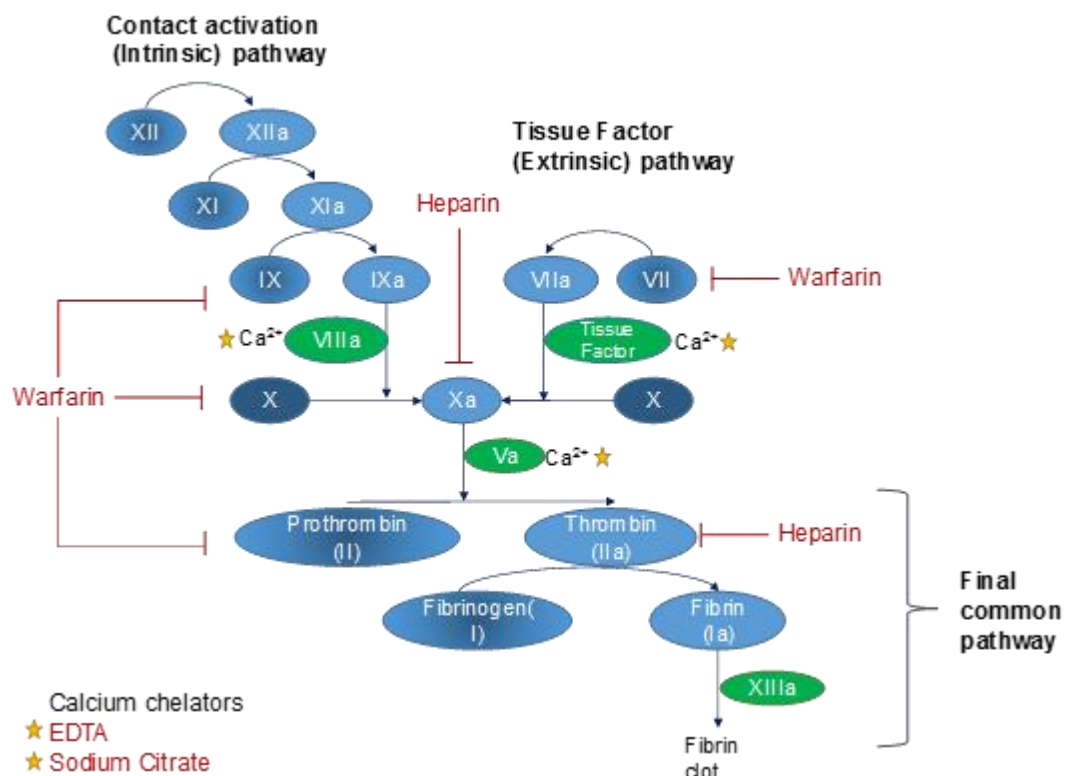
##### *1.6.4.1 Platelets*

Platelets, also known as thrombocytes, are fragments of cells released from megakaryocytes. They have no nucleus, are biconvex discoid in shape, are approximately 2-3  $\mu\text{m}$  in diameter, and are found only in mammals. The main function of platelets is haemostasis. Platelets circulate in the blood and gather at the site of

damage on the endothelium and essentially ‘plug the hole’ unless it is physically too large. Firstly, platelets adhere to the damaged endothelium where they become activated and secrete chemical messages to attract more platelets to the site. They then connect to one another (aggregation) and lead to the activation of the coagulation cascade and the development of a fibrinous clot (77).

#### 1.6.4.2 Coagulation Cascade

The coagulation cascade (Figure 1.11) consists of a series of pro-enzymes (serine proteases) and pro-cofactors which are activated sequentially to form thrombin via two different pathways- intrinsic and extrinsic - which combine in the final common pathway to form a fibrinous clot.



**Figure 1.11: The coagulation cascade and the points at which anticoagulants block the pathway.**

The tissue factor (formerly extrinsic) pathway is activated by the expression of tissue factor on the surface of injured cells. Tissue factor binds and activates factor VII to form a complex that activates factor X to Xa and factor IX which amplifies the activation of factor X with the aid of co-factor VIII bound to von Willebrand factor



(vWF). The contact activation (intrinsic) pathway is initiated by anionic surface-contact activation of factor XII to factor XIIa. Activation of factor XII forms an activation complex consisting of prekallikrein, high-molecular weight kininogen, and factor XI (78). Both pathways combine to form the ‘final common pathway’ whereby thrombin is generated by the action of the Xa/Va complex which cleaves prothrombin into thrombin. Thrombin then converts fibrinogen to fibrin monomers which combine to form a fibrin polymer clot. The clot becomes stabilised by factor XIII cross-linking the polymers. Platelets accelerate the process by providing membrane phospholipids which act as ‘docking’ stations for the coagulation factors. Thrombin is highly important in coagulation as it not only activates factors and promotes platelet aggregation, it binds thrombomodulin on the endothelial cell surface to activate protein C which inhibits coagulation (59).

Feedback loops prevent indefinite coagulation through monitoring the levels of active proteases in the blood and producing serum protein antithrombin which inactivates serine proteases, principally thrombin and factor Xa. Protein C and protein S are vitamin-K dependent proteins that act to inactivate factors Va and VIIIa as well as tissue plasminogen activator (TPA). Tissue factor pathway inhibitor inhibits this main *in vivo* coagulation pathway by inhibiting factors VIIa and Xa (59).

Fibrinolysis is the process whereby the fibrin clot is degraded by plasmin cleaved from plasminogen. This is activated through the release of TPA or exogenous agents such as streptokinase or urokinase-like plasminogen activator. Plasmin digests fibrin as well as factors V and VII.

#### 1.6.4.3 Anticoagulants

Anticoagulants consist of chemical substances which are used to prevent and control the clotting of blood. Anticoagulation therapy is used to prevent the formation and growth of dangerous clots in patients with thrombotic disorders such as coronary artery disease and deep vein thrombosis. The traditional anticoagulants are detailed below.

##### 1.6.4.3.1 Heparin

Heparin is a mucopolysaccharide that is not absorbed orally therefore is given intravenously or subcutaneously. It is an activator of antithrombin III which irreversibly inactivates prothrombin, Xa, IXa, and XIa. Heparin also inactivates

platelet function. Low molecular weight heparin preparations (MW < 5000) such as enoxaparin (Clexane®), deltaparin (Fragmin®), and tinzaparin (Innohep®) have an improved ability to inactivate factor Xa, are less effective on thrombin, and have a lesser effect on platelet function so tend to cause less bleeding. These variants of heparin have a longer plasma half-life and so daily subcutaneous administration is an effective prophylactic (59).

#### 1.6.4.3.2 Warfarin

Warfarin, also called Coumadin, is orally administered and prevents the promotion of the vitamin k-dependent  $\gamma$ -carboxylation of glutamic acid residues of factors II, VII, IX, and X. Within 24 h, there is a 50% drop in factor VII levels and factor II after 4 days. Protein C and S levels also fall leading to an initial increased risk of thrombosis. The therapeutic dose is very variable ranging from 0.5 to 20 mg/day (59). Warfarin dose must be monitored carefully as it is dependent on the amount of vitamin K in the body which is affected by diet (79). The time blood plasma takes to clot in seconds (prothrombin time; PT) is used for monitoring dose. The international normalised ratio (INR) calculates the ratio of PT of the test to normal PT (80).

## 1.7 Interactions of leukocytes with implantable continuous-flow LVADs

A typical LVAD operates at a flow rate of 5 L/min which means that for 5 L of blood circulating around the body, non-adherent leukocytes are repeatedly exposed to the LVAD at 1-minute intervals. It is plausible to assume that as brief exposure to high shear has been shown to sensitise platelets to subsequent low shear (81), leukocytes may be affected the same way.

The trajectory of an individual leukocyte is variable with most travelling through the primary flow path of the pump, and a small proportion through the secondary flow path. Residence time and exposure to shear stress will thus be variable. Contact with the biomaterial by the leukocyte is limited in the primary flow path, however, the secondary flow path generally has smaller gaps, higher shear, and low volumetric flow rates (82). Activation and adhesion of leukocytes in this area of the pump due to a combination of biomaterial, shear stress, and circulatory stasis is more apparent.

Leukocytes also contend with different types of biomaterials and surface finishes throughout the pump. The surface area of LVAD biomaterials varies greatly with the titanium alloy body having the greatest surface area, and bearings potentially the smallest. Whilst a biomaterial may cause leukocyte activation and adhesion, its surface area may render this unimportant when compared to mechanical benefits. In terms of surface finish, this also varies throughout the LVAD. Highly polished, smooth surfaces are used near the rotating impeller in long-term continuous-flow LVADs to reduce their thrombogenicity (83). However, many LVADs have parts of the pump coated with sintered titanium microspheres. The rationale behind this was to form a stable, densely adherent biological lining on the inside of the device to reduce the need for anticoagulation and to encourage cellular growth to incorporate the pump into the myocardium. The HMII has the inlet and outlet elbows as well as the intraventricular cannula coated with microspheres (84). The nature of the surface finish and the local wall shear stress may influence leukocyte adhesion.

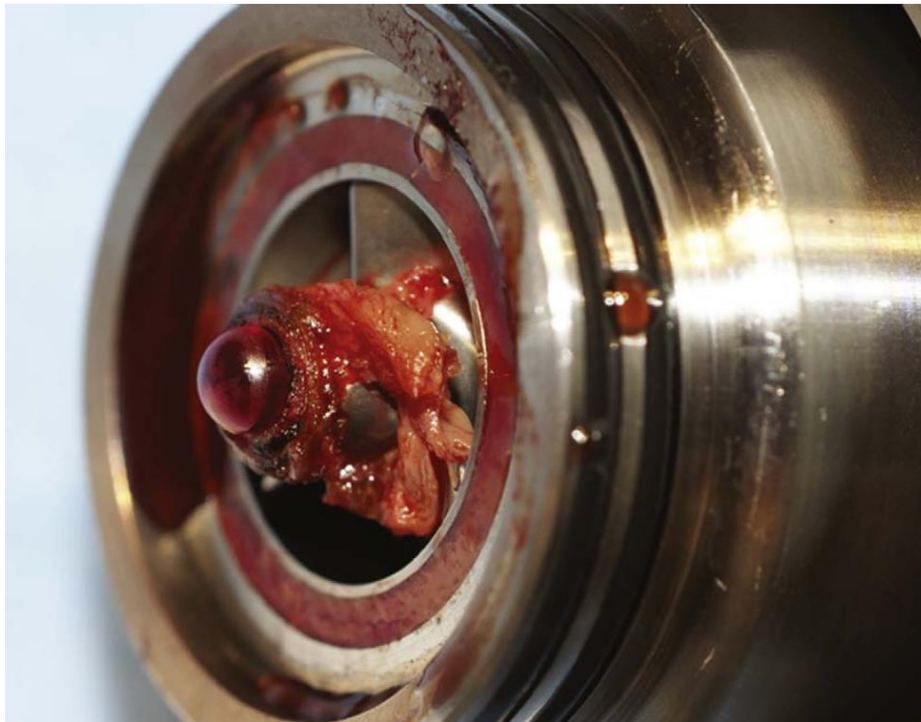
The interactions between leukocytes and the pump are important to understand the progression of common complications observed in VAD patients.

## 1.8 Complications of VADs

Despite the improvements in the quality-of-life and survival of patients with VADs, infection, stroke, bleeding, and thrombosis remain common complications. The nature of the implant and how it works contributes to the prevalence of such complications through the introduction of a foreign surface and artificial shear stress.

### *1.8.1 Thrombosis*

Thrombosis is the most fatal of the complications as the formation of a thrombus within the pump can lead to pump blockages and the need for replacement, whilst the breaking off from the clot into the circulation can result in a fatal embolism or stroke if not treated effectively. The origins of pump thrombosis remains poorly understood as the thrombus can be formed upstream of the VAD, or within the pump body, or present in the outflow graft due to turbulent flow (85). Pump-related factors include heat generation, graft kinking, shear stress, stasis, cannula position, and the foreign surface (86). The pump is not the only contributory factor as the patient and the management of the pump also influence the risk of thrombosis.



**Figure 1.12: Thrombus formation in the HeartMate II**

Image reproduced from Mokadam, N.A., *Thrombus formation in a HeartMate II*. European Journal of Cardio-Thoracic Surgery, 2011. **39**(3): p.414 with permission from Oxford University Press ©2011. Thrombus found on the inlet bearing of the HeartMate II upon explant (87)

Diagnosis of pump thrombosis (PT) can be strictly defined as confirmed during VAD exchange, explant, heart transplant, or death although the definition can include suspected cases (85). During multi-centre clinical trials for continuous-flow VADs such as the HeartMate II and the HeartWare HVAD between 2005 and 2012, confirmed PT was diagnosed in 2-3% of patients (88-91). However, despite these relatively low incidence rates, anticoagulation and anti-platelet therapy during implantation varies from centre to centre. Even more disturbingly, as time went by with more trials in different centres, the rate of PT was noticed to be increasing with reports of incidences as high as 11% (92-94). Most data between 2005-2012 was based on trials for the HeartMate II which is a relatively large axial flow pump with evident thrombus formation at the bearing (Figure 1.20). Improvements in design such as creating a smaller, centrifugal, magnetically-levitated pump have notably improved the PT rates as demonstrated by the recent 1-year clinical trial results with the HeartMate III where the PT rates were zero (95).

### 1.8.2 Infection

Device infection is a common complication for LVADs as well as other mechanical circulatory support systems. Various studies have demonstrated infection rates at anything between 7% and 72% of patients having some type of infection post-implantation with *Staphylococcus aureus* being the most prominent adversary (96). Device-related infections are defined as those which occur on the blood-contacting surface of a pump, outer surface of the pump, or at the driveline site. Many device infections are caused by biofilm-forming bacteria and fungi such as *Staphylococcus*, *Pseudomonas*, and *Candida* species which adhere and colonise on the large material surface. This limits attack by the immune system and can lead to sepsis if not treated effectively. Driveline infections are particularly problematic as the need to power the device leads to the requirement of an open wound which is vulnerable to infection whilst healing occurs. A risk factor for driveline infections is trauma to the driveline site (97, 98).



**Figure 1.13: Driveline infection**

Image reproduced from Chinn, R., Dembitsky W., Eaton L., et al., *Multicenter Experience: Prevention and Management of Left Ventricular Assist Device Infections*. ASAIO Journal, 2005 51(4) p. 461-470 [http://journals.lww.com/asaiojournal/Fulltext/2005/07000/Multicenter\\_Experience\\_Prevention\\_and\\_Management.23.aspx](http://journals.lww.com/asaiojournal/Fulltext/2005/07000/Multicenter_Experience_Prevention_and_Management.23.aspx) with permission from Wolters Kluwer Health, Inc. ©2005. Moderate driveline infection (99).

Whilst infections are relatively common place in VADs, the response to them differs to that of a healthy person. By the end-stage of HF, the patients suffer from chronic

inflammation due to the deformation of the heart and the attempt by the immune system to repair it (12). The immune system of these patients may be severely compromised by this leading to a difficulty in combatting further inflammatory stimuli (infection) (100). To exacerbate the issue, reduced cellular immunity has been reported in VAD patients 6 months' after implantation. VAD implantation has been linked to activation-induced cell death of T cells with increased expression of CD95 (Fas) by T cells leading to heightened apoptosis upon further stimulation by pathogens (101). Monocyte deactivation has also been noted in VAD patients where a reduced percentage of monocytes expressing HLA-DR in the early post-operative period was predictive of multiple organ failure, impaired recovery, and sepsis (102). These effects lead to an impairment of the leukocytes to function and elicit an effective attack against bacteria.

### *1.8.3 Bleeding*

Bleeding occurs when there is a defect in haemostasis such as low levels of platelets, dysfunctional platelets, and coagulation factors. Bleeding, particularly in the (GI) tract, occurs in one third of VAD patients who experience single or multiple bleeding events (103). A proposed cause of bleeding is the shear-induced degradation of high molecular weight von Willebrand factor (HMW-vWF). vWF is a large multimeric glycoprotein up to 20000 kDa in size produced by megakaryocytes and endothelial cells. It is stored in the platelet  $\alpha$ -granules and released into the plasma upon activation to act as a bridging molecule for platelet adhesion and aggregation at the sites of vascular injury (104). It has been suggested that the degradation of HMW-vWF and reduction of adhesive activity is due to excessive cleavage by ADAMTS-13 under persistently high levels of shear (105). This then leads to the development of acquired von Willebrand syndrome (AVWS) where there is a reduced ability of vWF to prevent bleeding (106). However, degradation of HMW-vWF and subsequent development of AVWS occurs soon after LVAD implantation, but not all patients have clinically relevant bleeding complications (105). This suggests that there are other mechanisms at work that lead to bleeding. One alternative is that LVAD implantation causes a reduction in pulse pressure leading to hypoperfusion in the GI lining (107). Combining this with increased intraluminal pressure can increase the risk of ruptured vessels due to the formation of arteriovenous malformations (108).

#### *1.8.4 Chronic right heart failure*

The majority of LVAD patients have some degree of right ventricular (RV) dysfunction. Consequently, RV failure complicates 10 – 40% LVAD implants (109, 110). LVADs decompress the LV and reduce LV end-diastolic pressure leading to a decrease in pulmonary artery pressure and improved RV function. However, increased cardiac output from the LVAD can worsen pre-existing RV failure, with continuous-flow LVADs causing aggressive decompression affecting RV contraction (110).

#### *1.8.5 Aortic insufficiency*

Aortic insufficiency (AI), also known as aortic regurgitation (AR), occurs when the aortic valve does not close tightly thus allowing blood to flow in the reverse direction (aorta into left ventricle) during ventricular diastole. AI may develop during support with continuous-flow LVADs. It has been proposed that this is due to commissural fusion and deterioration of the leaflet tissue, possibly due to failure of the aortic valve to open during support (111). To facilitate opening of the AV during support, running the pump at a lower speed or surgery to address the AI during implant are suggested options (111).

#### *1.8.6 Known complications in current VADs*

VADs that are currently approved for use pass through clinical trials with minimal adverse events and low haemolysis. However, complications appear later post-approval in various clinics. During *in vitro* testing, the HeartAssist 5 (HA5, ReliantHeart) reported haemolysis as 6 mg/dL (51) yet when run off design point in clinic, this increased to > 40 mg/dL (12% of cases) (112). Pump thrombosis has been noted as an adverse complication in the HA5 (113), the HMII (87, 114-117), and the HVAD (118, 119). Acquired von Willebrand syndrome and GI bleeding have been noted in the HMII (84), the Jarvik 2000 (120), and the HMIII (121).



## 1.9 Objectives

The overarching aim of this project was to gather data on the biocompatibility of medical devices to improve future designs of ventricular assist devices. A series of objectives were generated at the outset:

- Develop techniques for monitoring leukocytes for use during *in vitro* and pre-clinical studies.
- Evaluate changes in leukocyte behaviour in response to biomaterials relevant to VAD design.
- Evaluate thrombogenicity of biomaterials through coagulation assays and measuring platelet activation.
- Develop a method to image biomaterial discs to show cellular adhesion.
- Measure changes in leukocyte behaviour in response to shear stress at a biomaterial surface.
- Measure generation of leukocyte microparticles in response to shear stress using mock circulatory loops.
- Characterise leukocyte microparticle (LMP) activation status and parentage in multi-species.
- Compare the blood damage profiles of the MiniVAD with competitor devices.
- Translate the LMP assays from an *in vitro* to a pre-clinical setting.
- Measure the generation of LMPs throughout pre-clinical trials.
- Develop methods for characterising thrombus and the role leukocytes have in its formation.

## Chapter 2 Enabling technologies

### 2.1 Introduction

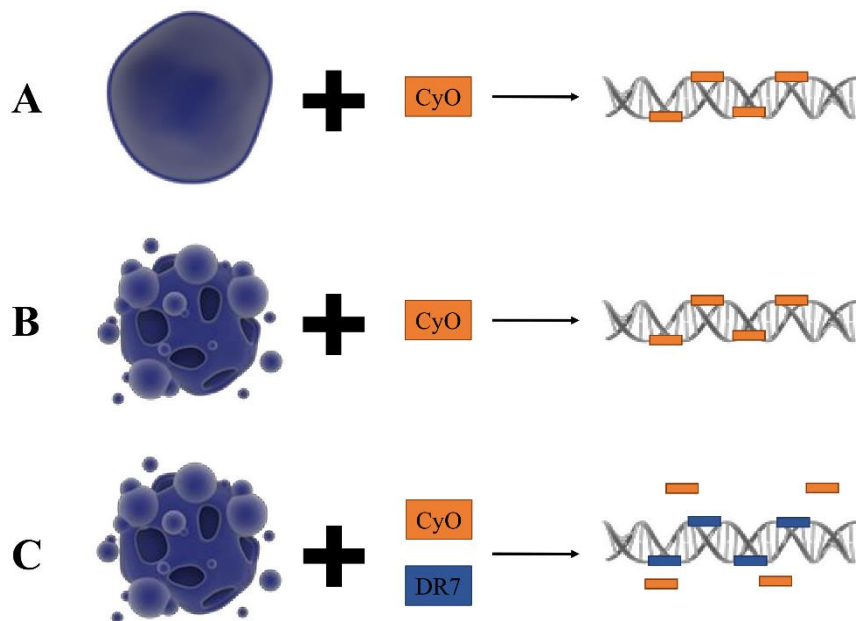
The research and development of ventricular assist devices (VADs) relies heavily on the use of blood from large animals such as cows, sheep, and pigs (122-124). The complications observed in VADs - infection; thrombosis; and bleeding - are linked to blood cell damage (101, 125-129) therefore it is necessary to monitor blood damage during *in vitro* and *in vivo* testing to improve pump design (63, 130). Haematology analysers can provide cell counts (63, 131), but cannot provide other information such as viability, cell activation, or microparticle formation and the type of haematology analyser greatly affects count accuracy (132). Therefore, other methodologies need to be used. Key amongst these is flow cytometry however given the dearth of tools for use on bovine, ovine, and porcine cells, method development is a requisite.

#### 2.1.1 DNA Dyes and absolute count beads

Flow cytometry is a highly sophisticated technique which has the main advantage of analysing the physical and chemical characteristics of particles in a large population within a short amount of time in a small volume (133). Depending on the instrument used, as many as 10-12 different antigens can be marked and evaluated giving a huge amount of information on the cell phenotype. Although some human monoclonal antibodies do cross-react with some large animal species (134, 135), specific antibodies suitable for flow cytometry for cows, sheep, and pigs are not commonplace (136, 137). The antibodies that are available are often unconjugated and require secondary reagents or fluorophore-conjugation kits which can be methodologically challenging and costly.

Flow cytometry using absolute counting bead standards is considered the 'gold standard' for cell subset enumeration in clinical samples (138). Multicolour flow cytometry using DNA dyes and absolute cell counting beads allow leukocytes to be counted as well as their viability determined (139) and also has the benefit of enabling more detailed analysis using conjugated antibodies. Anthraquinone DNA dyes such as CyTRAK Orange™ and DRAQ7™ have spectral properties rendering them suitable for several cytometry platforms and for multicolour assays. These could be used in

combination with absolute counting beads to provide cell counts and viability (140-142). CyTRAK Orange has an excitation max at 510 nm so can be used on both blue (488 nm) and green (523 nm) laser instruments. It emits at 580-720 nm with an emission max at 615 nm which is similar to the range for phycoerythrin (550-650 nm, emission max 578 nm). It is membrane permeable and stains both the DNA in the nucleus and double-stranded RNAs in the cytoplasm in all cells. DRAQ7 only enters cells with a compromised membrane (apoptotic/necrotic cells) but has a greater affinity for DNA and outcompetes CyTRAK Orange in these cells (Figure 2.1). DRAQ7 is excited by both blue (488 nm) and red (633 nm) lasers and emits at 650-800 nm and gives dual-positive dead cells (for example blue laser PE-Cy7 detector against red laser AlexaFluor700 detector) enabling easy gating (140).



**Figure 2.1: DRAQ7 outcompetes CyTRAK Orange in cells with a compromised membrane.**

CyTRAK Orange is a membrane permeable stain which binds DNA in cells with an intact membrane **A)** live cells and **B)** cells with a compromised membrane (fixed/apoptotic/necrotic). DRAQ7 stains the DNA of **C)** cells with a compromised membrane but outcompetes CyTRAK Orange when double-stained.

CyTRAK Orange can also be used to identify nucleated cells in fixed samples (142), which is advantageous over antigen-specific markers as the fixing process can irreparably alter antigen structure (143). This is useful during *in vivo* and clinical VAD

studies as fixed samples can be sent from study sites to a central site and batch processed (144, 145). Such an approach also requires effective blood preservation strategies.

### *2.1.2 Blood preservation*

Long-term stabilisation of cells is useful for the evaluation of cytometer performances in immunofluorescence assays, for training technicians, and to compare other immunofluorescence techniques essential for checking the performance of antigen quantitation methods (146). Large scale international collaborations, such as preclinical animal studies, can be confounded by the challenges of sample processing, storage, and shipment all of which can be ameliorated by the use of preservatives to fix fresh blood samples for an extended analysis lifetime (147). Doing this minimises variability between sites and machines as well as time and overall cost with the benefit of being able to ship, store and batch process samples. The high complexity, sensitivity and large amount of data that can be produced from flow cytometry analysis of samples makes blood preservation a very attractive technique to use (147). However, the blood preservation strategy must be optimised and any effects on measures made considered during downstream analysis.

The commercial fixative used in this study is provided by Streck Laboratories (Streck Inc., Omaha, NE, USA).

#### *2.1.2.1 Cyto-Chex® blood collection tubes (BCT)*

Cyto-Chex® BCT tubes are vacutainer tubes which contain Streck Cell Preservative, a stabilisation agent with formaldehyde donors (146), and EDTA anticoagulant. Streck Cell Preservative (SCP) can be purchased on its own and mixed 1:1 with whole, anticoagulated blood. It has been engineered to stabilise white blood cells for up to 7 days at room temperature (144), is considered the best fixative for conserving absolute cell counts and is recommended for intracellular staining (147).

Absolute T cell counts are preserved in healthy donors as well as good light scatter profiles for granulocytes, lymphocytes, and monocytes. Differentiation of various white blood cell populations is not compromised, and this is essential for accurate monitoring of immune cell total and subset counts. CD45<sup>+</sup>, CD19<sup>+</sup>, and CD16/56<sup>+</sup> NK cells all can be enumerated (144).

Cyto-Chex BCT vacutainers stored at room temperature in the dark have been trialled for the preservation of CD3, CD4, CD8, CD21 and CD45 expression on canine blood cells (148). Cell counts, blood smears, and flow cytometry analysis were well preserved for 7 days although a small, but significant decrease in relative percentage of lymphocytes was observed on day 7 (148). The expression of CD4, CD8, and CD21 in fixed blood remained comparable to unfixed day 0 blood. A significant decrease in the median fluorescent intensity (MFI) of CD3 and CD45 occurred on day 3 in fixed blood (148). These changes might be due to Cyto-Chex BCT modifying antigenic recognition of some markers in a manner similar to formaldehyde fixation either by reducing expression or altering antigen structure (145, 149). A separate study found a high increase in CD11b expression by unfixed canine neutrophils following collection and short-term storage was prevented by Cyto-Chex preservation (150). This phenomenon has been described in human blood fixed with Cyto-Chex BCT (151).

## 2.2 Objectives

- Establish a viability counting protocol for bovine and ovine leukocytes within whole blood using CyTRAK Orange and DRAQ7.
- Compare the counting accuracy of four types of absolute counting beads with a haematology analyser and determine which bead type is most suitable for each species.
- Evaluate the efficacy of preserving human, bovine, and ovine blood using Streck Cell Preservative with CyTRAK Orange as the measure.

## 2.3 Methods

### 2.3.1 *Blood collection ethics*

#### 2.3.1.1 *Human*

Human peripheral blood was collected from healthy adult volunteers with informed written consent. Blood was collected into either 3.2% sodium citrate or lithium heparin anticoagulant 9 mL Vacuette® tubes (Greiner Bio-One, Stonehouse, UK) (assay dependent). Venesection was performed by trained phlebotomists in the Joint Clinical Research Facility, Institute of Life Science. This study was approved by the Wales Research Ethics Committee 6 (13/WA/0190).

#### 2.3.1.2 *Bovine and ovine abattoir blood*

Fresh, whole bovine or ovine blood was drawn from the throat artery at a local abattoir under veterinary supervision. Blood was gravity-filled directly into a sterilised bottle primed with 14% anticoagulant solution (Citrate Phosphate Dextrose Adenine CPDA-1 Solution and antibiotics (50 mg/L gentamycin and 10 mg/dL antimycotic solution (Sigma-Aldrich, Dorset, UK)).

#### 2.3.1.3 *Ovine venepuncture*

Ovine blood was collected by venepuncture using an 11 G x 44 mm stainless steel needle from live sheep (sourced from Ig-Innovations Ltd, Llandysul, UK, project licence (PPL) number 40/3538). The blood was collected into 14% Citrate Phosphate Dextrose Adenine anticoagulant solution and antibiotics / antimycotics.

### 2.3.2 *Viability Counting Protocol*

#### 2.3.2.1 *CyTRAK Orange staining of leukocytes*

To evaluate whether CyTRAK Orange selectively stains leukocytes, human, bovine, and ovine blood (20 µL) was single- or double-stained with CD45-FITC (20 µg/mL human: ALB 12 Beckman Coulter; 5 µg/mL bovine/ovine: 1.11.32, AbD Serotec, Oxford, UK) according to the manufacturers' instructions. CyTRAK Orange was added (BioStatus, Leicestershire, UK) at a final concentration of 200 µM (1:25 dilution

with FACS buffer: 0.2% bovine serum albumin, 0.05% sodium azide, both Sigma Aldrich, in PBS), vortexed, and incubated in the dark at room temperature for 15 min. Red blood cells were lysed with EasyLyse (1:20 with H<sub>2</sub>O, DAKO supplied by Alere Ltd., Cheshire, UK). Samples were acquired immediately on the Navios for 60 secs (acquisition).

To confirm CyTRAK Orange negative events were non-DNA containing cells, e.g. platelets, human blood was double-stained with CyTRAK Orange and CD41-APC (0.25 µg/mL, clone P2, Beckman Coulter) in the same manner as above.

#### *2.3.2.2 Spectral Properties of DRAQ7 versus conventional viability dyes*

Human blood (100 µL) was single-stained with 5 µL DRAQ7 at a final concentration of 20 µM (stock diluted 1:15 in FACS buffer), 0.1 µg 7-Aminoactinomycin D (eBioscience, Hatfield, UK), or 50 ng Propidium Iodide (PI: stock diluted 1:100 in FACS buffer, Sigma Aldrich) for 15 min at room temperature in the dark. Red blood cells were lysed as described above and then 1% Triton-X-100 (Sigma Aldrich) was added prior to DRAQ7 staining to create a dead cell population after vigorously vortexing.

#### *2.3.2.3 CyTRAK Orange and DRAQ7 in combination with absolute counting beads*

Blood was diluted with PBS to obtain a haematocrit of  $30 \pm 2\%$  to standardise the samples (152) and then 100 µL was reverse pipetted, for enhanced accuracy, into a tube. Blood was single- and double-stained with CyTRAK Orange and/or DRAQ7, and red blood cells lysed as previously. After lysing, one of the following absolute counting bead preparations was reverse pipetted into the samples: 100 µL Cyto-Count™ (DAKO), 50 µL CountBright™, (Life Technologies, Paisley, UK), 50 µL AccuCount Ultra Rainbow Fluorescent Particles or 50 µL AccuCount Rainbow Fluorescent Particles, Low intensity (Ultra Rainbow and Rainbow: Spherotech supplied by Saxon Europe, Bedfordshire, UK). Samples were vortexed before acquisition to suspend beads in solution. 1000 bead events were acquired, and cell counts calculated from equations in the manufacturers' instructions.



### 2.3.3 *Preservation of whole blood with Streck Cell Preservative in vitro*

Blood diluted to a  $30 \pm 2\%$  haematocrit was mixed 1:1 with Streck Cell Preservative (SCP, Streck Laboratories, Omaha, NE, USA) with 1:1 PBS as a control. Samples were mixed thoroughly through inversion and stored at  $+2-8^{\circ}\text{C}$  for 7 days.

### 2.3.4 *Haematology*

Human blood, and animal blood during the DNA dyes work, was measured on the Cell-DYN Ruby clinical haematology analyser. The automatic veterinary haematology analyser, Abacus Jr Vet 5 (Diatron, Hungary), was available for the blood preservation study and used throughout to measure all animal blood samples. Animal blood preserved using SCP were measured in triplicate on the analyser daily for 7 days with corresponding control. Total leukocyte, neutrophil, monocyte, lymphocyte, and platelets were analysed for changes from baseline over time.

### 2.3.5 *Flow cytometry*

Blood sample (20  $\mu\text{L}$ ) was incubated at room temperature for 15 min with CyTRAK Orange (BioStatus, Leicestershire, UK) at a final concentration of 200  $\mu\text{M}$  (1:25 dilution with FACS buffer). Red blood cells were lysed with EasyLyse and the samples run on the Navios flow cytometer on a linear scale with a stopping gate of 10000 CyTRAK Orange positive ( $\text{CyO}^+$ ) events.

### 2.3.6 *Data analysis*

Veterinary haematology data was exported from the Abacus Jr Vet 5 and files converted to readable Excel files using DiatronLab (version 1.73, Diatron, Vienna, Austria). Clinical haematology data was exported from the Cell-DYN Ruby as Excel files. All data was compared to the baseline sample as a fold change and graphs were made in GraphPad Prism 7.02 (GraphPad Software, CA, USA).

Flow cytometry data LMD files were analysed in Kaluza 1.5a (Beckman Coulter).

### 2.3.7 *Statistical analysis*

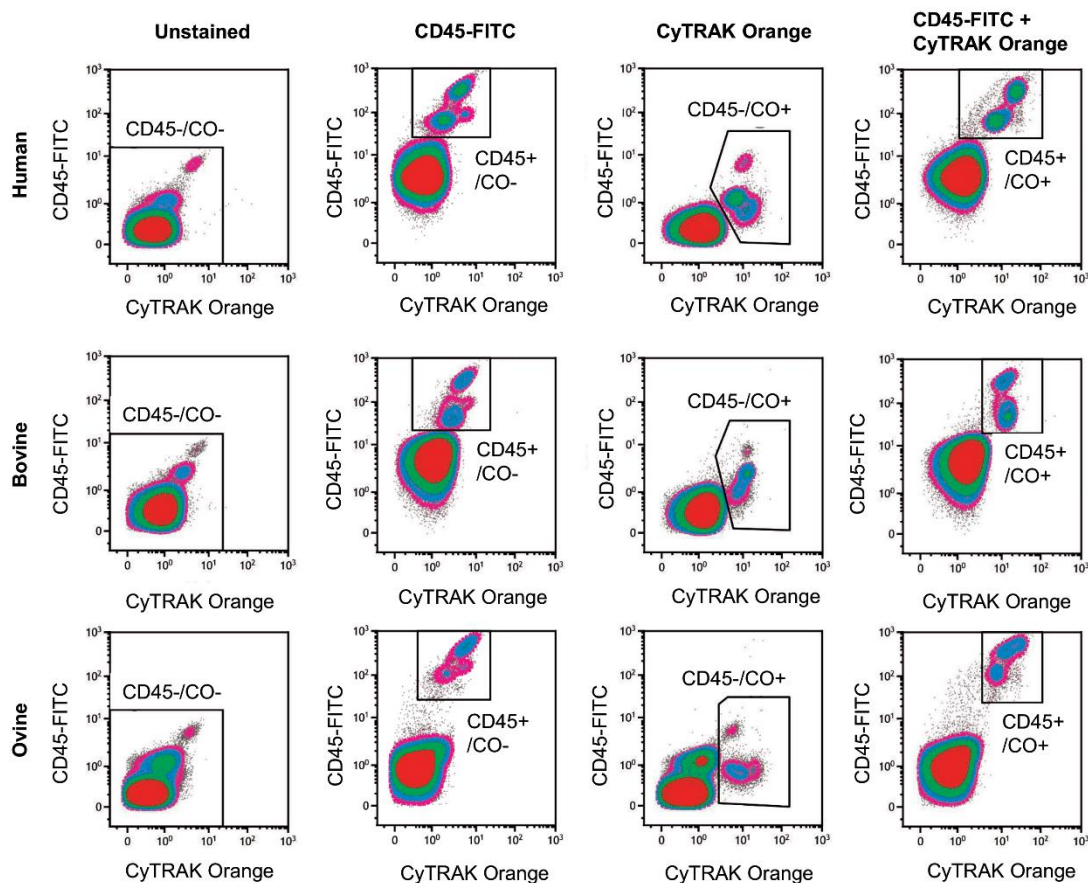
Statistical analysis was performed in GraphPad Prism 7. Repeated measures ANOVA with Sidak *post-hoc* test were used to compare SCP and control samples at each time

point. Dunnett's *post-hoc* test was used to show the effect of time on either SCP or control compared to the baseline sample. A p value of  $< 0.05$  was considered significant.

## 2.4 Results

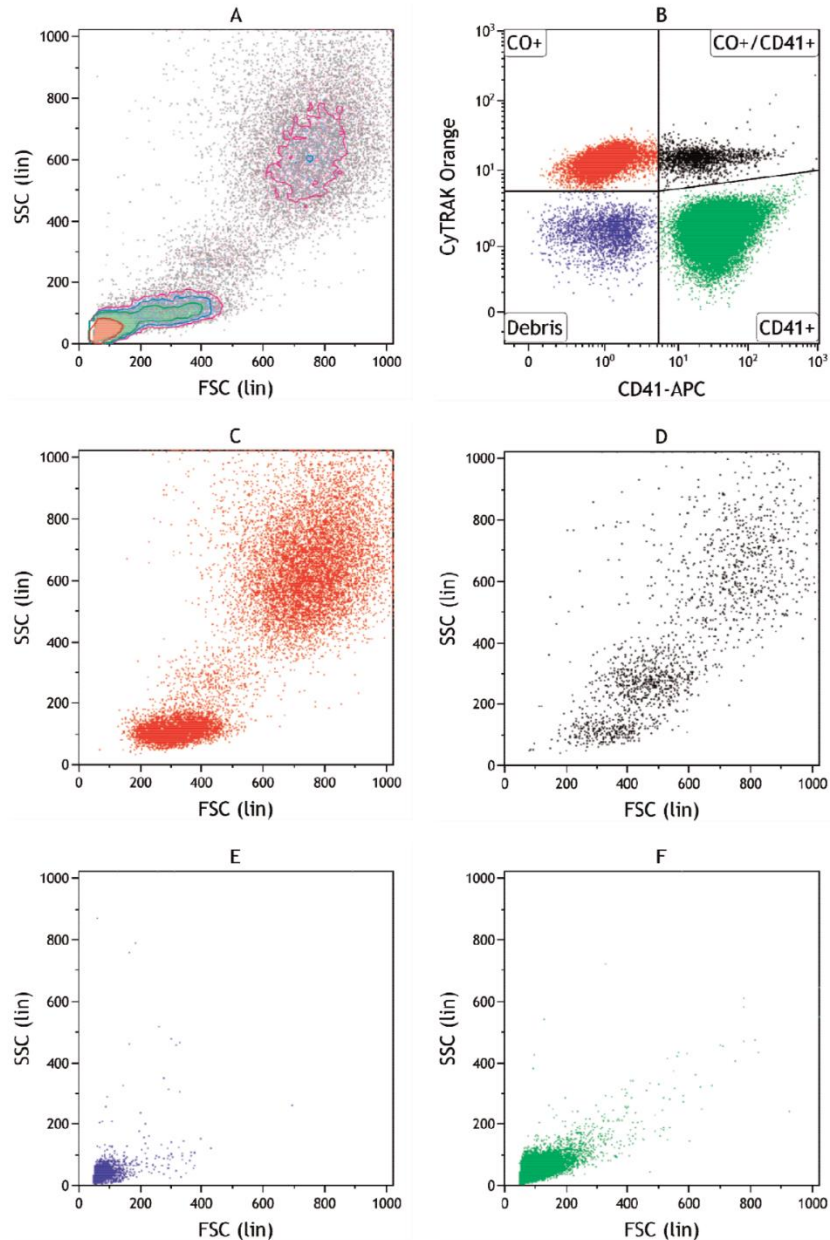
### 2.4.1 CyTRAK Orange selectively stains leukocytes

CD45, also known as the leukocyte common antigen (LCA), is expressed on all leukocytes: granulocytes, monocytes/macrophages, B- and T-lymphocytes (153). CyTRAK Orange specifically stained both human and non-human leukocytes as confirmed by the dual-positive staining for CyTRAK Orange and CD45-FITC (Figure 2.2). CyTRAK Orange negative events were confirmed as platelets, well recognised as DNA free cells (154) which stain positively for CD41-APC in human blood (Figure 2.3).



**Figure 2.2: Comparison of CD45+ staining and CyTRAK Orange staining in three species.**

Human, bovine, and ovine peripheral blood was stained with CD45-FITC, CyTRAK Orange, or both and samples were acquired for 60 secs. Double-stained samples generate a dual positive leukocyte population separated from the negative platelet population.

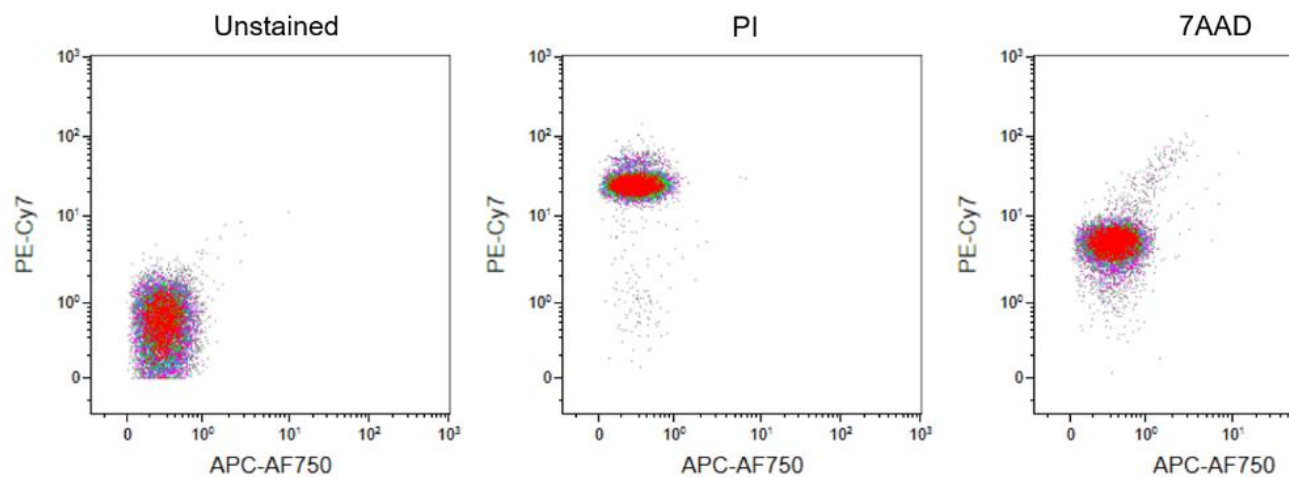


**Figure 2.3: CyTRAK Orange negative events are platelets.**

Whole human blood was double-stained with CyTRAK Orange and CD41-APC, followed by red blood cell lysis and acquisition on the Navios flow cytometer with a 60 s recording gate. **A)** Density contour forward and side scatter plot to show the outline of the various ungated cell populations. **B)** CD41-APC versus CyTRAK Orange dot plot gated for CD41+ platelets, CyTRAK Orange positive leukocytes, double-positive platelet-leukocyte aggregates, and double-negative debris. **C)** CyTRAK Orange positive events fall in the regions of lymphocytes, monocytes, and granulocytes (DNA-containing leukocytes). **D)** Double-positive events fall within the leukocyte regions, but not the platelet region, and are neither unspecific binding of the antibody to leukocytes, nor activated platelets binding to leukocytes. **E)** Double-negative cell debris falls in the region with the lowest forward and side scatter. **F)** CD41+ events fall in the low forward and side scatter region where platelets are to be expected.

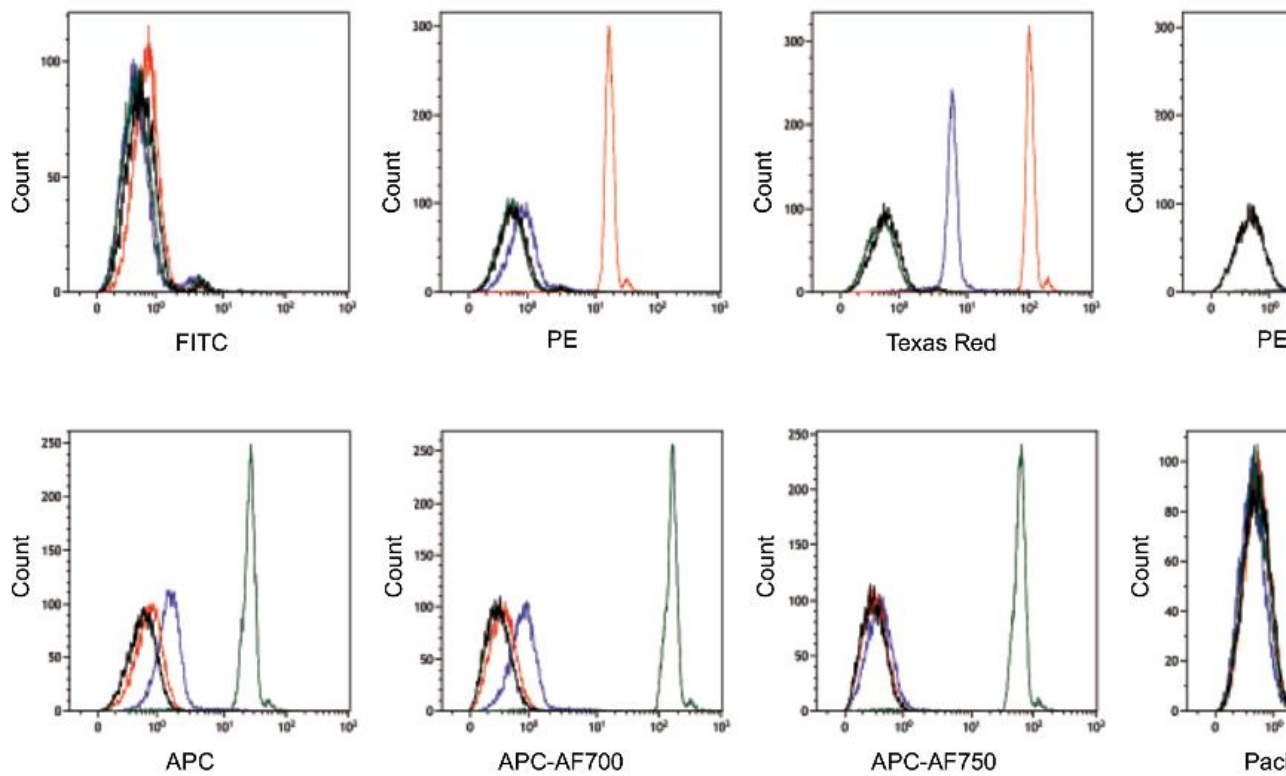
#### 2.4.2 Spectral properties of DRAQ7 versus conventional viability dyes

DRAQ7 stains cells with a compromised membrane induced through the use of the detergent Triton X-100. This allows for DRAQ7 when compared to more conventional dead cells dyes such as 7AAD and PI (Figure 2.5). After excitation by both red and blue laser allows dead cells to be gated as a dual positive population in multi-colour panels.



**Figure 2.4: Staining of human blood with DRAQ7.**

Human whole blood diluted to  $30 \pm 2\%$  haematocrit with PBS, mixed with 1% Triton X-100 to produce dead cells. This was used as a control then stained with PI, 7AAD, and DRAQ7. DRAQ7 shows dual positivity in both red (APC-AF750) and blue (PE-Cy7) channels.



**Figure 2.5: DRAQ7 emission profile compared to 7AAD and PI.**

Whole human blood single-stained with DRAQ7 (green), 7AAD (blue), or PI (red) and treated with 1% EDTA. After red blood cell lysis, the samples were acquired using a three laser Navios and a PMT detector.

### 2.4.3 Counting bead usability and repeatability

The development of a routine analysis method requires ease of use and simplicity to be conducted accurately every time. Therefore, different commercially available counting beads were evaluated. All counting bead standards, apart from Ultra Rainbow, came in a screw top bottle of varying volumes allowing for volume control. Ultra Rainbow beads arrived in a dropper bottle and the manufacturer claimed each drop held a volume of 50  $\mu$ L which is inconvenient should you wish to alter that volume.

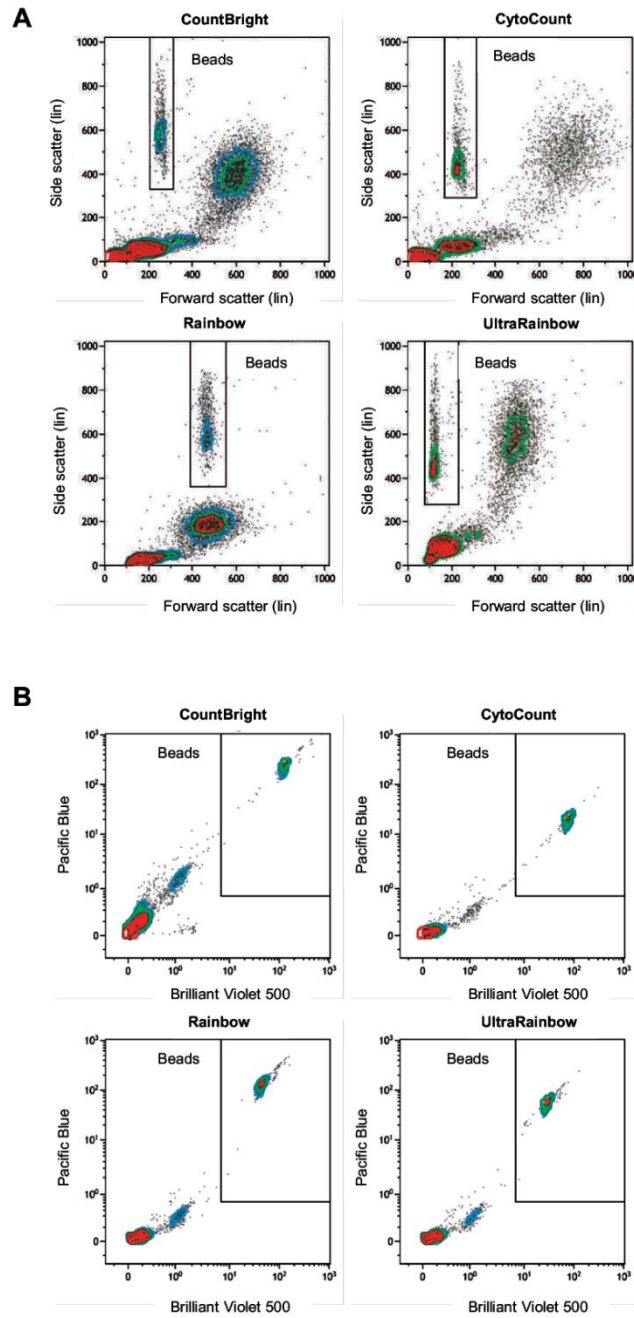
When samples containing the beads were acquired on a FSC versus SSC (Figure 2.6), the size of the Rainbow beads required the voltage settings to be adjusted to the point where the cell population was compressed and individual populations were difficult to discriminate. This is undesirable for routine analysis.

For these reasons, Rainbow and Ultra Rainbow beads were considered for exclusion from the study. To check whether these beads were superior in terms of repeatability before exclusion, CyTRAK Orange and DRAQ7 double-stained samples were tested in triplicate and the %CV obtained for all bead standards (Table 2.1). Rainbow and Ultra Rainbow were not superior in any of the species tested.

**Table 2.1: Coefficient of variance (%CV) for different cell counting bead types and species.**

Variation in counts yielded upon sample acquisition were calculated as average coefficient of variance (%CV) calculated from triplicate samples for human/bovine/ovine total leukocytes for different beads analysed using the Navios. Human samples: CytoCount and CountBright: n=2, Rainbow and Ultra Rainbow: n=1; bovine samples: CytoCount and CountBright: n=3, Rainbow and Ultra Rainbow: n=2. Ovine samples: n=3 for all bead types.

<b>Species</b>	<b>CountBright</b>	<b>CytoCount</b>	<b>Rainbow</b>	<b>Ultra Rainbow</b>
<b>Human</b>	4.1	1.5	17.7	9.3
<b>Bovine</b>	5.1	1.6	3.2	10.4
<b>Ovine</b>	7.2	4.9	6.7	11.1



**Figure 2.6: Scatter and emission profile of various counting bead standards.**

Whole bovine blood diluted to a haematocrit of  $30 \pm 2\%$  with PBS and red blood cells lysed before mixing with: CountBright, CytoCount, Rainbow, or Ultra Rainbow cell counting beads and acquired on the Navios flow cytometer. **A)** Density plot of forward scatter (FSC) against side scatter (SSC), both on linear axes. Each bead standard required a different FSC and SSC voltage thus changing the profile of the scatter. **B)** Contour density plot of the violet 550/40 (Brilliant Violet 500) detector against the 450/50 (Pacific Blue) detector, both on biexponential (logicle) axes. Bead standards can be distinguished easily from cellular and debris events.



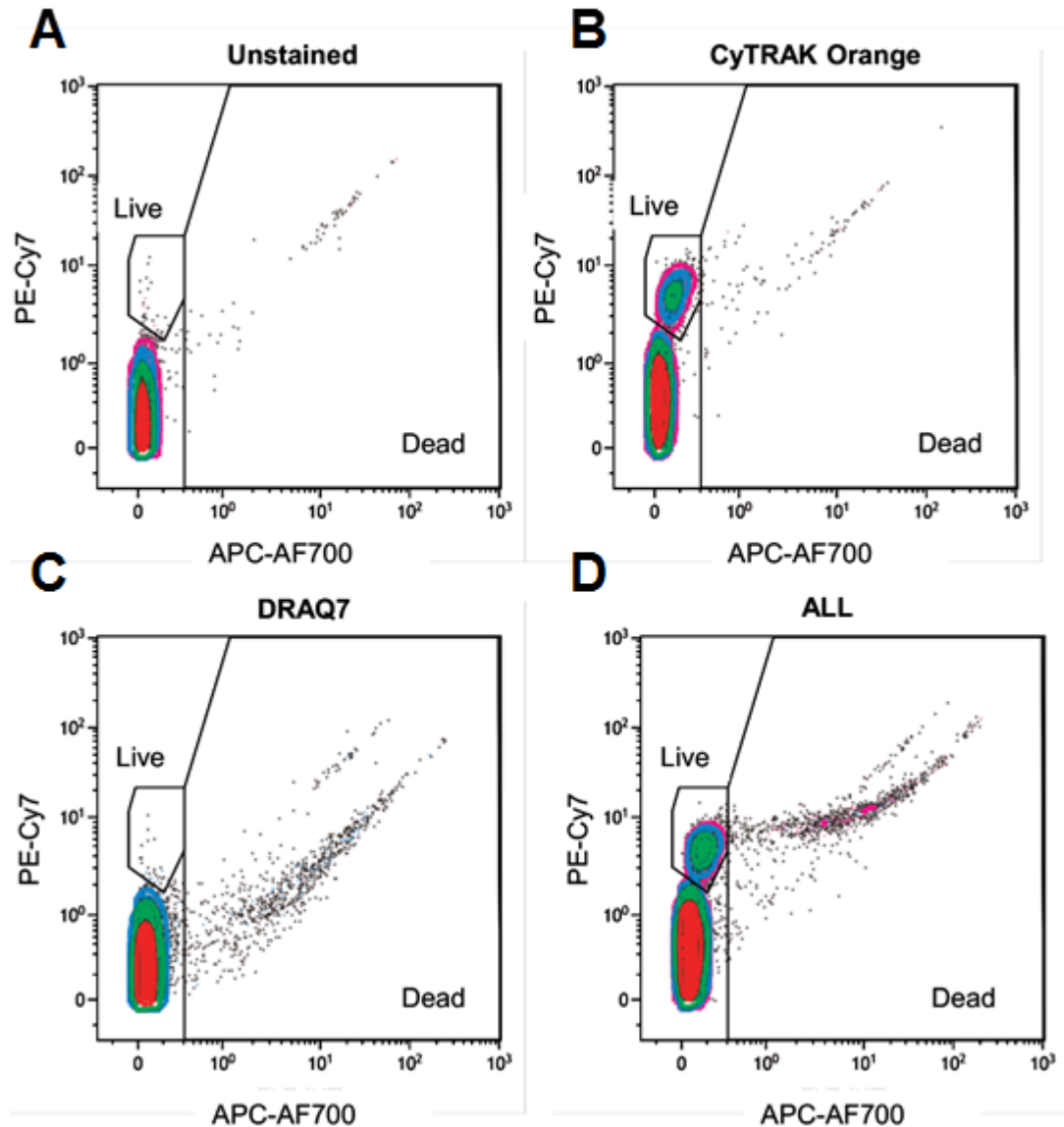
#### 2.4.4 Viability counts using CyTRAK Orange, DRAQ7, and absolute counting beads

The first gating step was to ensure that the bead standards did not interfere with the cell events. Beads were gated on a plot of the violet 550/40 detector (Brilliant Violet 500) against the 450/50 detector (Pacific Blue) on biexponential axes (logicles) (Figure 2.6B). Bead events were excluded from subsequent gating steps using a Boolean gate called “Cells” created using the rule (NOT “Beads”). The remaining events were displayed on a red laser detector (725/20: DRAQ7) versus a blue laser detector (695/30: CyTRAK Orange) density contour plot using logicle axes. This enables simultaneous detection of live (CyTRAK Orange) and dead (DRAQ7) events (Figure 2.7).

1000 bead events were acquired and the absolute count of live and dead cells in both single- and double-stained samples were calculated using the equations in the manufacturer’s instructions and accounting for blood dilution.

#### Equation 2.1: Equations for the calculation of cell counts for each bead type

<p><b>CountBright</b></p> $A/B \times C/D = \text{concentration (cells}/\mu\text{L)}$ <p>Where:</p> <ul style="list-style-type: none"> <li>A = number of cell events</li> <li>B = number of bead events</li> <li>C = assigned bead count of the lot (beads/50 <math>\mu\text{L}</math>)</li> <li>D = volume of sample (<math>\mu\text{L}</math>)</li> </ul>	<p><b>CytoCount</b></p> $A/B \times C \times Dil = \text{concentration (cells}/\mu\text{L)}$ <p>Where:</p> <ul style="list-style-type: none"> <li>A = number of cell events</li> <li>B = number of bead events</li> <li>C = CytoCount™ concentration (beads/<math>\mu\text{L}</math>)</li> <li>Dil = dilution factor of original sample</li> </ul>
<p><b>Rainbow</b></p> $A/B \times C/D = \text{concentration (cells}/\mu\text{L)}$ <p>Where:</p> <ul style="list-style-type: none"> <li>A = number of cell events</li> <li>B = number of bead events</li> <li>C = assigned bead count of the lot (beads/50 <math>\mu\text{L}</math>)</li> <li>D = volume of sample (<math>\mu\text{L}</math>)</li> </ul>	<p><b>UltraRainbow</b></p> $A/B \times C/D = \text{concentration (cells}/\mu\text{L)}$ <p>Where:</p> <ul style="list-style-type: none"> <li>A = number of cell events</li> <li>B = number of bead events</li> <li>C = assigned bead count of the lot (beads/50 <math>\mu\text{L}</math>)</li> <li>D = volume of sample (<math>\mu\text{L}</math>)</li> </ul>



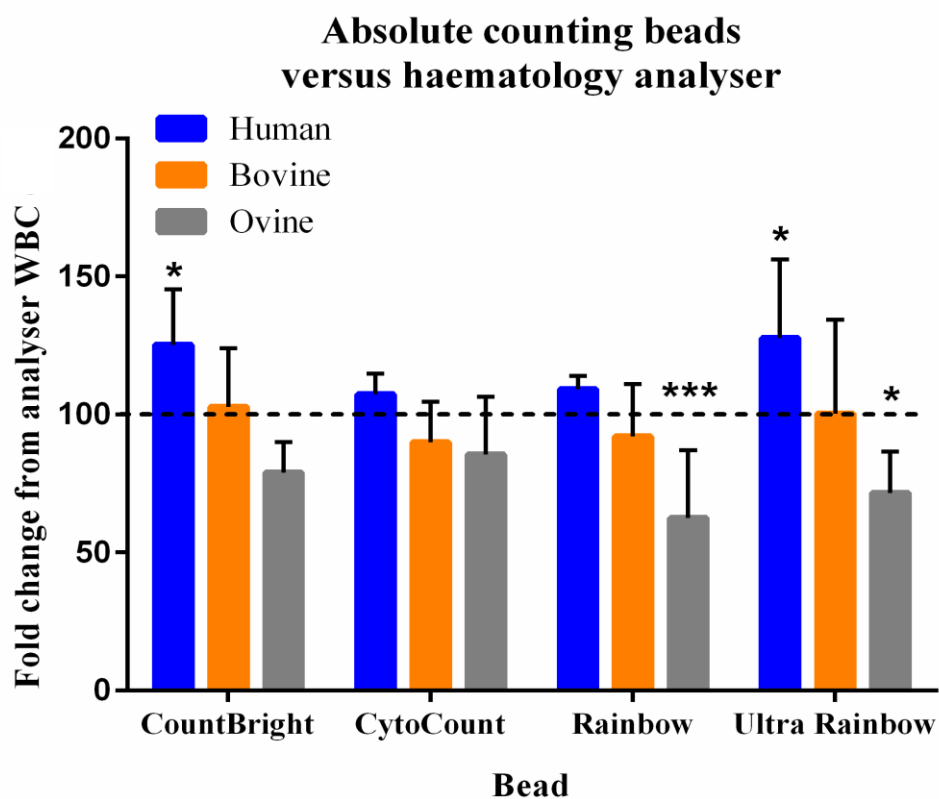
**Figure 2.7: CyTRAK Orange and DRAQ7 gating strategy.**

Whole bovine blood was diluted to haematocrit of  $30 \pm 2\%$  with PBS and red blood cells lysed before staining with either CyTRAK Orange, DRAQ7 or both then mixed with CytoCount beads and acquired on the Navios flow cytometer. Gating strategy: all counting bead standards were first gated based on their dual positivity in the two violet laser detectors (not shown) and then excluded from subsequent steps using Boolean gating (Cells = NOT Beads). “Cells” were displayed on density contour plots using the red laser (725/20: Alexa Fluor 700 or equivalent) detector on the x-axis and the blue laser (695/30: PE-Cy7 or equivalent) detector on the y-axis, both biexponential (logicle). Live and Dead gates were drawn using **A**) unstained, **B**) CyTRAK Orange single-stained, **C**) DRAQ7 single-stained, and **D**) double-stained samples. Event counts were obtained from the gates and inserted into the respective counting bead equations to obtain cell concentrations.

## 2.4.5 Efficiency of viability protocol in human, bovine, and ovine

### 2.4.5.1 Absolute counting beads versus haematology analyser

To evaluate the efficacy of the viability protocol and its superiority to the human haematology analyser (when a veterinary haematology analyser is unavailable), the total leukocyte count from the analyser was compared to the number of live and dead cells combined in the double-stained tube (Figure 2.8).



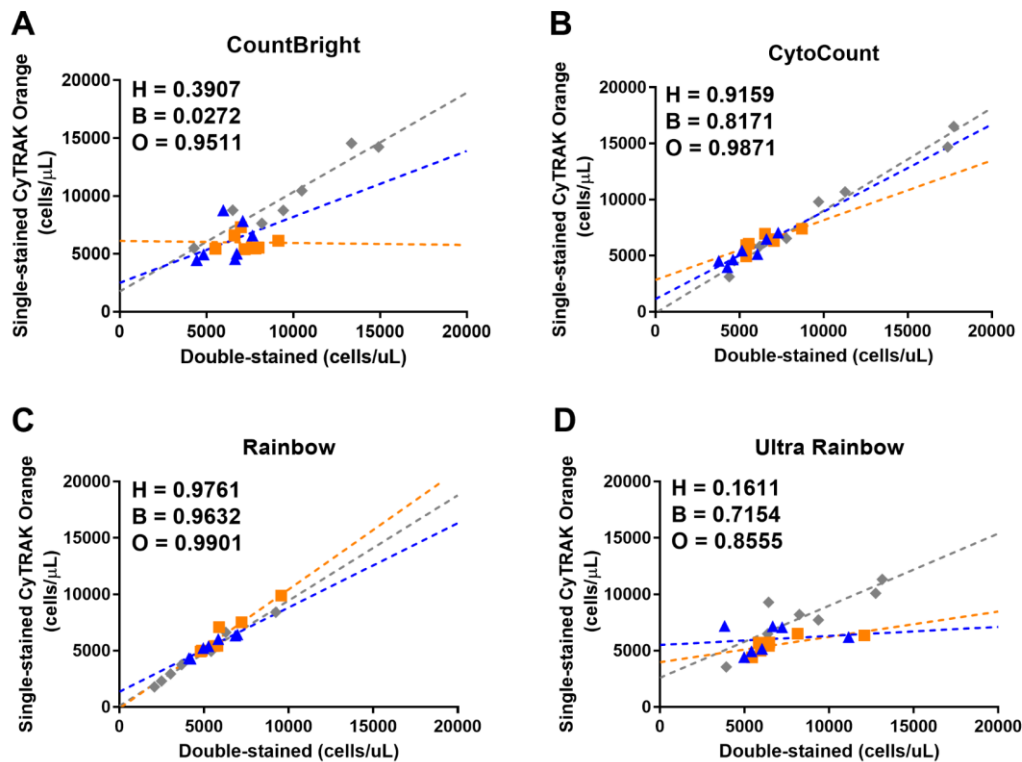
**Figure 2.8: Absolute counting beads versus haematology analyser for human, bovine, and ovine.**

Total number of live and dead cells in the double-stained tube as calculated using the bead equation was compared as a fold change to the total leukocyte count from the haematology analyser (Mean + SD, n = 7). A two-way ANOVA was used to compare analyser to bead count in each bead type and species (\* =  $p \leq 0.05$ , \*\* =  $p \leq 0.01$ , \*\*\* =  $p \leq 0.001$ ).

Two-way ANOVA revealed significant differences between the total cell count calculated by the beads and that of the analyser observed in: human CountBright ( $p = 0.035$ ); human Rainbow ( $p = 0.018$ ); ovine Rainbow ( $p = 0.0008$ ); and ovine UltraRainbow ( $p = 0.015$ ).

#### *2.4.5.2 Correlation between single- and double- stained blood*

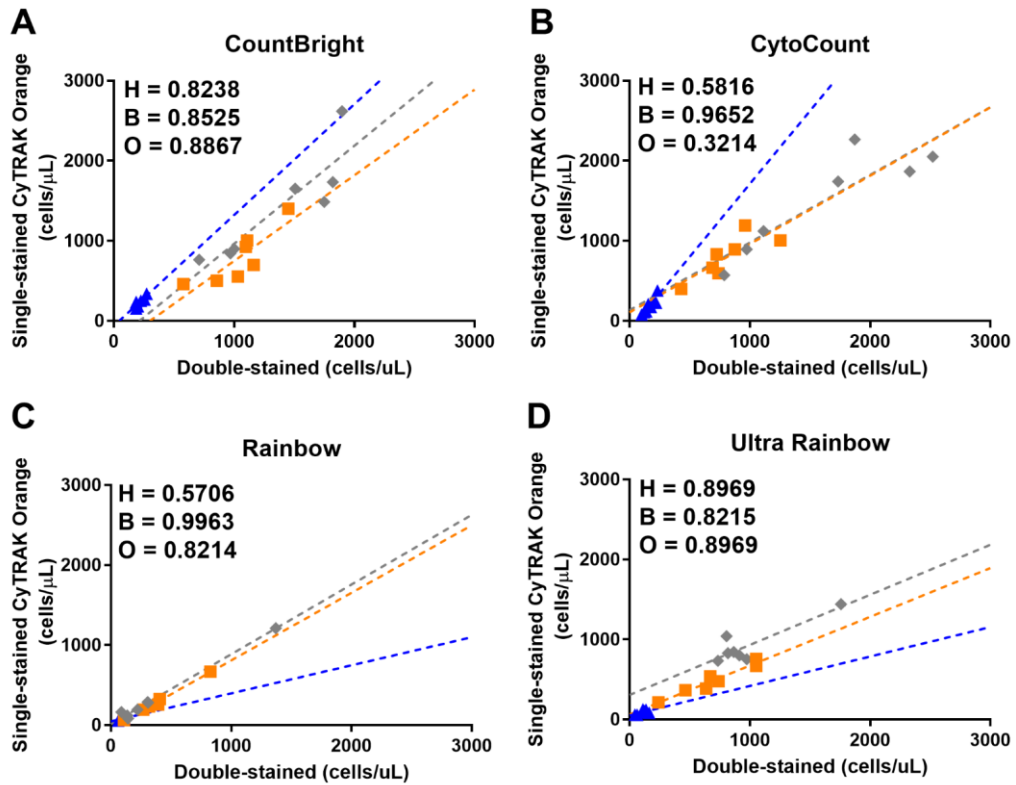
To ensure that CyTRAK Orange and DRAQ7 could be used together to effectively enumerate leukocytes, the single-stained cell count was compared to the double-stained live and dead cell count using all bead types for each species. Correlation between single-stained CyTRAK Orange blood and the live cell count in the double-stained tubes were compared (Figure 2.9). DRAQ7 single-stained blood was also compared to the dead cell count in the double-stained tube (Figure 2.10).



**Figure 2.9: Live cell count correlation between single- and double-stained blood for each bead/species.**

Diluted human (blue), bovine (orange), and ovine (grey) blood was single-stained with CyTRAK Orange or double-stained with CyTRAK Orange and DRAQ7. Absolute cell counts for CyTRAK Orange positive cells from each tube were compared for each bead type and species ( $n = 7$ ). All samples followed Gaussian distribution and Pearson  $r$  correlation was calculated.

The Rainbow beads gave the best correlation between single-stained CyTRAK Orange and the live cell count in the double-stained tube for all species with a Pearson  $r > 0.96$  (Figure 2.9C). However, considering the Rainbow and Ultra-Rainbow beads were considered for exclusion, the second-best beads for each species were CytoCount for human and bovine (Pearson  $r = 0.9159$  and  $0.8171$  respectively; Figure 2.9B), and CountBright for ovine (Pearson  $r = 0.9511$ ; Figure 2.9A).



**Figure 2.10: Dead cell count correlation between single- and double-stained blood for each bead/species.**

Diluted human (blue), bovine (orange), and ovine (grey) blood was single-stained with CyTRAK Orange or double-stained with CyTRAK Orange and DRAQ7. Absolute cell counts for DRAQ7 positive cells from each tube were compared for each bead type and species ( $n = 7$ ). Pearson  $r$  correlation was calculated for normally distributed samples, Spearman's for non-normally distributed (marked with \*).

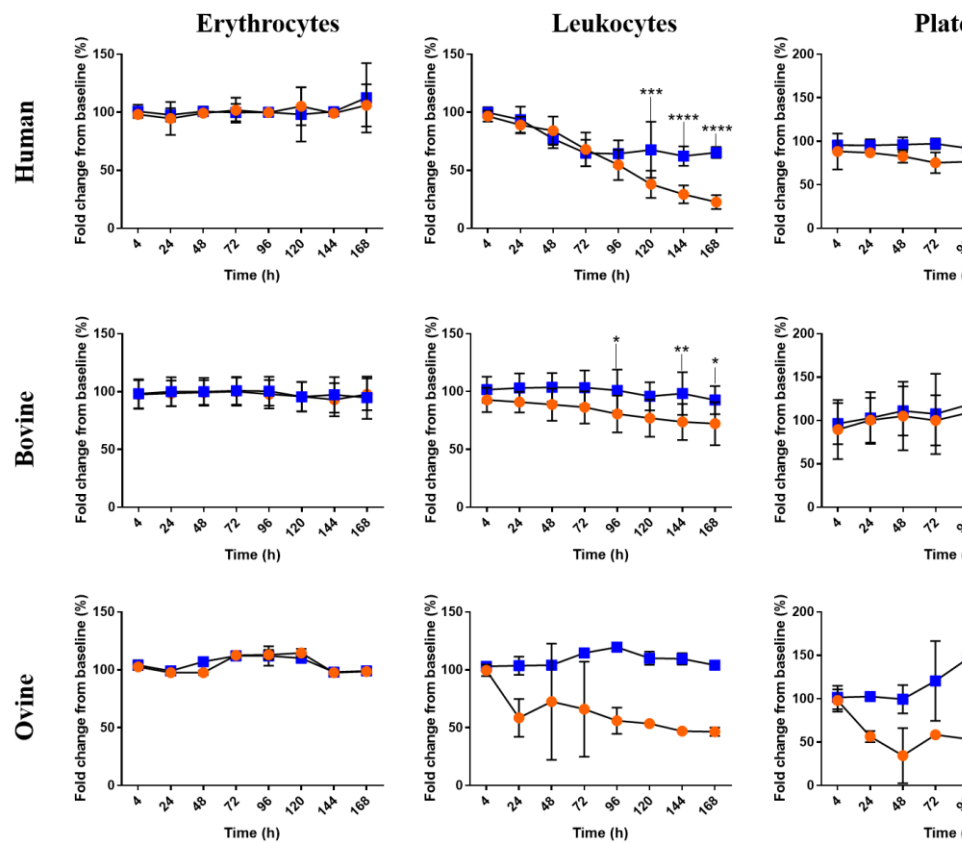
Dead cell counts between the single- and double-stained tubes correlated better for each bead type than the live cell counts. Rainbow beads correlated best for bovine (Pearson  $r = 0.9953$ ; Figure 2.10C), but second best was CountBright (Pearson  $r = 0.8525$ ; Figure 2.10A). CytoCount correlated best for human and ovine dead cells (Pearson  $r = 0.8969$  for both; Figure 2.10B). These results show that there are different optimal bead/species combinations, however, if only one bead option were available, CytoCount would be the best choice.

## *2.4.6 Streck Cell Preservative in vitro*

The DNA dyes work involved the use of ovine blood from the abattoir. It was later found that ovine abattoir blood is not suitable as stress and death triggers mechanically young erythrocytes to be released from the sheep spleen, resulting in poor quality blood (156). A source of ovine venepuncture blood was found for the blood preservation work as it is better quality and comparable to the future preclinical MiniVAD trials (Chapter 5 - VADs: From bench to bedside).

### *2.4.6.1 Haematology*

To monitor the effectiveness of SCP as a preservative for leukocytes, cell counts were measured daily on a haematology analyser and compared to the baseline (diluted blood at time 0) counts as a fold change.

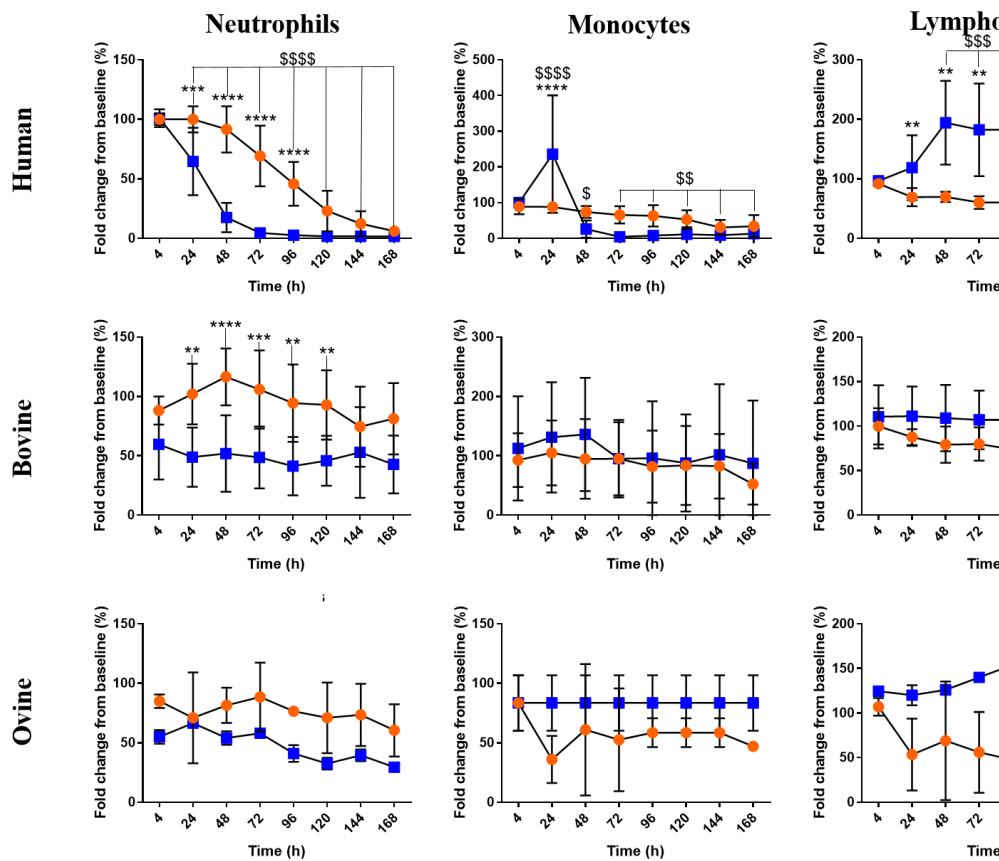


**Figure 2.11: Erythrocyte, leukocyte, and platelet count**

Human (n = 6), bovine (n = 8), or ovine (n = 2) blood was preserved 1:1 in SCP (blue squares) w control (orange circles). Samples were read on the appropriate analyser in triplicate every day for 7 fold change to the baseline. ‘\*’ = Significance between Streck and control; ‘\$’ = significance of Stre



Due to lack of resources and a clotted sample, only data from two sheep were available and no statistics could be calculated. Erythrocyte counts for both control and SCP blood remained stable in all species as did the platelet counts (excluding ovine for lack of data). However, SCP is designed to preserve leukocytes, and this is where species differences in counts were noticeable. Bovine and ovine preserved leukocytes remained stable over the 7-day period, whereas human leukocytes progressively declined for 72 hours before reaching a plateau (Figure 2.11). The reason for this progressive decline can be seen when considering the human leukocyte subsets (Figure 2.12). After 24 hours, the SCP neutrophil count is significantly different from baseline ( $p < 0.0001$ ) and continually declines thereafter. The monocyte count in SCP human blood is also significantly reduced at 48 hours ( $p = 0.03$ ) and onwards whereas the lymphocyte count increases from 48 hours onwards ( $p = 0.002$ ).



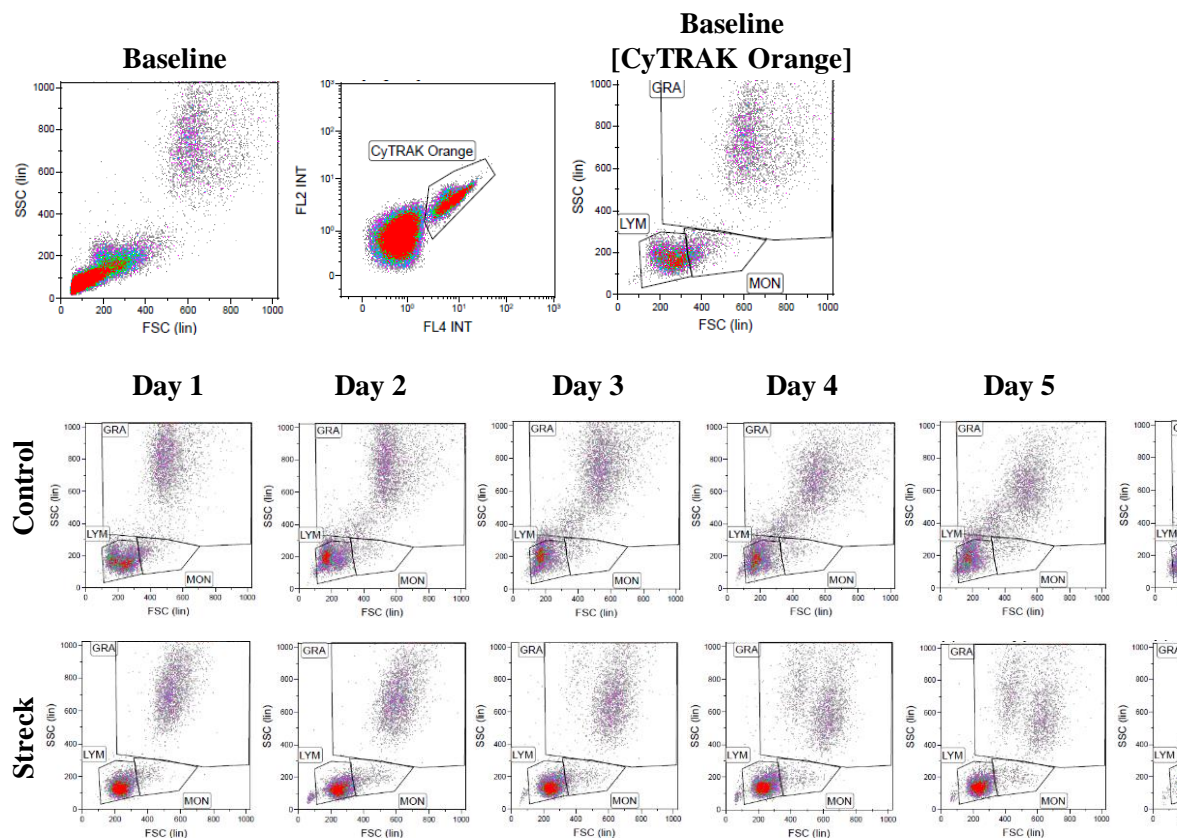
**Figure 2.12: Leukocyte differential cell counts.**

Human (n = 6), bovine (n = 8), or ovine (n = 2) blood was preserved 1:1 in SCP (blue squares) with blood (orange circles). Samples were read on the appropriate analyser in triplicate every day for 7 days and the results were compared to the baseline. ‘\*’ = Significance between Streck and control; ‘\$’ = significance of Streck compared to the baseline.

It appears that SCP is better at preserving bovine and ovine blood which may in part be due to the ratio of non-granular lymphocytes which is higher than in human (157). Neutrophils are the most abundant subset in humans (158) and fixing of these cells is different due to the granularity (146, 159). The fixing process alters the scatter characteristics of neutrophils and may be 'seen' by the haematology analyser as lymphocytes (due to the increase in the human lymphocyte population).

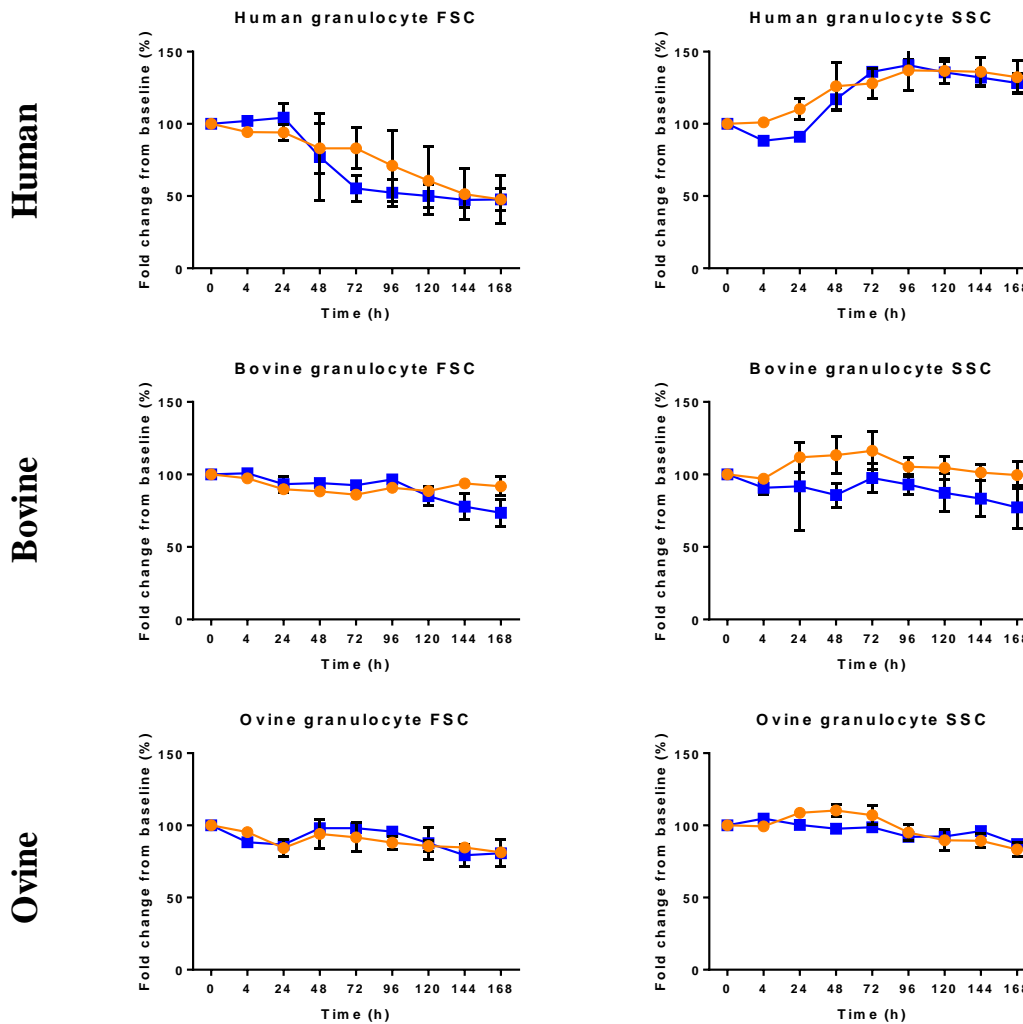
#### *2.4.6.2 Flow Cytometry*

To use the assays developed in-house, preserved blood must be flow cytometry compatible. Therefore, FSC and SSC of CyTRAK Orange stained leukocytes was measured over 7 days in preserved and control blood.



**Figure 2.13: Forward- vs side-scatter of CyTRAK Orange positive leukocytes over time in Streck**  
 Diluted ovine blood mixed 1:1 with Streck Cell Preservative or PBS as a control was stored at +2-8°C, red blood cells lysed, and then 10000 CyTRAK Orange positive (CyO<sup>+</sup>) events recorded every day for 5 days. Leukocytes were identified on a FL2 vs FL4 plot and then displayed on a FSC versus SSC plot.

In blood preserved in SCP, the FSC/SSC characteristics of the granulocytes change over time with a noticeable splitting of the population (Figure 2.13). This is the likely reason why there is a large decrease in the number of neutrophils recorded on the haematology analysers (Figure 2.12). This is particularly noticeable in human samples where there is a sharp drop in FSC and increase in SSC in the SCP samples (Figure 2.14) and is less apparent in bovine and ovine samples.



**Figure 2.14: Change in forward and side scatter of granulocytes for each species over time.**

The X-median (FSC) and Y-median (SSC) of the granulocyte population plotted as a fold change from baseline over time for human, bovine, and ovine blood preserved in SCP (blue squares) or control PBS (orange circles).

## 2.5 Discussion

The purpose of the work in this chapter was to develop assays which would improve the analysis opportunities for non-human leukocytes while always enabling their comparisons to human leukocytes throughout *in vitro*, *in vivo*, and clinical studies for LVADs. The study has shown that CyTRAK Orange and DRAQ7 can be used in combination for a quick, simple, flow cytometric viability assay for assessing the leukocytes of multiple species relevant to LVAD testing. Furthermore, these DNA dyes can be used in conjunction with absolute count beads to accurately count the number of live and dead leukocytes, something that is not possible when using only haematology analysers (160).

CyTRAK Orange has been shown to only stain leukocytes with CyTRAK Orange negative events confirmed as being CD41 positive platelets in human blood. The advantage of using CyTRAK Orange to identify leukocytes is the ability to stain the leukocytes of multiple species without the need for the purchase of costly CD45-antibodies, a pan-leukocyte marker. Other dyes which could have been used instead include the Vybrant Dye-cycle dyes (Violet, Orange, Green), the SYTO 59-64 dyes, LDS 751, and Hoechst 33342 (160). However, these dyes have a relatively short stability (6-12 months), require storage at -20°C, longer incubation times (except Hoechst 33342), and Vybrant Dye-cycle dyes require incubation before and after staining at +37°C. CyTRAK Orange is supplied ready to use with a long shelf life if kept at +2-8°C, stains cells within 15 min, and is compatible with parallel antibody staining as there is no need for incubation at higher temperatures.

DRAQ7 was chosen for this study as it has desirable spectral characteristics in comparison to more traditional viability dyes such as 7AAD and Propidium Iodide (PI). Its dual laser excitation and far-red emission result in double positive dead cell populations, freeing detectors otherwise occupied by the likes of 7AAD and PI (PE and APC respectively). This makes DRAQ7 more suitable for multi-colour panels, particularly for those developed for large animal species where antibodies are often only available in PE, FITC, or APC fluorochromes.

CyTRAK Orange and DRAQ7 were combined with absolute count beads to create a simple viability assay. Four varieties of counting beads, CountBright, CytoCount,

Rainbow, and Ultra-Rainbow, were tested to assess which would be the best. Firstly, due to the need to scale down blood volumes, Ultra-Rainbow were ultimately excluded due to their dropper bottle presentation which allowed only a drop of 50  $\mu$ L used. Secondly, Rainbow beads were also ultimately excluded due to their size/side scatter characteristics which meant dramatic changes in SSC voltage were required to visualise both beads and cells on the same dot plot causing compression of the cell population making it difficult to discriminate individual populations by their scatter characteristics. With only two bead varieties left, CountBright and CytoCount, the best choice would appear to be CytoCount as the repeatability, forward-vs side-scatter, single- and double-staining correlation in all species were superior.

Use of the developed viability assay has proved useful on live blood cells. However, *in vivo* and clinical studies are often outsourced to specialist potentially far-flung facilities and assay variability linked to the use of different machines and operators can hamper data analysis. To overcome this problem, blood fixatives have been developed to enable preservation of blood for up to a week providing time for transportation of blood to a single site (144, 147). SCP has been shown to successfully preserve human, bovine, and ovine blood for up to 7 days. Despite this success, the haematology analysers have difficulty in identifying individual leukocyte populations in preserved blood, most notably in human neutrophils. This may be due to the ‘splitting’ (by FSC) of the granulocyte population over time in the SCP samples which can be observed by flow cytometry. It has been suggested that this is caused by the rearrangement of and differing fixation time of granules which does not affect non-granular cells such as monocytes and lymphocytes (146, 159).

Despite the altered FSC profile of granulocytes, SCP preserves blood well. CyTRAK Orange can stain fixed leukocytes which allows use of this dye for analysis. The use of CyTRAK Orange and absolute count beads could be used to accurately count leukocyte populations where the haematology analysers cannot. In contrast, DRAQ7 is not a fixable viability dye and would need to be replaced with others such as VivaFix™ (Bio-Rad, CA, USA) or Zombie Fixable Viability dyes (BioLegend, London, UK), if viability measures were required.

## 2.6 Conclusion

CyTRAK Orange can be used to identify total leukocytes in fixed and unfixed human, bovine, and ovine blood samples. In unfixed blood, CyTRAK Orange can be used with DRAQ7 to provide a viability assessment in human and bovine blood, although ovine abattoir blood does not work as well. The use of ovine blood from the abattoir has been replaced by a source of ovine venepuncture since for any testing due the poor cell viability and high levels of haemolysis caused by the contracting spleen in times of stress (156). In combination with absolute count beads such as CountBright and CytoCount, concentration and viability analysis of leukocytes can be conducted. In fixed blood, CyTRAK Orange and count beads could be used to more accurately count leukocyte subsets in comparison with haematology analysers which struggle to identify populations due to alterations in size and shape. With the addition of antibodies, these DNA dyes and beads offer an excellent methodology for the analysis of leukocytes during the testing of blood-handling devices such as LVADs from bench to bed-side.



# Chapter 3 Biomaterials: Foreign surface blood interactions

## 3.1 Introduction

### *3.1.1 Definition of a biomaterial*

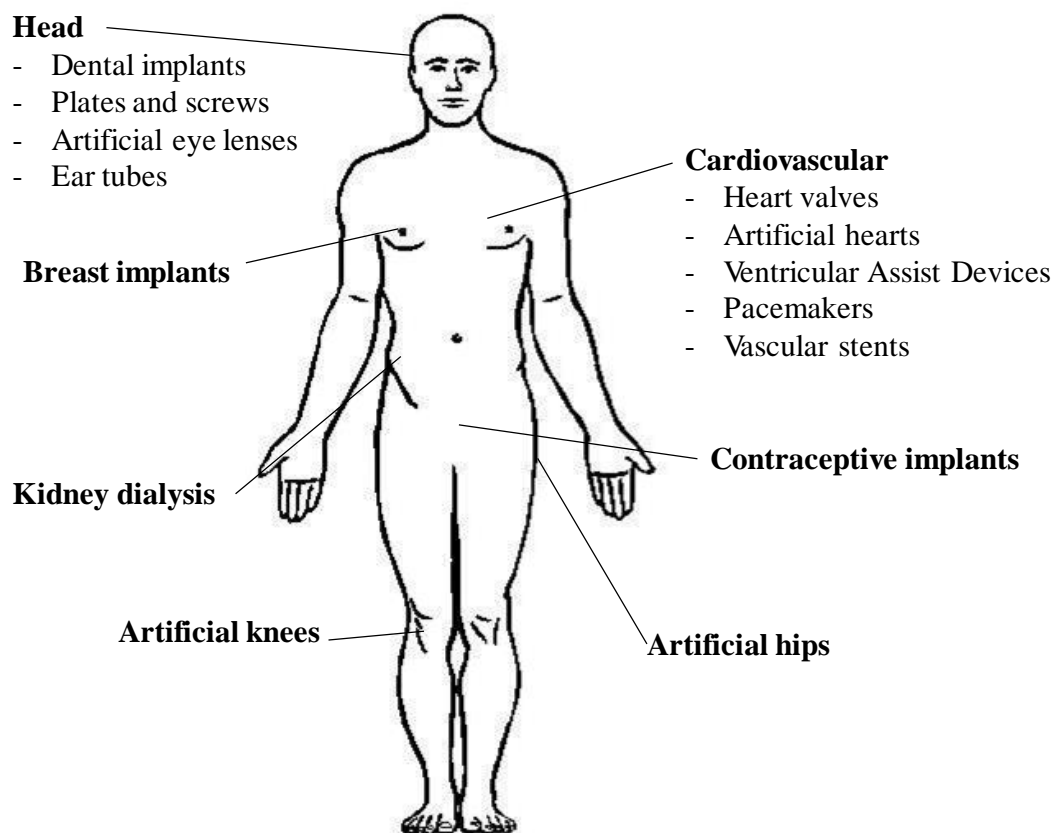
The International Union of Pure and Applied Chemistry (IUPAC) defines a biomaterial as ‘a material exploited in contact with living tissues, organisms, or microorganisms’ (161). A biomaterial can be derived from natural or synthetic sources utilising a variety of chemical approaches involving metallic components, polymers, ceramics, or composite materials. They are often used or adapted for medical purposes and become part of the living structure or function as a biomedical device. Often devices are made from multiple materials that can affect the immune response or tissue integration differently. First and foremost, the choice of biomaterial is based on its acceptability by the human body. It should not cause allergy, inflammation, nor toxicity immediately or post-operatively and can last until death. Success of the biomaterial implant is based on its properties, biocompatibility, and the health of the recipient (162).

### *3.1.2 History of biomaterials*

Throughout history, humans have used the world around them to solve problems such as creating weapons for more efficient hunting, using fire to cook, making shelter from trees, and unsurprisingly, using it to fix their bodies. Dental implants from as early as 600 AD have been found from Mayan people who fashioned teeth from shells (163), and in 200 AD, the Romans in France used iron with some success (164). The first reporting to assess *in vivo* biocompatibility was performed in dogs using gold, silver, lead, and platinum by H. S. Levert in 1829 (165). By the early 20<sup>th</sup> century, surgeons and doctors were turning increasingly to metals, ceramics and, post-World War One, plastics, in order to save their patients with little restriction on such experimental trials (166). Nevertheless, the actions of these surgeons led to a surge in the use of materials to repair the body.

In 1949, Sir Harold Ridley was the first to implant intraocular lenses made from Perspex® poly(methyl methacrylate) and changed the course of history by improving the quality of life for millions of cataract sufferers (167). Major advances in kidney dialysis were accomplished by the creation of the Quinton-Scribner shunt made from Dacron®, Teflon, and silicone (168). In 1964, the National Heart and Lung Institute of the NIH aimed to have a total artificial heart available by 1970. By 1966, Dr Michael DeBakey had implanted a left ventricular assist device, and in 1969 Dr Denton Cooley and Dr William Hall implanted a polyurethane total artificial heart (169).

### 3.1.3 Biomaterial applications



**Figure 3.1: Types of medical implant**

Implants, prostheses, and devices are manufactured from a wide variety of materials including polymers, metals, ceramics, and their composites (170). Some examples of synthetic biomedical materials include (170):

- Polymeric: silicone, polymethylmethacrylate-late (PMMA), polyethyletherketone (PEEK), polyurethane (PU).

- Metallic: stainless steel, titanium and its alloys, gold, platinum, silver, cobalt-chromium based alloys.
- Ceramic: alumina ( $\text{Al}_2\text{O}_3$ ), carbon, zirconia ( $\text{ZrO}_2$ ), hydroxyapatite ( $\text{Ca}_{10}(\text{PO}_4)_6(\text{OH})_2$ ).

These materials are used in an extensive list of applications such as joint replacements, bone plates, artificial ligaments/tendons, dental implants, sutures/clips/staples, contact lenses, heart valves, blood vessel prostheses, stents and grafts, and as drug delivery systems.

### *3.1.4 Foreign body reaction to biomaterials*

Despite their extensive use in medicine, biocompatibility of biomaterials is relatively poorly understood. When a biomaterial is implanted into the body, no matter how biocompatible the material is deemed it is considered foreign by the body. The function of the immune system is to react and remove this ‘foreign body’ from the host. The nature of this response is highly dependent on the characteristics of the material and its interaction with its environment.

#### *3.1.4.1 Protein adsorption*

The first biological matter a device will encounter is protein. Protein adsorption is a complex process driven by forces such as van der Waals, hydrophobic, and electrostatic interactions between the protein and the surface of the implant (171). Initially, the protein must overcome repulsive forces before it can adsorb. This is achieved by a conformational change to provide the entropy required to overcome electrostatic repulsion (170, 171). External parameters can influence the efficacy of protein adsorption: an increase in temperature provides proteins with more energy to diffuse towards the material, whereas pH governs the electrostatic state of protein and proteins-surfaces of opposite charges accelerate the migration of proteins to the surface (171).

Protein adsorption is important for cell/bacterial adhesion, reaction to tissue implants, inflammation, infection, tissue healing, and coagulation (172). The accumulation of these proteins turns an ‘inert’ biomaterial into a biologically active surface (173).

#### 3.1.4.2 Cellular activation

The matrix which is formed by plasma proteins on the surface of the biomaterial activates platelets and leukocytes in a composition dependent fashion (172, 174-177). The composition of the protein matrix adsorbed onto the material is highly variable but consists largely of the most abundant proteins in the blood: fibrinogen, albumin, and globulins. Platelet activation occurs through interaction with fibrinogen in particular leading to platelet-platelet aggregation (178). These immobilised platelets are then able to recruit and activate blood-borne leukocytes, mainly neutrophils and monocytes, which contribute to the building of thrombus through adhesion whilst also releasing cytokines for further recruitment to the site (179). Activation of blood cells can occur very quickly in response to biomaterials with intracellular calcium flux in T cells within 2 minutes (180), platelets present on the surface within 10 minutes, and up-regulation of CD11b on granulocytes observed as early as 30 minutes (174). Adherence and activation of leukocytes and platelets are well described for several commonly used biomaterials such as titanium, low density polyethylene (LDPE), Pellethane®, and polytetrafluoroethylene (PTFE) using *in vitro* models. This evidence is provided by changes in the expression of adhesion molecules such as decreased L-selectin, and increased CD11b expression, an increase in inflammatory cytokine concentration (e.g. TNF $\alpha$ , MCP-1, IL-8) and the release of reactive oxygen species (ROS) (181-185).

For ventricular assist devices (1.3 Ventricular assist devices (VADs)), titanium alloy is the most commonly used material as the VAD body for it has high strength, high fatigue resistance, and enhanced corrosion resistance which makes it durable for long-term implantation (173, 186). Other key components of VADs are the bearings and impeller which have been made from ruby alumina (187), sapphire (188), and zirconium (35). Biocompatibility testing of these materials, which can be grouped as ceramic materials, has been limited to their applications in dental or joint implants (189, 190).

#### 3.1.5 Progressing biocompatibility

Coatings have been suggested as a solution for materials with desirable mechanical properties but poor biocompatibility. Diamond-like carbon (DLC) is a chemically inert nanocomposite coating with properties of natural diamond such as high hardness, low

friction, and high corrosion resistance (191, 192). DLC has been deemed biocompatible through prolonged clotting time, and suppressed platelet and complement activation (193). These features of DLC could potentially reduce pump thrombosis and the need for pump replacements in VAD patients.

## 3.2 Objectives

The main objectives of this chapter are:

- To develop an experimental model which can quickly verify the biocompatibility of any material in terms of both blood proteins and cells before they are used for medical devices.
- To analyse the effects of common VAD biomaterials on proteins, erythrocytes, leukocytes, and platelets.
- To develop a method for imaging opaque biomaterials for the study of cell adhesion.

## 3.3 Methods

### *3.3.1 Ethics*

As per 2.3.1 Blood collection ethics - 2.3.1.1 Human

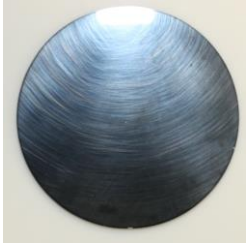




### *3.3.2 Biomaterial discs*

#### *3.3.2.1 Cleaning and set-up*

The following biomaterial discs: Stainless steel; Titanium (Ti6Al4V alloy); Single-crystal sapphire; Zirconia Toughened-Alumina (ZTA); Silicon Nitride (all from SAK Equipment Ltd., East Sussex, UK) were used. Discs measured 60 mm in diameter apart from ZTA which was 45 mm and were highly polished to achieve minimal surface roughness. The stainless-steel disc was coated with diamond-like carbon (Wallwork Heat Treatment Ltd., Birmingham, UK) (Table 3.1).

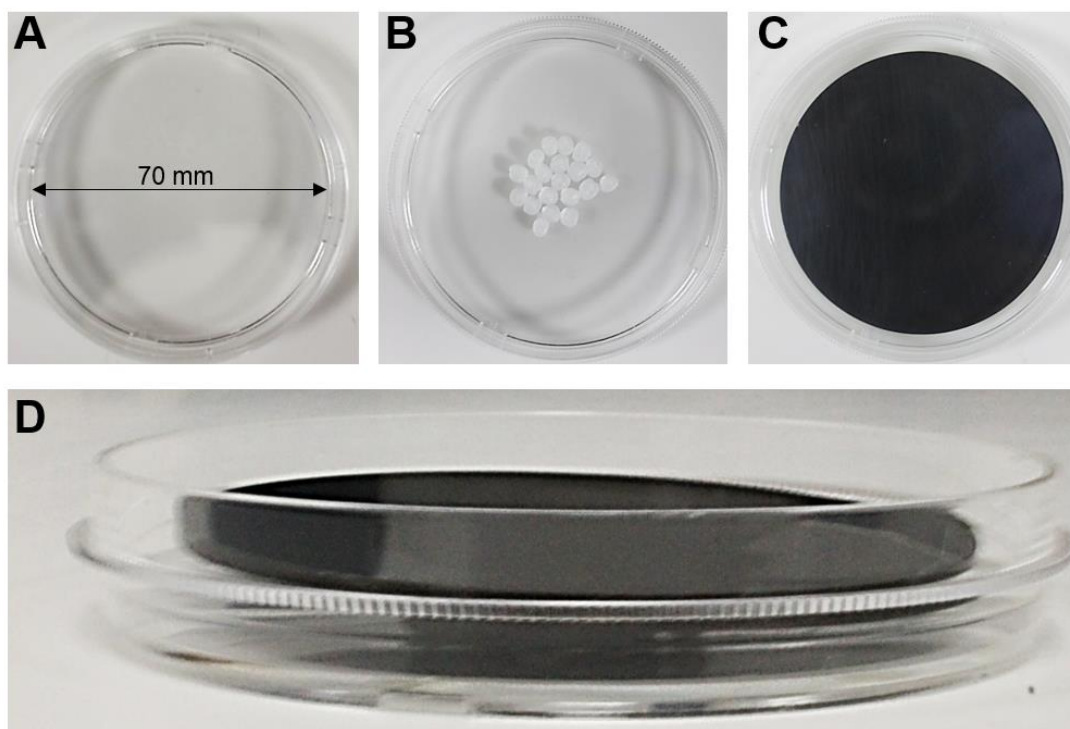
**Table 3.1: Biomaterial specifications**

Blood contact ratio calculated as biomaterial surface area (SA) compared to SA of the petri dish with beads ( $3630 \times (20 \times 12.57) = 3881.4 \text{ mm}^2$ ). Percentage of blood in contact with the biomaterial is reported (biomaterial SA / (biomaterial SA + petri dish and beads SA)).

Name and abbreviation	Image	Ø (mm)	h (mm)	SA (mm <sup>2</sup> )	Surface roughness (Ra, µm)	Blood contact (%)
Diamond-like carbon coated stainless steel (DLC)		60	2	6032	0.774	60.8
Single-crystal sapphire (Sap)		60	4	6409	0.044	62.3
Silicon Nitride (SiN)		60	4	6409	0.029	62.3
Titanium alloy (Ti)		60	2	6032	0.099	60.8
Zirconia-toughened alumina (ZTA)		45	3	4072	0.047	51.2



Discs were cleaned prior to experiments using equipment that had been cleaned and sprayed with 70% ethanol before use (Fisher Scientific, Loughborough, UK). Discs were sonicated in 3% neutracon® in dH<sub>2</sub>O (Decon Laboratories Ltd., East Sussex, UK) at +40°C for 10 min and then sonicated in 250 mL warm soapy dH<sub>2</sub>O (Ecover washing up liquid, Ecover UK Ltd, Basingstoke, UK) for 3 min followed by a 3 min sonication in fresh dH<sub>2</sub>O. The discs were air-dried and then sprayed with 70% denatured ethanol and left to dry on lint-free cloths. The polypropylene beads (Fred Aldous Ltd., Manchester, UK) used to balance the discs in the dishes were sprayed with 70% denatured ethanol, air-dried, then rinsed in sterile PBS before use.



**Figure 3.2: Biomaterial set-up.**

Twenty polystyrene beads were clustered together in a 70 mm sterile tissue culture dish (A&B). The biomaterials were then balanced on these beads (C&D) prior to addition of blood.

70 mm sterile tissue culture dishes (Cole Parmer, London, UK) were set up in the tissue culture hood with 20 beads clustered together in each (Figure 3.2). The biomaterials were rinsed in sterile PBS and then carefully placed on top of the beads. UV light was left on inside the tissue culture hood for 30 min to minimise further contamination before experiment commenced.

### 3.3.3 *Biomaterial- induced contact activation*

#### 3.3.3.1 *Experimental set-up*

Healthy human blood was collected using 9 mL 3.2% sodium-citrate Vacuettes® and cell counts measured using an automated haematology analyser (CELL-DYN Ruby; Abbott Laboratories, Maidenhead, UK). Blood was diluted with phosphate buffered saline (PBS, pH 7.4, Life Technologies) to a haematocrit of  $30 \pm 2\%$ . 12.5 mL of diluted blood was added to each dish containing the biomaterial. 2.5 mL PBS was added to each dish; negative control had just PBS and beads, positive control contained 2.5 mL Kaolin (Sigma Aldrich) solution (4 mg/mL in sterile PBS, vigorously shaken) and beads. The dishes were incubated for 1 h on a shaker plate at  $+37^{\circ}\text{C}$ . After this time, the blood was removed and centrifuged at  $1000 \times g$ , 10 min, no brake to give platelet rich plasma (PRP). The plasma was removed and subjected to centrifugation at  $2000 \times g$ , 15 min, with brake to remove platelets and debris. Final plasma was stored in aliquots at  $-80^{\circ}\text{C}$  until analysis.

#### 3.3.3.2 *Clotting time*

Frozen plasma samples were thawed at room temperature and then warmed to  $+37^{\circ}\text{C}$  prior to assay. 80  $\mu\text{L}$  plasma was added to a 96-well flat-bottomed plate pre-warmed to  $+37^{\circ}\text{C}$  in the microplate reader (BMG Labtech, Germany). Plasma was recalcified with a calcium buffer (25 mM Tris, 75 mM NaCl, 20 mM  $\text{CaCl}_2$ , 0.02% sodium azide buffer- all from Sigma Aldrich) and absorbance at 405 nm measured every 12 seconds (secs) for 20 min. The  $\frac{1}{2} V_{\text{max}}$  was calculated and expressed in secs.

#### 3.3.3.3 *Peptidase activity*

Frozen plasma samples were handled as in 3.3.3.2. 80  $\mu\text{L}$  of plasma kallikrein substrate S-2302 (Chromogenix, ILWW, MA, USA) (4 mM stock diluted 1:10 with 50 mM Tris, 100 mM NaCl, 500  $\mu\text{M}$  EDTA, 0.02% sodium azide buffer – all from Sigma Aldrich, unpublished method from Thrombosis Research Institute, Chelsea, London, UK) was added to the plasma. The plate was shaken immediately and then the absorbance at 405 nm read over 5 min. Increase in absorbance is directly proportional to enzymatic activity and is calculated through the difference in absorbance between 0 and 5 min. Results are expressed in milli-OD/min (mOD/min).

#### 3.3.3.4 *Thrombin activity*

The thrombin activity assay was described in 3.3.3.3 with thrombin substrate S-2238 (Chromogenix, ILWW, MA, USA) (2 mM stock diluted 1:8 with tris-buffered saline) used instead of kallikrein substrate.

#### 3.3.4 *Biomaterial-induced cell activation*

Healthy human blood was collected in lithium heparinised Vacuette® tubes and 15 mL added to each petri dish containing the biomaterials. Beads only served as a negative control. Dishes were incubated for 2 h at +37°C on a shaker plate set to 50 rpm (Titramax 1000, Heidolph Instruments, Schwabach, Germany) before blood was removed for assays. An initial time-lapse study involving sampling points at 2, 4, and 8 h (8.1.1 Time-course data) revealed that 2 h was appropriate for observable activation and so this time point was selected.

#### 3.3.5 *Haemolysis*

Three 1 mL aliquots of blood were centrifuged at 4200 x g for 7 min. Plasma (100 µL) was added to a 96-deep well plate (StarLab Ltd., Milton Keynes, UK) and mixed with 1 mL 0.1% Na<sub>2</sub>CO<sub>3</sub>. 170 µL was transferred to a 96-well plate (Greiner Bio-One) and absorbance read at 380, 415, and 450 nm using a microplate spectrophotometer (POLARstar Omega, BMG Labtech, Ortenburg, Germany). The amount of plasma-free haemoglobin was calculated using Equation 3.1.

#### **Equation 3.1: Calculation of haemoglobin concentration in plasma samples**

$$pfHb = (167.2 \times A_{415} - 83.6 \times A_{380} \times A_{450}) \times \frac{1}{1000} \times 1/DR$$

Where:

*pfHb* = plasma free haemoglobin (g/L)

$A_n$  = the absorbance peak at  $n$  (nm)

*DR* = Dilution ratio of plasma/Na<sub>2</sub>CO<sub>3</sub> solution (194)

#### 3.3.6 *Haematology*

A complete blood count using the Cell-DYN Ruby clinical haematology analyser was generated in triplicate for each blood sample.

### 3.3.7 Flow cytometry

Cells stained as described below were analysed within 2 h using a 10 colour, 3 lasers, Navios Flow Cytometer (Beckman Coulter, High Wycombe, UK). The instrument was turned on at least 1 h prior to run to allow lasers to warm up and for quality control checks. To check instrument performance, FlowCheck and FlowSet beads (both Beckman Coulter) were run. All samples were recorded without compensation which was applied later in data analysis. Voltages were set on unstained samples.

#### 3.3.7.1 Platelet activation

For platelet activation, blood was stained with 200 ng/ $\mu$ L CD42b-FITC (clone HIP1, IgG1 $\kappa$ , eBioscience). CD42b is a glycoprotein expressed at the platelet surface that decreases with platelet activation (195). Samples were vortexed and incubated on ice in the dark for 30 min. Red blood cells were lysed with 1 mL BD FACs lysing solution (BD Bioscience, Oxford, UK), vortexed, and incubated in the dark at room temperature for 15 min. Tubes were centrifuged (7 min, 515 x g, +4°C), the supernatant discarded, and the samples washed again by centrifugation before being acquired on the Navios. 50,000 platelets were acquired on a logarithmic scale based on a gate using typical forward and side scatter characteristics. Blood stimulated for 20 min with phorbol 12-myristate 13-acetate (PMA, Sigma Aldrich) at a final concentration of 4  $\mu$ M was used as positive control for activated platelets.

#### 3.3.7.2 Platelet aggregates

The aggregation assay was performed using 12.5 ng/ $\mu$ L CD15-Krome Orange (clone 80H3, IgM, Beckman Coulter), 500 ng/ $\mu$ L CD14-Pacific Blue (clone M5E2, IgG2a, BioLegend, London, UK) and 12.5 ng/ $\mu$ L CD41-APC (clone P2, IgG1, Beckman Coulter); CD41 is a platelet marker, CD15 a neutrophil marker and CD14 a monocyte marker – co-expression on an event identified using flow cytometry is indicative of aggregates containing these cells (196). Samples were vortexed and incubated on ice in the dark for 30 min. Red blood cells were lysed with 600  $\mu$ L EasyLyse (Dako, Ely, UK), vortexed, and incubated in the dark at room temperature for 15 min. Tubes were run on a logarithmic scale with 10,000 CD15<sup>+</sup> events as the stopping gate.

### 3.3.7.3 *Leukocyte analysis*

Whole blood was stained with the following: CD15 and CD14 as above; 100 ng/ $\mu$ L CD3-APC-AF750 (clone UCHT1, IgG1 $\kappa$ , Beckman Coulter); 25 ng/ $\mu$ L CD62L-PE (clone DREG-56, IgG1 $\kappa$ , eBioscience); 100 ng/ $\mu$ L CD11b-APC (clone CBRMI/5, IgG1 $\kappa$  eBioscience); 220 ng/ $\mu$ L fMLP receptor-FITC (clone REA169, IgG1, Miltenyi Biotec, Woking, UK). Samples were vortexed, incubated, and lysed as described in 3.3.7.2. EasyLyse was chosen instead of FACs lyse here as it is formaldehyde free and therefore will not affect dead cell staining. 1  $\mu$ L DRAQ7, final concentration of 20  $\mu$ M (BioStatus, Leicester, UK), was added before running the samples (160). Whole blood stimulated with 10 ng/mL LPS for 4 h at +37°C, 5% CO<sub>2</sub>-in-air as in 3.3.8.1 was used as a positive control and unstained samples were used for gating purposes. Blood exposed to 1% Triton-X 100 (Fisher Scientific) was used to determine DRAQ7 positive cell gates. AbC beads (Life Technologies, Paisley, UK) were stained singly with each antibody and used for compensation. Within 2 hours of staining, samples were acquired on the Navios flow cytometer (Three lasers (violet: 405 nm, blue: 488 nm, red: 638 nm and the standard filter configuration as supplied by the manufacturers, Beckman Coulter) using linear forward scatter (FSC) versus side scatter (SSC) scale, flow rate set to high, and stop gate on 10,000 CD15<sup>+</sup> events which would allow for acquisition of approximately 10,000 total lymphocytes and 1,000 monocytes. Compensation and data analysis were performed using Kaluza 1.3 (Beckman Coulter).

### 3.3.8 *Cell culture supernatants and plasma processing*

#### 3.3.8.1 *Whole blood culture*

Whole blood cultures (100  $\mu$ L blood/300  $\mu$ L RPMI + 2 mM GlutaMax + 0.1 mM 2-mercaptoethanol (Life Technologies)) were left unstimulated or stimulated with 10 ng/mL *E. Coli OIII:B4* lipopolysaccharide (Ultrapure LPS, Invivogen, Toulouse, France). After 24 h incubation at +37°C, 5% CO<sub>2</sub>-in-air cell free supernatants were harvested by centrifugation (+4 °C, 515 x g, 7 min). These were stored at -20°C until analysis.

#### 3.3.8.2 *Cytokine analysis*

Levels of inflammatory cytokines (interleukin 1 beta: IL-1 $\beta$ , tumour necrosis factor alpha: MCP-1/TNF $\alpha$ , monocyte chemoattractant protein-1: CCL2/MCP-1, interleukin

6: IL-6, interleukin 8: CXCL8/IL-8, and interleukin 10: IL-10) were first measured through multiplex analysis using LEGENDplex (BioLegend) on the Navios Flow Cytometer (Beckman Coulter) according to the manufacturer's instructions (8.1.2 Human inflammatory multiplex panel). Levels of IL-1 $\beta$ , TNF $\alpha$ , IL-6, IL-8 in cell free supernatants were then measured using specific ELISAs (DuoSet, R&D Systems, USA) according to the manufacturer's instructions.

#### *3.3.8.3 Endotoxin testing*

Endotoxin concentration in the unstimulated cell culture supernatants was assessed using the Pierce Limulus Amebocyte Lysate (LAL) Chromogenic Endotoxin Quantification Kit (Thermo Fisher Scientific, Gloucester, UK) according to the manufacturer's instructions.

#### *3.3.8.4 Soluble CD62L*

Soluble L-selectin in plasma was measured using a specific ELISA (DuoSet ELISA DY728, R&D Systems, Oxford, UK) according to the manufacturer's instructions.

### *3.3.9 Microscopy*

#### *3.3.9.1 Staining of biomaterial discs with CyTRAK Orange*

Biomaterial discs were carefully rinsed with PBS after incubation with heparinised blood for 2 h. Discs were left in 1% glutaraldehyde (Sigma Aldrich) for 1 h at room temperature in a fume hood then washed with PBS 3 times for 15 mins each. 1 mL CyTRAK Orange (BioStatus) diluted in PBS to a final concentration of 5  $\mu$ M was pipetted onto the surface of the biomaterial and incubated for 30 min at room temperature shielded from light. Discs were washed in PBS once for 15 mins prior to imaging.

#### *3.3.9.2 Confocal imaging*

A cover slip was attached to the biomaterial discs using cellotape and placed over the x40 lens with oil immersion. Biomaterial discs were analysed using the LSM710 META inverted confocal microscope (Zeiss) equipped with 405 nm diode laser (blue), 488 nm argon laser (green), and the 633 nm HeNe laser (red).

### 3.3.9.3 *Image analysis*

Images from the confocal microscope were analysed using ImageJ 1.50i (Wayne Rasband, National Institutes of Health, USA). The number of leukocytes present on each material was counted using the ‘analyse particles’ tool.

### 3.3.10 *Data and statistical analysis*

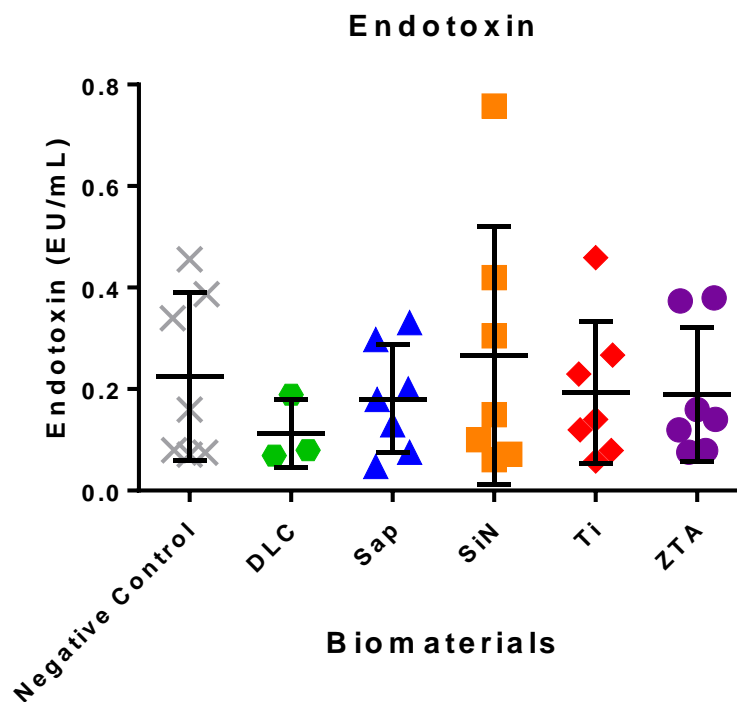
Flow cytometry data LMD files were exported and analysed using automatic compensation in Kaluza 1.5a (Beckman Coulter) using data from the AbC bead samples, baseline sample for autofluorescence, and the DRAQ7 stained Triton-X-100 sample.

GraphPad Prism 7.02 (GraphPad Software Inc., La Jolla, CA) was used for all statistical analysis. Gaussian distributions were tested using D’Argostino and Pearson omnibus normality or Kolmogorov-Smirnov tests. Comparisons between baseline and biomaterials were analysed using one-way analysis of variance (ANOVA) or the Kruskal-Wallis nonparametric test. Repeated measures ANOVA was used for time course samples. Tukey or Dunn’s tests were applied *post hoc*. A p value  $\leq 0.05$  was considered significant.

## 3.4 Results

### 3.4.1 Endotoxin

Endotoxins are heat-stable LPS substances present in the outer membrane of gram-negative bacteria released upon cell lysis (197). Presence of endotoxin on the biomaterials would compromise the results as it would not be possible to know if activation was due to the biomaterials or contamination.



**Figure 3.3: Endotoxin levels.**

Unstimulated, biomaterial-exposed-cell culture supernatants were analysed for endotoxin ( $n = 7$ ). 1 EU/mL is approximately 0.1 ng endotoxin/mL.

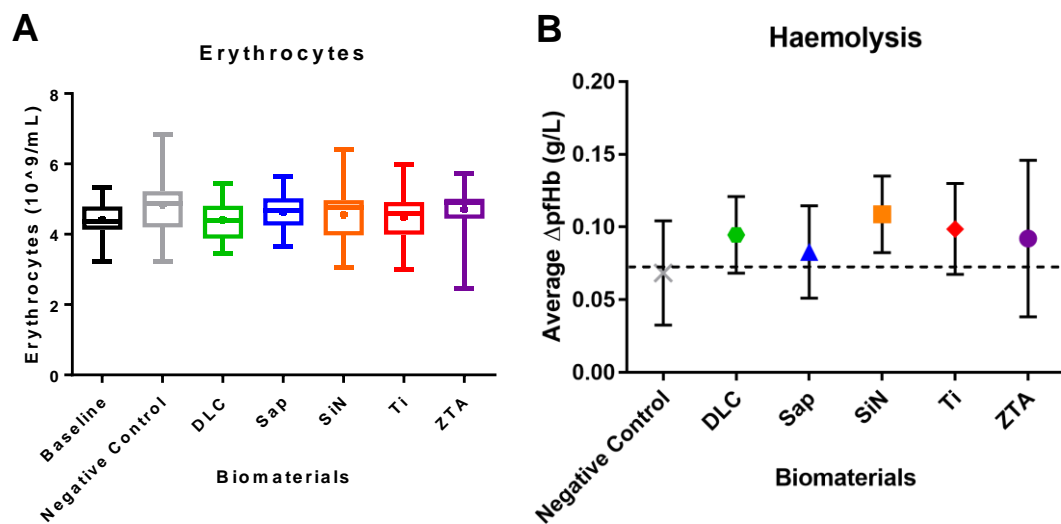
Endotoxin levels in all the samples were less than 1 EU/mL (approximately 0.1 ng/mL) indicating that the cleaning method was adequate and that cellular activation, for leukocytes, is due to the actions of the material and not residual bacterial components.

### 3.4.2 The effect of biomaterials on erythrocytes

Before in-depth analysis of less prominent blood components (leukocytes, platelets, proteins) could be done, it was important to check that the biomaterials were not



negatively impacting the more abundant red blood cells (erythrocytes). The biomaterials studied did not significantly affect the total erythrocyte count ( $n = 16$ ; Figure 3.4A). Additionally, the health of the erythrocytes was measured using the Harboe assay which enables calculation of the concentration of plasma-free haemoglobin in the plasma due to haemolysis. The measurement of haemolysis is a key regulatory requirement for implantable devices such as VADs (198) and was a parameter to be considered in biomaterial testing. Additionally, plasma-free haemoglobin (pfHb) can upregulate tissue factor expression on macrophages (199) which could influence leukocyte activation measurements on other subsets. There was no significant increase in haemolysis in blood incubated with biomaterials comparison to the baseline (time 0 sample;  $n = 9$ ; Figure 3.4B).

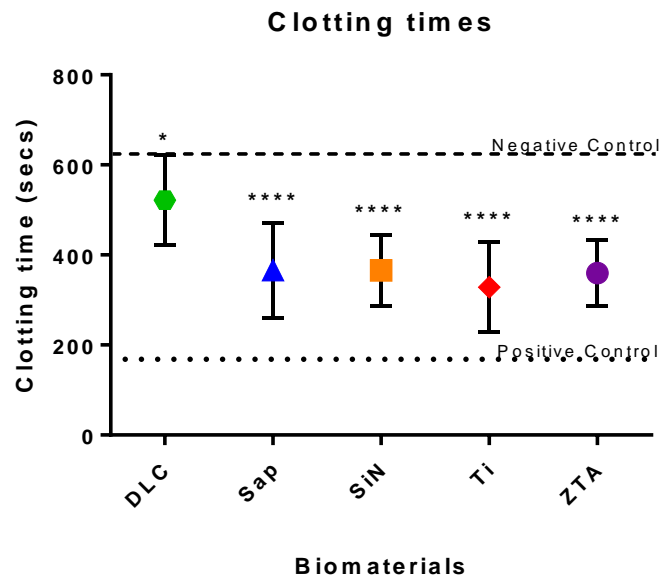


**Figure 3.4: The effects of various biomaterials on erythrocyte counts and haemolysis.**

Whole heparinised blood was exposed to each of the biomaterials - diamond-like carbon coated stainless steel (DLC), single-crystal sapphire (Sap), silicon nitride (SiN), titanium alloy (Ti), and zirconia toughened alumina (ZTA) - for 2 hours and A) erythrocyte counts measured using an automated haematology analyser ( $n = 16$ ); and B) haemolysis measured as a change in concentration of plasma free haemoglobin ( $\Delta$ pfHb;  $n = 9$ ) at time 0 and after 2 h incubation with each biomaterial. There was no significant difference between biomaterials and the time baseline (as shown by dashed line)

### 3.4.3 The effect of biomaterials on the coagulation cascade

Pump thrombosis leads to the requirement for pump replacements and incidences of embolism. This adverse event is controlled with anticoagulant and anti-platelet therapy but the effect of the pump on the creation of thrombus could be related to the choice and location of biomaterials. Certain biomaterials may be more thrombogenic than others and knowing this early in development could reduce negative outcomes in clinic. The following assays measure the activity of the coagulation cascade.

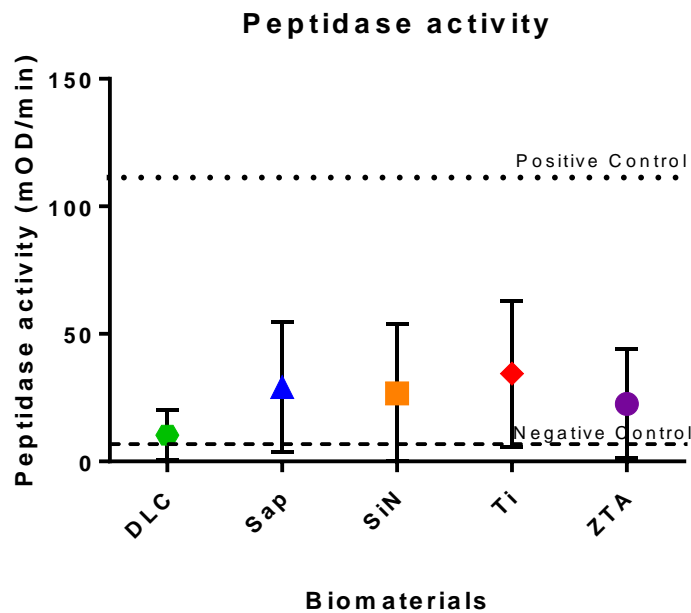


**Figure 3.5: The effects of various biomaterials on clotting time.**

Whole sodium-citrated blood was exposed to each of the biomaterials - diamond-like carbon coated stainless steel (DLC), single-crystal sapphire (Sap), silicon nitride (SiN), titanium alloy (Ti), and zirconia toughened alumina (ZTA) – for 1h. Negative control was blood diluted with PBS and positive control was blood incubated with 4mg/mL Kaolin solution. Platelet-poor plasma was used to measure time taken to clot after exposure to calcium (n = 11, \* =  $p \leq 0.05$  \*\*\*\* =  $p \leq 0.0001$  from negative control).

A decrease in the time for plasma to clot upon re-calcification is a measure of increased activity of the coagulation cascade and indicative that the material is thrombogenic. Clotting time of plasma from blood exposed to the biomaterials (Figure 3.5) was decreased by all the biomaterials ( $p \leq 0.0001$  compared to negative control except DLC where the difference was  $p = 0.027$ ). None of the biomaterials affected clotting time

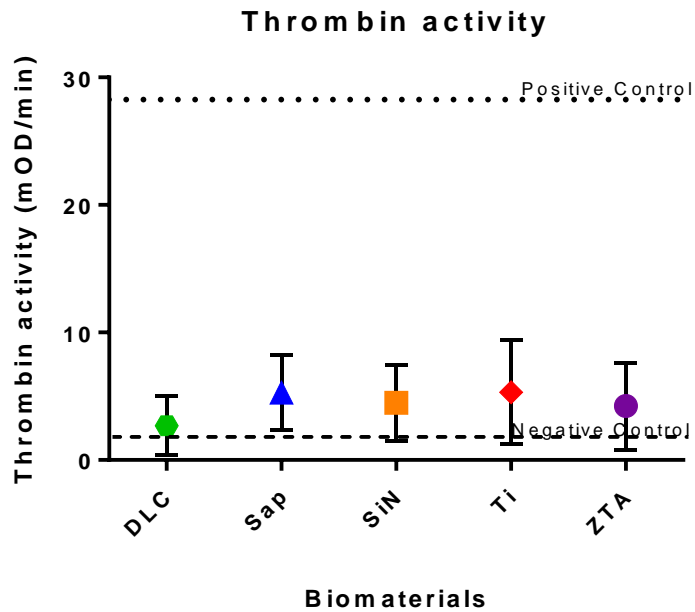
of plasma to the same extent as the positive control ( $p \leq 0.0001$  compared to positive control).



**Figure 3.6: The effects of various biomaterials on peptidase activity.**

Whole sodium-citratated blood was exposed to each of the biomaterials - diamond-like carbon coated stainless steel (DLC), single-crystal sapphire (Sap), silicon nitride (SiN), titanium alloy (Ti), and zirconia toughened alumina (ZTA) – for 1h. Negative control was blood diluted with PBS and positive control was blood incubated with 4mg/mL Kaolin solution. Peptidase activity was measured as directly proportionate to the increase in absorbance at 405 nm over 5 mins ( $n = 11$ ).

The intrinsic pathway of the coagulation cascade is initiated by factor XII (FXII) which becomes proteolytically active upon induction by negatively charged surfaces (200). Active FXII causes a cascade of serine proteases to cleave peptide bonds down the coagulation pathway. Peptidase activity was measured as the maximum absorbance at 405nm after 5 mins due to cleavage of the peptidase chromogenic substrate S-2302 (Figure 3.6). There was no significant difference between the biomaterials and the negative control ( $p \leq 0.0001$ ). There was significant difference between all biomaterials and the positive control ( $p \leq 0.0001$ ).



**Figure 3.7: The effects of various biomaterials on thrombin activity.**

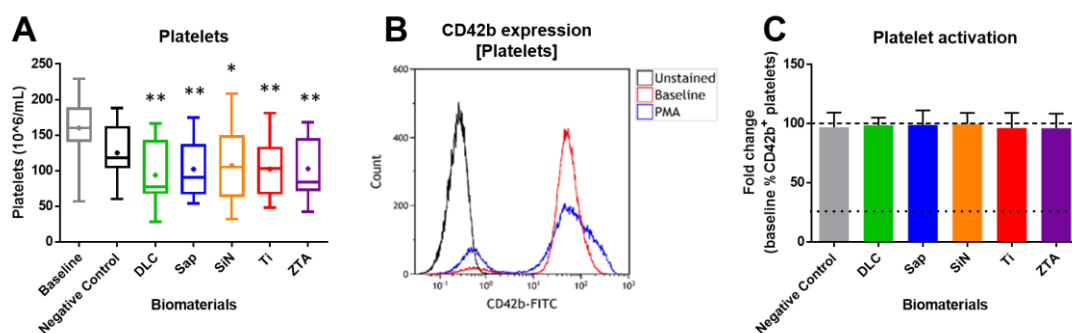
Whole sodium-citratated blood was exposed to each of the biomaterials - diamond-like carbon coated stainless steel (DLC), single-crystal sapphire (Sap), silicon nitride (SiN), titanium alloy (Ti), and zirconia toughened alumina (ZTA) – for 1h. Negative control was blood diluted with PBS and positive control was blood incubated with 4mg/mL Kaolin solution. Thrombin activity was measured as directly proportionate to the increase in absorbance at 405 nm over 5 mins (n = 11).

Thrombin is a serine protease that converts soluble fibrinogen to fibrin in the final common pathway of the coagulation cascade. Thrombin activity was measured as the maximum absorbance at 405nm after 5 mins due to cleavage of the peptidase chromogenic substrate S-2238 (Figure 3.7). There was no significant difference between the biomaterials and the negative control ( $p \leq 0.0001$ ). There was significant difference between all biomaterials and the positive control ( $p \leq 0.0001$ ).

### 3.4.4 The effect of biomaterials on platelets

#### 3.4.4.1 Platelet activation

Platelets are a key component of the coagulation process. Upon activation, platelet morphology changes from round to the presence of pseudopodia which allow platelets to aggregate with other platelets and cells to create a thrombus (201). Platelet count after 2 h incubation was significantly reduced compared to time 0 baseline sample in response to all biomaterials: DLC ( $p = 0.004$ ); Sap ( $p = 0.006$ ); SiN ( $p = 0.02$ ); Ti ( $p = 0.007$ ), and ZTA ( $p = 0.009$ ) (Figure 3.8A). Platelet activation was measured through decreased CD42b expression (Figure 3.8B). After 2 hours, there was no significant change with biomaterials compared to baseline blood for CD42b expression (Figure 3.8C).



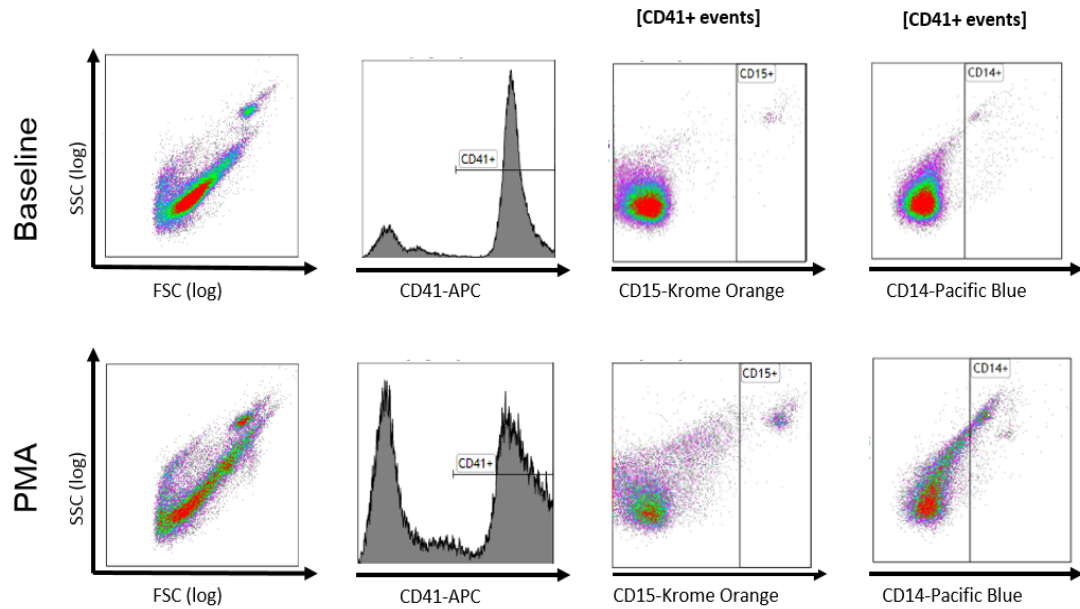
**Figure 3.8: The effects of various biomaterials on platelet counts and activation status**

Whole heparinised blood was exposed to each of the biomaterials - diamond-like carbon coated stainless steel (DLC), single-crystal sapphire (Sap), silicon nitride (SiN), titanium alloy (Ti), and zirconia toughened alumina (ZTA). A) Platelet count was measured on an automated haematology analyser after 2 h ( $n = 16$ ); B) Flow cytometry histogram showing the expression of CD42b on platelets at baseline (red) and after activation with PMA (blue), an unstained control is also shown (black). C) Platelet CD42b expression at 2 hours shown as percentage of baseline expression at time 0 ( $n = 6$ ; \*  $p \leq 0.05$ , \*\*  $p \leq 0.01$ , \*\*\*  $p \leq 0.001$ , \*\*\*\*  $p \leq 0.0001$ ).

#### 3.4.4.2 Platelet-platelet and leukocyte-platelet aggregates

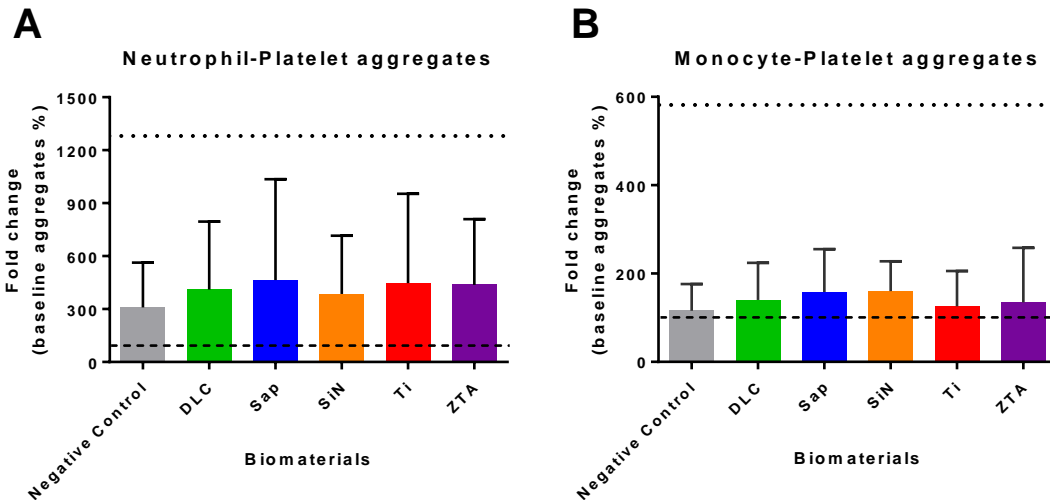
Platelet-platelet and leukocyte-platelet aggregates are suggestive of thrombus build-up (202). Co-expression of CD41 (a platelet marker), CD15 (a neutrophil marker), and CD14 (a monocyte marker) on a flow cytometry event is indicative of aggregates

containing these cells (196) (Figure 3.9). None of the biomaterials had a significant effect on the formation of neutrophil-platelet (Figure 3.10A) and monocyte-platelet aggregates (Figure 3.10B) at 2 hours.



**Figure 3.9: Gating strategy for leukocyte-platelet aggregates.**

Whole heparinised blood was exposed to each of the biomaterials - diamond-like carbon coated stainless steel (DLC), single-crystal sapphire (Sap), silicon nitride (SiN), titanium alloy (Ti), and zirconia toughened alumina (ZTA) – and samples taken at 2 hours. Samples were stained with CD41, CD15, and CD14 acquired on a logarithmic scale. Platelets were identified by their expression of CD41 and gated as CD41<sup>+</sup>. CD41<sup>+</sup> events were plotted on SSC versus CD15-Krome Orange or CD14-Pacific Blue to identify aggregates containing neutrophils or monocytes, respectively. Baseline blood stimulated with PMA was used as a positive control.



**Figure 3.10: The effects of biomaterials on neutrophil-platelet and monocyte-platelet aggregates.**

Whole heparinised blood was exposed to each of the biomaterials - diamond-like carbon coated stainless steel (DLC), single-crystal sapphire (Sap), silicon nitride (SiN), titanium alloy (Ti), and zirconia toughened alumina (ZTA) - for 2 hours. Samples were then stained with CD14, CD15, and CD41. The percentage of dual-positive cells (CD14<sup>+</sup>/CD41<sup>+</sup> or CD15<sup>+</sup>/CD41<sup>+</sup>) was compared to the time 0 baseline (dashed line) as fold change (n = 5). Baseline blood stimulated with PMA for positive control is shown as a dotted line.

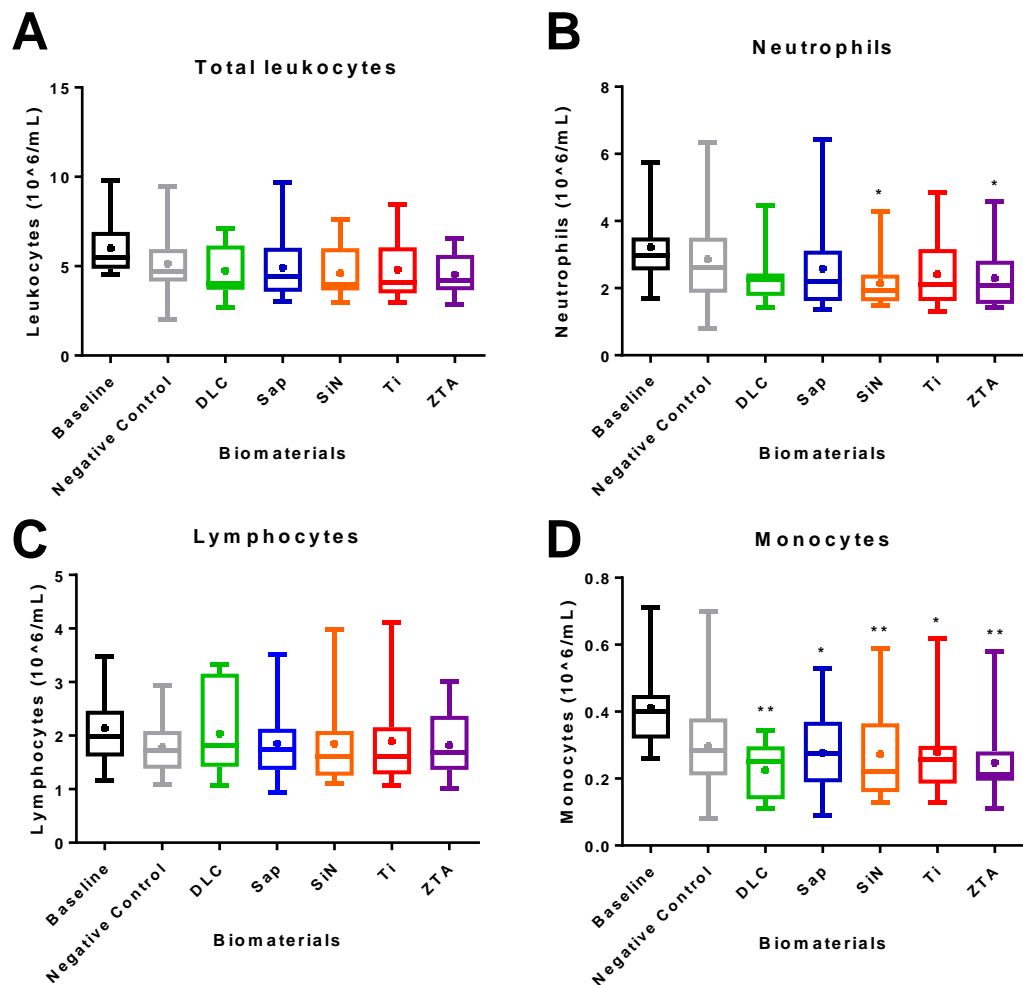
### 3.4.5 The effect of biomaterials on leukocytes

Leukocytes influence the inflammatory and repair phases surrounding implanted materials. Alterations in the function of leukocytes can lead to chronic inflammation, poor wound repair, poor resistance to infection, and can even contribute to the formation of thrombus. The early interactions between biomaterials and leukocytes is important for the future success of the implant as changes to leukocyte function caused by the biomaterials of choice could cost dearly.

#### 3.4.5.1 Leukocyte cell counts

A decrease in leukocyte count could be the result of activation/damage that changes cell morphology or adherence of the cells to the materials. The biomaterials used did have significant effects on neutrophil and monocyte counts in comparison to the baseline sample at time 0 for some of the biomaterials (n=16; Figure 3.11B and D). Neutrophil counts were reduced significantly in the presence of; SiN (p = 0.014) and ZTA (p = 0.045). Monocyte counts were decreased significantly in the presence of all

the biomaterials: DLC ( $p = 0.004$ ), Sap ( $p = 0.042$ ), SiN ( $p = 0.007$ ), Ti ( $p = 0.017$ ) and ZTA ( $p = 0.002$ ) (Figure 3.11C).



**Figure 3.11: The effects of various biomaterials on total leukocyte and subset counts.**

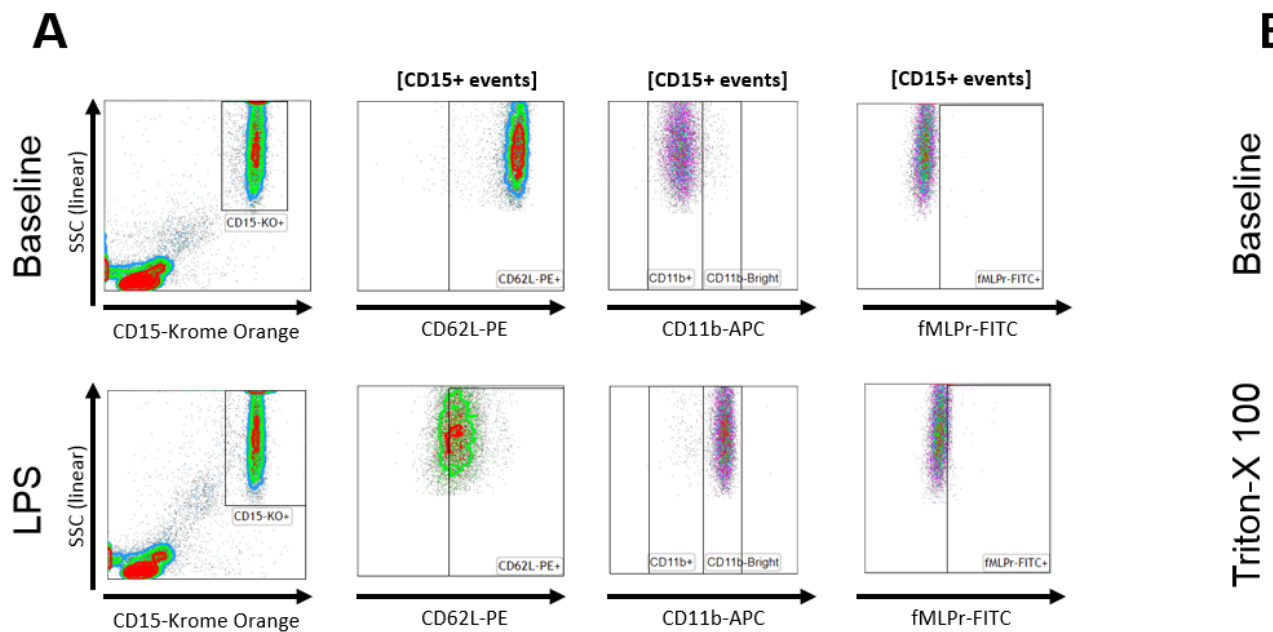
Whole heparinised blood was exposed to each of the biomaterials - diamond-like carbon coated stainless steel (DLC), single-crystal sapphire (Sap), silicon nitride (SiN), titanium alloy (Ti), and zirconia toughened alumina (ZTA) - for 2 hours and complete cell counts measured on an automated haematology analyser. A) Total leukocytes, B) neutrophils, C) monocytes, and D) lymphocytes ( $n = 16$ ); \*  $p \leq 0.05$ , \*\*  $p \leq 0.01$  on statistical comparison to time 0 baseline.

Lymphocyte counts were not significantly affected which is unsurprising as lymphocyte adhesion to biomaterial surfaces takes longer than 2 hours and requires the presence of adherent macrophages or foreign body giant cells (FBGCs) (203).



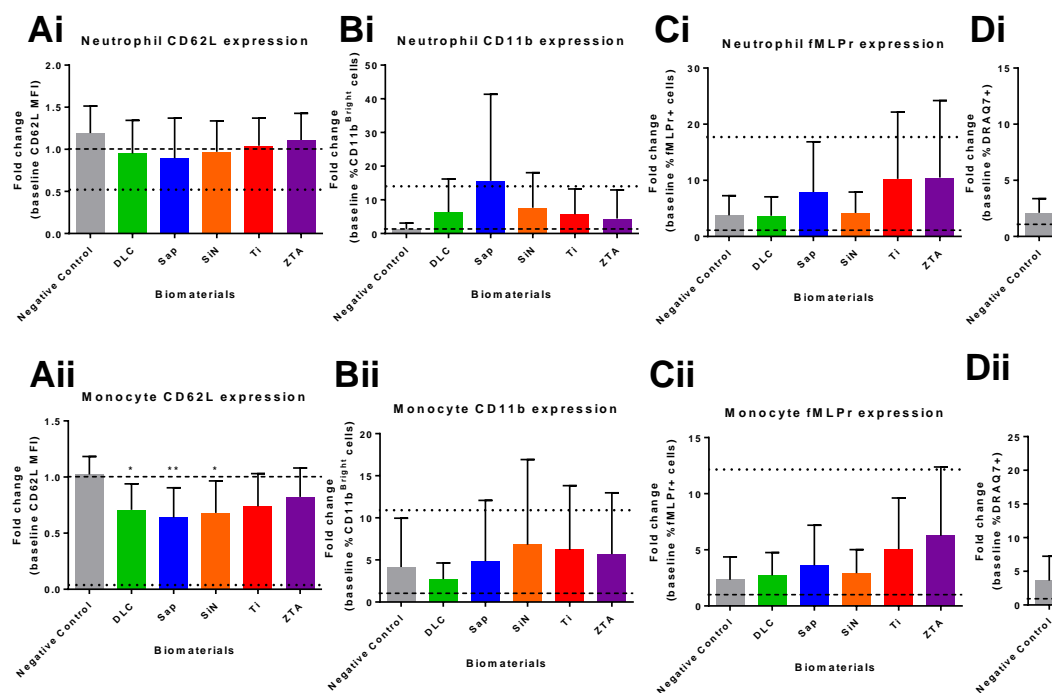
#### 3.4.5.2 *Leukocyte activation and death*

To account for the decrease in cell count and to see whether the leukocytes were becoming activated or dying, flow cytometry was used to identify neutrophils, monocytes, T lymphocytes, and monitor phenotype changes. The activation markers, L-selectin (CD62L), CD11b, and fMLPr were used to determine the activation status of the leukocyte subsets. L-selectin is a cell adhesion molecule constitutively expressed on leukocytes and shed upon activation (204). CD11b is part of the  $\beta$ 2 integrin complement receptor 3 which becomes upregulated upon activation (182). FMLPr is expressed upon stimulation by bacteria and plays a role in chemotaxis (205).



**Figure 3.12: Gating strategy for leukocyte activation and death.**

Baseline (time 0 sample) and baseline blood stimulated with 10 ng/mL LPS for 4 hours (positive control) were stained with CD3, CD14, CD15, CD62L, CD11b, fMLP receptor (fMLPr), and DRAQ7. Samples were analyzed for activation profiles of leukocyte subsets with neutrophils shown as an example here. A) Neutrophils were gated using SSC/CD15-Krome Orange. CD15<sup>+</sup> events were then plotted using SSC versus CD62L-PE, CD11b-APC according to baseline samples with high expression of CD62L, dim expression of CD11b (CD11b<sup>dim</sup>) in stimulated samples. B) 1% Triton-X 100 was added to lysed baseline blood, vortexed vigorously, and analyzed as a dead cell control. DRAQ7 positive events (DRAQ7<sup>+</sup>) identified dead cells and a gate was used as a dead cell negative control.



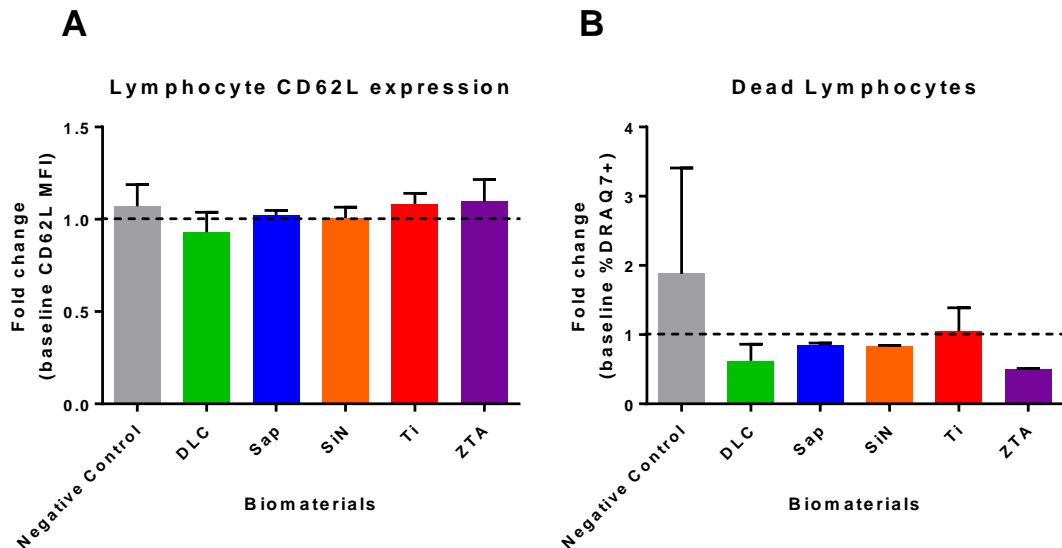
**Figure 3.13: The effect of various biomaterials on neutrophil and monocyte activation and death.**

Whole heparinised blood was exposed to each of the biomaterials - diamond-like carbon coated sapphire (Sap), silicon nitride (SiN), titanium alloy (Ti), and zirconia toughened alumina (ZTA) - for 15 minutes. Leukocyte activation was measured by the change in median fluorescent intensity (MFI) of CD62L on **i**) CD15<sup>+</sup> neutrophils (n = 9) and **ii**) CD14<sup>+</sup> monocytes; **C**) Change in percentage of CD11b<sup>Bright</sup> cells on **i**) CD15<sup>+</sup> neutrophils and **ii**) CD14<sup>+</sup> monocytes (n = 6); **C**) Change in percentage of fMLPr<sup>+</sup> cells on **i**) CD15<sup>+</sup> neutrophils and **ii**) CD14<sup>+</sup> monocytes (n = 5); **D**) Percentage of **i**) CD15<sup>+</sup> neutrophils and **ii**) CD14<sup>+</sup> monocytes cells that were DRAQ7<sup>+</sup>.

(n = 5). All were compared to the time 0 baseline as a fold change (dashed line). The LPS positive c  
(\* p ≤ 0.05, \*\* p ≤ 0.01).

Changes in leukocyte activation - decreased L-selectin (CD62L), increased CD11b<sup>Bright</sup> cells, and increased fMLP receptor - were measured as mean fluorescence intensity (CD62L) or percentage positive (CD11b, fMLP receptor) on CD15<sup>+</sup> neutrophils, CD14<sup>+</sup> monocytes and CD3<sup>+</sup> T cells (Figure 3.12). Changes in expression for neutrophils and monocytes are presented as fold change compared to baseline (time 0 sample; Figure 3.13). Expression of CD11b on lymphocytes is restricted to the CD8<sup>+</sup> subset (206) and fMLPr is expressed on innate immune cells (205), not lymphocytes, so this was not done.

Expression of CD62L (n = 9) on neutrophils and lymphocytes (Figure 3.13Ai & Figure 3.14A) was not significantly affected by the biomaterials whereas expression of CD62L on monocytes (Figure 3.13Aii) was significantly decreased in the presence of DLC (p = 0.049), Sap (p = 0.009), and SiN (p = 0.026). A decrease in CD62L expression by monocytes through activation-induced shedding led to the hypothesis that levels of soluble CD62L in the fluid phase would be increased. However, there was no significant increase in soluble CD62L (Figure 3.15).

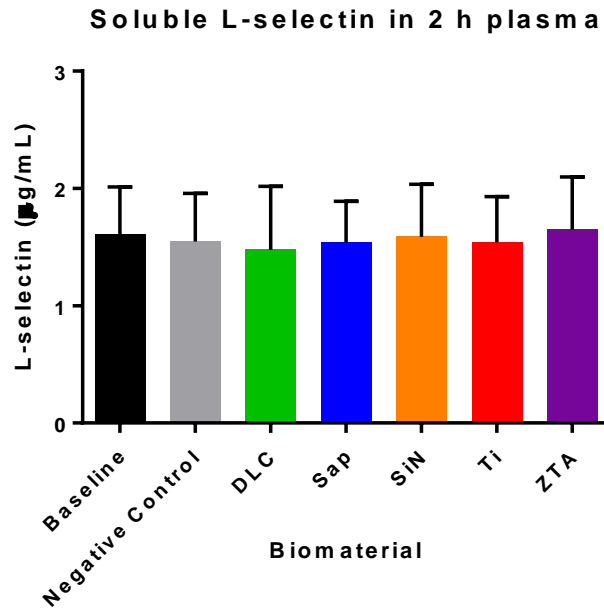


**Figure 3.14: The effect of various biomaterials on lymphocyte activation and death.**

Whole heparinised blood was exposed to each of the biomaterials - diamond-like carbon coated stainless steel (DLC), single-crystal sapphire (Sap), silicon nitride (SiN), titanium alloy (Ti), and zirconia toughened alumina (ZTA) - for 2 hours. Samples were then stained with CD62L, CD3 and DRAQ7. Change in A) median fluorescent intensity (MFI) of CD62L; and B) percentage of DRAQ7+ dead cells. There were no significant differences in comparison to baseline (all n = 3).

The percentage of cells with high expression of (CD11b<sup>Bright</sup>) after exposure to biomaterials did not differ significantly in comparison to baseline for either neutrophils or monocytes (Figure 3.13Bi, Bii). Lymphocyte expression CD11b is reported to be low so these data are not shown for T cells (206).

Incubation alone increased fMLP receptor expression by neutrophils and monocytes after 2 h incubation with no significant effects of biomaterial (Figure 3.13Ci & ii). Expression of fMLP receptor on T cells was not observed.



**Figure 3.15: The effects of various biomaterials on soluble CD62L.**

Whole heparinised blood was exposed to each of the biomaterials - diamond-like carbon coated stainless steel (DLC), single-crystal sapphire (Sap), silicon nitride (SiN), titanium alloy (Ti), and zirconia toughened alumina (ZTA) - for 2 hours. Samples were centrifuged and the plasma analysed for soluble L-selectin using specific ELISA. There were no significant differences in comparison to baseline (n = 8).

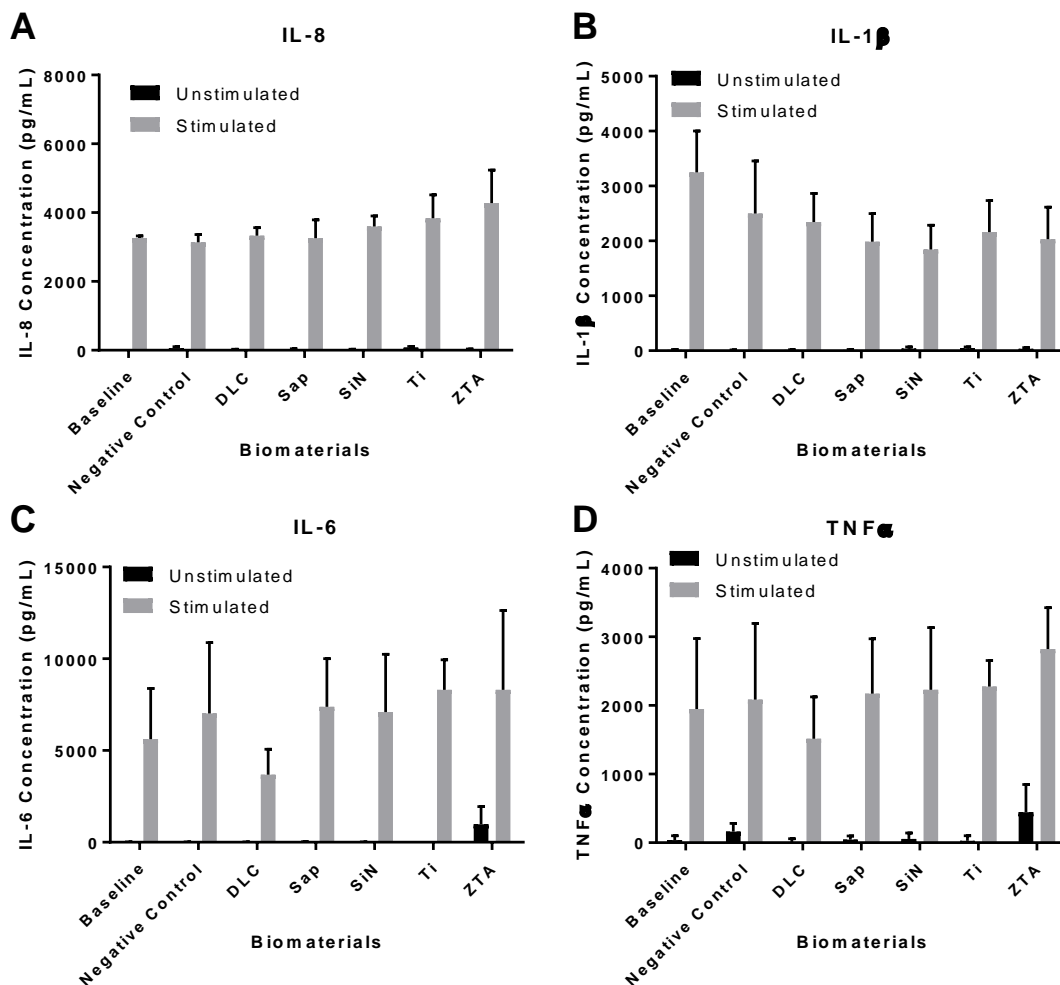
Cell death was monitored throughout using DRAQ7 (160) and there was no significant effect of biomaterials exposure on cell death within each of the leukocyte subsets of interest (Figure 3.13Di & ii and Figure 3.14B).

#### 3.4.5.3 Cytokine production

As there were phenotypic differences in leukocytes, especially monocytes, upon exposure to biomaterials any functional effect was then considered by studying the response to the prototypic inflammatory stimuli LPS. LPS induced a significant increase in inflammatory cytokine levels with all biomaterials in keeping with the expected effects of LPS exposure of whole blood. Levels of the pro-inflammatory cytokines IL-8, IL-1 $\beta$ , IL-6, TNF- $\alpha$ , MCP-1 and the anti-inflammatory cytokine IL-10 were measured initially using a multiplex flow cytometry based approach (8.1.2 Human inflammatory multiplex panel) to indicate a focus on IL-8 (Figure 3.16A; n =

7), IL-1 $\beta$  (Figure 3.16B; n = 7), IL-6 (Figure 3.16C; n = 5), and TNF $\alpha$  (Figure 3.16D; n = 5) using single-plex ELISA analysis.





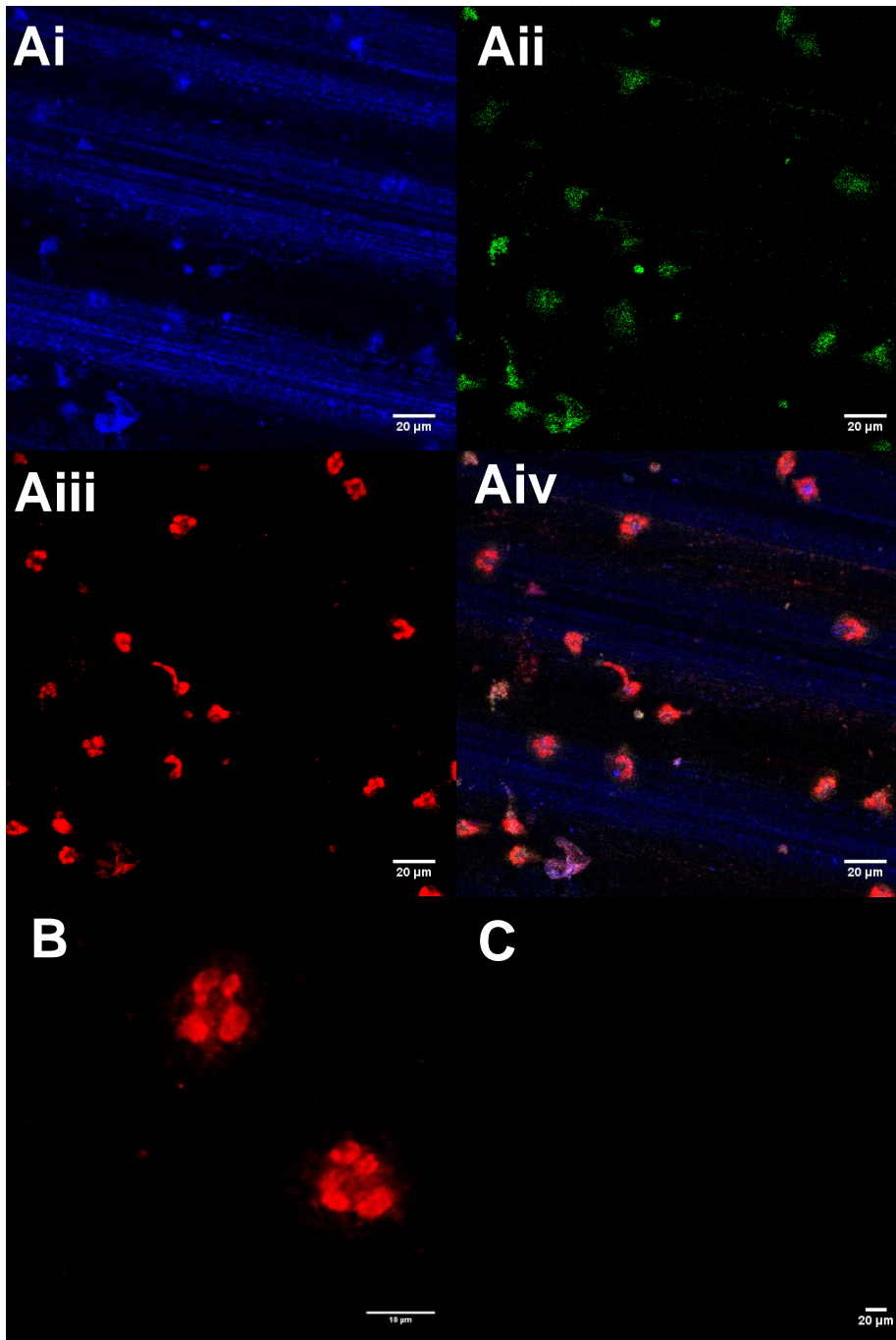
**Figure 3.16: The effects of biomaterials on cytokine response in both LPS-stimulated and unstimulated blood**

Whole heparinised blood incubated with various biomaterials - diamond-like carbon coated stainless steel (DLC), single-crystal sapphire (Sap), silicon nitride (SiN), titanium alloy (Ti), and zirconia toughened alumina (ZTA) - for 2 h was cultured either in media alone (unstimulated) or with media containing 10 ng/mL LPS (stimulated) for a further 24 h in 5% CO<sub>2</sub>, 37°C. Pro-inflammatory cytokines **A**) IL-8 (n = 7), **B**) IL-1 $\beta$  (n = 7), **C**) IL-6 (n = 5), and **D**) TNF $\alpha$  (n = 5) were measured with specific ELISAs. No significant difference in comparison to time 0 baseline were seen.

While LPS induced significant increases in each of the cytokines of interest, there was no significant difference between biomaterials in either unstimulated or LPS-stimulated cytokine responses although elevated levels of IL-6 and TNF $\alpha$  in unstimulated samples were seen with ZTA.

#### *3.4.5.4 Leukocyte adhesion*

Leukocyte adhesion is the final piece of the puzzle into how biomaterials affect leukocytes. Decrease in platelet and monocyte counts as well as the monocyte activation seen in some of the materials indicated that these cells had become adhered to the biomaterial.

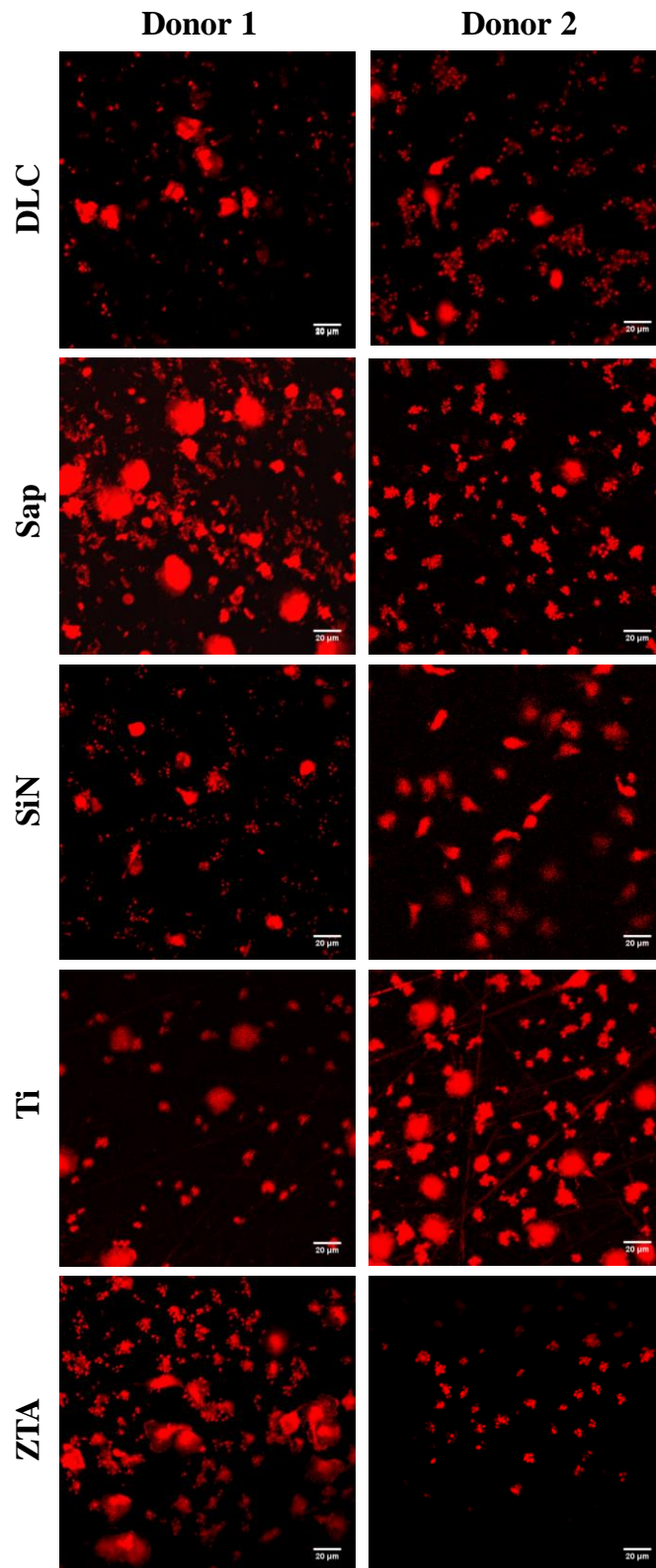


**Figure 3.17: Confocal microscope images of leukocytes present on rough titanium.**

A disc of titanium alloy with a rough surface was incubated with whole human blood for 2 hours. After rinsing, the disc was fixed with 1% glutaraldehyde solution and stained with CyTRAK Orange. A coverslip was taped onto the disc and the sample analysed using the confocal inverted microscope using the **Ai**) 405nm diode (blue), **Aii**) 488 nm argon, and **Aiii**) 633 nm HeNe laser **Aiv**) shows the merged image with the grooves in the titanium fluorescing blue whilst the nuclei of leukocytes are stained red shown in **(B)**. The disc was cleaned and re-imaged to ensure no cellular debris was left shown in **(C)**.

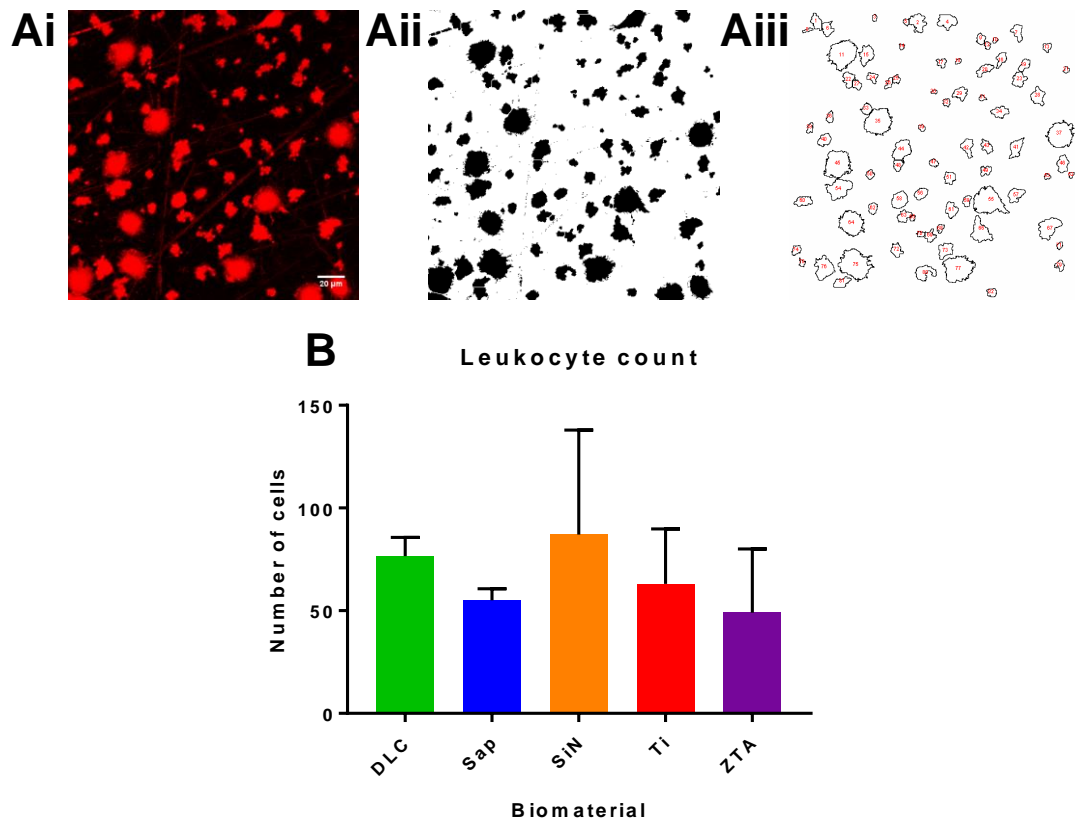
Imaging of reusable opaque materials is very difficult and required some careful consideration. The solution was to stick a coverslip onto the material and lay it face down onto the lens of the confocal microscope. It was then vital that the lens did not scrape along the biomaterial and as it was impossible to focus on cells with bright-field, getting into the right plane was a case of trial and error. The autofluorescence of the materials was also problematic so manipulation of the laser gains was necessary. Fortunately, all the biomaterials (except ZTA) had large blue autofluorescence (Figure 3.17Ai) and minimal fluorescence in the green and red laser channels.

The biomaterials were fixed in 1% glutaraldehyde post-incubation with human blood with the intention of detecting platelets using the glutaraldehyde-induced fluorescence technique (GIFT). The reaction of GIFT is not fully understood but may be related to the formation of Schiff bases by cross-linking with free amino groups of proteins and phospholipids (207). GIFT has the advantage of being simple and inexpensive due to it not requiring antibodies/stains to detect platelets – particularly on such a large surface as the discs – and causes platelets to fluoresce in the green channel. Despite the use of GIFT in other publications, it did not appear to work here in combination with these biomaterials as there are no green areas the size of platelets ( $\sim 2 \mu\text{m}$ ) observable (Figure 3.17Aii), potentially due to the maximum magnification of x40 available for use with the discs.



**Figure 3.18: CyTRAK Orange positive leukocytes present on the biomaterial discs**

All biomaterial types were incubated for 2 h with human blood, rinsed, fixed with 1% glutaraldehyde, and stained with CyTRAK Orange. The nuclei of the leukocytes are stained red and the number of leukocytes present varies depending on biomaterial type.



**Figure 3.19: ImageJ analysis and leukocyte counts on biomaterials**

Images acquired on the confocal microscope (**Ai**) were converted to black and white (**Aii**) images with holes filled in and lines put between cells using the ‘watershed’ function (**Aiii**). The number of cells was counted using the ‘analyse particles’ function and displayed as a graph ( $n = 2$ ) (**B**).

Despite the set-back with the platelet analysis, CyTRAK Orange worked well to stain the nucleus of leukocytes adhered to the discs. Getting the correct focus using the red laser was challenging but it was possible to identify neutrophils from their multi-lobed nucleus (Figure 3.17: DLC & SiN) and likely monocytes adhered to the discs. Counting of CyTRAK Orange positive cells was achieved using ImageJ (Figure 3.19). There was no significant difference observed between the cell counts on the discs.

### 3.5 Discussion

Rapid, robust, and affordable screening approaches for assessing the potential total blood damage effects of multiple biomaterials are desired to minimise adverse events in medical device patients. The model developed here allows for red blood cells, platelets, and leukocytes to be studied simultaneously in an experimental system which is recognised by the International Standards (208). The biomaterial discs used in this study were manufactured to have a smooth surface and were cleaned thoroughly to reduce the presence of contaminants; endotoxin levels were below 1 EU/mL. The method was designed to allow the effects of the biomaterials to emerge without requiring complicated experimental rigs. Initial time course analysis revealed that incubation times longer than 2 hours introduced time-related artefacts, thus more detailed analysis was performed at the 2 h time-point for the rest of the study. Two hours may seem like a relatively short period, but it allows robust early stage evaluation and a comparison of the biomaterials of interest before progressing to more complex studies incorporating experimental conditions better representative of the *in vivo* scenario where residence time is transient but repetitive. Importantly, the model used also allows the research question to be refined based on these early stage findings. Reasonable volumes of blood can be used in this model to reveal functional impact on the cells of interest. Scalable experimental approaches and flow cytometry are useful for this purpose.

The titanium alloy Ti6Al4V is the biomaterial of choice for the VAD body (186) and is therefore the largest surface area for blood contact. Titanium can be thrombogenic by promoting the formation of a surface protein matrix composed of fibrinogen, thrombin, complement factors, and coagulation cascade proteins such as kallikrein that encourages cell activation and adhesion (175). In this study, titanium caused a significant decrease in platelet count, but no measurable platelet activation nor platelet aggregates, and no effects on erythrocytes or leukocytes. This correlates with the results from Chang & Gorbet who demonstrated that there was no increase in platelet activation or platelet-neutrophil/platelet-monocyte aggregates in whole blood flowing over a TiAl64V wire under shear stress ( $100\text{ s}^{-1}$ ) did not significantly increase platelet activation nor platelet-neutrophil/platelet-monocyte aggregates (209). Titanium can also cause high levels of TNF $\alpha$  (~600 pg/mL) in PBMCs cultured for 24 h (210) and

a reduction in TNF $\alpha$  in MNCs stimulated with LPS (211) which was not observed in this study. However, titanium disc implants in rats have shown low levels of TNF $\alpha$  (~25 pg/mL), IL-1 $\beta$  (~15 pg/mL) and IL-1 $\alpha$  (~100 pg/mL) in the exudate after 1 h and even 3 h (183) further promoting the need to test these biomaterials with whole blood rather than isolated cells to mimic the *in vivo* response.

Ceramic materials such as Sap, SiN and ZTA used in this study are desirable bearing materials due to their potential to resist wear damage, their hardness, and their wettability (212, 213). Biocompatibility testing of these materials has so far been limited to bone growth (214), tissue implantation (189), or protein adsorption (215, 216). This study is the first to analyse the effects of these materials on blood cells using whole blood. We found monocytes were the most affected cell type with a significant decrease in number when exposed to SiN and ZTA and a decrease in monocyte expression of CD62L on Sap and ZTA. All ceramic biomaterials showed a decrease in platelet count. It is possible that these cell types are adhering to the discs. Use of these materials as VAD bearings, could lead to the build-up of thrombus such as that seen in the single-crystal alumina (ruby) bearing of the HeartMate 2 (87, 191).

To overcome biocompatibility issues in mechanically desirable materials, coatings with excellent biocompatibility have been introduced. DLC is one such coating which rapidly adsorbs albumin and inhibits fibrinogen adsorption (191) so strongly reduces platelet adhesion and activation, prolongs clotting time, and suppresses complement convertase activation (193). In this study, DLC exposure was associated with a significant decrease in monocyte and platelet count and decreased monocyte CD62L expression – a response like that of the ceramics indicating some monocyte activation. DLC has been shown to slightly increase monocyte adhesion (217), with DLC coated Ti6Al4V favouring cell adhesion over uncoated (218) as well as platelet retention (219).

Due to the findings that platelets and monocytes are the key cell target type, ongoing work involves optimising methods for visualising cells adhered to the biomaterial surface. A limitation of this study is the continued contact of the blood cells with the biomaterials when residence time would normally be measured in milliseconds rather than hours, and the absence of shear stress. The findings prompted the addition of shear stress to the model using a rheometer in the next chapter (Chapter 4). A real value of



the simple model we describe here will be the ability to use blood from heart failure patients of which only a limited volume will be available. The use of blood from the target patient group is critical as pre-existing inflammation with chronic heart failure means that leukocytes, particularly monocytes, are already activated (10, 220). Platelet activity might also be elevated (221) which could affect biomaterial interaction. This possibility has been described: platelet adherence on low and medium thrombogenic polymer-based biomaterials was increased for patients with coronary artery disease compared to healthy controls (222).

### 3.6 Conclusion

Assessing the biocompatibility of any materials involved in medical devices is needed to progress their design and minimise patient complications. This simple yet effective model provides a useful screening tool to evaluate how various blood cell populations interact with biomaterials used in blood-handling devices such as VADs, especially in the target patient population. It allows quick identification of the cells most susceptible to activation by a certain biomaterial – such as monocytes exposed to DLC and the ceramics – using powerful techniques such as flow cytometry that enables the study of multiple cell populations in small sample volumes. These methods also go further than the tests recommended by the International Standards providing a more thorough look at the leukocyte response, such as cytokine release, which is important when designing a device for patients with a disease characterised by inflammation. These techniques can then eliminate biomaterials with poorer biocompatibility and focus the research and development of blood-handling devices during *in vitro* and *in vivo* testing.

# Chapter 4 Shear stress cell activation and damage

## 4.1 Introduction

### 4.1.1 Definition of shear

#### 4.1.1.1 Newtonian and non-Newtonian Fluids

A fluid is a substance that will deform continuously under force. Fluids can be described as Newtonian and non-Newtonian. A Newtonian fluid remains at a constant viscosity regardless of any external stressors placed upon it such as mixing or sudden force application (223). Water is considered Newtonian as its viscosity remains constant, no matter how much shear is applied. This is a linear relationship between the viscosity and shear stress (223).

In contrast, a non-Newtonian fluids viscosity will change under the application of shear stress. The simplest example of a non-Newtonian fluid is corn-starch mixed with water whereby impacting a force will cause the atoms to rearrange and the solution to behave like a solid. This is called ‘shear-thickening’ whereas ‘shear-thinning’ has the opposite effect where impacting a force causes the fluid to behave like a liquid, such as paint, ketchup, and toothpaste (223).

When modelling rotary blood pumps, it is common practice to assume blood is Newtonian to ease simulations and experiments. However, blood viscosity depends on haematocrit, temperature, and concentration of plasma proteins, which are all affected by specific flow conditions (224). Cellular distribution also changes depending on vessel diameter with smaller diameters (such as capillaries) causing cells to accumulate in the centre and lowering the viscosity (224). Erythrocytes have the unique mechanical properties of deformability and reversible aggregation during stasis which is why blood is a non-Newtonian fluid.

#### 4.1.1.2 Laminar and turbulent Flow

Laminar flow occurs when fluid travels smoothly in a regular path where the velocity, pressure, and other flow properties at each point in the fluid remain constant. Laminar flow over a horizontal surface can be thought of as flowing in thin layers, or laminae, all parallel to each other. This type of flow is common only in places where the flow channel is relatively small, moving slowly, and the viscosity is high. Blood flow through a capillary is laminar (225).

Turbulent flow is more common and is defined as a type of fluid which undergoes irregular fluctuations where the flow speed at a point is continuously changing in direction and magnitude appearing random. Wind and river flow are considered turbulent as is the flow of blood in arteries (226).

#### 4.1.1.3 Shear rate, shear stress, and viscosity

Shear rate ( $\gamma$ ) is defined as the gradient of velocity in a flowing fluid in reciprocal seconds (Equation 1). It can be thought of as the change in velocity between adjacent laminae of fluid passing over each other divided by their separation (227).

#### Equation 4.1: Shear rate equation

$$\gamma = \frac{dV}{dx}, \text{ units} = \text{s}^{-1}$$

Shear stress ( $\tau$ ) is the force acting per unit area between adjacent laminae (units = Pa), also thought of as the drag force between laminae (227).

Viscosity is defined as the internal resistance to flow, or friction between laminae in the flow. In fluids, viscosity is defined in terms of shear rate ( $\gamma$ ) and shear stress ( $\tau$ ) (Equation 2) (227).

#### Equation 4.2: Viscosity equation

$$\eta = \frac{\tau}{\gamma}$$

Trauma to the formed elements in blood (leukocytes, erythrocytes, platelets, and proteins) is influenced by both the magnitude of shear stress and the exposure time.

### *4.1.2 Physiological shear stress*

Arteries consist of several layers of tissue, the intima which contacts the blood flow, with the media and adventitia providing mechanical support. The pulsatile blood pressure originating from the heart drives blood throughout the vascular system causing wall shear stress on the endothelial layer of the vessels. This frictional force is opposed by the tension, stretch, and deformation of the endothelium. The flow and pressure of the blood results in internal stressors and deformation of the vessel wall components such as fibrin and cells which trigger and release biochemical reactants that maintain the physical function of the blood vessels. This ability to deform under stress is related to the remodelling of blood vessels under extra strain from hypertension, diabetes, and atherosclerosis (228).

Cells can counteract the effect of shear stress through rearranging their cytoskeleton. Physiological shear stress values vary from 0.05-12 Pa depending on the vessel type and the size of the organism. In large arteries, the shear stress range is 1 – 4 Pa (229), and in large veins 0.1-0.5 Pa (230).

### *4.1.3 Shear stress on blood components*

#### *4.1.3.1 Erythrocytes*

Erythrocytes (or red blood cells; RBCs) are the largest constituent of blood and have a normal lifespan of 120 days in a healthy person (61). Haemolysis is the premature damage to these cells and the body can adapt to some haemolysis, but in excess can lead to haemolytic anaemia (231). The release of plasma free haemoglobin due to haemolysis can also lead to kidney damage due to nephrotoxicity (232). Four basic mechanisms encompass both pathological and mechanical inducers of haemolysis: colloid osmotic lysis; perforation of the cell; excessive deformation or fragmentation of RBCs; and erythrophagocytosis. Deformation and fragmentation is the most important when it comes to the effects of shear stress on RBCs. High shear ( $\geq 600$  Pa caused by medical devices (81)) leads to leakage of plasma free haemoglobin through small, reversible openings in the membrane, but catastrophic shear causes rupturing (233). The viscoelastic behaviour of RBCs means that their susceptibility to lysis is influenced not only by shear stress, but time exposure.

#### 4.1.3.2 *Proteins*

Von Willebrand Factor (vWF) is a protein in the blood which is sensitive to shear stress and linked to gastrointestinal bleeding in VAD patients (234). vWF is a large multimeric glycoprotein which circulates in varying sizes (between 500 and 20000 kDa) in the blood plasma. It is produced in the Weibel-Palade bodies of the endothelium and the  $\alpha$ -granules of platelets (104). The primary function of vWF is to bind proteins and platelets together at wound sites to repair damage. Deficiency of vWF leads to patients tending to bleed (235). High shear due to disease or a medical device can lead to acquired von Willebrand syndrome (AVWS) due to the mechanical degradation of high molecular weight into low molecular weight vWF (236). Controversially, most LVAD patients have AVWS, but not all of them have clinically relevant bleeding complications (105).

#### 4.1.3.3 *Platelets*

Thrombus formation is problematic in mechanical devices such as mechanical heart valves. The flow conditions of these devices lead to the disruption of haemodynamic conditions which briefly exert high shear stresses (10-800 Pa) on platelets (237, 238). In a study by Sheriff et al., platelets exposed briefly to high shear stress (6 Pa for 40 s) showed some activation but when platelets were exposed to lower shear stress alone they became activated 20-times faster than those that had not been exposed to higher shear first (81). This is defined as platelet sensitisation and can be very problematic in terms of thrombus formation.

#### 4.1.3.4 *Leukocytes*

Work on the effects of shear stress on leukocytes is sparse. In the 1970s, Dewitz et al., used a concentric cylinder viscometer to shear whole blood for 10 min. This caused a significant impact on white blood cell viability, count, and enzyme release in the range of 10 – 60 Pa, much lower than critical for red blood cells (239, 240). Rotary blood pumps tested for 6 h with human blood have also shown white blood cell damage through trypan blue exclusion further suggesting white blood cells are more vulnerable to mechanical trauma than red blood cells (241).

Human leukocytes respond to fluid shear stress by retraction of pseudopods (lamellipodia, filopodia, and other forms) and membrane detachment (242). This

response serves as a key mechanism to maintain circulatory leukocytes in spherical shape without pseudopod formation preventing trapping in capillaries and allowing normal passage through microcirculation (243). During inflammation, adherent leukocytes must produce pseudopodia to migrate across the endothelium into the tissue which indicates that there is a fundamental regulatory mechanism for leukocyte shear stress response in inflammation. Application of shear stresses ( $\sim 1.5 \text{ dyne/cm}^2$  or  $0.15 \text{ Pa}$ ) on adherent leukocytes on a glass surface caused instant pseudopod retraction irrespective of the shape of the pseudopod. The number of leukocytes with pseudopod formation without treatment was significantly decreased by application of shear stress ( $5 \text{ dyne/cm}^2$  or  $0.5 \text{ Pa}$ )(243).

Shive et al., used scanning electron microscopy (SEM) to show that the phagocytic ability of neutrophils diminishes under high shear stress ( $> 0.6 \text{ Pa}$ ) in comparison to low shear stress ( $0 - 0.2 \text{ Pa}$ ) through scanning electron microscopy (SEM). The method used involved seeding bacteria onto cardiovascular device materials, adding isolated neutrophils to the discs and then subjecting them to shear. The SEM revealed that neutrophils subjected to high shear stress were apparently incapable of interacting with the bacteria, becoming compact and irregularly-shaped, with condensed nuclei and F-actin (used for pseudopod extension in phagocytosis). Those subjected to lower shear stresses maintained the characteristic multi-lobed nuclei with a larger, more spread morphology and retained bactericidal activity (185). Another study identified an immediate retraction of neutrophil pseudopodia at the application of  $\sim 0.4 \text{ dyne/cm}^2$  and neutrophil granule velocity significantly enhanced by shear stress ( $1 \text{ dyne/cm}^2$  or  $0.1 \text{ Pa}$ ) *in vitro* (242). The continuous application of shear stress enhances random granule velocity and reduction in cell stiffness. These phenomena suggests that shear stress mediates water entry into the cell thereby reducing F-actin (242), causing cell swelling/lysis (239), and depression of proliferative responses in T cells (244).

Pseudopod retraction by leukocytes in response to shear stress is suppressed at elevated concentrations of inflammatory mediators such as platelet activating factor (PAF) and formyl-methionyl-leucyl-phenylalanine (FMLP). After stimulation with inflammatory mediators, the number of leukocytes that retract their pseudopods after exposure to fluid shear stress is reduced in a dose-dependent manner (243). This response is of interest to VAD developers as heart failure is an inflammatory disease and the

leukocyte response to the additional pump shear stress is likely to be different to that of a healthy patient.

#### *4.1.4 Medical device shear stress*

Elevated shear stress is a common factor affecting blood contacting medical devices. VADs and other cardiovascular devices cause artificially high shear-stresses held responsible for adverse bleeding events due to von Willebrand factor degradation (1.8.3 Bleeding). There are also oxygenators which exchange oxygen and carbon dioxide in the blood during cardiopulmonary bypass (CPB), and haemodialysis machines for those suffering kidney failure that expose blood to high shear stresses. A study on three different designs of oxygenator which had different levels of shear stress across the oxygenator did not show significant differences in haemolysis but did show an increase in white blood cell count in all three designs (245). This was not thoroughly investigated but the shear stress in the oxygenators was well below the critical value of 200 – 300 Pa for haemolysis but over that tolerated by platelets and white blood cells (245). Another study comparing hollow fibre and flat sheet membrane oxygenators measured a significant increase in elastase, a leukocyte activation marker, in the flat sheet at the end of CPB compared to baseline (246). Haemorheologic alterations have also been cited in haemodialysis patients who have increased plasma volume, whole blood viscosity, and haematocrit and show erythrocyte shape changes, decreased RBC aggregation and increased platelet aggregation (247, 248).



## 4.2 Objectives

This chapter investigates shear stress as a vital component and contributor to adverse events in VADs. The work aims to identify the effect shear stress has on leukocytes through the following:

- To use the CentriMag™ at different operating conditions to measure the effect of continuous-flow shear on leukocytes and other blood components.
- To evaluate the biomaterials used in static conditions with whole blood in a shear environment using a rheometer.
- To measure the effect of the biomaterial/shear stress combination on leukocytes activation and evaluate effect on leukocyte function.
- Use the results to make recommendations to the development of the MiniVAD.

## 4.3 Methods

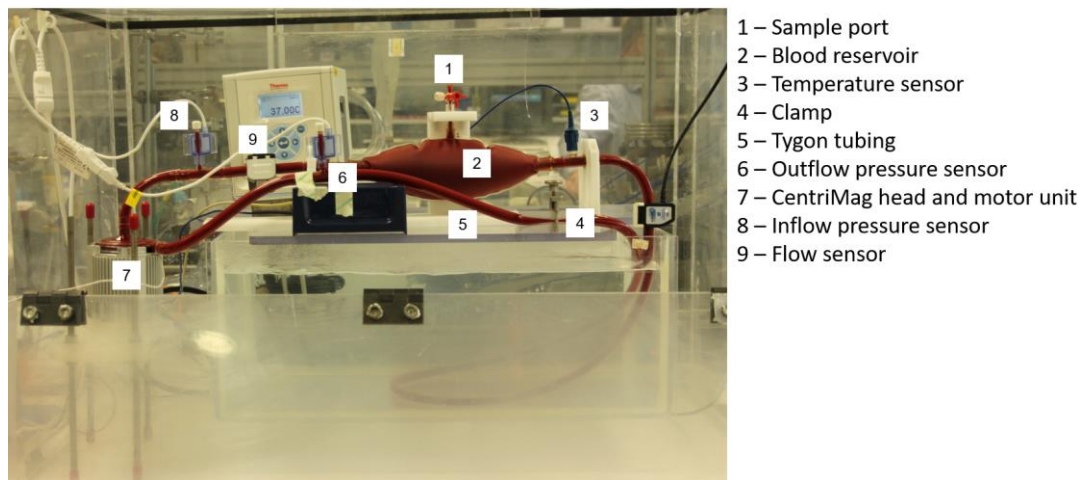
### 4.3.1 CentriMag™ at different operating conditions

#### 4.3.1.1 Blood collection

See 2.3.1.3 Ovine venepuncture.

#### 4.3.1.2 Loop set-up

The test loop is set up using a custom designed blood reservoir with a 3-way luer sample port attached to the CentriMag™ head (Thoratec, Pleasanton, CA, USA) using 2 m Tygon tubing (12.7 mm x 9.5 mm, Fisher Scientific). Pressure (PRESS-S-000, PendoTECH, Princeton, NJ, USA) and temperature sensors (PendoTECH) were attached to the loop using a barbed tee fitting luer as well as an ultrasonic flow sensor (ME8-PXL, Transonic Systems Inc., Ithaca, NY, USA) hooked on to the loop (Figure 4.1). The blood bladder bag was suspended on a mount over a water bath with part of the loop submerged.



**Figure 4.1: The mock circulatory loop**

1x PBS solution (Fisher Scientific) is filled into the loop and run for 20 min then removed prior to test. Bovine blood from the local abattoir that had the haematocrit adjusted to  $30 \pm 2\%$  using PBS (Life Technologies) was gravity-filled into blood bags and then drained into the loop ensuring all air was removed via the sampling port. Pressure and flow were adjusted using a clamp to comply with the ASTM and this was monitored throughout the testing period along with temperature and speed. Static

blood contained in a bag in a +37°C water bath was included as a negative control. Blood samples were removed 5 min after the start of the test and every hour for the 6-hour duration. The first 1 mL of blood drawn using a syringe was discarded, then a further 5 mL was drawn, and this was spilt into 4 tubes for assays.

#### 4.3.1.3 *CentriMag operating conditions*

The extracorporeal ventricular assist device CentriMag® CP (Abbott Vascular, Santa Clara, CA, USA) was tested using an *in vitro* testing circuit under constant haemodynamic conditions using three different operating conditions: herein called *standard*, *low flow*, and *high speed*. The *standard* operating conditions have been described in detail elsewhere (63) and followed the ASTM standards (152, 249). Briefly, the flow rate was  $5 \pm 0.25$  L/min, the differential pressure across the pump was adjusted using a custom-made clamp to  $100 \pm 3$  mmHg, and the speed was 2,200 rpm. The *low flow* condition differed by using a flow rate of  $1 \pm 0.25$  L/min, and the *high speed* condition differed by using 3,300 rpm.

#### 4.3.2 *Rheometry*

##### 4.3.2.1 *Blood collection*

See 2.3.1.1 Human.

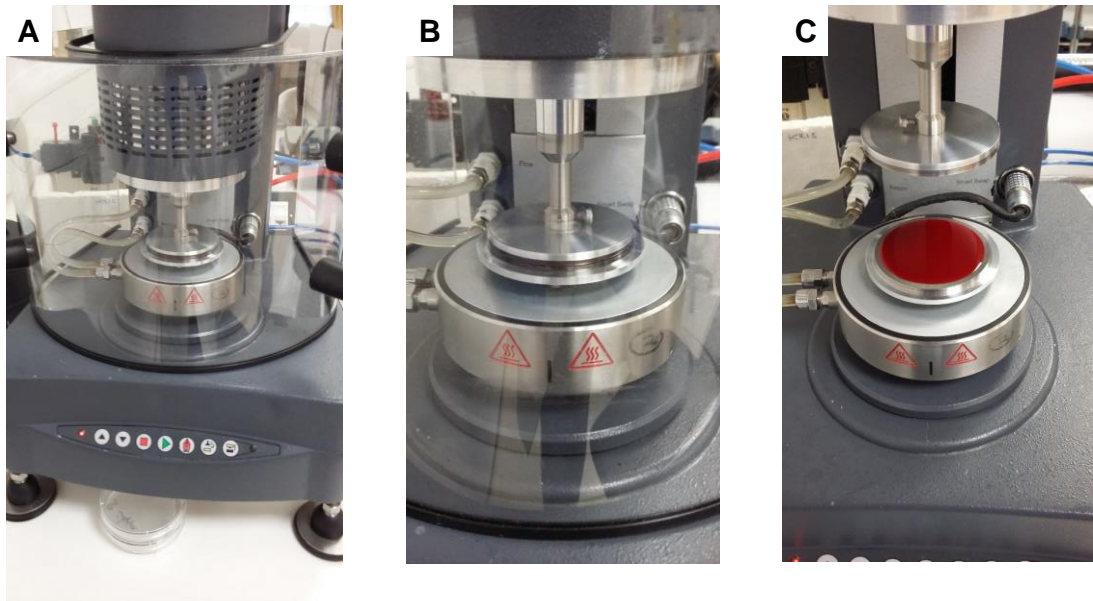
##### 4.3.2.2 *Calibration*

The ARG2 rheometer (TA Instruments, New Castle, DE, USA) was used to create shear stress. The rheometer was calibrated through measuring the instrument inertia and then a 60 mm parallel Peltier plate (aluminium) was attached. The Peltier inertia and friction were calibrated before bringing the Peltier down to the plate geometry to set the ‘zero gap’. Once the ‘zero gap’ had been calculated by the machine, final calibration for the rotational mapping was completed (standard, 2 iterations).

##### 4.3.2.3 *Shearing whole blood between parallel plates and biomaterials*

Using the TRIOS software (TA Instruments) a procedure was set up for the use of the 60 mm parallel Peltier plate with the environment set to +37°C. The gap between geometry plate and Peltier plate was set to 400 µm which would allow approximately

1.2 mL of blood to be pipetted onto the surface. The soak time was set to 30 secs, the duration set to 300 secs, and the shear rate used was either  $0\text{ s}^{-1}$  or  $1000\text{ s}^{-1}$ . The blood was added and then the Peltier brought down to the 'loading gap' for the procedure to begin. After shearing, as much blood as possible was removed from the surface yielding  $\sim 500\text{ }\mu\text{L}$  for analysis.



**Figure 4.2: Rheometer model**

**A & B)** Biomaterial discs (Ti here) were attached in parallel to the geometry (bottom plate) and Peltier (top plate) using crystal bond adhesive. Blood was placed between the biomaterial discs for 5 min at  $+37^{\circ}\text{C}$  with/without shear ( $0\text{ s}^{-1}$  /  $1000\text{ s}^{-1}$ ). Sample was pipetted from the surface after elapsed time **(C)**.

Attachment of the biomaterial discs required heating the geometry plate to  $+80^{\circ}\text{C}$  and applying Crystal Bond Adhesive (Agar Scientific, Stanstead, UK) with a melting temperature of  $+66^{\circ}\text{C}$ . One biomaterial disc was laid onto the geometry, the other glued to the Peltier. Adjustments were made so that the discs were parallel with one another and then the geometry temperature brought down to  $+25^{\circ}\text{C}$ . Calibration for the Peltier was performed as above between samples to ensure the rheometer was balanced and inducing the correct level of shear.

### 4.3.3 Flow Cytometry

#### 4.3.3.1 Leukocyte microparticles

20  $\mu$ l blood samples from time points 5, 120, 240, and 360 min were stained with 0.2  $\mu$ g CD45-PE, clone 1.11.32, mouse IgG1 (Thermo Fisher Scientific) for 30 min on ice in the dark. The red blood cells were lysed by adding 600  $\mu$ L EasyLyse (1:20 with dH<sub>2</sub>O, DAKO, Alere, Cheshire, UK), followed by vortexing and 15 min incubation at room temperature in the dark. Necrotic cells were stained with 0.1  $\mu$ g 7AAD solution (eBioscience) at room temperature in the dark for 15 min before acquisition. As a positive control for 7AAD staining of dead cells, 1 ml baseline blood was treated with 3  $\mu$ M staurosporine solution (Sigma Aldrich) at room temperature for at least 4 h prior to staining with CD45-PE and 7AAD. Untreated blood single-stained CD45-PE and was used to set the 7AAD-gate.

Leukocytes were gated and displayed on a contour density dot plot with 7AAD against CD45-PE. The healthy cell gate was set using the Staurosporine-treated control to just outside the main contour of the healthy 7AAD-negative population. Any events to the right of this border were considered 7AAD-positive necrotic leukocytes. Fragmented white blood cells (LMPs) still display CD45 but no longer contain DNA and because of their reduced size and complexity, and therefore lower side scatter, end up below the healthy leukocytes in the gate designated CD45<sup>+</sup> MP (Appendix Figure 8.5).

#### 4.3.3.2 Activated leukocyte microparticles

20  $\mu$ l blood samples from time points 5, 120, 240, and 360 min were stained with a panel including activation and lineage markers. The antibodies used were 2  $\mu$ g anti-CD11b-FITC (clone CC126, IgG2b, AbD Serotec), 0.1  $\mu$ g anti-CD21-PE (clone LB21, IgG1, AbD Serotec) (250), 0.1  $\mu$ g anti-CD14-BDV500 (clone M5E2, IgG2a,  $\kappa$ , BD Bioscience), and 3 pg anti-HLA-DR-PE-Cy7 (clone LN3, IgG2b,  $\kappa$ , eBioscience).

The gating strategy was drawn using the baseline samples and comparing the pattern differences to the pumped samples which were obvious. FMOs for all antibodies, and isotype controls for the activation markers CD11b and HLA-DR, were prepared but

did not prove useful in this lyse, no wash protocol. Isotype controls were useful for setting the gates for the cells but not the microparticles.

#### 4.3.3.3 *Neutrophil and monocyte activation*

Whole blood (20  $\mu$ L) was stained with CD14, CD15, CD62L, and CD11b and processed as in 3.3.7.3.

#### 4.3.3.4 *Phagocytosis*

BioParticles (*E. coli* K-12 strain, fluorescein conjugate, Thermo Fisher) were reconstituted in PBS with sodium azide added to a final concentration of 2 mM. The BioParticles were vortexed 3 x 15 secs and then sonicated 3 x 20 secs. Number of BioParticles per  $\mu$ L were counted using CountBright beads (described in Chapter 2). Initial optimisation experiments used 100:1 and 10:1 ratios of BioParticle to leukocyte which indicated that 10:1 gave optimal fluorescence to continue with (Appendix Figure 8.7).

Whole blood was added to FACS tubes and 10  $\mu$ L of BioParticles (diluted 1:10 with PBS) was added. Samples were incubated in a shaking water bath set to +37°C for 30 min. Phagocytosis was stopped through the addition of 2.5  $\mu$ L cytochalasin D (final concentration 200 nM, Sigma). Tubes were then placed on ice and 3 mL ice cold PBS added before centrifugation (+4°C, 515 xg, 7 min). Supernatants were discarded and the tubes washed in ice cold PBS again. Blood was stained with CD14-PB and CD15-VG (see 3.3.7.3). 3 mL FACS lyse (BD Bioscience) was added and samples vortexed vigorously to encourage full lysis of red blood cells. Samples were incubated for 15 min in the dark on ice then centrifuged. Samples were then washed in 1 mL ice-cold PBS with 12.5  $\mu$ L 0.2  $\mu$ m-filtered trypan blue (251). Samples were then fixed in 200  $\mu$ L FACS fix (BD Bioscience).

#### 4.3.3.5 *Radical Oxygen Species assay*

Stock solution of ROS assay stain concentrate (eBioscience) was reconstituted in 40  $\mu$ L of DMSO and stored in aliquots at -20°C. ROS assay stain stock was diluted with 1X ROS assay buffer (eBioscience). 100  $\mu$ L of 1X ROS assay stain was added per 1 mL blood and incubated for 60 min at +37°C, 5% CO<sub>2</sub>. Blood stimulated for 60 min

with 1  $\mu$ M phorbol 12-myristate 13-acetate (PMA) was used as a positive control. Stained blood was then sheared as per 4.3.2.3. 20  $\mu$ L of sheared blood sample was added to a tube, red blood cells lysed using EasyLyse, and then acquired on the Navios flow cytometer. The median fluorescence intensity of ROS was measured in the FL1 (FITC) channel.

#### 4.3.4 Cytokine analysis

##### 4.3.4.1 Whole blood cultures

See 3.3.8.1.

##### 4.3.4.2 Proteome profiling

All reagents were brought to room temperature before proceeding with the Human Cytokine Proteome Profiler Array (R&D Systems) as per manufacturer's instructions. In brief, each membrane was incubated for 1 h with Array buffer 4 serving as a blocking buffer. Whole blood culture supernatant (200  $\mu$ L) was added to 500  $\mu$ L Array buffer 4 and adjusted to a final volume of 1.5 mL with Array buffer 5. Reconstituted Human Cytokine Array Detection Antibody Cocktail (15  $\mu$ L) was added to each sample and incubated for 1 h. Samples were then incubated overnight at +2-8°C in dishes containing the membranes. Membranes were washed the following day 3 times in 1X wash buffer for 10 min each then 2 mL diluted Streptavidin-HRP (1:2000 with Array Buffer 5) added to each membrane for 30 min. Membranes were washed 3 times again and then membranes incubated for 1 min with Amersham ECL Western Blotting Detection Reagent (GE Healthcare). Membranes were exposed for 10, 30, 60, and 120 secs on the ChemiDoc XRS Scanner (Universal Hood II, Bio-Rad, CA, USA). Pixel intensity was calculated using ImageJ and the negative control subtracted from each dot to obtain relative pixel intensity used for graphs and statistical analysis.

##### 4.3.4.3 ELISA

Cytokines of interest were identified on the proteome profile and chosen for further analysis with ELISA. Levels of MIF (Human MIF DuoSet, R&D Systems) and IL-1 $\alpha$  (Human IL-1 $\alpha$  DuoSet, R&D Systems) were measured using specific ELISAs.

#### 4.3.5 *Data and statistical analysis*

Flow cytometry data was analysed as described in 3.3.10. Comparisons between samples were analysed using two-way ANOVA with multiple comparisons. Dunnett's test was applied *post hoc*. A p value of  $\leq 0.05$  was considered significant.



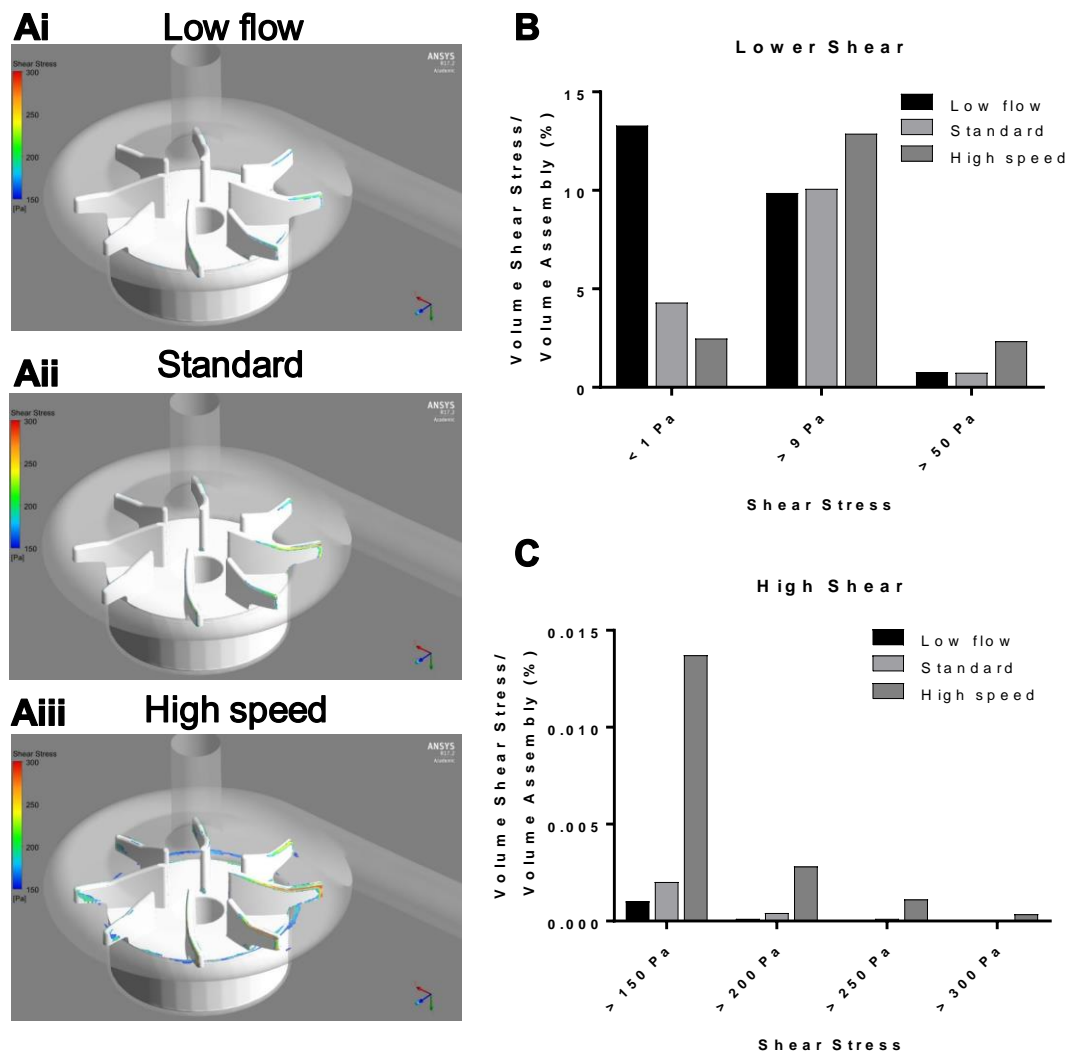
## 4.4 Results

### 4.4.1 *The effect of different CentriMag operating conditions on ovine blood*

Ovine blood was run through a mock circulatory loop powered by the CentriMag at 3 different operating conditions (Table 4.1) to induce different levels of shear (Figure 4.3).

**Table 4.1: CentriMag operating conditions**

	<b>Low flow</b>	<b>Standard</b>	<b>High speed</b>
<b>Speed (rpm)</b>	2200 ± 0	2200 ± 82	3300 ± 0
<b>Flow (L/min)</b>	1.00 ± 0.03	5.03 ± 0.08	4.96 ± 0.06
<b>Pressure (mmHg)</b>	105.29 ± 1.91	82.98 ± 4.59	212.23 ± 19.14
<b>Milligrams normalised index of haemolysis (mgNIH) at 360 min</b>	1.05 ± 0.89	0.38 ± 0.15	2.82 ± 2.80
<b>Baseline haematocrit (%)</b>	30.33 ± 2.57	30.78 ± 1.49	29.25 ± 3.88
<b>Baseline haemoglobin (g/L)</b>	116.27 ± 15.55	116.03 ± 15.05	108.11 ± 12.36
<b>Sample size (n)</b>	4	5	5



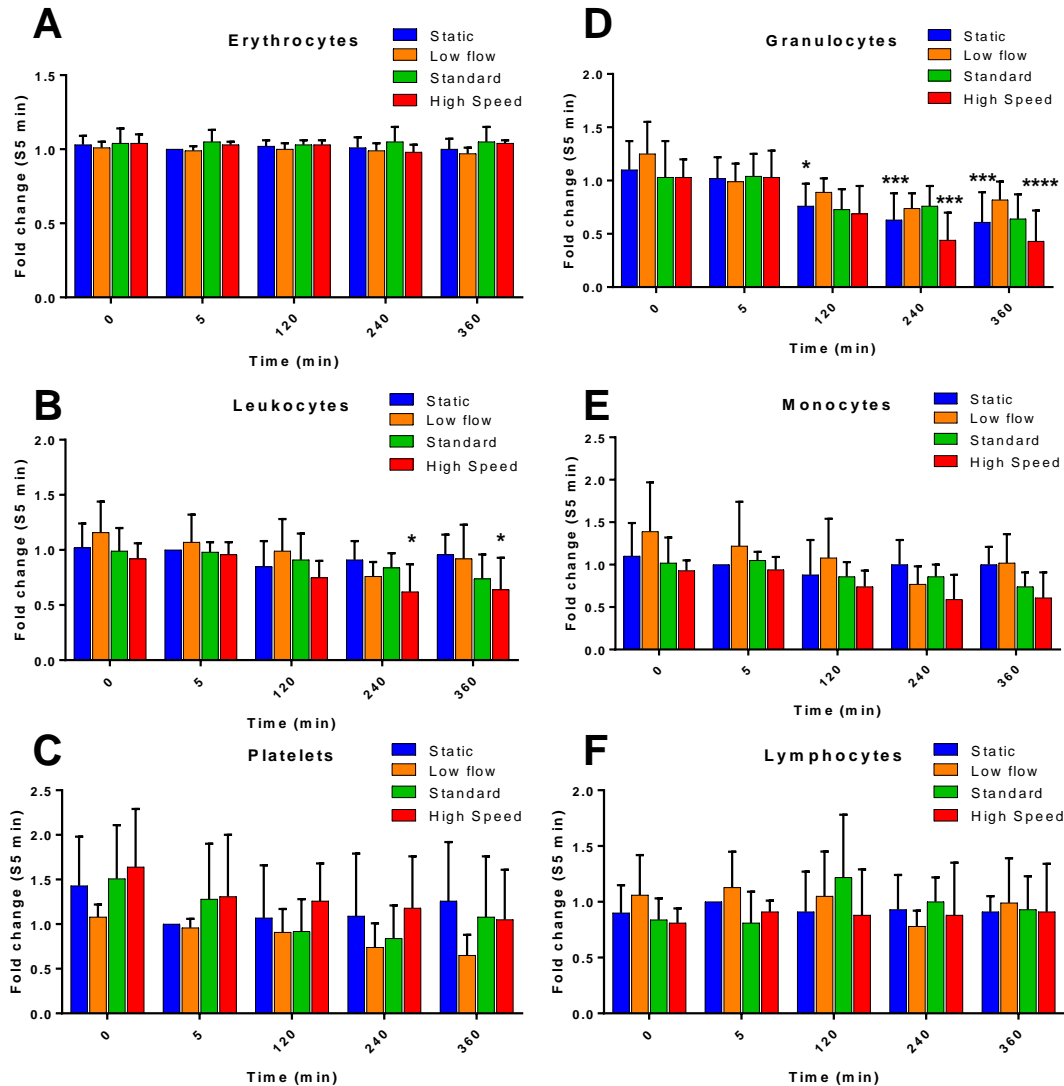
**Figure 4.3: Computational fluid dynamic results of shear in the CentriMag™**

**Ai-Aiii)** CFD images of each operation condition in the CentriMag™ showing areas of shear stress. **B)** Graph of areas with lower shear stresses and **C)** graph of areas with higher shear stresses in that one simulation. Images provided courtesy of A. Molteni (CFD engineer, Calon Cardio – Technology Ltd.)

#### 4.4.1.1 Haematology

The first indicator of the effect these different operating conditions had on blood cells was measured through complete cell counts (Figure 4.4). There was no significant difference in the erythrocyte count for static or pumped samples. Leukocyte counts at 240 min and 360 min were decreased significantly in the *high speed* condition ( $p = 0.026$  &  $0.047$  respectively). Granulocyte count was significantly decreased in the static at 120, 240, and 360 min samples ( $p = 0.048$ ,  $0.0003$ , &  $0.0001$ ) and in the *high*

*speed* condition at 240 and 360 min ( $p = 0.0001$  &  $< 0.0001$  respectively) in comparison to baseline. There was no significant change in monocyte, lymphocyte, nor platelet count.

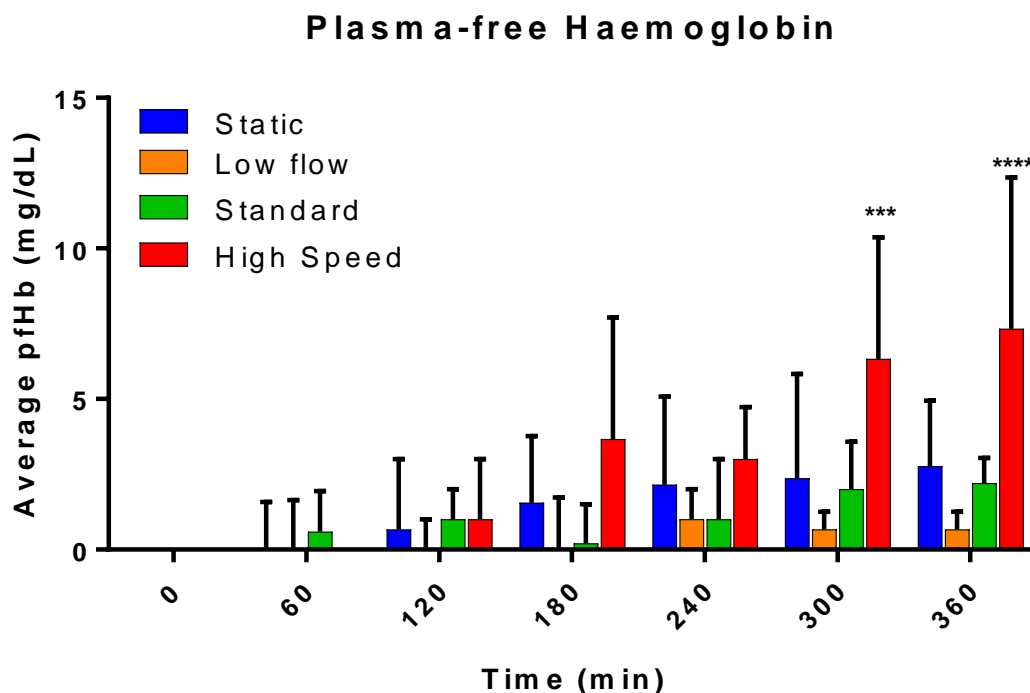


**Figure 4.4 Haematological analysis of blood run in the CentriMag™ loop under different operating conditions**

Ovine blood was diluted to a haematocrit of  $30 \pm 2\%$  using PBS, loaded into the CentriMag™ loop and run at either *low flow*: 2,200 rpm, 1 L/min ( $n = 4$ ), *standard* conditions: 2,200 rpm, 5 L/min ( $n = 5$ ), or *high speed*: 3,300 rpm, 5 L/min ( $n = 5$ ). A 500 mL bag of ovine blood was left in the  $+37^\circ\text{C}$  water bath as a static control. Blood samples were removed every hour for 6 hours. Average complete cell counts (cells/ $\mu\text{L}$ ) from blood samples run in triplicate compared as fold change to static 5 min sample (S5min) for **A**) erythrocytes, **B**) leukocytes, **C**) platelets, **D**) granulocytes, **E**) monocytes, and **F**) lymphocytes for each time point.

#### 4.4.1.2 Haemolysis

As per 3.3.5. Plasma-free haemoglobin is an important measure for blood damage assays as the haemoglobin can activate platelets and leukocytes.



**Figure 4.5 Haemolysis in the CentriMag™ at different operating conditions**

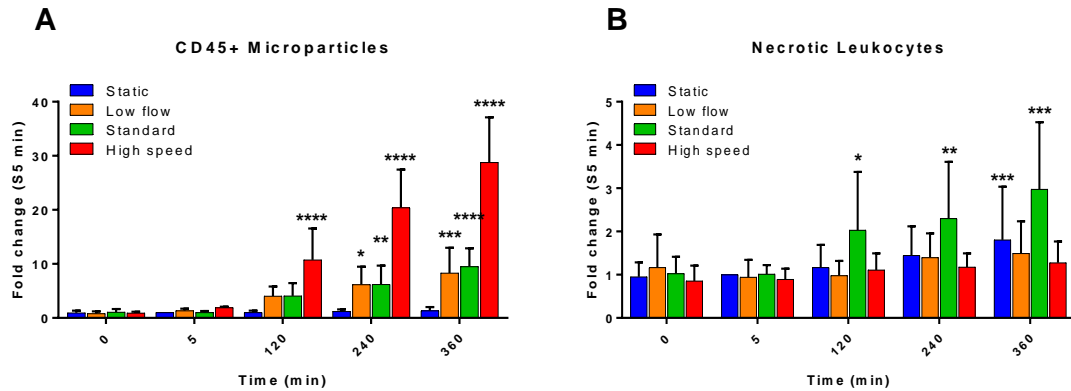
Ovine blood was diluted to a haematocrit of  $30 \pm 2\%$  using PBS, loaded into the CentriMag™ loop and run at either *low flow*: 2,200 rpm, 1 L/min ( $n = 4$ ), *standard* conditions: 2,200 rpm, 5 L/min ( $n = 5$ ), or *high speed*: 3,300 rpm, 5 L/min ( $n = 5$ ). A 500 mL bag of ovine blood was left in the  $+37^\circ\text{C}$  water bath as a static control. Blood samples were removed every hour for 6 hours. Plasma-free haemoglobin (mg/dL) was measured using the Harboe assay.

The pfHb levels for all testing conditions increased over time as is expected (Figure 4.5). The *high speed* conditions generated the highest levels of pfHb measuring  $7.3 \pm 5.0$  mg/dL at 360 min which was significantly greater than the baseline ( $p < 0.001$ ).

#### 4.4.1.3 Leukocyte microparticles and death

Leukocyte-derived microparticles (LMPs) are membrane vesicles released when leukocytes come under stress (252). LMPs have both pro-inflammatory and pro-

thrombotic effects so are associated with both infection and thrombosis (253-255). All operating conditions caused a significant increase in CD45<sup>+</sup> LMPs (gating strategy see Appendix Figure 8.5) compared to baseline (*low flow* 240 min:  $p = 0.012$ , *standard* 240 min:  $p = 0.006$ , *high speed* 120 min:  $p < 0.001$ ; Figure 4.6A).



**Figure 4.6: Leukocyte-derived microparticles and necrotic cells**

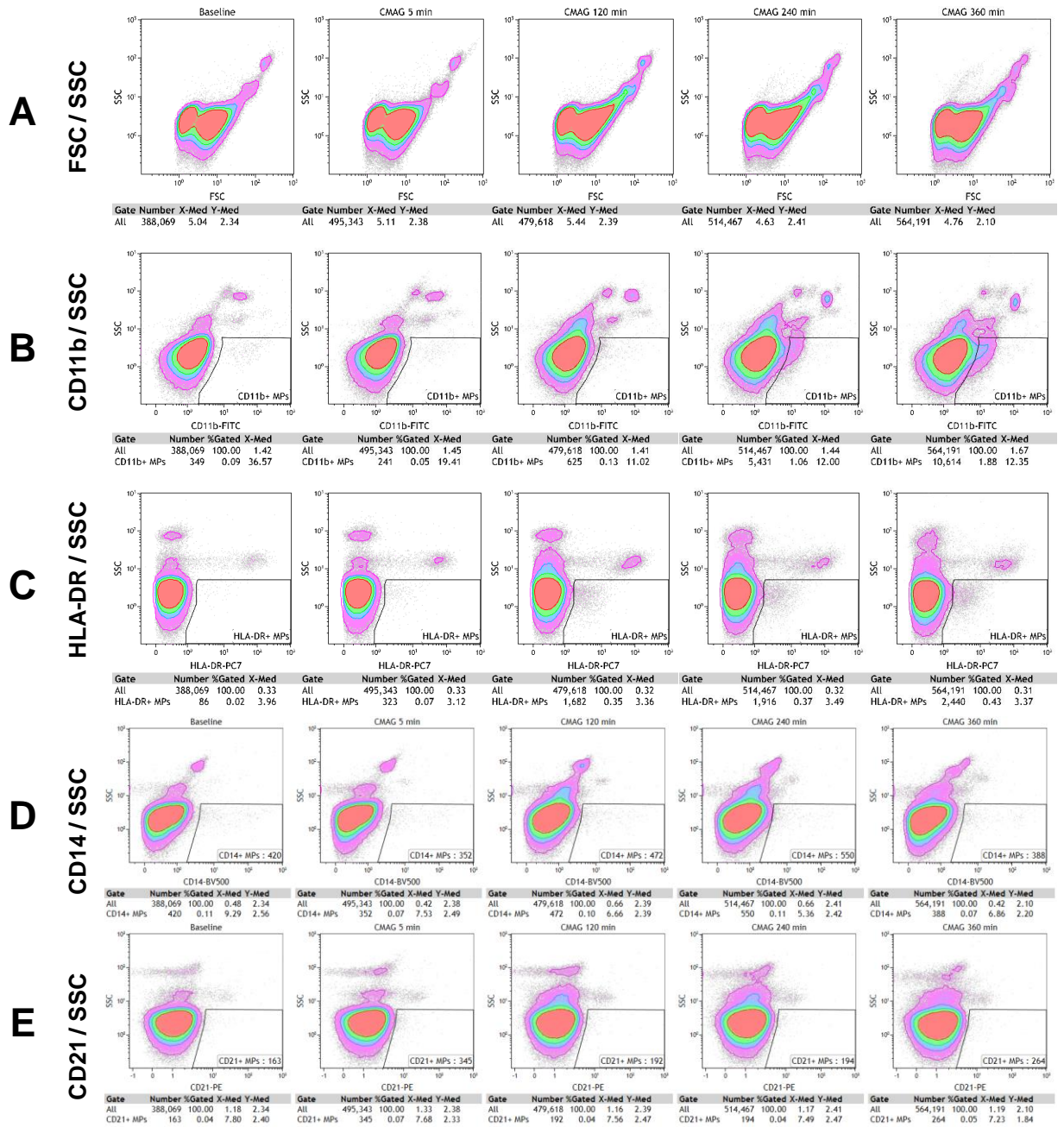
Blood samples taken from the loop were stained with the leukocyte marker CD45 and the dead cell dye 7AAD. Samples were analysed through flow cytometry and the number of CD45<sup>+</sup> microparticles and number of 7AAD<sup>+</sup> (necrotic cells) were plotted over time for each of the conditions: *static* ( $n = 14$ ), *low flow*: 2,200 rpm, 1 L/min ( $n = 4$ ), *standard* conditions: 2,200 rpm, 5 L/min ( $n = 5$ ), or *high speed*: 3,300 rpm, 5 L/min ( $n = 5$ ).

The *standard* operating condition caused a significant increase in necrotic leukocytes at 120, 240, and 360 min ( $p = 0.028$ ,  $0.002$ , &  $0.0002$  respectively; Figure 4.6B). After 360 min, the static control also showed a significant increase in necrotic leukocytes ( $p = 0.0004$ ).

#### 4.4.1.4 Characterising microparticles

As there was an increase in LMPs, next step was to characterise them further through identifying their parent-cell type. The lack of commercially available ovine antibodies limited the flow cytometry panel CD14 (monocytes), CD21 (B cells), and the activation markers CD11b (present on granulocytes, monocytes, and a subset of lymphocytes) and HLA-DR (present on monocytes and a subset of lymphocytes). Each of the markers increased over time in all operating conditions (Figure 4.7).

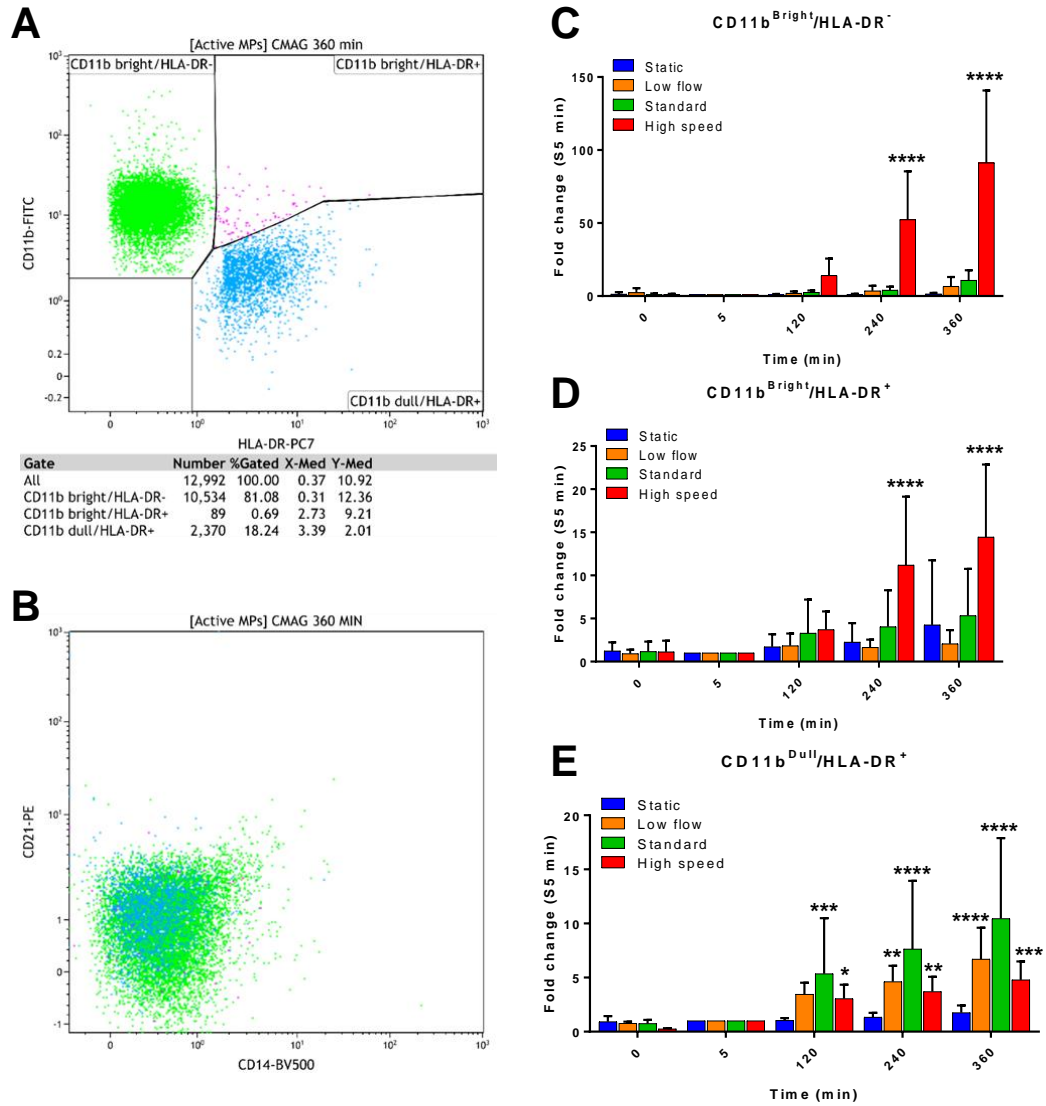
### Scatter profile and MP formation at 'High speed'



**Figure 4.7: Scatter profiles for each antibody at each time point for the high speed condition**

Ovine blood was pumped through the CentriMag™ at *high speed* (3300 rpm) for 5, 120, 240, and 360 min and compared to the baseline sample. Samples were stained with CD14, CD21, CD11b, and HLA-DR. An initial increase is observed in the **A**) FSC/SSC and an increase in the frequency of **B**) CD11b<sup>+</sup>, **C**) HLA-DR<sup>+</sup>, **D**) CD14<sup>+</sup>, and **E**) CD21<sup>+</sup> MPs.

LMPs generated during pump testing expressed CD11b and/or HLA-DR in three distinct sub-populations: CD11b<sup>bright</sup>/HLA-DR<sup>+</sup>, CD11b<sup>dull</sup>/HLA-DR<sup>+</sup>, and CD11b<sup>bright</sup>/HLA-DR<sup>-</sup> (Figure 4.8A). All three populations were negative for CD14 and CD21 expression and therefore are unlikely to come from monocyte or B cells. The CD11b<sup>bright</sup>/HLA-DR<sup>-</sup> parental lineage are likely to be granulocytes due to their high expression of CD11b (Figure 4.7B) and lack of HLA-DR expression (Figure 4.7C). HLA-DR expression was limited to the lymphocyte area of SSC (Figure 4.7C) and therefore the likely parental lineage for CD11b<sup>dull</sup>/HLA-DR<sup>+</sup> LMPs might be T cells. The CD11b<sup>bright</sup>/HLA-DR<sup>+</sup> subset of LMPs could be a further activated subset of either two populations as T cells can increase their CD11b expression (256) and activated neutrophils can increase their HLA-DR expression (257).



**Figure 4.8: CD11b and HLA-DR expression on LMPs**

Ovine whole blood pumped in the CentriMag (CMAG) at high speed (3,300 rpm) for 360 min. Blood was stained with antibodies targeting CD14, CD21, CD11b, and HLA-DR, and MPs expressing CD11b and/or HLA-DR were gated. A Boolean gate named ‘Active MPs’ was created (CD11b<sup>+</sup> OR HLA-DR<sup>+</sup> MPs) and displayed. **A**) Activated MPs form three distinct populations when displayed on CD11b versus HLA-DR axes. **B**) The three populations are CD14<sup>+</sup>/CD21<sup>-</sup>, and therefore likely to be generated from granulocytes (CD11b) and T cells (HLA-DR) based on the baseline cell surface marker expression. **C.** CD11b<sup>Bright</sup>/HLA-DR<sup>-</sup> LMPs, **D**) CD11b<sup>Bright</sup>/HLA-DR<sup>+</sup> LMPs **E**) CD11b<sup>Dull</sup>/HLA-DR<sup>+</sup> LMPs in the operating conditions: *static* (n = 14), *low flow*: 2,200 rpm, 1 L/min (n = 4), *standard* conditions: 2,200 rpm, 5 L/min (n = 5), or *high speed*: 3,300 rpm, 5 L/min (n = 5).



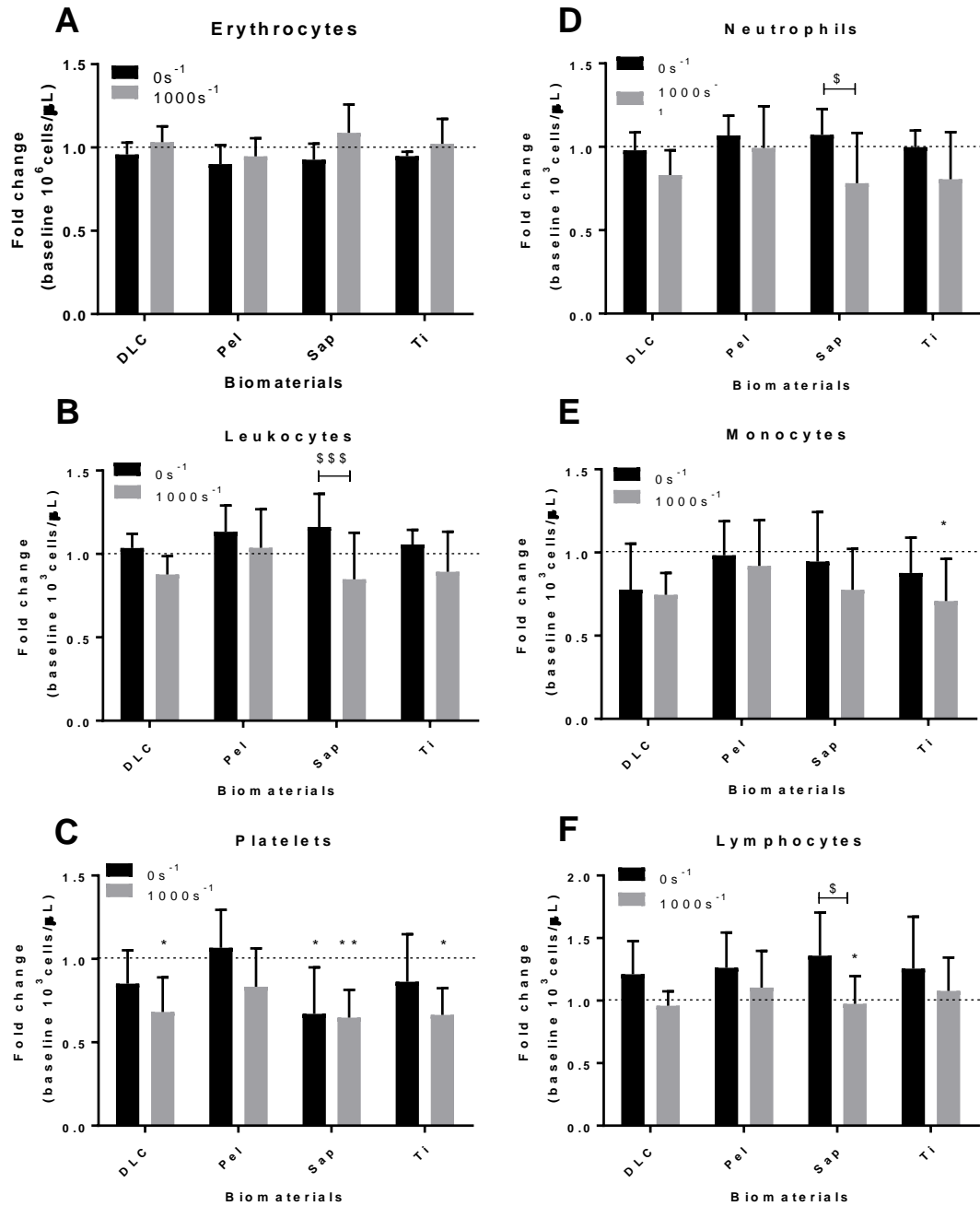
The *high speed* condition caused a significant increase in the CD11b<sup>bright</sup>/HLA-DR<sup>-</sup> compared to the static control by 240 min ( $p < 0.0001$ ; Figure 4.8C). The *high speed* also caused a significant increase for the CD11b<sup>bright</sup>HLA-DR<sup>+</sup> LMPs ( $p$  at 240 min  $< 0.0001$ ; Figure 4.8D). The CD11b<sup>dull</sup>HLA-DR<sup>+</sup> LMPs significantly increased during all pumping conditions compared to baseline (*low flow* 240 min  $p = 0.007$ , *standard* 120 min  $p = 0.0001$ , *high speed* 120 min  $p = 0.047$ ; Figure 4.8E).

#### 4.4.2 *The effect of biomaterials and shear on leukocyte counts, activation, and death*

After the CentriMag study it was clear that leukocytes are significantly affected by different shear stresses. However, VADs are composed of different materials and the blood encounters these materials under shear when pumped through the VAD. To replicate this, a rudimentary model using a rheometer with the biomaterials from the static study (Chapter 3) was used. Due to model constraints, only three of the biomaterials were used, a metal (titanium alloy), a ceramic (single-crystal sapphire), and a coating (diamond-like carbon coating) with the standard Peltier base plate (copper disc with a hardened chromate surface) to represent just shear.

##### 4.4.2.1 *Haematology*

As standard, the complete blood cell counts were measured on the clinical haematology analyser (Figure 4.9). The erythrocyte counts were not affected by biomaterials or shear. Blood sheared on Sap had a significantly lower leukocyte count than non-sheared ( $p = 0.004$ ) which translated to significantly lower neutrophil ( $p = 0.017$ ; Figure 4.9D) and lymphocyte ( $p = 0.034$ ; Figure 4.9F) counts. The monocyte count was significantly lower in comparison to baseline when sheared on Ti ( $p = 0.049$ ; Figure 4.9E). The platelet count was lowered on Sap without shear ( $p = 0.015$ ) and on DLC ( $p = 0.038$ ), Sap ( $p = 0.017$ ), and Ti ( $p = 0.026$ ) when sheared at those surfaces (Figure 4.9C).

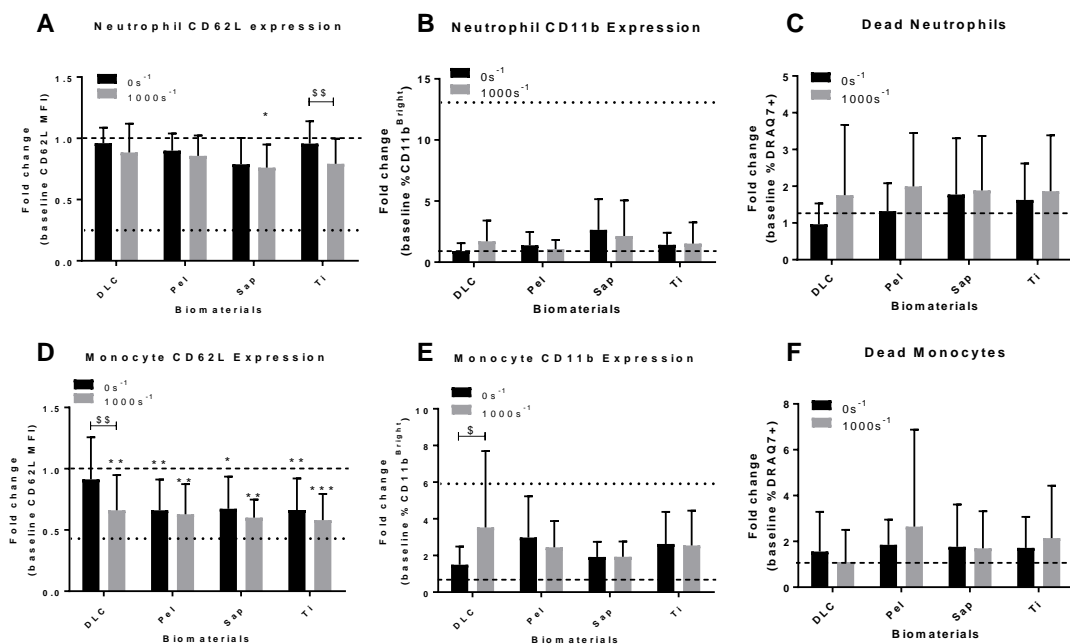


**Figure 4.9: Complete cell counts before and after shear on different biomaterials**

Human whole blood was placed between biomaterial discs - diamond-like carbon coated stainless steel (DLC), single-crystal sapphire (Sap), and titanium alloy (Ti) - attached onto a rheometer. Shear ( $1000\text{ s}^{-1}$ ) or no shear ( $0\text{ s}^{-1}$ ) was applied for 5 min before analysis on an automated haematology analyser ( $n = 7$ , difference between sample and baseline = \*  $p \leq 0.05$ , \*\*  $p \leq 0.01$ , \*\*\*  $p \leq 0.001$ ; difference between shear and non-shear \$  $\leq 0.05$ , \$\$  $\leq 0.01$ , \$\$\$  $\leq 0.001$ ).

#### 4.4.2.2 Leukocyte activation

Complete cell counts revealed a decrease in neutrophil and lymphocyte counts when sheared on the Sap surface and an overall decrease in monocyte count when sheared on the three biomaterials (significant decrease for Ti). Therefore, the activation status of these cell types was considered (Appendix Figure 8.4).



**Figure 4.10: Leukocyte activation and death before and after shear on different biomaterials**

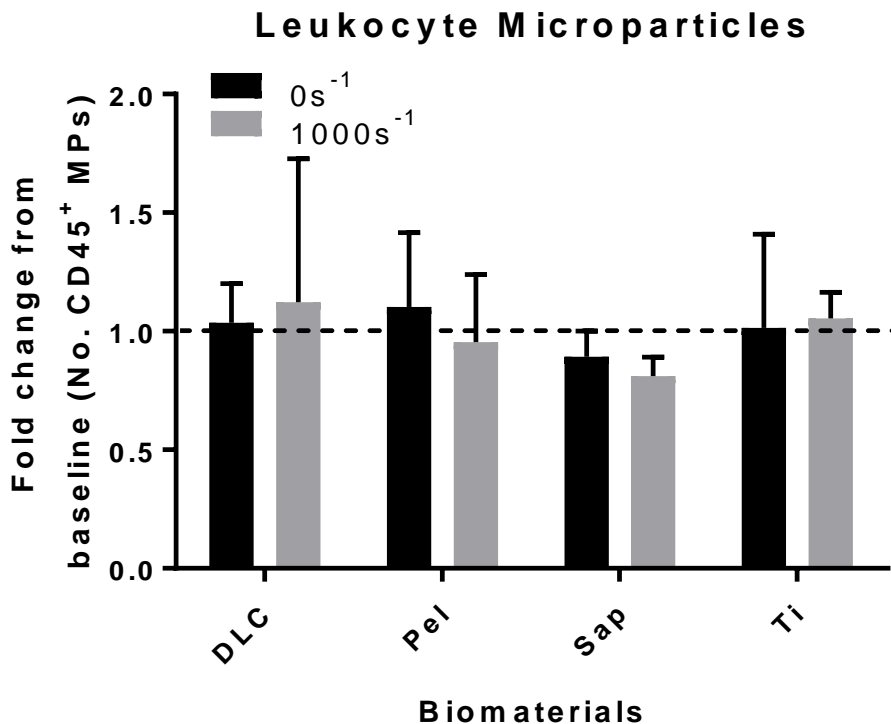
Human whole blood was placed between biomaterial discs - diamond-like carbon coated stainless steel (DLC), single-crystal sapphire (Sap), and titanium alloy (Ti) - attached onto a rheometer. Shear (1000 s<sup>-1</sup>) or no shear (0 s<sup>-1</sup>) was applied for 5 min. Leukocyte activation was investigated by: **A**) Change in median fluorescent intensity (MFI) of CD62L on **A**) CD15<sup>+</sup> neutrophils and **D**) CD14<sup>+</sup> monocytes; Change in percentage of CD11b<sup>Bright</sup> cells on **B**) CD15<sup>+</sup> neutrophils and **E**) CD14<sup>+</sup> monocytes. Percentage of **C**) CD15<sup>+</sup> neutrophils and **F**) CD14<sup>+</sup> monocytes cells are dead as determined by DRAQ7. All were compared to the time 0 baseline as a fold change (dashed line). The LPS positive control is indicated with a dotted line (n = 9; difference between sample and baseline = \* p ≤ 0.05, \*\* p ≤ 0.01, \*\*\* p ≤ 0.001; difference between shear and non-shear \$ ≤ 0.05, \$\$ ≤ 0.01, \$\$\$ ≤ 0.001).

L-selectin expression was significantly decreased in blood sheared on Sap compared to the baseline (p = 0.030; Figure 4.10A) but did not differ to the non-sheared sample whereas shearing on the Ti surface decreased expression significantly compared to non-shear (p = 0.003). CD11b<sup>Bright</sup> expression of neutrophils did not significantly change compared to samples exposed to biomaterials both either with or without shear (Figure 4.10B). Monocyte activation evidenced by decreased L-selectin expression

was significantly apparent in all the samples in comparison to baseline with and without shear (Figure 4.10D), although shearing on DLC showed a significant increase in CD11b<sup>Bright</sup> expression compared to baseline ( $p = 0.016$ ). This correlates with the static biomaterial study (Chapter 3 Figure 3.13) where L-selectin expression was decreased significantly on monocytes exposed to DLC and Sap. There was no significant effect on cell death for either neutrophils and monocytes in response to any of the biomaterials (as in Chapter 3) or shear (Figure 4.10C&F).

#### 4.4.2.3 *Leukocyte microparticles*

LMPs were a prominent feature of the effect of shear stress on leukocytes during the CentriMag<sup>TM</sup> work (4.4.1.3). Therefore, the blood from the rheometer experiments was stained with CD45/7AAD to determine whether small shear stress levels for a shorter period may increase their prevalence. However, this was not the case as neither biomaterial nor shear increased the number of CD45<sup>+</sup> MPs already present in the baseline sample (approx. 500 LMPs) (Figure 4.11; gating strategy Appendix Figure 8.5).



**Figure 4.11: Leukocyte microparticle generation before and after shear on different biomaterials.**

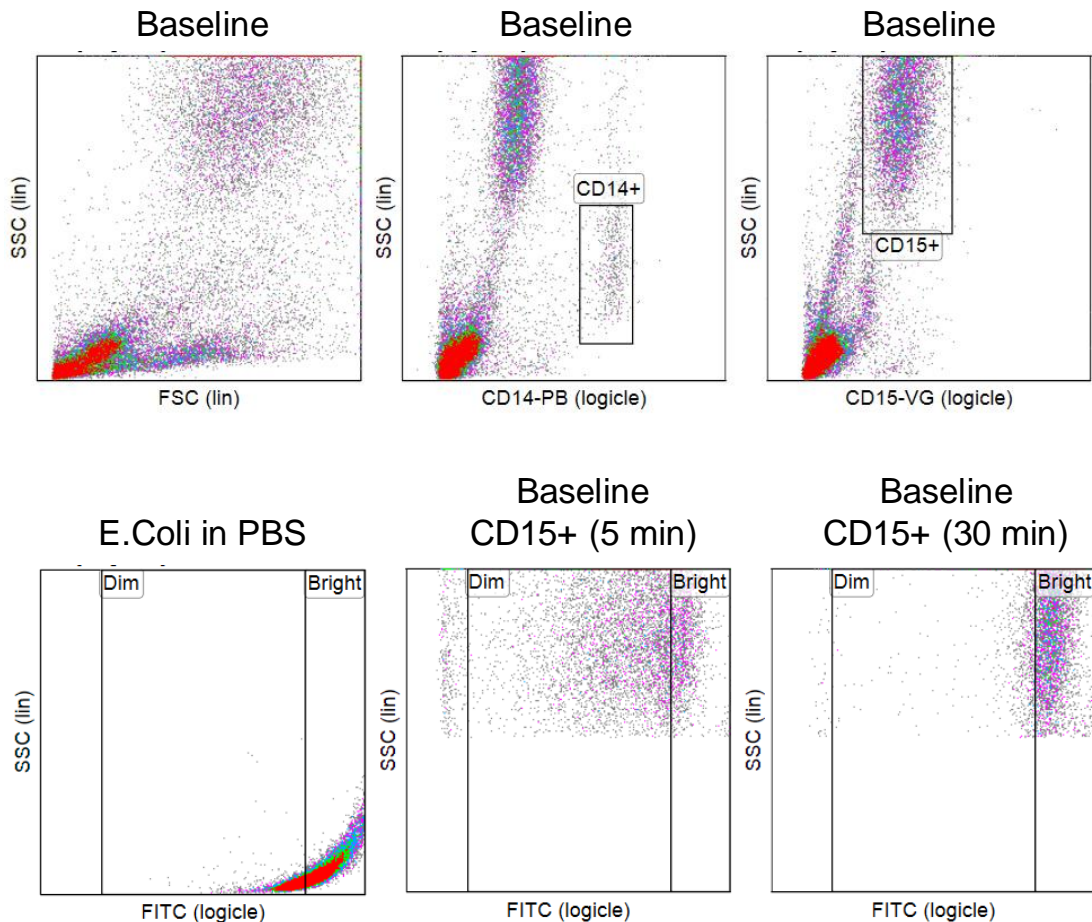
Human whole blood was placed between biomaterial discs- diamond-like carbon coated stainless steel (DLC), single-crystal sapphire (Sap), and titanium alloy (Ti) - attached onto a rheometer. Shear ( $1000\text{ s}^{-1}$ ) or no shear ( $0\text{ s}^{-1}$ ) was applied for 5 min. ( $n = 3$ ). The blood was stained with CD45 and 7AAD before acquiring on the flow cytometer. The number of CD45<sup>+</sup> MPs was compared as a fold change to the baseline sample.

#### 4.4.3 *The effect of biomaterials and shear on leukocyte functionality*

The finding that leukocytes were becoming activated under these conditions prompted research into their functionality. Phagocytes such as monocyte/macrophages and neutrophils engulf invading pathogens through a process called phagocytosis. The pathogen is encapsulated in a phagosome which fuses with lysosomes containing enzymes, proteins, and peptides that are toxic to the pathogen, thus destroying it (258). Neutrophils and monocyte/macrophages also destroy pathogens through producing toxic ROS which include hydrogen peroxide ( $\text{H}_2\text{O}_2$ ), nitric oxide (NO), and superoxide anion ( $\text{O}_2^-$ ) (258).

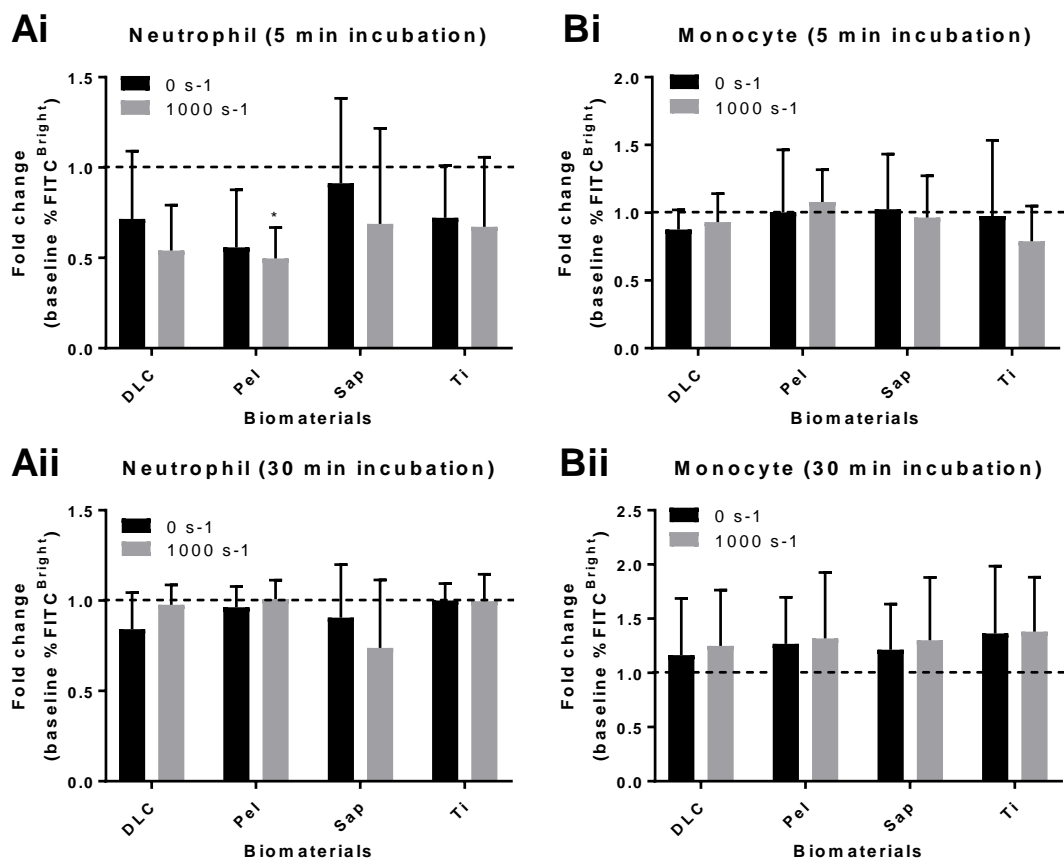
#### 4.4.3.1 Phagocytosis

Phagocytic function was measured through adding fluorescent *E. Coli* bioparticles to blood that had been in contact with the biomaterials with/without shear. The bioparticles were incubated with the blood for 5 min to observe initial phagocytosis and 30 min to full phagocytosis. These times were decided based on optimisation work for the phagocytosis assay (Appendix Figure 8.7). Monocytes and neutrophils are the phagocytes of interest and were identified with antibodies to CD14 and CD15, respectively (Figure 4.12).



**Figure 4.12: Gating strategy for phagocytosis.**

Baseline blood was incubated in a +37°C shaking water-bath with fluorescent *E. coli* bioparticles for 5 min and 30 min. Phagocytosis was stopped through the addition of cytochalasin D and two washes with ice-cold PBS. Samples were stained with CD14 and CD15 antibodies, red blood cells were lysed, then samples were washed with ice cold PBS containing trypan blue to quench the bioparticles on the cell surface. *E.coli* bioparticles in PBS were used to gate the Bright population indicating full phagocytosis for neutrophils (CD15<sup>+</sup>- shown in figure as example) and monocytes (CD14<sup>+</sup>).



**Figure 4.13: Phagocytic ability of neutrophils and monocytes before and after shear on different biomaterials**

Human whole blood was placed between biomaterial discs - diamond-like carbon coated stainless steel (DLC), single-crystal sapphire (Sap), and titanium alloy (Ti) - attached onto a rheometer. Shear ( $1000\text{ s}^{-1}$ ) or no shear ( $0\text{ s}^{-1}$ ) was applied for 5 min. Samples were added to tubes and incubated in a  $+37^{\circ}\text{C}$  shaking water-bath with fluorescent *E. coli* bioparticles for 5 min and 30 min. Phagocytosis was compared to the baseline sample and measured as neutrophils ( $\text{CD15}^{+}$ ) or monocytes ( $\text{CD14}^{+}$ ) that were in the *E. coli*<sup>Bright</sup> region at 5 minutes (**Ai** and **Bi**, respectively) and 30 minutes and compared to the baseline sample (**Aii** and **Bii**, respectively) ( $n = 6$ ;  $* p \leq 0.05$ ).

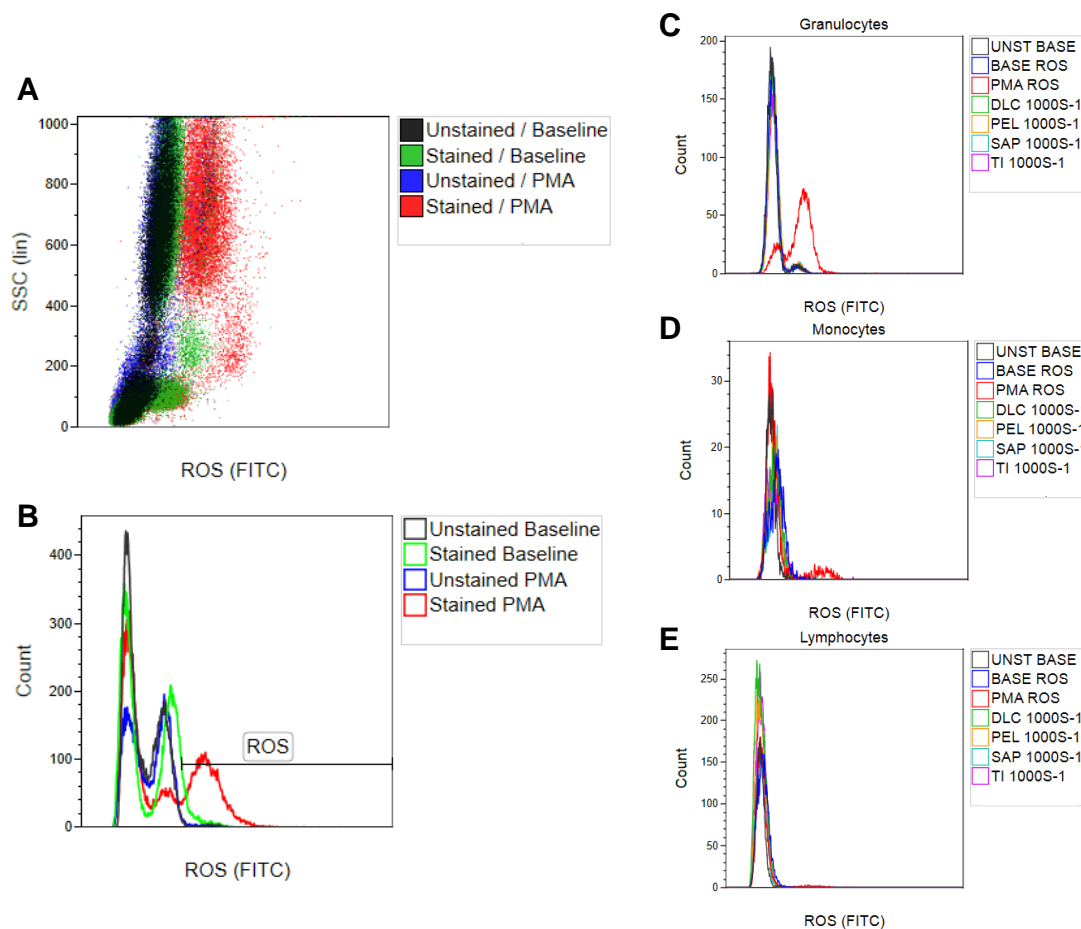
The only significant difference in phagocytic ability compared to baseline was observed in the sheared Pel sample for the neutrophils incubated for 5 min ( $p = 0.035$ ; Figure 4.13Ai). Although not significant, the phagocytic ability of neutrophils appeared lower in DLC and Ti with no shear compared to baseline and all samples that were sheared (Figure 4.13Ai). Incubation with the bioparticles for 30 min did not show a significant difference in the neutrophil phagocytic ability compared to baseline,

although it was lower in the sheared Sap sample (Figure 4.13Aii). These results suggest that the biomaterials, particularly DLC and Ti, have attenuated the immediate neutrophil response to pathogens which is exacerbated by the addition of shear stress. This is rectified after a longer period of incubation with the bioparticles although neutrophils from the blood sheared on Sap are still not at the same phagocytic ability as the baseline. Monocytes on the other hand were unaffected by biomaterial or shear in that their phagocytic ability with 5 and 30 min incubation was not significantly impaired (Figure 4.13Bi&Bii).

#### *4.4.3.2 ROS production*

As there was some attenuation of phagocytic response from the neutrophils, especially during the immediate response, it was hypothesised that the production of reactive oxygen species might be affected by biomaterials and shear.





**Figure 4.14: ROS production before and after shear on different biomaterials**

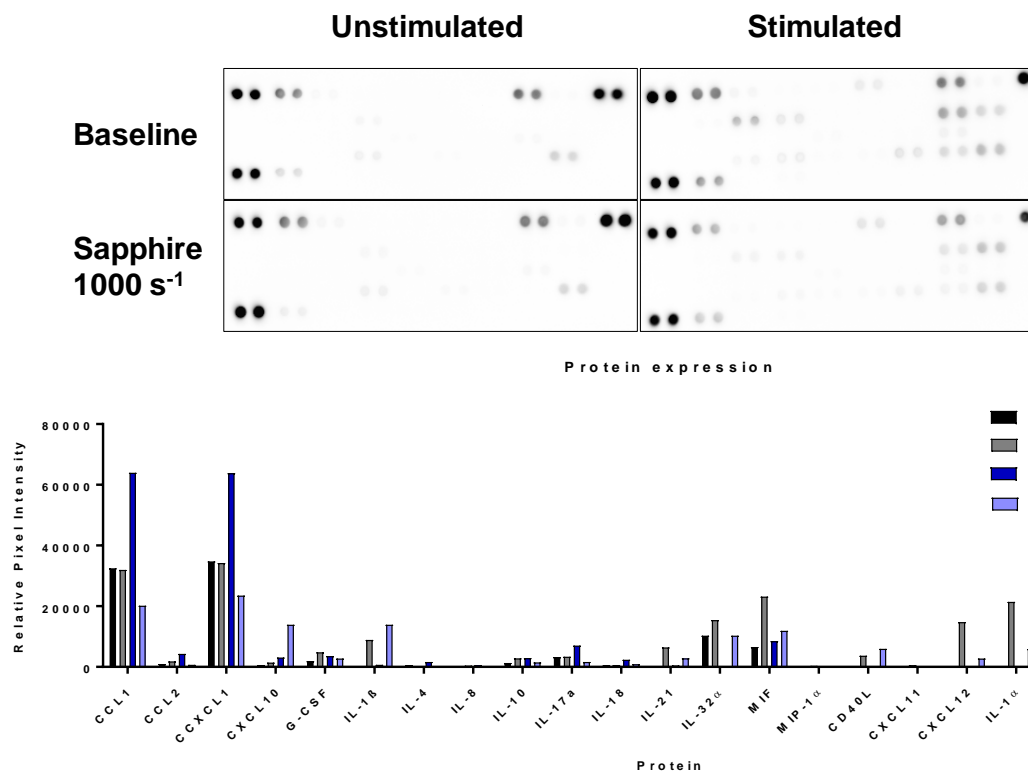
Blood was incubated at +37°C for 1 h with 1X ROS assay stain before being placed between biomaterial discs- diamond-like carbon coated stainless steel (DLC), single-crystal sapphire (Sap), and titanium alloy (Ti) - attached onto a rheometer. Shear ( $1000 \text{ s}^{-1}$ ) or no shear ( $0 \text{ s}^{-1}$ ) was applied for 5 min ( $n = 3$ ). Baseline blood stimulated with 1  $\mu\text{M}$  PMA was used as a positive control. **A)** Overlay dot-plot for controls with and without ROS stain, **B)** Overlay histogram for controls with and without ROS stain. ROS production in **C)** granulocytes, **D)** monocytes, and **E)** lymphocytes from blood sheared between biomaterials.

The positive control PMA gave a measurable ROS response from both neutrophils and monocytes (Figure 4.14). ROS production was not evident for neutrophils or monocytes when sheared between the biomaterials ( $n = 3$ ).

#### 4.4.3.3 Cytokine production

The impact on leukocyte function can be measured through changes in cytokine production in general and when under pathogen-stimulation. To determine which cytokines/chemokines might be affected by the biomaterials and shear, cell-free

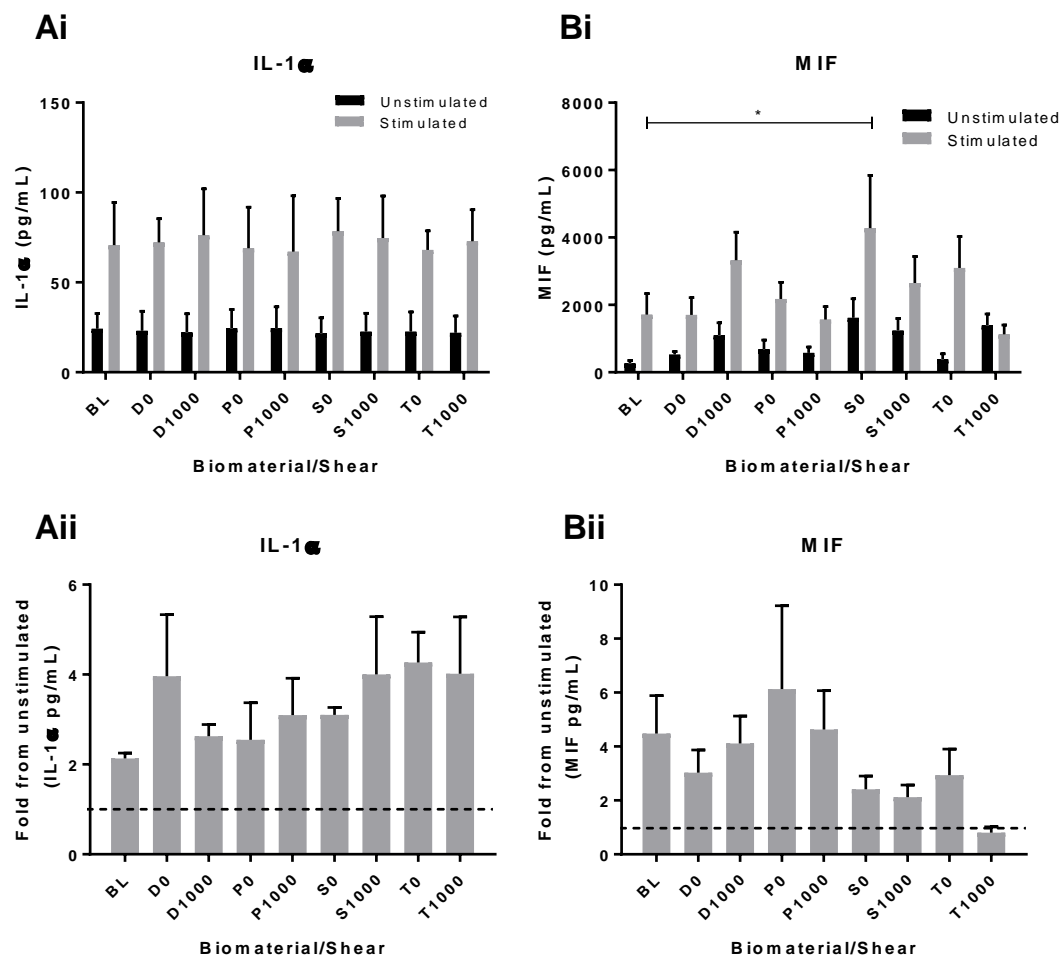
supernatants from baseline and Sap  $1000\text{ s}^{-1}$  unstimulated and stimulated with  $10\text{ ng/mL}$  LPS samples were used in a proteome profiler array (Figure 4.15).



**Figure 4.15: Proteome profile.**

Baseline blood and blood that had been sheared for 5 min at  $1000 \text{ s}^{-1}$  between single-crystal sapphire for 24 h at  $+37^\circ\text{C}$ , 5%  $\text{CO}_2$ . Supernatants were harvested and processed with the manufacturer's instructions (n = 1).

Several cytokines/chemokines such as IL-21, IL-32 $\alpha$ , and IL-12 showed potentially interesting results with regards to the differences in concentrations between baseline and Sap (Figure 4.15). Macrophage inhibitory factor (MIF) and interleukin 1 alpha (IL-1 $\alpha$ ) are cytokines related to neutrophils and monocytes and their concentrations were lower in the LPS stimulated Sap 1000 s<sup>-1</sup> compared to the baseline LPS stimulated blood sample. This prompted further analysis of MIF and IL-1 $\alpha$  ELISAs (Figure 4.16).



**Figure 4.16: IL-1 $\alpha$  and MIF expression before and after shear on different biomaterials**

Human whole blood was placed between biomaterial discs - diamond-like carbon coated stainless steel (DLC), single-crystal sapphire (Sap), and titanium alloy (Ti) - attached onto a rheometer. Shear ( $1000\text{ s}^{-1}$ ) or no shear ( $0\text{ s}^{-1}$ ) was applied for 5 min. The samples were cultured with or without  $10\text{ ng/mL}$  LPS for 24 h at  $+37^\circ\text{C}$ ,  $5\% \text{ CO}_2$ . Supernatants were harvested and processed for **Ai**) IL-1 $\alpha$  and **Aii**) as a fold change from the unstimulated sample ( $n = 4$ ) and **Bi**) MIF and **Bii**) as a fold change from the unstimulated sample ( $n = 7$ ; \*  $p \leq 0.05$ , dashed line represents unstimulated sample) ELISA.

There was no significant difference compared to baseline in any of the samples for IL-1 $\alpha$  ( $n = 4$ ; Figure 4.16A). There was a significant increase between the baseline stimulated and Sap  $0\text{ s}^{-1}$  stimulated for MIF concentration ( $n = 7$ ). When compared as a fold change from the unstimulated samples, an attenuated response to LPS in the samples sheared on Ti was observed.

## 4.5 Discussion

An increase in the understanding of shear-dependent blood trauma is important to develop safer VADs as high shear stresses within the pumps is causative of haemolysis (259), platelet activation (81), leukocyte damage (239), and degradation of vWF (260). *In vitro* testing of shear stress on the different blood components can aid in the design of VADs. Combining shear stress and VAD biomaterials in a simple model can provide a wealth of information previously untapped, especially if guided by the known effects of VADs from both *in vitro* and *in vivo* analysis.

The CentriMag centrifugal extracorporeal pump manifests a low blood damage profile due to the large gaps and slower moving rotors (63). *In vitro* haemolysis levels observed in the CentriMag are very low (NIH = 0.0029 (261)) which makes it an excellent benchmark control for the testing of VADs. The advantage of the CentriMag in this study was that the speed and flow rate could be adjusted to produce different levels of shear stress within the pump defined as *low flow*, *standard*, and *high speed*. The focus of VAD testing has always been on the red blood cells, but this does not give a complete view of what is happening to the blood. This is evident in that although haemolysis was highest at 6 hours in the *high speed* condition compared to the static, the erythrocyte count was unaffected by the different operating conditions, whereas the leukocyte count was. The *high speed* condition caused a significant decrease in granulocyte and monocyte counts but not in the more abundant (in sheep (157)) lymphocyte population. Both the *low flow* and *high speed* conditions significantly decreased the platelet counts. This decrease could be associated with platelet activation in that both lysis and aggregation can lead to an observed reduction in numbers. Platelet activation is caused by an increase in residence time (262) (*low flow*) and by high shear stress (81, 263) (*high speed*). However, it must be noted that to achieve the *low flow* operating condition, it was necessary to tighten the flow resistor (clamp) quite severely. This small gap may have had an impact on results through increasing activation and microparticle generation.

The decrease in leukocyte counts could be linked to the significant increase in CD45<sup>+</sup> LMPs observed at the 6 h timepoint under all operating conditions, but most significantly under *high speed* conditions. Characterisation of these LMPs is novel but does have its limitations. The antibodies in the 4-colour panel were chosen based

on their availability as directly conjugated to fluorochromes for replicability and for their cross-reactivity with ovine, bovine, and human blood cells for translational research. Three distinct LMP populations were identified: CD11b<sup>Bright</sup>HLA-DR<sup>+</sup>, CD11b<sup>Dull</sup>HLA-DR<sup>+</sup>, and CD11b<sup>Bright</sup>HLA-DR<sup>-</sup> which were all negative for CD14 and CD21 suggesting they are not from monocytes or B cells. Therefore, it is hypothesised that the CD11b<sup>Bright</sup>HLA-DR<sup>-</sup> and CD11b<sup>Dull</sup>HLA-DR<sup>+</sup> LMPs must come from granulocytes and T cells, respectively. Unfortunately, directly conjugated granulocyte and T cell markers for ovine are currently unavailable. The different trends in LMP production across the different pumping conditions supports the likelihood that the CD11b<sup>Bright</sup>HLA-DR<sup>-</sup> and CD11b<sup>Dull</sup>HLA-DR<sup>+</sup> LMPs are derived from different cell populations which respond different to the shear stress stimuli. Given that the granulocyte count significantly decreases in the *high speed* condition, and the CD11b<sup>Bright</sup>HLA-DR<sup>-</sup> LMP population is significantly increased further under these same conditions supports the granulocyte parentage hypothesis as CD11b is present on activated neutrophils (264). The parentage of CD11b<sup>Dull</sup>HLA-DR<sup>+</sup> LMPs are a little more challenging to confirm and are possibly derived from T cells or CD21 negative B cells that express HLA-DR (265) – but this remains to be proven.

The CentriMag study showed that leukocytes were differentially affected by shear stress alone and this could have implications for adverse events. However, the CentriMag and its accompanying circulatory loop is made almost exclusively from polymers which are largely absent from VADs. To study the effect of combined shear stress and VAD candidate biomaterials had in conjunction on leukocytes, a rheometer model was developed. Through attaching the biomaterial discs used in the previous chapter (Chapter 3) to a rheometer, it was possible to shear healthy human blood between relevant biomaterials representative of the VAD body (Ti), a bearing candidate (Sap), and a coating option (DLC). The rheometer model does not accurately replicate the VAD as it incorporates large gaps, long residence time, and can only achieve a maximum shear stress of 1000 s<sup>-1</sup>. However, it is a good starting point to look at previously unknown effects on leukocytes using small blood volumes.

It was decided that application of the rheometer model for 5 min was sufficient for two reasons:

1) the time was adequate for the user to add the blood, set the rheometer up, run, and then remove the blood without excessive haste,

2) 5 min was long enough that observable changes could be seen.

Blood was left between the parallel biomaterial discs without shear to observe the effect of the biomaterial alone, and then sheared at  $1000 \text{ s}^{-1}$  to look at the effect biomaterial and shear have in combination.

As expected, there was no significant difference in erythrocyte counts compared to the baseline sample, but leukocyte counts did differ. When blood was sheared on a Sap surface, the leukocyte count was decreased which translated to a decrease particularly in neutrophils in comparison to the non-sheared sample. The monocyte count was significantly decreased in the sheared Ti sample, but the lymphocyte counts were unaffected by the biomaterials with/without shear. Decreases in leukocyte count under shear have been noted in the past when Dewitz et al., sheared whole blood for 10 min and noticed a 25% decrease in leukocyte count at 60 Pa and membrane disruption at 15 Pa (239) – although these are significantly higher shear stresses than in our study. These decreases, unlike in the CentriMag study, were not related to an increase in  $\text{CD45}^+$  LMPs as these remained comparable to the baseline sample. Platelet counts were significantly reduced on non-sheared Sap, and when sheared on DLC, Sap, and Ti. As noted above, these decreased platelet counts could be related to platelet activation, but this was not measured in this study as it was analysed extensively with these biomaterials by Dr Rebecca Hambly (266).

Given that a decreased leukocyte count was not associated with the emergence of LMPs, the activation status of the leukocytes in the blood samples were more insightful. No significant increase in dead neutrophils or monocytes was observed. Neutrophil expression of CD62L was decreased in the sheared Sap blood and there was a significant decrease between non-sheared and sheared blood on Ti. L-selectin on neutrophils is cleaved from the surface ‘during rolling on a ligand-bearing surface under hydrodynamic shear flow’ according to Lee et al., and the mechanical shedding depends on the shear stress applied (267). There was no significant increase in neutrophil CD11b expression. In the study, fluid shear stress was applied to whole blood on a glass surface which significantly down-regulated CD18 expression in comparison to neutrophils that were not sheared (268). In monocytes, CD62L was



decreased in all samples regardless of biomaterial type, as observed in Chapter 3, or the application of shear. Interestingly, CD11b expression was significantly increased in the sheared DLC monocytes which relates to the increased adhesion of monocytes observed in Chapter 3 and by Linder et al. (217). These results suggest that while neutrophils and monocytes are susceptible to the effects of shear and biomaterials there are differences in the response profile perhaps reflecting their differing but overlapping functions in the body. There was no significant increase in death amongst neutrophils or monocytes.

The host response to pathogens largely depends on the first defence provided by neutrophils which engulf pathogens via phagocytosis and the generation of ROS. Diminished phagocytic ability has been noted in neutrophils adhered to cardiovascular device material subjected to physiological shear stresses for 60 min (185). Functional assays have also been cited as ‘a more appropriate way to evaluate the effect of shear stress on leukocytes rather than simple cell counts’ (269). Whilst there were no significant differences in the phagocytic ability of neutrophils and monocytes in comparison to baseline, some interesting observations were made. Neutrophils from blood that had been in contact with DLC, Ti, and the Pel showed a lower immediate phagocytic ability (5 min incubation) which was exacerbated by the addition of shear stress compared to the baseline sample. This appeared resolved when incubated for longer (30 min) with the *E. Coli* Bioparticles apart from in sheared Sap neutrophils which had reduced phagocytosis. These alterations in phagocytic ability were not evident in the monocyte population. In terms of ROS production, studies on ROS production under shear appears to largely focus on endothelial cells not leukocytes (270). Finally, the functional cytokine output in response to a commonly used prototypic inflammatory stimuli – LPS - was considered (271). Instead of simply measuring the same cytokines as shown in Chapter 3 or used by other investigators (183, 272, 273), an array approach was used first to better identify candidates for further analysis. Cytokine production (IL-1 $\alpha$  and MIF) was also relatively unaffected by the biomaterials/shear although there was a significant increase in MIF on non-sheared Sap challenged with LPS compared to the baseline sample. MIF is involved in cell-mediated immunity and is considered an inflammatory cytokine that regulates macrophage function (274). Macrophages release MIF upon stimulation with LPS (275) with high levels of MIF in circulation known to exacerbate sepsis (276). With

this in mind, Sap inducing higher levels of MIF than the baseline when stimulated with LPS could predispose the VAD patients to sepsis. However, reanalysing these samples as a fold change to the unstimulated to eliminate background MIF, an attenuated response to LPS could be seen in the Sap and Ti with the application of shear exacerbating this in Ti samples. This suggests that these materials can cause immunosuppression. Many pathogens, trauma, burns, and major surgery can cause acute immunosuppression leading to a diminished capability of responding to infection (277). The combination of major surgery and implantation of a VAD that is largely composed of titanium alloy could potentially increase patient susceptibility to infection.

## 4.6 Conclusion

The rheometer model does have its limitations but the assay possibilities that can be applied to it are vast. Even with the small blood volume yield ( $\sim 500 \mu\text{L}$ ), complete cell counts, flow cytometry, and whole blood cultures can be done to achieve a wealth of results. The results from Chapter 3 suggested that Sap may be causing higher levels of leukocyte activation than the other materials. The rheometer work has shown that Sap is still causing alterations to leukocytes and this is only exacerbated by shearing – a big problem as Sap is considered for VAD bearings, an area of very high shear and prone to thrombus generation. Another advantage of the use of the rheometer model is that only small blood volumes can be used ( $\sim 1.2 \text{ mL}$ ) which is perfect for paediatric or heart failure patient blood where only small volumes are cleared by ethics.

The ideal model for the assessment of shear on blood would be to design an adjustable device which could be incorporated into the current mock circulatory loops. This ‘Shear Rig’ was under development by Calon but has been postponed due to financial, resource, and time-constraints. However, the design specifications of the device would have allowed a range of shear stresses (low and high), very short exposure times (milliseconds), adjustable gap height, multiple passages of blood, and interchangeable biomaterial sleeves. In future, this device could be assembled, and the assays developed in this chapter used to generate highly useful information on how VADs affect the blood to improve the design faster and with better results.

# Chapter 5 VADs: From bench to bedside

## 5.1 Introduction

The development of a VAD is a long process which requires rigorous testing before approval for use in clinic is given. Before development begins, a set of criteria on the physical design of the VAD is put into place (Table 5.1). These designs are aided and changed per results from computational fluid dynamics and *in vitro* testing. Once a design has been deemed successful in the laboratory, the VAD is manufactured for preclinical studies involving implantation into large animals for a minimum of 30 days. Following successful preclinical trials, the VAD design is frozen and manufactured to complete a clinical trial.

**Table 5.1: Specifications for the MiniVAD**

As specified in the PhD thesis by former Calon C.T.O. Dr G. Foster (278)

Category	Criteria
<b>Haemodynamics and engineering</b>	1. Flow throughput of 0 – 7 L/min
	2. Centrifugal hydraulic (HQ) characteristic
	3. Power consumption of less than 6 watts at 5 L/min and 100 mmHg (good efficiency)
	4. Very low noise and vibration
	5. Durability of 10+ years
<b>Size and implantability</b>	1. Sufficiently small to allow implantation in a wide range of patients
	2. Amenable to implantation via a mini thoracotomy
<b>Cost</b>	1. Able to be manufactured at a total cost of less than 50% of existing VADs
<b>Blood damage and biocompatibility</b>	1. Haemolysis of less than NIH 0.004 g/100L
	2. Very low level of pump-induced thrombus
	3. All materials should be biocompatible

### *5.1.1 In vitro testing*

The VAD is a blood handling device and as such must not induce significant damage and thus harm rather than treat. The most important parameter of blood trauma in VADs is haemolysis whereby damage to the red blood cells leads to leakage of haemoglobin causing anaemia, liver damage, pulmonary hypertension and thrombosis which can lead to device failure (279). The haemolysis test is the first test any VAD developer must do and has been standardised in ASTM F1841-97: Standard Practice for Assessment of Haemolysis in Continuous Flow Blood Pumps (152). The summary of practice in the ASTM denotes blood, test loop, pump conditions and evaluation to reliably measure haemolysis comparatively (Table 5.2).

**Table 5.2: Summary of practice from ASTM F1841-97**

<b>Category</b>	<b>Criteria</b>
<b>Blood(249)</b>	1. Obtained from human volunteers, cattle, or pigs with normal body temperatures, no physical signs of disease, and acceptable haematological profiles.
	2. Collection via venepuncture using a 14G or larger needle is recommended although slaughterhouse blood can be used.
	3. Anticoagulant for use can be citrate phosphate dextrose adenine solution (CPDA-1) or heparin sulphate
	4. Any blood with plasma-free haemoglobin above 20 mg/dL should not be used.
	5. The haematocrit should be adjusted to $30 \pm 2\%$ by haemodilution with phosphate buffered saline.
<b>Test loop</b>	1. Loop consists of 2 m of 9.5 mm ID polyvinylchloride tubing and a reservoir with a sampling port.
	2. Primed blood volume is $450 \pm 50$ mL
	3. A screw clamp is positioned at the outlet to set the pressure.
	4. Pressure sensors are connected at the inlet and outlet of the pump.
	5. Flow rate is monitored using a flow probe.
	6. A thermistor is connected to the loop to measure blood temperature.
<b>Pump conditions</b>	1. Pump flow rate is set to $5 \pm 0.25$ L/min.
	2. Circulating blood temperature set to $+37^{\circ}\text{C} \pm 1^{\circ}\text{C}$ .
	3. Total pressure head is set to $100 \pm 3$ mmHg.
<b>Evaluation</b>	4. The free plasma haemoglobin is determined by clinically approved assay methods.

To assess the pump's effects on erythrocytes, a recirculation test is performed for 6 h with samples withdrawn every hour to be tested for haemolysis. The results are expressed as NIH (Equation 5.1) and compared with a static control (blood in bag kept at +37°C). An NIH of 0.01 g/100L when pressure is 100 mmHg is deemed acceptable for long-term implantation (280).

**Equation 5.1: Normalised Index of Haemolysis (NIH)**

$$NIH \text{ g/100L} = \Delta pfHb \times V \times \frac{100 - Hct}{100} \times \frac{100}{Q \times T}$$

where:

$\Delta pfHb$  = increase of plasma free haemoglobin concentration (g/L) time

$V$  = circuit volume (L)

$Q$  = flow rate (L/min)

$Hct$  = haematocrit (%)

$T$  = sampling time (min)

Haemolysis is the only assay specifically required for VAD testing but a wide range of tests on other blood components such as platelets and white blood cells is left up to the desires of the VAD developer. The International Standard ISO-10993-4: Selection of tests for interactions with blood (208) comments on coagulation, complement system, haematology, platelets, and thrombosis tests for blood contacting devices but stresses that the testing cannot be specified due to limitations in knowledge and precision of tests. In terms of VADs, the ISO only defines thrombosis, haematology, and the complement system tests for consideration. During *in vitro* testing in mock circulatory loops, this has been largely ignored by VAD developers in favour of more extensive assays in preclinical animal models. Calon on the other hand has worked to develop assays of the other blood cell types, namely platelets and leukocytes. The effects of the VentrAssist implantable rotary blood pump (Ventracor Ltd., Sydney, Australia), and the RotaFlow centrifugal pump (Maquet Holding GmbH & Co. KG, Rastatt, Germany) on leukocyte numbers, necrosis, and microparticle generation has been investigated (131). The blood damage assays were further developed to include

platelet activation and vWF degradation to benchmark the CentriMag™ as an appropriate control for testing VADs (63).

### 5.1.2 Preclinical testing

When the *in vitro* testing of a VAD has concluded to a satisfactory level, implantation into animals is the next step. Animal models for VADs include calves (137, 281), sheep (282, 283) and pigs (284, 285) due to heart size and haemodynamics being comparable to that of humans. The type of species selected depends on the study type with calves growing too fast for long-term studies (30+ days), and the nature of pigs to roll around making studies with cables attached difficult. (156).

To progress to clinic, results from *in vivo* studies must obey good laboratory practice (GLP) and the requirements of a GLP study are in Table 5.3.



**Table 5.3: Good laboratory practice specifications**

<b>Category</b>	<b>Criteria</b>
<b>Facility</b>	1. Facility contains all appropriate equipment and materials
	2. Suitable size, construction, and location to minimise outside conditions which may interfere with validity of results.
	3. Adequately separates different activities.
	4. Appropriate storage of test and reference material
	5. Waste disposal should not jeopardise study through contamination and waste collection, storage, and disposal should be appropriate.
	6. Apparatus, reagents, and test systems should be suitable located and of appropriate quality/design.
	7. Quality control system is in place.
<b>Personnel</b>	1. Fully qualified and records of qualifications kept.
	2. Must exercise safe working conditions
	3. Personnel with health conditions should be excluded.
	4. Labelling and record keeping must be exemplary.
<b>Study director</b>	1. Needs to buy into the study plan and seek authorisation for any variation of the study plan.

The study protocol is set in place by the contract research organisation (CRO) which has the ethical approval to carry out the study including high level surgical protocol and follow-up animal care. The VAD development team then checks the details to ensure that it fits for the specific device e.g. collection of pump data (flow, speed, power) and the biological data (complete blood counts, biochemistry, plasma-free haemoglobin). Non-GLP studies can also be conducted to see if the VAD produces significant adverse events and the results are not presented during the approval to enter clinical trials phase.

As well as haemolysis, platelet activation and aggregation assays are common during animal trials as they are potentially useful for identifying thrombosis. Snyder et al., analysed platelet activation and microaggregation in calves implanted with the HeartMate II finding elevated platelet activation that did not return to pre-op levels in comparison to the sham surgery controls (286). An increase in platelet activation was also consistent with animal and pump complications in sheep implanted with the PediaFlow (consortium of University of Pittsburgh, Carnegie Mellon University, Children's Hospital of Pittsburgh, World Heart Corporation, and LaunchPoint Technologies, LLC (287)) (288). Leukocyte-platelet aggregates and monocyte tissue factor expression have also been studied in sheep and cows implanted with the HeartMate II with a noticeable increase post-implantation (289, 290).

### *5.1.3 Clinical testing*

After completion of a GLP study with at least 6 animals with minimal haemolysis, no pump thrombus at 60+ days, and no adverse events (mechanical, electrical, or biological), the pump can move into clinical trials. Medical device trials are conducted differently to drug trials mainly because you cannot implant into a healthy patient and 'blind' or 'double blind' controls are near impossible (291). A VAD clinical trial will start as a pilot study of 10 – 30 patients who fit the criteria (end-stage heart failure that no longer responds to medication and with little/no chance of a heart transplant) (292). The pilot study reveals any immediate problems with the VAD over a 6 month trial period and provides preliminary information on the safety and performance of the device. The pivotal study then increases the patient population to 150-300 to determine effectiveness and adverse event rates (291). Successful completion of the pivotal study allows for approval, such as the CE mark, to be granted. At this stage, post-approval studies collect long-term data and monitor adverse event rates (291).

The testing of VADs in humans lends itself to a wider range of assay possibilities due to the availability of reagents. It is here that inflammatory biomarkers, such as IL-6, and the presence of microparticles from platelets, leukocytes, and endothelial cells are being studied as markers of adverse events (126, 293-295). A more in depth analysis of the activation status of leukocytes, particular T and B cells of adaptive immunity,

has also been studied in clinical VAD studies showing defects in immune cell response through deactivation and over-activation (101, 102, 296).

## 5.2 Objectives

One of the unique aspects of Calon as a company is the focus on blood damage research with the intention of broadening knowledge in the field, improving VAD design long before implantation, and discovering potential new markers for adverse events which would allow for early intervention. Therefore, the aims of this chapter are to:

- Devices testing *in vitro* to analyse:
  - Haemolysis
  - Haematology
  - Platelet activation
  - Leukocyte microparticles
- Create *in vitro* blood damage profiles of collected parameters for:
  - MiniVAD
  - CentriMag™
  - Heartmate II
  - HVAD
- Device testing *in vivo* to analyse:
  - Leukocyte microparticles and correlations to other parameters
  - Thrombus formation and leukocyte involvement

## 5.3 Methods

### 5.3.1 *In vitro* testing

#### 5.3.1.1 *Ethics and blood collection*

See 2.3.1.2 – bovine abattoir collection

#### 5.3.1.2 *Loop set-up*

See 4.3.1.2.

Test devices (MiniVAD, HeartMate II, and HVAD) were cleaned as per WI-0073\_01: Pump and equipment cleaning. In brief, the devices were sonicated in a 5% Neutracon® solution (Decon Laboratories Ltd., East Sussex, UK) at +50°C for 10 min. Devices were rinsed in tap water and then submerged in 100% ethanol for 1 min before being left out to dry. Before being entered in to the loop, the devices were rinsed in 1X sterile PBS (Life Technologies). To connect the devices to the loop, a pump hat (made by Calon) is placed over the outflow of the pumps.

#### 5.3.1.3 *Haemolysis*

See 3.3.5. and Equation 3.1.

#### 5.3.1.4 *Haematology*

See 2.3.4.

#### 5.3.1.5 *Platelet activation*

Blood samples from the pump test were mixed 1:1 with Streck Cell Preservative (Streck) to preserve the activation status of platelets and left at +2-8°C overnight. CD41/CD61 complex antibody, CAPP2A (IgG1, WSUMAC, USA), was diluted 1:50 in FACS buffer and 5 µL added to 20 µL fixed blood for 30 min on ice in the dark. Samples were lysed with 2 mL BD FACS lysing solution (1:10, BD Bioscience), vortexed, and incubated for 15 min at room temperature in the dark before centrifugation at +4°C, 515 xg, 7 min. The supernatant was discarded and the sample stained with 5 µL of R-PE F(ab')<sub>2</sub> fragment goat anti-mouse IgG (H+L) diluted 1:20 in FACS buffer for 20 min on ice in the dark. Samples were washed in 2 mL FACS buffer and centrifuged. The supernatant was discarded and the cells resuspended in

200  $\mu\text{L}$  BD CellFix (1:10, BD Biosciences) for up to 48 h before acquisition on the flow cytometer. 50000 platelets were acquired based on a gate on the forward- vs side-scatter (log scale) plot. A decrease in CAPP2A signal is indicative of platelet activation (156).

#### 5.3.1.6 *Leukocyte microparticles and death*

##### 5.3.1.6.1 CD45/7AAD

Blood (20  $\mu\text{L}$ ) from the pump test and a positive control (1 mL baseline blood stimulated with 1.87  $\mu\text{g}/\text{mL}$  staurosporine for 4 h) was stained with 0.2  $\mu\text{g}$  CD45-PE (Thermo Fisher) and incubated on ice in the dark for 30 min. Red blood cells were lysed with 600  $\mu\text{L}$  EasyLyse (Dako supplied by Alere Ltd.) and incubated in the dark at room temperature for 15 min after vortexing. 0.1  $\mu\text{g}$  7AAD (eBioscience) was added, the samples vortexed, and incubated for 15 min. Samples were run on the flow cytometer for 60 s acquisition time.

##### 5.3.1.6.2 Activated leukocyte microparticles

As in 4.3.3.2 with the inclusion of 1  $\mu\text{g}$  MM1A (IgG1) for bovine T cells and MM20A for bovine granulocytes (IgG1, Washington State University Monoclonal Antibody Center, WA, USA). These antibodies were conjugated in the lab using Lightning Link APC kit for MM1A (Novus Biologicals, Abingdon, UK) and the Zenon Pacific Blue Conjugation Kit for MM20A (Life Technologies) per the manufacturers' instructions.

##### 5.3.1.6.3 Microparticle differentiation

To confirm that the microparticles were from leukocytes and not platelets, waste blood from human polycythaemic patients was pumped in the CentriMag for 6 h. Human blood was used as conjugated CD41 was unavailable for large animal species. 20  $\mu\text{L}$  blood from baseline, staurosporine, 5, 120, 240, 360 min was single-stained 0.1  $\mu\text{g}$  CD45-PE, 0.6  $\mu\text{g}$  CD41-FITC, 0.1  $\mu\text{g}$  7AAD, or a combination of all (Appendix Figure 8.6).

### 5.3.2 *In vivo testing*

#### 5.3.2.1 *Ethics*

Under the study protocol, animals received humane care in compliance with the ‘European convention for the protection of vertebrates used for experimental and other scientific purposes’ and ‘European directive 86/609/ECC’, formulated by the Council of Europe. The testing facility conducted the study in accordance with national and international legal requirements; and according to the study protocol approved by the University of Leuven’s Animal Ethics Committee; and this Sponsor approved ‘study’ protocol.

#### 5.3.2.2 *Leukocyte microparticles in preserved blood*

Blood samples were drawn via venepuncture into CPDA-1 anticoagulant tubes (Greiner Bio-One) and Cyto-Chex BCT tubes from sheep implanted with the MiniVAD at the following times: PRE (before surgery); POD1 (post-operative day 1); POD2; WEEK 1; WEEK 2; WEEK 3; WEEK 4; TERM (just before euthanasia). CPDA-1 blood was mixed 1:1 with Streck Cell Preservative and stored at +2-8°C with the Cyto-Chex BCT tubes until being packed on ice for shipping to the laboratory (within 24 h of sample being taken). Blood samples (20 µL) were incubated on ice in the dark for 30 min with the following antibodies (Table 5.4):

**Table 5.4: Antibodies for pre-clinical samples**

Tube	CD45-PE	CD14-BV500	CD21-PE	CD11b-FITC	HLA-DR-PeCy7
1: Unst	-	-	-	-	-
2	0.2 µg	-	-	-	-
3	0.2 µg	-	-	2 µg	3 pg
4	-	0.1 µg	0.1 µg	2 µg	3 pg

Red blood cells were lysed with EasyLyse and run immediately on the Navios flow cytometer for 60 sec acquisition time on a log scale.

### 5.3.2.3 *Clot structure*

#### 5.3.2.3.1 Fixation

Biological matter from the MiniVAD pumps implanted into sheep for 30 days and the explanted HeartAssist 5 (ReliantHeart Inc. Houston, TX, USA) was carefully removed and either stored in 10% neutral-buffered formalin for 72 h at room temperature (for paraffin-embedding) or in 1% glutaraldehyde (Sigma Aldrich) overnight and then placed in 70% ethanol at +2-8°C for long term storage.

#### 5.3.2.3.2 Paraffin-embedding and slicing

Formalin-fixed tissue was placed into a Tissue-Tek cassette (VWR, Lutterworth, Leicestershire, UK) and labelled with a pencil. The cassette containing the sample was dehydrated in a series of ethanol incubations: 70% for 40 min; 80% for 40 min; 90% for 40 min; then 100% for 40 min twice. Cassette was then placed into HistoChoice clearing agent (Sigma Aldrich) for 10 min twice. Paraffin wax granules were melted at +65°C until clear and runny then the sample removed from the cassette and placed into the wax with gentle agitation for 7 min. A tissue mould was partially filled with paraffin before positioning the tissue in the mould. The body of the cassette was placed onto the mould and paraffin wax added until the top of the cassette was filled. Paraffin was cooled for 30 min and then the mould placed on ice to remove the final paraffin-embedded sample.

Sections of paraffin-embedded samples were cut at 5 µm thickness on a rotary microtome. Slices were floated on a water bath at +37°C onto poly-L-lysine coated microscope slides (Leica). The wax melted onto the slide by heating at +65 °C for 20 min. Slides were dried overnight and room temperature and stored at +2-8°C.

#### 5.3.2.3.3 Carstairs staining method

Slides were rehydrated via the following steps: HistoChoice 10 min twice; 100% ethanol 10 mins twice; 95% ethanol 5 min; 70% ethanol 5 min; 50% ethanol 5 min; rinsed in dH<sub>2</sub>O then hydrated in PBS for 10 min. Slides were then submerged in 5% ammonium (III) iron sulphate solution (CN Technical Services Ltd., Cambridgeshire, UK) for 5 mins, rinsed in tap water, then stained with Mayer Haematoxylin (CN Technical Services Ltd.) for 5 min. Slides were rinsed in tap water then stained with Picric acid-orange G solution (CN Technical Services Ltd.) for 30 min, rinsed once in



dH<sub>2</sub>O, then stained in Ponceau Fuchsin (CN Technical Services Ltd.) for 3 min. Slides were rinsed in tap water and submerged in 1% phosphotungstic acid solution (Sigma Aldrich; 1g dissolved in 100 mL dH<sub>2</sub>O) for 60 secs followed by rinsing in tap water. Slides were submerged in aniline blue (CN Technical Services Ltd.) for 1 h followed by rinses in several changes of dH<sub>2</sub>O. The slides were cleared twice for 3 min with HistoChoice then dehydrated with 100% ethanol three times for 1 min each before DPX was used to mount the coverslip.

#### 5.3.2.3.4 Scanning electron microscopy

The sample that had been stored in 1% glutaraldehyde was dehydrated with a series of graded concentrations (30% to 100 %) of ethanol. The dehydrated sample was then rinsed with 50% hexamethyldisilane solution (HMDS) in 100% ethanol for 10 minutes in a fume hood and then three times in 100% HMDS and left overnight to dry. The sample was coated with a thin layer of gold (~15 nm) using sputter coating and was imaged using scanning electron microscopy (Hitachi 4800) (297).

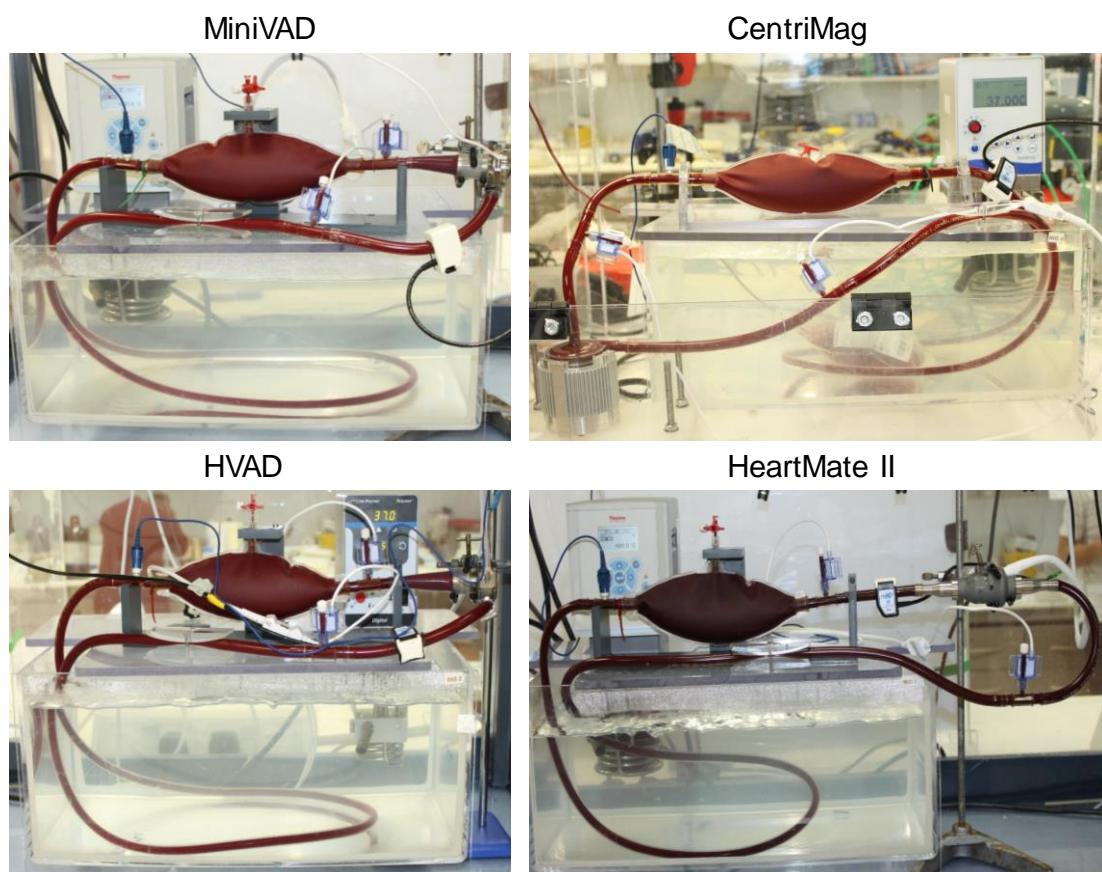
#### 5.3.3 *Data and statistical analysis*

As described in 4.3.5.

## 5.4 Results

### 5.4.1 Benchmarking study

The purpose of the benchmarking study was to use the assays developed as part of this thesis (see 4.3.3.1 and 4.3.3.2) on competitor pumps compared to the MiniVAD. The HVAD and HMII were donated to Calon from collaborators. The devices were cleaned using protocols set in place by the engineering team and assembled for laboratory testing. The CentriMag was used as the control for these tests as haemolysis is very low and reproducible in this pump (63). Therefore, if the normalised index of haemolysis (NIH) value for CentriMag after completion of the test was  $\geq 0.002$  g/ 100 L the blood was considered of low quality and the experiment was discarded and repeated.

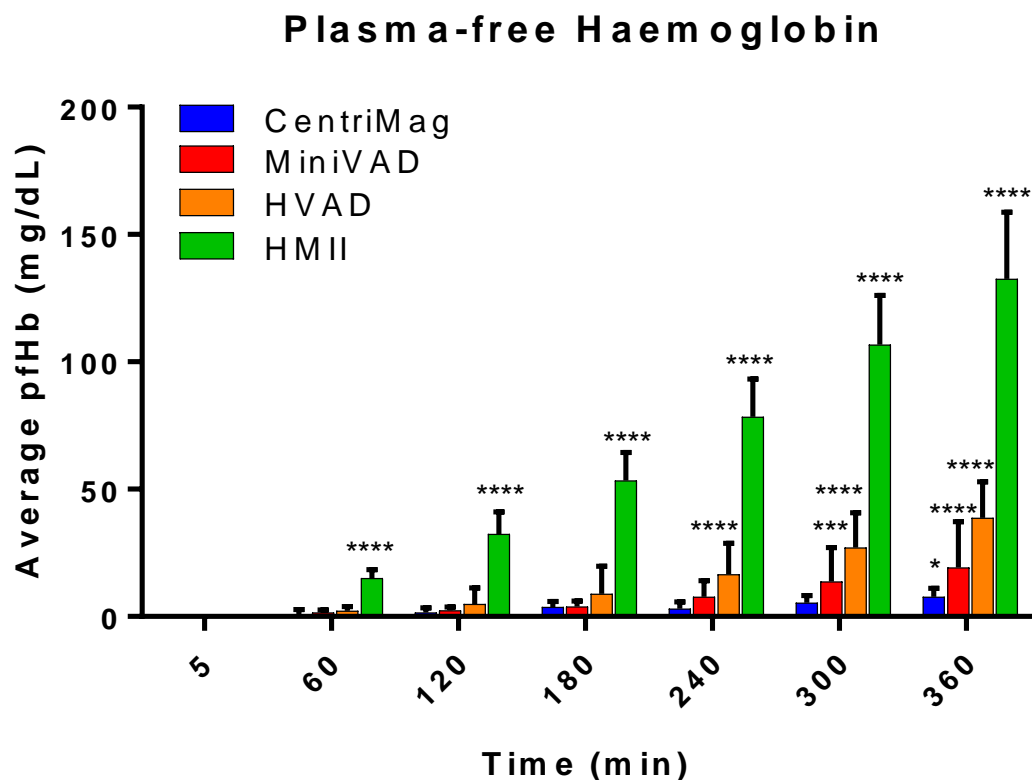


**Figure 5.1: The devices used in the Benchmarking study**

The MiniVAD, HVAD, HeartMate II, and the CentriMag were connected to the mock circulatory loop according to the ASTM. 1X PBS was circulated within the loops for 20 min to check pump function. The PBS was drained and bovine blood adjusted to a packed cell volume of  $30 \pm 2\%$  gravity filled into the loops.

### 5.4.1.1 Haemolysis

As previously mentioned, haemolysis is the standard measurement required for regulatory approval. As the HVAD and HMII are used in clinic and have been since 2008, their performance in the Calon designed test rig for the most basic blood damage assessment was the first step into determining how different designs impact the blood *in vitro*.



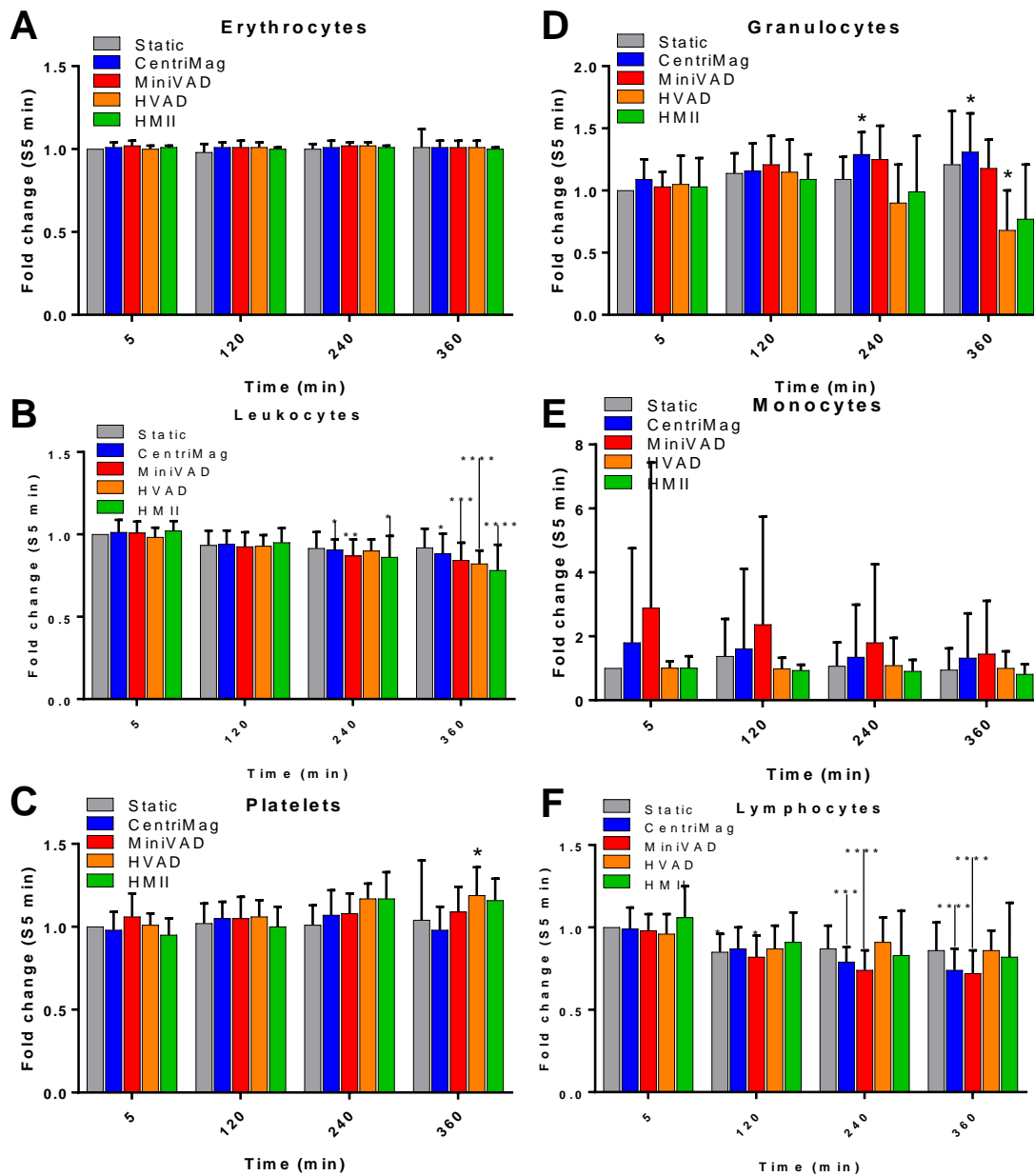
**Figure 5.2: Haemolysis**

Bovine blood was diluted to a haematocrit of  $30 \pm 2\%$  using PBS, loaded into the loops with the CentriMag (blue,  $n = 15$ ); MiniVAD (red,  $n = 11$ ); HVAD (orange,  $n = 10$ ); HMII (green,  $n = 5$ ). A 500 mL bag of ovine blood was left in the  $+37^\circ\text{C}$  water bath as a static control (grey,  $n = 15$ ). Blood samples were removed every hour for 6 hours. Plasma-free haemoglobin was measured using the Harboe assay (mg/dL).

Plasma-free haemoglobin increased with time as expected. This increase was significantly higher than the baseline sample in the HMII after only 60 min of pumping ( $p = 0.001$ ), after 240 min in the HVAD ( $p = 0.001$ ), and 360 min in the MiniVAD ( $p = 0.001$ ) and the CentriMag ( $p = 0.038$ ).

#### 5.4.1.2 *Haematology*

Four tubes were available after each sample point. Three tubes were centrifuged for the haemolysis assay and the fourth was reserved for whole blood assays. This tube was run in triplicate on the Abacus Jr Vet 5.



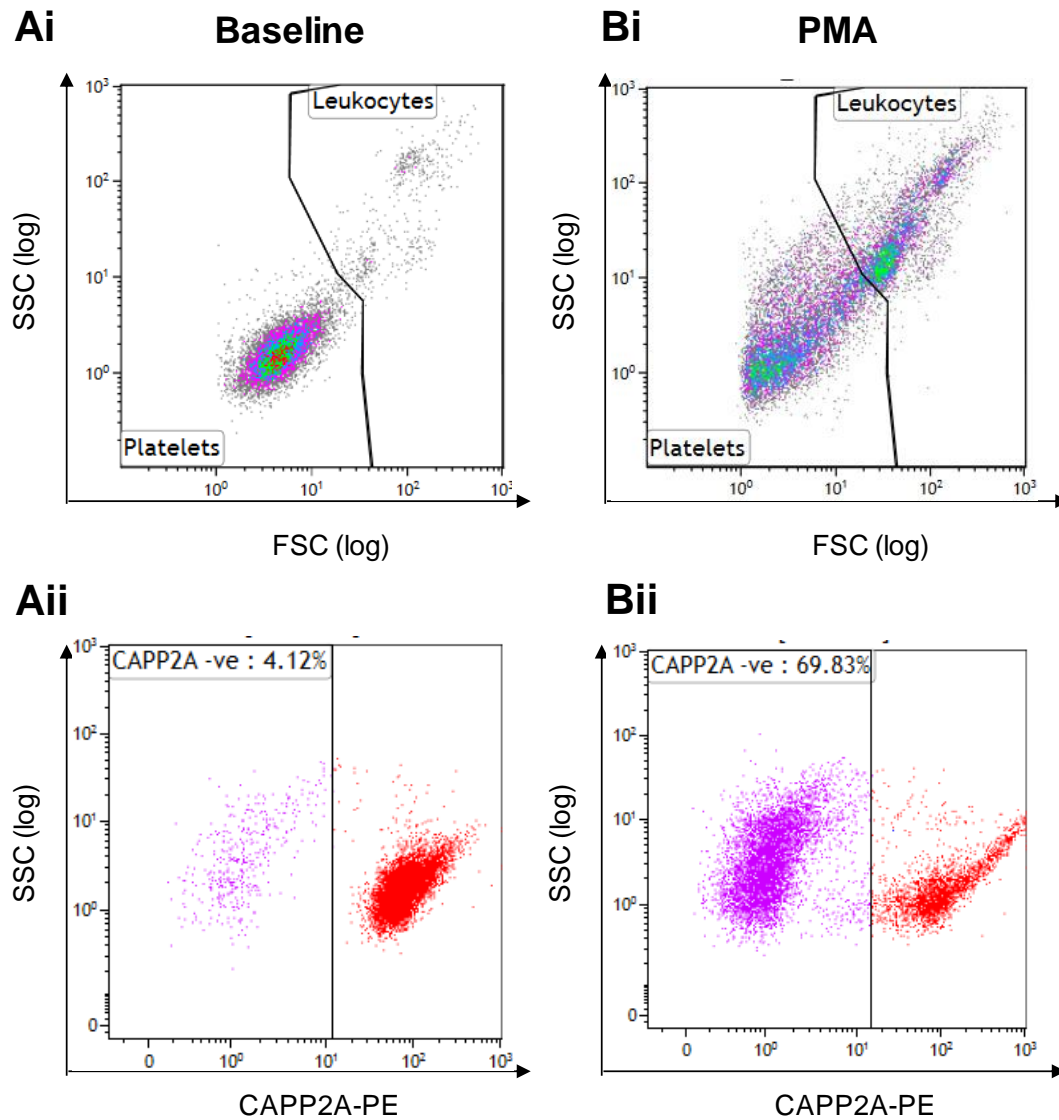
**Figure 5.3: Haematology**

Bovine blood was diluted to a haematocrit of  $30 \pm 2\%$  using PBS, loaded into the loops with the CentriMag (blue,  $n = 15$ ); MiniVAD (red,  $n = 11$ ); HVAD (orange,  $n = 10$ ); HMII (green,  $n = 5$ ). A 500 mL bag of ovine blood was left in the  $+37^\circ\text{C}$  water bath as a static control (grey,  $n = 15$ ). Blood samples were removed every hour for 6 hours. Average complete cell counts (cells/ $\mu\text{L}$ ) from blood samples run in triplicate for **A**) erythrocytes, **B**) leukocytes, **C**) platelets, **D**) granulocytes, **E**) monocytes, and **F**) lymphocytes for each time point.

The erythrocyte count was unaffected by the pumps and the platelet count was only significantly increased after 360 min in the HVAD ( $p = 0.03$ ). The leukocyte count was significantly decreased after 240 min and 360 min in the MiniVAD ( $p = 0.0047$  &  $0.0002$  respectively), at 240 min and 360 min in the HMII ( $p = 0.035$  &  $0.0001$ ), and at 360 min in the HVAD ( $p = 0.0001$ ) and the CentriMag ( $p = 0.013$ ). To shed light on which leukocyte subset is mostly affected by the pumps, the granulocyte, monocyte, and lymphocyte count was measured. Granulocytes were significantly decreased by the CentriMag at 240 and 360 min ( $p = 0.026$  &  $0.014$ ) and by the HVAD at 360 min ( $p = 0.03$ ). The monocyte count was not affected by the pumps but the lymphocyte count was significantly decreased by the CentriMag at 240 min and 360 min ( $p = 0.026$  &  $0.014$ ) and the HVAD at 360 min ( $p = 0.03$ ).

#### *5.4.1.3 Platelet activation*

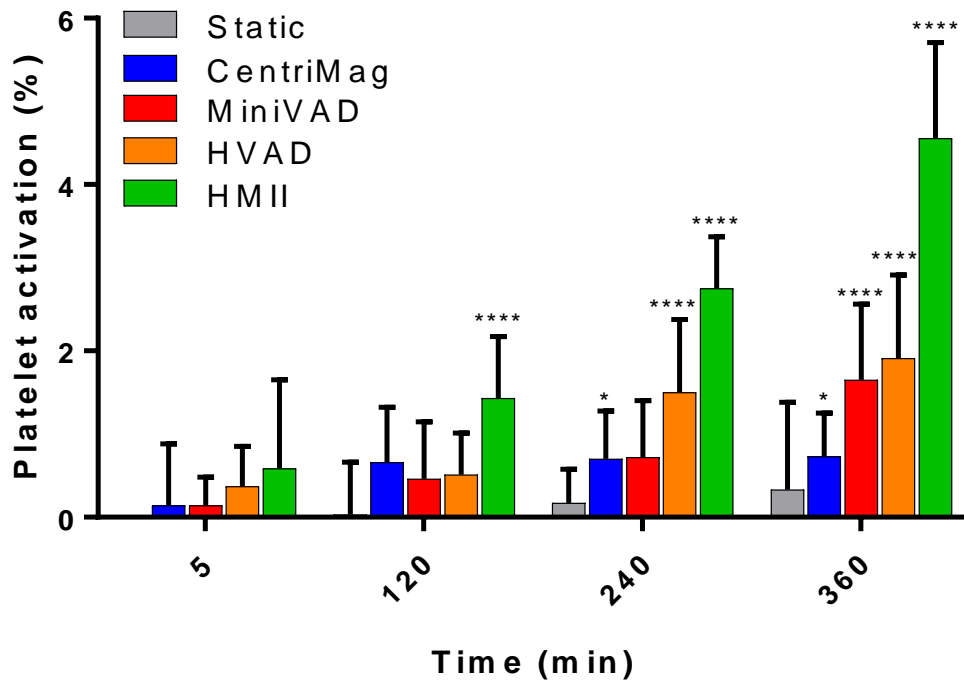
The level of platelet activation can give some indication as to how thrombogenic the pumps are. Platelet activation was measured using the bovine-specific antibody CAPP2A which is the ruminant equivalent of the CD41/CD61 complex (156). This complex changes conformation upon platelet activation and a down-regulation in its expression can be measured using flow cytometry (Figure 5.4) (156).



**Figure 5.4: Gating strategy for measuring platelet activation**

Bovine blood was diluted to a haematocrit of  $30 \pm 2\%$  using PBS (**A**) baseline. A positive control was stimulated with  $1 \mu\text{M}$  PMA for 20 min (**B**). Blood was stained with CAPP2A and PE-secondary antibody to detect resting platelets. After lysing of red blood cells, washing, and fixing, the samples were acquired on the flow cytometer. Percentage of cells negative for CAPP2A were deemed 'activated platelets'. **Ai & Bi**) Forward vs side scatter on a log scale with platelet and leukocyte gates set to known characterisation, **Aii & Bii**) Expression of CAPP2A on platelets.

## Platelet activation



**Figure 5.5: Platelet activation**

Bovine blood was diluted to a haematocrit of  $30 \pm 2\%$  using PBS, loaded into the loops with the CentriMag (blue,  $n = 17$ ); MiniVAD (red,  $n = 9$ ); HVAD (orange,  $n = 10$ ); HMII (green,  $n = 8$ ). A 500 mL bag of ovine blood was left in the  $+37^\circ\text{C}$  water bath as a static control (grey,  $n = 19$ ). Blood samples were stained with CAPP2A and a decrease in its expression on platelets ( $\% \text{CAPP2A}^+$ ) was identified as activation.

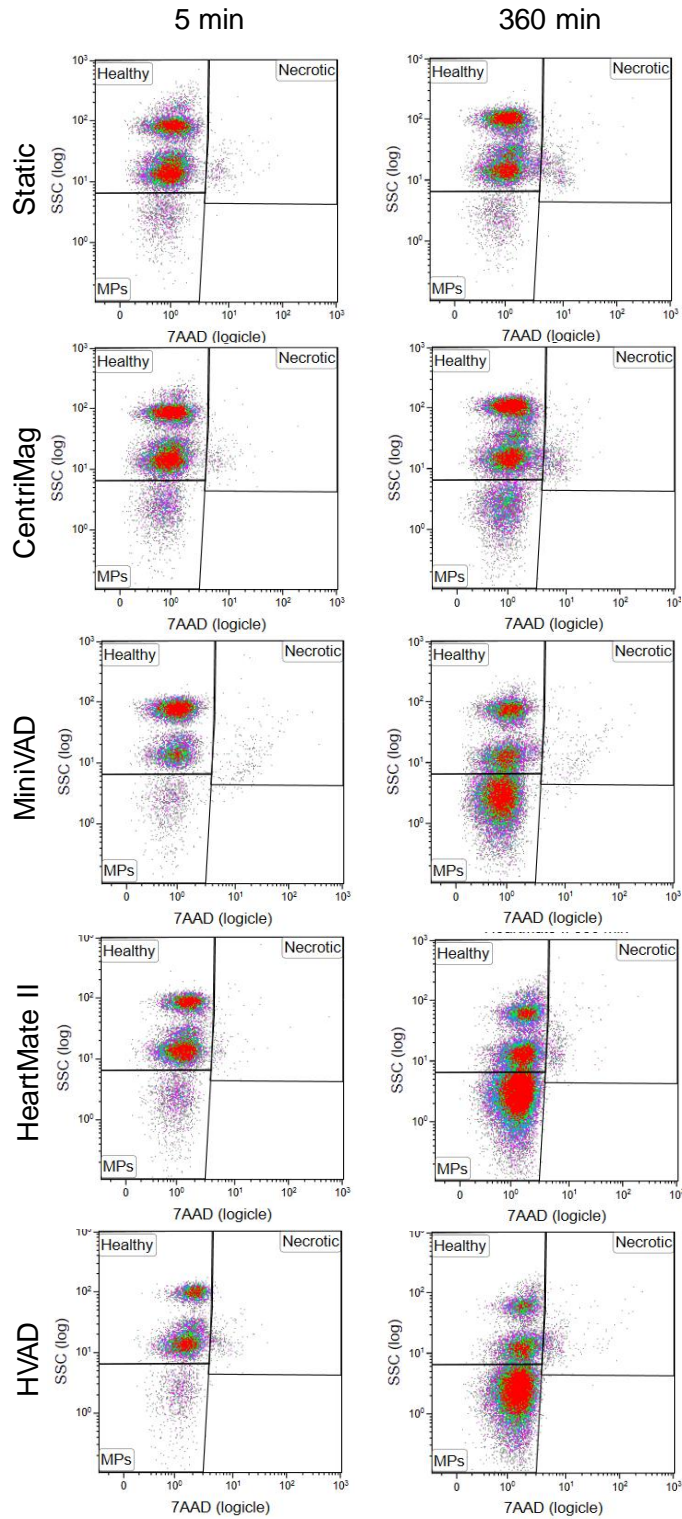
Platelet activation was significantly increased in comparison to the 5 min static control in the HMII at 120, 240, and 360 min ( $p \leq 0.0001$ ). This significance was also observed in the HVAD at 240 min, and the MiniVAD at 360 min. Platelet activation in the CentriMag was significantly increased compared to the 5 min static control at 240 min ( $p = 0.041$ ) and at 360 min ( $p = 0.029$ ).

### 5.4.1.4 Leukocyte microparticles and death

In Chapter 4, different operating conditions were reported to change the number of leukocyte-derived microparticles present after 6 h circulation in the CentriMag. Therefore, LMPs potentially could be used as a biomarker for the efficacy of pump

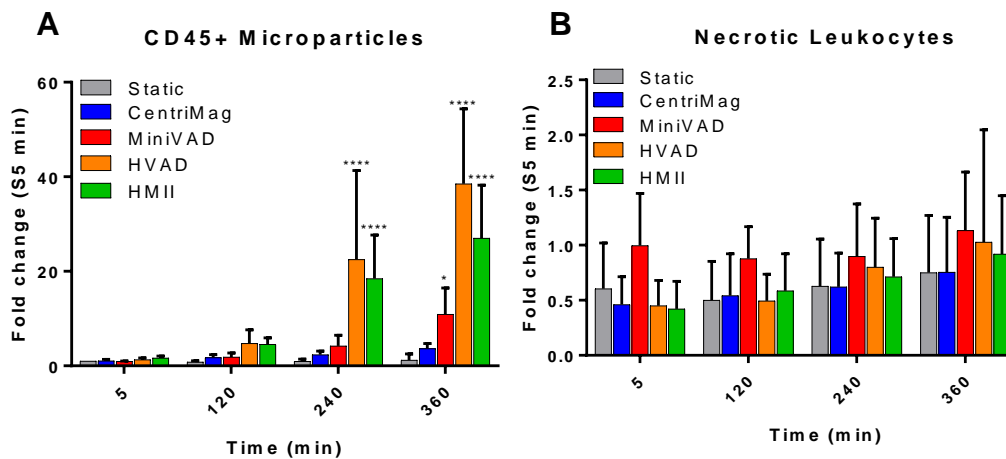


design and measure of thrombogenicity. Gating strategy for the LMPs is shown in (Figure 5.6) for the 5 and 360 min timepoint for each pump.



**Figure 5.6: Leukocyte microparticles gating strategy for benchmarking study**

Bovine blood samples stained with CD45-PE and 7AAD and acquired for 60 secs on the Navios flow cytometer. CD45<sup>+</sup> events were displayed on SSC vs 7AAD plot to display healthy, necrotic, and leukocyte microparticles.



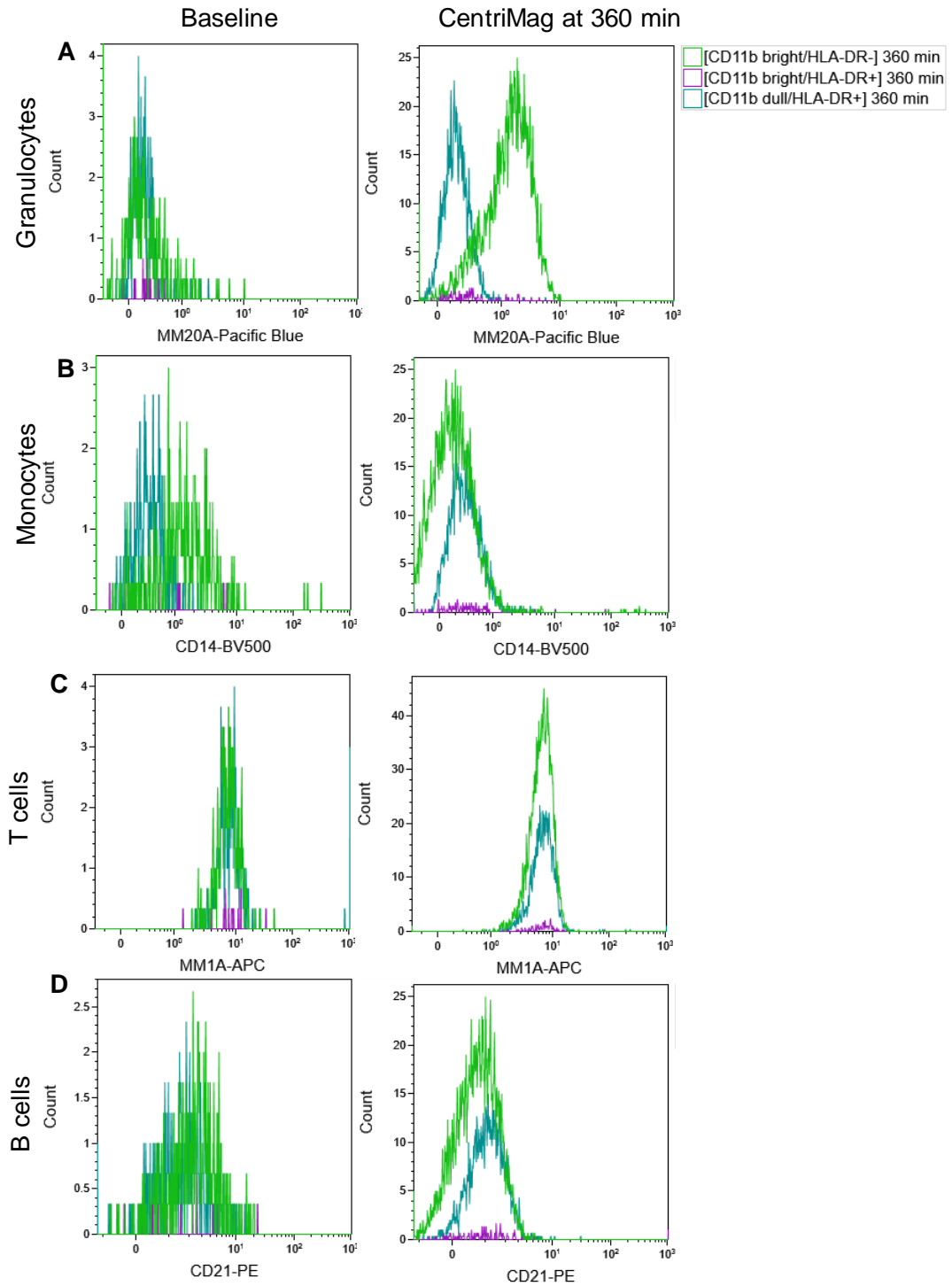
**Figure 5.7: Leukocyte microparticles and necrotic leukocytes**

Bovine blood was diluted to a haematocrit of  $30 \pm 2\%$  using PBS, loaded into the loops with the CentriMag (blue,  $n = 15$ ); MiniVAD (red,  $n = 4$ ); HVAD (orange,  $n = 9$ ); HMII (green,  $n = 10$ ). A 500 mL bag of ovine blood was left in the  $+37^\circ\text{C}$  water bath as a static control (grey,  $n = 15$ ). Blood samples were stained with CD45-PE and 7AAD to identify **A.** number of LMPs and **B.** number of necrotic leukocytes.

After 240 min circulation in the loops, the HMII and HVAD showed a significant increase in the number of LMPs in comparison to the static at 5 min ( $p \leq 0.0001$ ). The MiniVAD reached a significant difference at 360 min ( $p = 0.024$ ) (Figure 5.7A). There was no significant difference in necrotic leukocytes (Figure 5.7B).

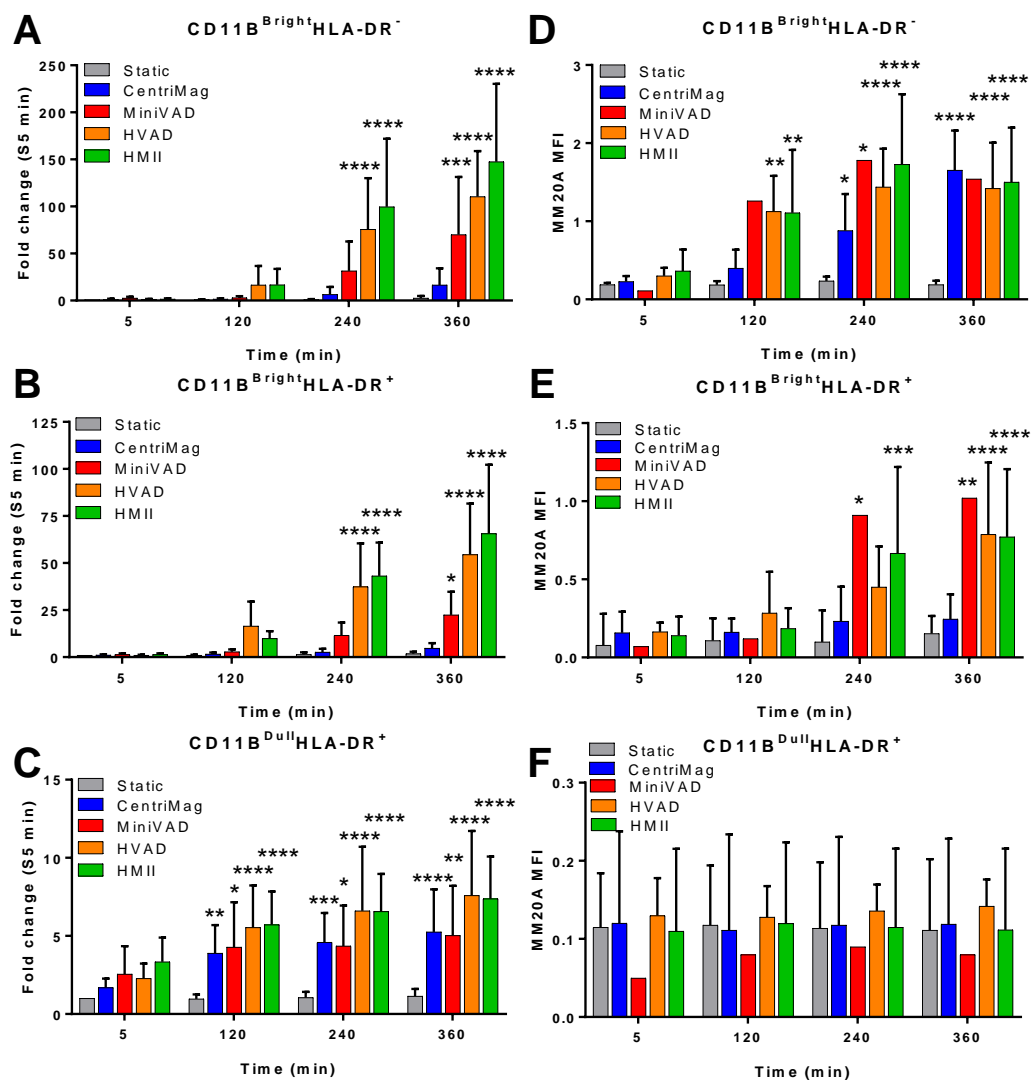
#### 5.4.1.5 Activated leukocyte microparticles

Characterisation of the LMPs was achieved using a 6-colour flow cytometry panel to identify granulocytes (MM20A), monocytes (CD14), T cells (MM1A), B cells (CD21) and the activation markers CD11b and HLA-DR. Gating of active LMPs was achieved as described in Shear stress chapter figures with the additional expression of MM1A or MM20A used to determine parentage (Figure 5.8).



**Figure 5.8: Parentage of activated leukocyte microparticles**

Active microparticles were defined as events with low SSC and positive for CD11b and/or HLA-DR (Green = CD11b<sup>bright</sup>HLA-DR<sup>-</sup>, purple = CD11b<sup>bright</sup>HLA-DR<sup>+</sup>, and blue = CD11b<sup>dull</sup>HLA-DR<sup>+</sup>). Co-expression of MM20A, CD14, MM1A, or CD21 on these active microparticles indicates lineage from **A**) granulocytes, **B**) monocytes, **C**) T cells, or **D**) B cells, respectively.



**Figure 5.9. Activated leukocyte microparticles.**

Bovine blood was diluted to a haematocrit of  $30 \pm 2\%$  using PBS, loaded into the loops with the CentriMag (blue,  $n = 13$ ); MiniVAD (red,  $n = 5$ ); HVAD (orange,  $n = 8$ ); HMII (green,  $n = 9$ ). Blood from 5, 120, 240, and 360 min were stained with MM20A, MM1A, CD14, CD21, CD11b, and HLA-DR and the number of microparticles with the following expression: **A.** CD11b<sup>Bright</sup>HLA-DR<sup>-</sup>, **B.** CD11b<sup>Bright</sup>HLA-DR<sup>+</sup>, and **C.** CD11b<sup>Dull</sup>HLA-DR<sup>+</sup>, plotted for each pump type as a fold from the 5 min static control. **D., E. and F.** show the MM20A MFI for each active MP population.

The number of each type of microparticle increased over time in all implantable pumps (MiniVAD, HVAD, HMII). The CD11b<sup>Bright</sup>HLADR<sup>-</sup> LMPs (Figure 5.9A) were increased significantly after 240 min in the HVAD and HMII ( $p = 0.0001$  for both) and after 360 min in the MiniVAD ( $p = 0.0006$ ). The CD11b<sup>Bright</sup>HLADR<sup>+</sup> LMPs (Figure 5.9B) were increased significantly after 240 min in the HVAD and HMII ( $p =$

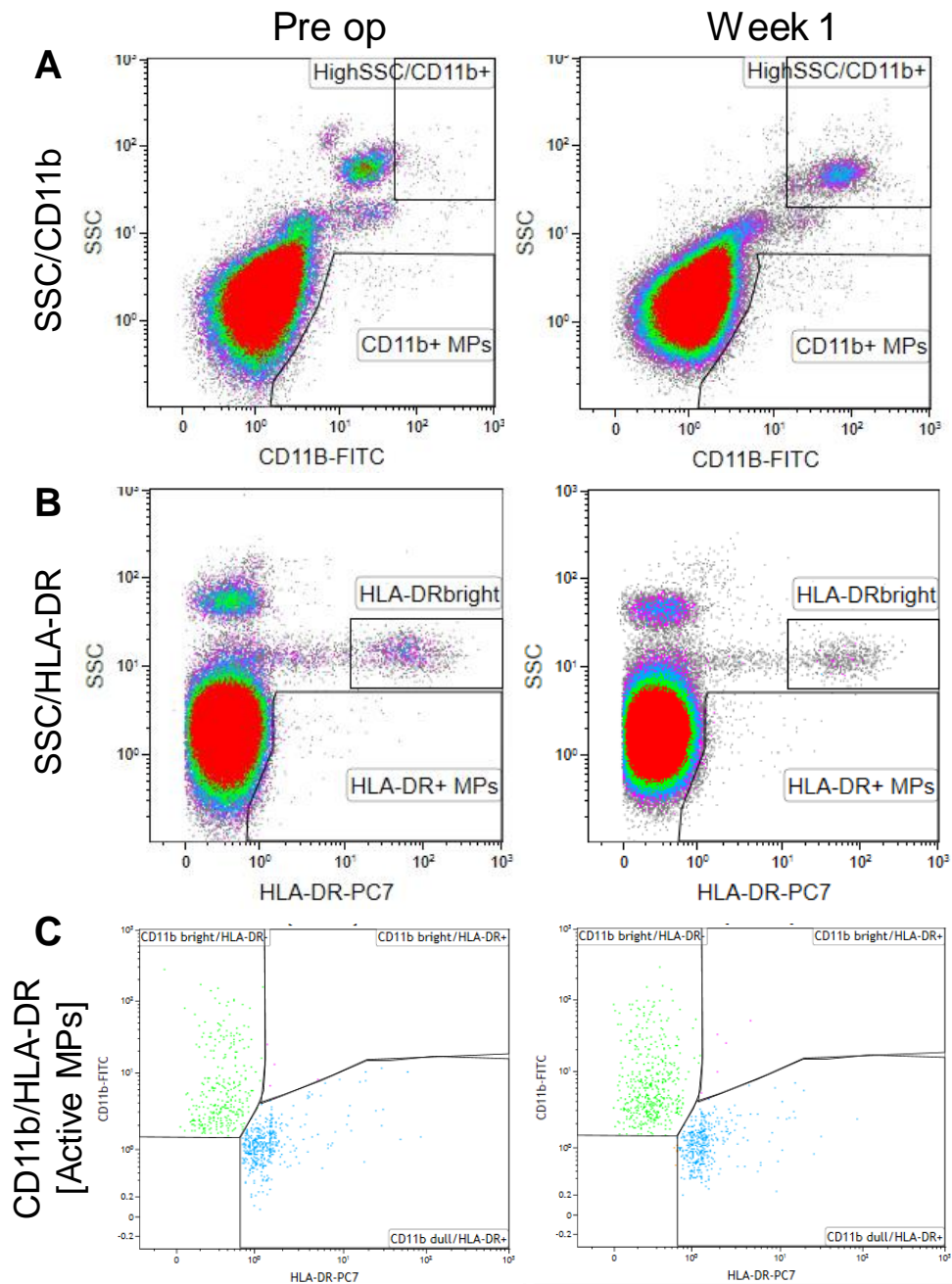
0.0001 for both) and after 360 min in the MiniVAD ( $p = 0.011$ ). The pattern of activated MPs was changed with the CD11b<sup>Dull</sup>HLADR<sup>+</sup> (Figure 5.9C). After 120 min, all pumps had a significantly increased CD11b<sup>Dull</sup>HLADR<sup>+</sup> LMP population (CentriMag:  $p = 0.008$ ; MiniVAD:  $p = 0.042$ ; HMII & HVAD:  $p \leq 0.0001$ ).

In the previous chapter (Chapter 4) it was suspected that the CD11b<sup>Bright</sup>HLADR<sup>-</sup> and CD11b<sup>Bright</sup>HLADR<sup>+</sup> populations could be derived from granulocytes but due to the lack of an ovine granulocyte marker it was not possible to prove this. MM20A detects bovine granulocytes (298) and could be used to determine the lineage of these LMPs. The MFI of MM20A significantly increased after 120 min in the HMII and HVAD ( $p = 0.003$ ;  $n = 6$  &  $0.004$ ;  $n = 5$  respectively), and after 240 min in the MiniVAD and CentriMag ( $p = 0.025$ ;  $n = 1$  &  $0.011$ ;  $n = 8$  respectively) for the CD11b<sup>Bright</sup>HLADR<sup>-</sup> population (Figure 5.9D). After 360 min, there was no longer a significant difference observed in the MiniVAD ( $p = 0.051$ ), however, this was only for one test ( $n = 1$ ). The MFI of MM20A also significantly increased on the CD11b<sup>Bright</sup>HLADR<sup>+</sup> LMPs (Figure 5.9E) after 240 min for the MiniVAD and HMII ( $p = 0.026$  &  $0.0004$  respectively) and after 360 min for the HVAD ( $p = 0.0001$ ). CD11b<sup>Dull</sup>HLADR<sup>+</sup> did not express MM20A (Figure 5.9F) and therefore confirms that this population must come from another leukocyte subset. However, the bovine T cell marker, MM1A, was not detected on these LMPs (Figure 5.8C) so they either come from a different population or they no longer possess the marker for their lineage.

#### 5.4.2 Pre-clinical trials – leukocyte microparticles

After successfully achieving an NIH of below 0.01 g/100 L, the MiniVAD entered non-GLP *in vivo* trials. The MiniVAD was implanted into 8 sheep for up to 30 days. Blood samples were taken at pre-determined time points during the study and preserved directly in Cyto-Chex blood collection tubes (Cyto-Chex BCT, Streck) or drawn into CPDA-1 tubes and mixed 1:1 with Streck Cell Preservative (SCP). Both preservatives vary slightly in their chemical formula (Cyto-Chex has K3-EDTA as its anticoagulant combined with SCP) but have different advantages. The Cyto-Chex-BCT are designed for collection via venepuncture resulting in sterile blood and is practical for the phlebotomist to use, whereas this is not feasible for *in vitro* testing making the SCP more appropriate. Both approaches were used for the preclinical trial

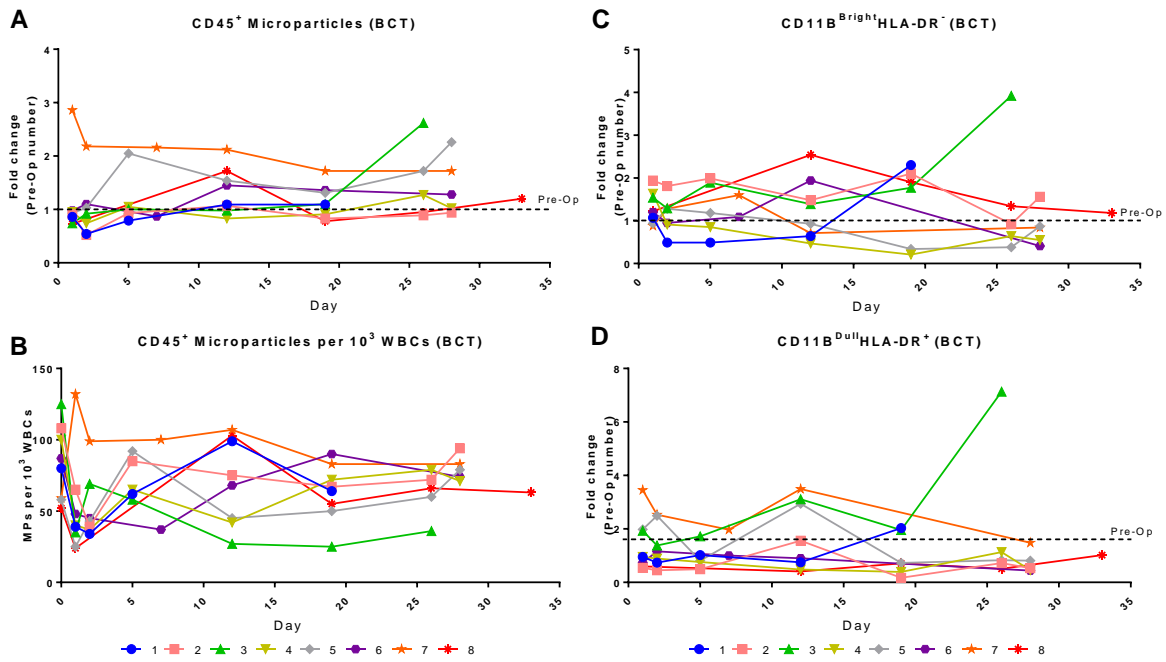
to compare how well they preserved the blood and whether the flow cytometry results obtained were comparable. The main purpose was to use the *in vitro* developed LMP assays on the blood collected from implanted animals to see whether LMPs could be used as a biomarker of pump performance and adverse events (e.g. thrombosis). This could only be achieved through using blood preservatives (as tested in Chapter 2) due to the preclinical trials happening in Leuven, Belgium and required shipping to Swansea.



**Figure 5.10: Preclinical activated leukocyte microparticles**

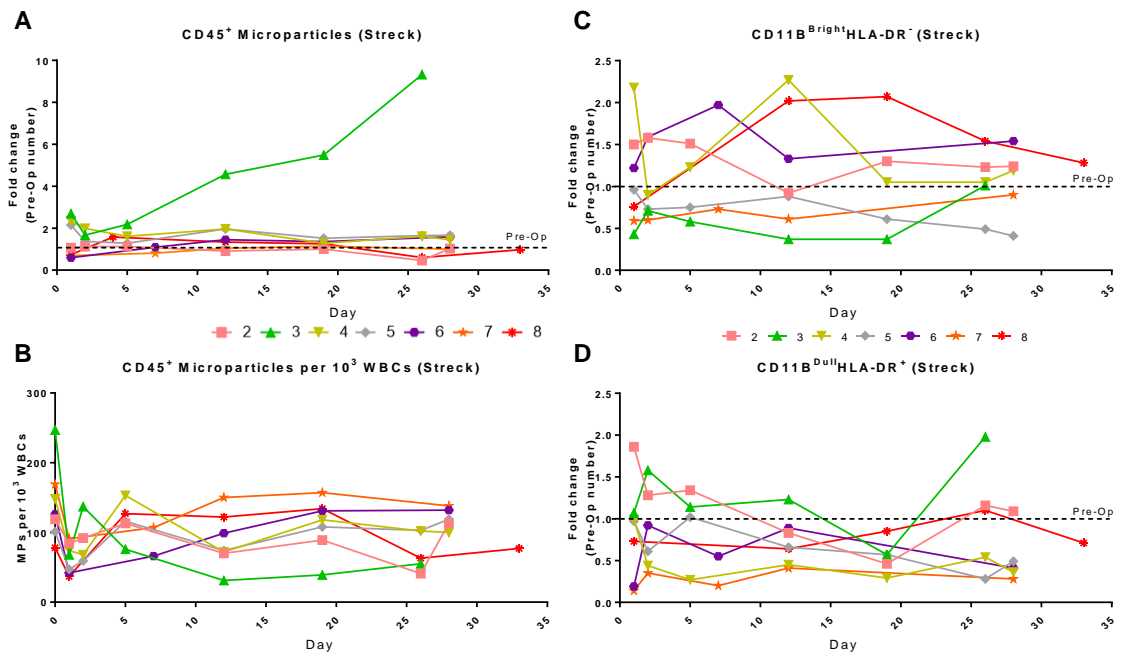
Blood from sheep implanted with the MiniVAD was collected via venepuncture into CPDA-1 anticoagulant, then mixed 1:1 with Streck Cell Preservative before shipping to Swansea at  $+2-8^{\circ}\text{C}$  (pre-op and week 1 samples shown here). Samples were stained with CD14, CD21, CD11b, and HLA-DR. Events with a low SSC were defined as microparticles (MPs) (A & B) and plotted on a CD11b-FITC vs HLA-DR PeCy7 to determine activation status: CD11b<sup>Bright</sup>HLA-DR<sup>-</sup>, CD11b<sup>Bright</sup>HLA-DR<sup>+</sup>, or CD11b<sup>Dull</sup>HLA-DR<sup>+</sup> (C).





**Figure 5.11: Leukocyte- derived microparticles in blood taken from VAD-implanted sheep into Cyto-Chex-BCT tubes.**

Blood was drawn via venepuncture into Streck BCT and shipped to the lab within 48 h. Blood was stained with CD45, CD14, CD21, CD11b, and HLA-DR and the number of microparticles plotted: **A.** CD45<sup>+</sup> MPs (fold change from pre-op), **B.** CD45<sup>+</sup> MPs per 10<sup>3</sup> WBCs, **C.** CD11b<sup>Bright</sup>HLA-DR<sup>-</sup> MPs (fold change from pre-op) and **D.** CD11b<sup>Dull</sup>HLA-DR<sup>+</sup> MPs (fold change from pre-op). Each colour represents a sheep number.



**Figure 5.12: Leukocyte-derived microparticles from blood taken from VAD-implanted sheep and mixed with Streck Cell Preservative.**

Blood was drawn via venepuncture into CPDA-1 tubes. Blood from this tube was mixed 1:1 with Streck Cell Preservative and shipped to the lab within 48 h. Blood was stained with CD45, CD14, CD21, CD11b, and HLA-DR and the number of microparticles plotted: **A.** CD45<sup>+</sup> MPs (fold change from pre-op), **B.** CD45<sup>+</sup> MPs per 10<sup>3</sup> WBCs, **C.** CD11b<sup>Bright</sup>HLA-DR<sup>-</sup> MPs (fold change from pre-op) and **D.** CD11b<sup>Dull</sup>HLA-DR<sup>+</sup> MPs (fold change from pre-op). Each colour represents a sheep number.

The two variations of the Streck preservative proved very different in terms of microparticle numbers, marker expression, and general pattern over time. Overall, the BCT tubes while more practical generally, arrived in the laboratory in Swansea in poor condition (leakage, clots, and cracked tubes) which is most likely due to not inverting the tubes immediately on collection of blood. It is likely that the SCP samples give a more accurate representation of LMPs as the preservative was mixed directly with the blood via a pipette.

The number of CD45<sup>+</sup> LMPs did not change significantly from pre-op levels during the time of implantation in 7 of the 8 sheep (Figure 5.11 & Figure 5.12A). When compared as a ratio to the WBC count, there was an initial decrease in the number of CD45<sup>+</sup> LMPs at post-operative day 1 (POD1) which increased slightly and levelled

out over time (Figure 5.11 & Figure 5.12B). The activation profile of the LMPs fell into two categories (Figure 5.10C:CD11b<sup>Bright</sup>HLA-DR<sup>-</sup> and CD11b<sup>Dull</sup>HLA-DR<sup>+</sup>) instead of the three-observed *in vitro* but it was very difficult to determine what was happening over time for these MPs (Figure 5.11C&D, Figure 5.12.C&D).

The anomaly during the study was KULOV-03 which was diagnosed with arrhythmogenic right ventricular cardiomyopathy during the necropsy. This correlated with an increasing number of white blood cells over time and thereby an increase in the number of CD45<sup>+</sup> LMPs (Figure 5.11A & Figure 5.12A) although the ratio was not remarkably different to the other sheep (Figure 5.11B & Figure 5.12B).

### 5.4.3 Pre-clinical trials – clot structure

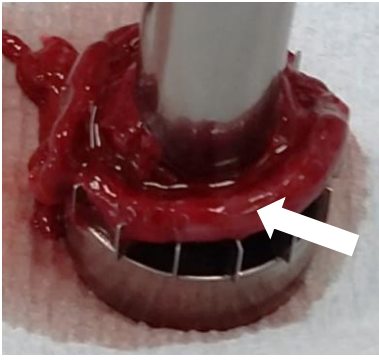
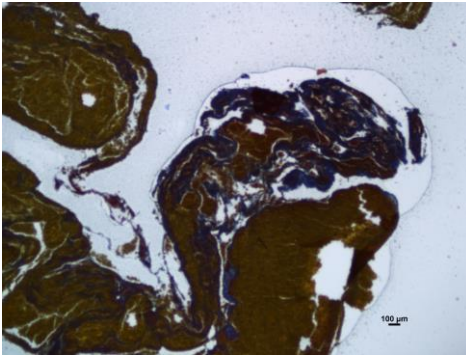
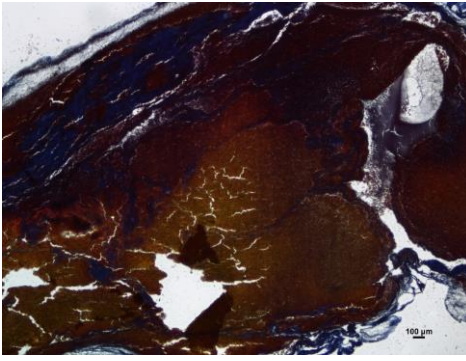
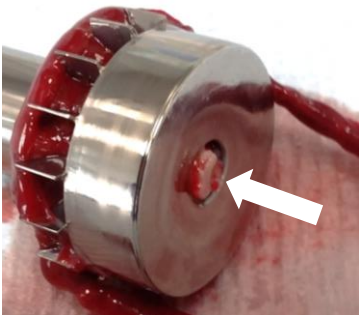
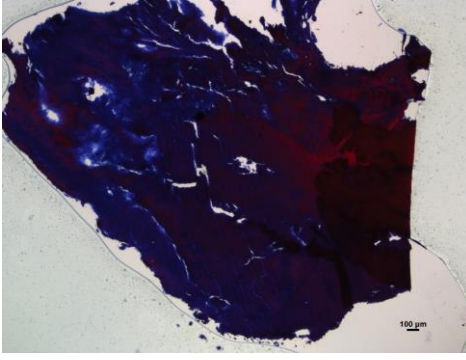
Thrombosis continually plagues VAD developers and pump thrombus leads to stroke, pump blockage, pump replacement, and death. It is a common adverse event associated with VADs with reported rates approximately 0.02 events per patient per year (89). Creating thrombus during *in vitro* testing is extremely difficult and very little research is done on clots during *in vivo* studies. Hastings et al., successfully formed thrombi *in vitro* using the Revolution centrifugal pump (Sorin Group, Milan, Italy) and stained the samples using the Carstairs' method (299). This inspired the work for thrombi found in the MiniVAD post-implant in sheep.

#### 5.4.3.1 Histological staining

The Carstairs' Method was designed in the 1960's to differentiate fibrin from platelets in a histological sample when the role of thrombus in atherosclerosis was picking up interest. Routine stains such as haematoxylin-and-eosin stain could identify fibrin, but platelets had the same tinctorial characteristic making these methods not so useful for thrombi (300). Carstairs altered combinations of traditional stains to allow differentiation and identification of fibrin (bright red), platelets (navy), collagen (bright blue), and red blood cells (clear yellow) in his self-named method (300). This method is used to stain formalin-fixed paraffin-embedded samples (FFPE) which allows for long-term storage of samples at room temperature.

**Table 5.5: Histological staining of samples obtained from the pump implanted into KULOV-08.**

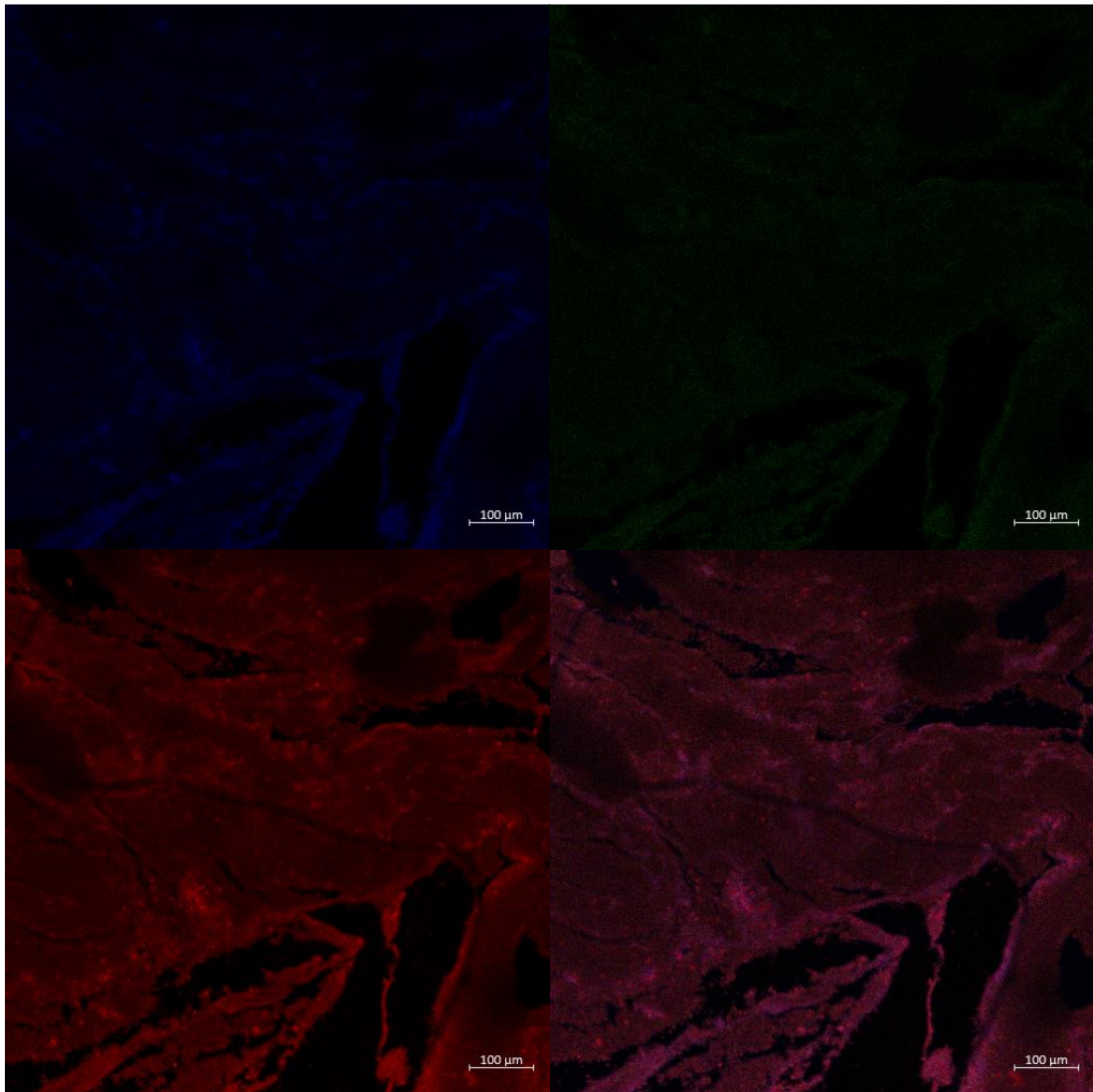
Biological build-up (supposed thrombi) were carefully removed from areas of the pump and fixed in 10% neutral-buffered formalin for 72 h to ensure full fixation. Samples were dehydrated, cleared, and paraffin-embedded. A microtome was used to slice 5  $\mu\text{m}$  thick slices which were mounted onto slides before being stained with the Carstairs' method. Slides were imaged using a light microscope with the higher magnifications (x4) showing the fibrin (bright red), platelets (navy), collagen (bright blue), and red blood cells (clear yellow) clearly.

Location	Image	Slide (x4 mag)
A. On top of rotor blades		
B. Outflow	N/A	
C. Outlet bearing		

Unfortunately, KULOV-08 was the only pump where the biological build-up was available to be processed in the laboratory whereas the other pump samples were sent back to Leuven which does not use this method. Before staining, the samples were either characterised as a ‘red clot’ (red blood cell based) or a ‘white clot’ (platelet based) related to their appearance to the naked eye (301). When stained with the Carstairs method, this staining showed to match the initial characterisation. The red thrombus on top of the rotor blades was formed from mainly red blood cells and some platelets. The rotor blades are an area of high shear and it is plausible that the platelet area was formed on the blades, and the red blood cells accumulated on top to form the red thrombus (Table 5.5A). This is like the outflow sample of red thrombus which has a core of red blood cells, surrounded by platelets and fibrin (Table 5.5B) which could have been where the titanium alloy of the outflow contacted the blood and formed a cellular matrix. This matrix would then have caught the red blood cells as they flowed past in the lower shear area of the pump forming a small thrombus. The final sample is from the outlet bearing. This is an area of very high shear, where a white clot, known to form under areas of elevated fluid shear stress, was formed (302). This is consistent with the staining as the whole sample is dominated by an organised structure of platelets, and fibrin (Table 5.5C).

#### 5.4.3.2 *Fluorescent staining*

CyTRAK Orange has been used throughout this thesis to identify leukocytes. To see whether there were leukocytes present in the thrombus found in KULOV-08, the coagulation on the rotor was stained with CyTRAK Orange and analysed using the confocal microscope.



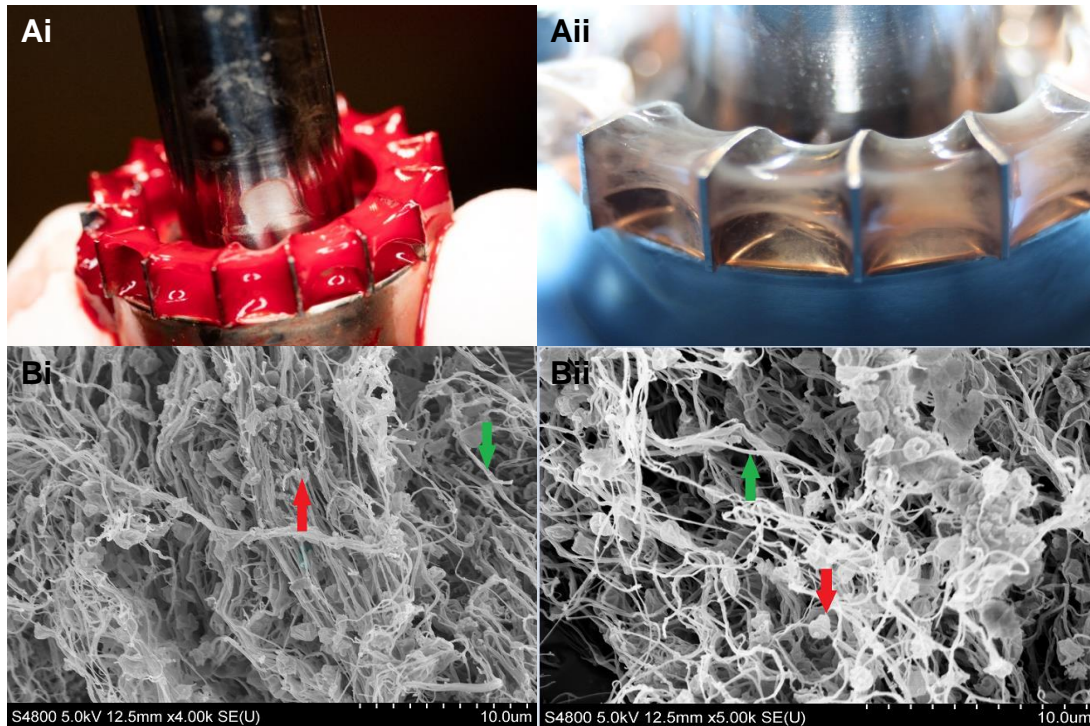
**Figure 5.13: Sample from on top of the rotor stained with CyTRAK Orange.**

A 5 µm slice of the FFPE red clot from the rotor of KULOV-08 MiniVAD was deparaffinised, rehydrated, and stained with CyTRAK Orange for 30 min. The slide was washed three times in PBS before mounting with DPX and a coverslip. The slide was imaged on the confocal microscope at x10, x20, and x40 magnification. Figure shows the x10 image as this was the most focused when detected in the blue (top left), green (top right), red (bottom left), and overlaid (bottom right).

It is possible to see bright red spots within the thrombus sample which indicate the presence of leukocytes. Upon increasing the magnification, it was difficult to focus on these cells to determine the shape of the nucleus and attempt to characterise the leukocytes as polymorphonuclear or mononuclear. Further work using specific antibodies would aid in this characterisation of leukocytes contained within the thrombus.

### 5.4.3.3 Scanning electron microscopy

The pump explanted from KULOV-07 was placed in water after explant and therefore there was lysis of the red blood cells (Figure 5.14Aii) and potential damage to the other cells. To see whether it was still possible to observe a thrombotic structure in this ‘webbing’, the sample was outsourced for scanning electron microscopy (SEM by Dr N. Badiei, Centre for Nanohealth, Swansea University).



**Figure 5.14: SEM of biological matter found on KULOV-07 MiniVAD rotor.**

Biological matter found on the rotor of the MiniVAD explanted from KULOV-07 and processed for SEM analysis. **Ai.** Rotor post-explant, **Aii.** Rotor post-arrival in the lab having been kept in water, **Bi.** SEM image x4000 magnification (red arrow = platelet, green arrow = fibrin), **Bii.** SEM image x5000 magnification.

SEM revealed a dense network of fibrin strands connected by platelets (Figure 5.14Bi & Bii). The presence of platelets and fibrin here correlates with the area in the histology slide for the biological matter found on top of the KULOV-08 rotor which stained for platelets (Table 5.5.A). This area was most likely in contact with the blades in a similar fashion to KULOV-07 (Figure 5.14Ai).


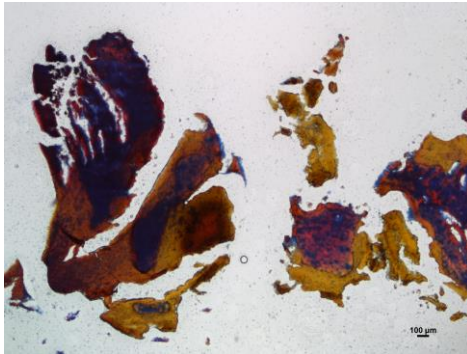

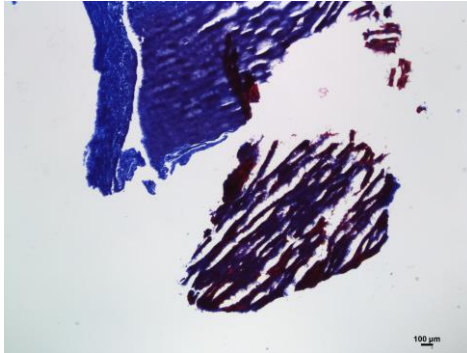

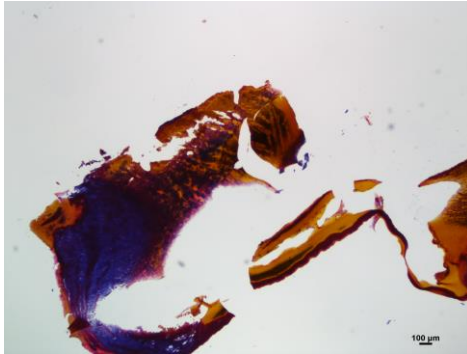
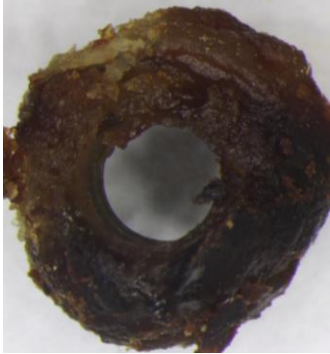
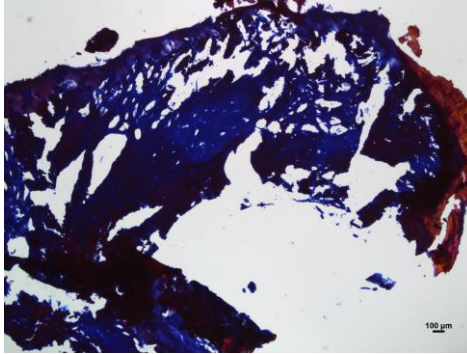
#### *5.4.4 Non-Calton explanted VAD*

To finalise the work for this chapter, Calon received a HeartAssist 5 (ReliantHeart Inc.) explanted from a patient in 2012 which had been taken apart and preserved in formalin. This pump had a wide variety of biological build-up in various areas providing an opportunity to analyse thrombus from a clinical implanted VAD.



5.4.4.1 *Histological staining*

**Table 5.6: Samples from the HA-5 stained using the Carstairs' method**

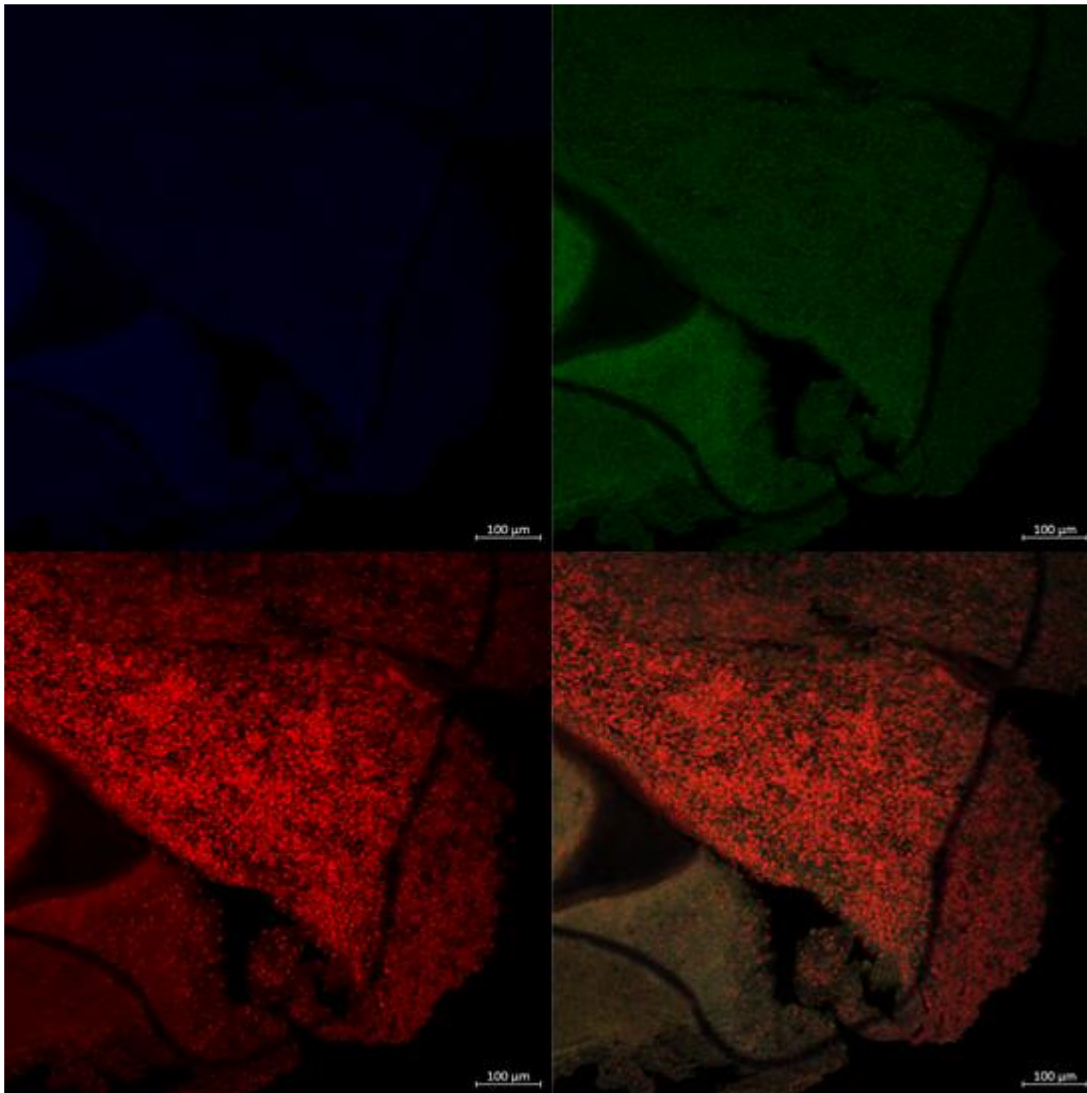
Location	Image	Slide (x4 mag)
<p><b>A.</b> Rotor blade</p>		
<p><b>B.</b> Outflow</p>		
<p><b>C.</b> Outlet bearing</p>		
<p><b>D.</b> Inlet bearing</p>		

Carstairs' staining of the HA-5 samples showed that thrombi formed in different areas of the pump had very different compositions (Table 5.5). To the naked eye, the rotor blade to the naked eye was part white and part red clot which matches the histological staining showing a large area dominated by platelets, collagen, and fibrin to the top left of the image and the rest of the image showing similar areas surrounded by red blood cells (Table 5.5A). The outflow, a white clot, was dominated by the staining for platelets and fibrin (Table 5.6B) which is different to the outflow sample in the MiniVAD (Table 5.5B). The outlet bearing sample in the HA-5 was also different to that observed in the MiniVAD in that there were red blood cells surrounding the platelet-fibrin mass (Table 5.6C) as opposed to just platelets and fibrin (Table 5.5C). The inlet bearing proved the most fascinating sample as a large circle of matter had formed around the bearing during its use. As suspected, this area of high shear formed a circle of platelets connected by fibrin strands with an outside layer of red blood cells which may have adhered to the growing platelet matrix as the blood flowed through the inlet from the left ventricle (Table 5.6D).

There are several reasons for the differences between the *in vivo* MiniVAD implants and the clinical HA-5 which include species, pump design, implantation time, drug/anticoagulation regime, among many other factors that could have influenced the composition of the thrombi.

#### 5.4.4.2 *Fluorescent staining*

As an example of a 'white and red clot', the outflow sample from the HA-5 was stained with CyTRAK Orange and imaged with the confocal microscope.



**Figure 5.15: Confocal image of HA-5 outflow stained with CyTRAK Orange.**

A 5  $\mu\text{m}$  slice of the FFPE red clot from the outflow of the HeartAssist 5 was deparaffinised, rehydrated, and stained with CyTRAK Orange for 30 min. The slide was washed three times in PBS before mounting with DPX and a coverslip. The slide was imaged on the confocal microscope at x10, x20, and x40 magnification. Figure shows the x10 image as this was the most focused when detected in the blue (top left), green (top right), red (bottom left), and overlaid (bottom right).

A dense area of bright red spots shows a large infiltration of leukocytes in one part of the thrombus, whereas there are leukocytes in the lower left of the sample, but these are sparser (Figure 5.15). This area of sparse leukocyte infiltration correlates with the KULOV-08 samples (Figure 5.13) which was a ‘red clot’ and therefore this area of the HA-5 is probably the red part of the sample. This would suggest that a ‘white clot’ is more likely to contain leukocytes – but further work on this is required.

## 5.5 Discussion

Since its inception in the 1950s, VAD technology has improved greatly with the creation of smaller devices with better blood handling capabilities. VADs are becoming more acceptable as destination therapy and with that comes a desire to make a long-lasting pump with few adverse events so that a patient may live more than 10 years with a relatively good quality of life. The most recent VAD on the market is the HeartMate 3 (Thoratec) which received market approval for use in the European Union in 2015. The 1-year results have shown no pump thrombosis, failure, or haemolysis but still high levels of GI bleeding (12%), driveline infections (16%), and stroke (18%) (95) showing that despite the improved technology, VADs remain prone to haemocompatibility-related problems.

Thorough *in vitro* testing has the potential to reduce the number of animals required for *in vivo* pre-clinical trials which is not only controversial, but costly and time-consuming. *In vitro* testing during the early design and development phase using food-grade waste blood from local abattoirs succeeds in cost savings and a faster design turnover. Cows, sheep, and pigs are widely used *in vivo* models and therefore the blood from these species is used for *in vitro* mock circulatory loops. In our studies, we have used venepuncture sheep blood (Chapter 4) and bovine abattoir blood. Procuring blood via venepuncture is preferable largely due to the sterility and the lower level of trauma. However, a maximum of ~800 mL of blood can be taken via venepuncture from a sheep which only allows for the filling of one mock circulatory loop. Therefore, bovine blood from the abattoir was used throughout the benchmarking study as up to 5 L can be acquired.

Post-explant competitor devices were donated from various collaborators and were cleaned and restored to working order by the engineering team, although the devices would never be fully restored to their original pre-implant condition. All the devices were run at a flow rate of 5 L/min and pressure at 100 mmHg as standard and compared to the CentriMag to compare their blood-handling abilities. An increase in haemolysis as calculated by the amount of plasma-free haemoglobin was immediately evident after 60 min circulation in the HMII and substantially increased at the end of the 6h test. In clinic, axial flow pumps such as the HMII have been shown to have higher rates of haemolysis than centrifugal pumps with approximately 3% patients reported

(303, 304). The order of least to most haemolysis was: CentriMag < MiniVAD < HVAD < HMII and none of the pumps had any effect on the erythrocyte cell count. The same trend was observed with platelet activation with the HMII exhibiting the highest level after 6 h. Shared trends in haemolysis and platelet activation are suggestive of a link between the two. Singhal et al., demonstrated that extracellular haemoglobin activates platelets through binding to GP1B $\alpha$  in a concentration-dependent manner (305) therefore the high levels of plasma-free haemoglobin in the HMII might be at least partially responsible for the higher levels of platelet activation. The HMII was compared to the HeartAssist-5 (HA-5) in a study by Chiu et al., using a mock circulatory loop and showed a 2.5 fold higher platelet activation than the HA-5 (306). This higher platelet activation was attributed to the recirculation and stagnant areas within the HMII leading to thrombus formation within the pump (87, 307).

Leukocytes play a role in both infection and thrombosis making them key elements in adverse events. Increased microparticle formation from platelets, leukocytes, and endothelial cells has been demonstrated clinically with VAD patients (308). These microparticles express anionic phospholipids, such as phosphatidylserine (PS), which are essential for initiating and propagating coagulation (309). PS can also induce endothelial damage in inflammatory environments (310). The LMP trend observed was different to the haemolysis and platelet activation assays with the order of least to most LMPs as follows: CentriMag < MiniVAD < HMII < HVAD. After 240 min circulation, the HVAD and HMII showed significantly higher numbers of CD45<sup>+</sup> LMPs ( $p \leq 0.0001$ ) with the MiniVAD only reaching a significance at 360 min ( $p = 0.024$ ). The decrease in leukocyte count potentially correlates with the increase in the number of MPs, but this is only evident at 360 min indicating that substantial levels of microparticles affect the haematology count.

The leukocyte subset counts seem to correlate better with the activation status of the LMPs characterised as CD11b<sup>Bright</sup>HLADR<sup>-</sup>, CD11b<sup>Bright</sup>HLADR<sup>+</sup>, and CD11b<sup>Dull</sup>HLADR<sup>+</sup>. The CD11b<sup>Bright</sup>HLADR<sup>-</sup> LMPs significantly increased after 240 min in the competitor pumps and after 360 min in the MiniVAD. The same trend for CD11b<sup>Bright</sup>HLADR<sup>+</sup> was also apparent. These populations were positive for MM20A, suggesting that these activated MPs are shed from granulocytes (264) and linked to the significant decrease in the granulocyte count in the HVAD and HMII. Woolley et al., looked at temporal leukocyte numbers and MAC-1 expression on granulocytes from

patients implanted with HMII or HVAD. Leukocyte counts increased significantly at POD14 but declined to below preoperative level at POD60 in both devices. MAC-1 expression (a complement receptor consisting of CD11b and CD18), was significantly higher in the HMII than the HVAD from POD14 through to POD60 (127) which correlates with the HMII having the highest number of CD11b<sup>Bright</sup>HLADR<sup>-</sup> LMPs.

The CD11b<sup>Dull</sup>HLADR<sup>+</sup> LMPs show a different trend with the number of LMPs increasing significantly in all pumps, including the CentriMag, which suggests that the act of artificially pumping blood in a mock loop activates leukocytes no matter what the design. Here, the population increases significantly from the static 5 min control after 120 min of pumping with the HVAD and HMII having similar numbers, and the MiniVAD comparable to the CentriMag. When comparing to the previous work on different operating conditions in the CentriMag (4.4.1), the *standard* operating condition produced the most CD11b<sup>Dull</sup>HLADR<sup>+</sup> LMPs with the *high speed* producing the least after 6h. In contrast, the MiniVAD and HVAD run at speeds of approximately 3250-4000 rpm yet the MiniVAD produced a similar number of CD11b<sup>Dull</sup>HLADR<sup>+</sup> LMPs to the CentriMag operating at standard conditions, and the HVAD produced more. This would suggest that design greatly influences the production of these LMPs, not just operating condition. An increase in HLA-DR expression is a sign of T cell activation (311) although the CD11b<sup>Dull</sup>HLADR<sup>+</sup> LMPs were not positive for the bovine T cell marker MM1A. The lack of expression of MM1A does not necessarily mean that these LMPs are not derived from T cells, it may be that the antigen that MM1A detects is no longer present. CD4, CD8 and CD25 are possible antigens that could be on T cell derived microparticles as has been found in human blood from hepatitis patients (312) – but antibodies for these in bovine/ovine species are not readily available. There was a decrease in lymphocyte number over time in all the pumps which would indicate that these LMPs are lymphocyte-derived. Pulsatile-flow devices have shown a selective reduction in CD4<sup>+</sup> T cells, defective proliferative responses to stimuli such as staphylococcal enterotoxin B, and higher levels of apoptosis in CD4<sup>+</sup> and CD8<sup>+</sup> T cells in comparison to medically treated NYHA class IV patients (101, 125, 313, 314). An increase in the number of CD11b<sup>Dull</sup>HLADR<sup>+</sup> LMPs in all the pumps here suggests that they are affected in continuous-flow devices. The impact of continuous-flow devices on T cells has recently found that the

implantation of a VAD increases the percentage of T regulatory cells (Tregs) (315), which could impact LMP production.

Overall, the blood damage profile of the MiniVAD is substantially better than the competitors but not yet equal to the CentriMag. The competitors should be given some leeway as they are explanted pumps which have seen better days and this could influence their efficacy in our *in vitro* tests. The leukocyte assays employed for *in vitro* testing reveal that the MiniVAD appears to have less of an impact on granulocytes than the competitor devices. Neutrophils, a subset of granulocytes, have a dose-response relationship with shear as demonstrated using a cone and plate viscometer measuring L-selectin shedding (316). Hence the MiniVAD may have lower shear or fewer areas of high shear compared to the competitors and therefore has less of an effect on granulocytes. If this remains true in clinic, then it is possible that infection rates in MiniVAD patients should be low. Despite this, the MiniVAD still affects lymphocytes which could be more problematic for longer term adaptive immunity. T cells migrate against fluid flow whereas neutrophils migrate with it (317), making it difficult for T cells to move against shear when it is higher than physiological levels so making them more susceptible to damage. Despite this, the MiniVAD and CentriMag showed similar numbers of CD11b<sup>Dull</sup>HLADR<sup>+</sup> LMPs, lower than those in the HMII and HVAD at 360 min which is promising.

The *in vitro* study of the MiniVAD led to finalisation of a design that could be tested *in vivo*. The aim of the *in vivo* study was to implant the MiniVAD for 30 days in sheep with no haemolysis and no pump thrombus at the time of explant. Eight sheep were implanted in total from February 2015- September 2016 all with variations of the MiniVAD design which was altered and tested over time under the orders of the Chief Technology Officer (CTO). Therefore, it is not possible to compare the sheep to one another. The leukocyte assays developed in the lab were used on preserved blood from the sheep taken at pre-op, POD1, POD2, and then weekly until termination. The efficacy of SCP as a blood preservative was discussed in Chapter 2 and deemed successful at preserving leukocytes for a maximum of 5 days. The SCP does not contain anticoagulant and is added to anticoagulated blood at a 1:1 ratio which can be altered dependent on users' needs. Alternatively, Cyto-Chex-BCT are used in clinic to directly draw blood via venepuncture in the same way as typical vacutainer anticoagulant tubes. Streck BCT contains the SCP and K3-EDTA as the anticoagulant.

Both options were used during the *in vivo* study to compare preservation efficacy with the aim of using BCT exclusively for *in vivo* and SCP for *in vitro* studies.

Throughout the trial, the Cyto-Chex-BCT arrived in poor condition with a few being cracked and many clotted potentially due to poor mixing. Therefore, it is likely that the MP analysis of blood from these tubes was compromised so the SCP tubes are considered a more accurate representation. There was no significant change in the number of CD45<sup>+</sup> LMPs compared to pre-op and when calculated as a ratio of the WBC number, there was an initial decrease at POD1 which increased at POD2 and remained level for the duration of implant. The trauma of surgery causes an inflammatory response and therefore an increase in leukocyte count (acute leukocytosis) within the first 24 hours is normal (318). The activated MPs were also unremarkable although only two populations, the CD11B<sup>Bright</sup>HLA-DR<sup>-</sup> and the CD11B<sup>Dull</sup>HLA-DR<sup>+</sup> were identifiable with the CD11B<sup>Bright</sup>HLA-DR<sup>+</sup> LMPs found *in vitro* virtually absent. Fixation of cells is known to cause alterations which randomise epitope availability to the antibodies (319) so LMPs that are double positives might only be detected as single positive. To test this would require taking fresh blood from the implanted sheep and running the samples at the location, which is not feasible.

The final part of this chapter focuses on the structure of biological build-up found in the MiniVAD pumps upon explant from the sheep and that found in an explanted HA-5 from a VAD-patient. Nothing of this sort has been published, although this is a sensitive commercial matter and, potentially, work has been done internally in other blood-handling device companies. Thrombus formation occurs when there are abnormalities in blood flow, the vessel wall, and components of the blood. These three features are known as Virchow's triad (320) which have been further refined as (321, 322):

- Circulatory stasis – abnormalities in haemorheology and turbulence
- Vascular wall injury – abnormalities in the endothelium
- Hypercoagulable state – abnormalities in the coagulation and fibrinolytic pathways and platelet function

VADs cause abnormalities in all three of these areas with circulatory stasis occurring within areas of the pump with poor flow, vascular wall injury occurring due to the



foreign material contacting the endothelium, and the hypercoagulable state due to blood trauma.

To the naked eye, it is easy to categorise clots per their colour but that does not give a sufficiently in-depth view. Red clots, also known as venous thrombi, feature enmeshed erythrocytes and are commonly observed in deep vein thrombosis (DVT) where venous return is impaired (301, 323). White clots, or arterial thrombi, are platelet- and fibrin-rich, fast-growing, and typically grow in areas of fast blood flow (324, 325). Three areas of the explanted MiniVAD from one sheep were preserved and analysed with the Carstairs staining method to detect platelets, fibrin, collagen, and red blood cells. The images revealed that the red clot found on the rotor may have begun forming before being switched off as there was an area of structured platelets where the clot contacted the rotor. This area may have only been small at first but would have attracted adhering red blood cells to coagulate there whilst explant surgery (~ 4h) was occurring, thus hiding the initial clot and risking being discarded as unimportant. In fact, the SEM from another explanted MiniVAD (KULOV-07) revealed that the webbing was formed from platelets and fibrin strands. The lysis of the red blood cells from this web upon its mistaken storage in water revealed that thrombus formation began on the rotor blade. Had the original matter been preserved correctly, it is possible that the Carstairs staining would have shown the same pattern as in KULOV-08.

The sample from the outflow was like the rotor clot but there was more evidence of fibrin in the area. This suggests that platelets had adhered to the titanium alloy of the outflow cannula and begun to form a matrix (326), becoming more fibrin rich as the thrombus grew (324, 325). This matrix would then capture red blood cells as they flowed past into the aorta as evidenced by the clear yellow staining. The white clot found at the outlet bearing was consistent with the hypothesis that white clots are formed from platelets and protein as this clot was exclusively dominated by platelets, collagen, and fibrin with red blood cells absent from the area. The outlet bearing is an area of very high shear and the composition is consistent with findings that such areas cause platelet activation leading to risk of clot formation and pump blockage (301).

With the lack of publications surrounding the composition of thrombus from VADs, it was difficult to predict how these thrombi translated to those in other pump designs

and clinic. Also, the animals used in the trial were not anticoagulated nor given antiplatelet agents (as in normal clinical practice) which may have led to the formation of thrombi where in clinic there would not have been. Fortunately, in 2012, a HA-5 was donated to Calon and had been preserved in formalin until its rediscovery in May 2017. The HA-5 had thrombus in many areas including the rotor, the inlet and outlet bearings, and the outflow. On comparison with the thrombi found in KULOV-08 for the same areas, the composition of the clots showed some notable differences. The rotor sample from the HA-5 showed areas that were dominated by platelets with visible fibrin formation surrounded by a denser layer of red blood cells. Fibrin had not been visible in the rotor sample for the KULOV-08 and the platelet area was small and less organised than that observed in the HA-5. This would suggest that the thrombus on the HA-5 rotor had been developing for longer than the one found in KULOV-08, unfortunately it is not known how long the HA-5 was implanted for. Additionally, the HA-5 outflow sample consisted of a platelet-fibrin matrix whereas the KULOV-08 was dominated by red blood cells. The bearing samples for both pumps were more similar though in that they both showed dominant platelet-fibrin-collagen matrices. These differences can be attributed largely to the difference in species, pump design, medication/anticoagulation therapies, and duration of implant yet they provide an excellent first attempt into identifying the steps of thrombus formation in VADs.

The preliminary work on the thrombus samples leant itself to opportunities to determine whether leukocytes could be detected within the thrombus. For this, the slides were stained with CyTRAK Orange and imaged with the confocal microscope. The thrombi found on the rotor of KULOV-08 and the outflow of the HA-5 was chosen due to their different colours (red and white respectively). When comparing the two images at x10 magnification, there were obvious differences in the density of leukocyte infiltration. The KULOV-08 clot had sparse bright red spots indicative of leukocytes through the edges of the thrombus. The HA-5 on the other hand had a very dense population of leukocytes in one area, and another area (perhaps a red clot area within the sample) with fewer leukocytes. The discovery of fewer leukocytes in the red clot areas confirms the suspicion that red clots are artefacts of low/no flow and the lack of a mature matrix. The red clot did have a platelet area evident in the histology slides which was confined to one edge and where the leukocytes are co-located in the fluorescent image. It is possible that leukocytes contribute to the building of 'red'

thrombus through neutrophil extracellular traps (NETs) which contribute to the development of venous thrombus in DVT with RBCs being shown to adhere to NETs (327, 328).

The white clot has time to form a complex matrix consisting of activated platelets, fibrin, and collagen. Activated platelets can modulate leukocyte activation through cytokine release to form leukocyte-platelet aggregate and recruitment of leukocytes to the arterial thrombus (329). Leukocytes contribute to the building of arterial thrombi through the exposure of tissue factor on macrophages/monocytes and TF-positive microparticles (330-332). The research on the leukocyte contribution to thrombus is limited and warrants further investigation.

## 5.6 Conclusion

The MiniVAD was tested against two competitor devices which are used routinely used in clinic for the treatment of end-stage heart failure. These tests were conducted before proceeding to animal trials and show that substantial *in vitro* testing can be used to improve pump design in terms of blood damage long before implantation. From the most basic assessment of red blood cell damage through haemolysis testing to considering the effect on platelets and leukocytes, the MiniVAD appears superior at handling blood than the HMII and HVAD, almost to the same degree as the CentriMag. The incorporation of leukocyte microparticle assays into *in vitro* testing is a first publicly shown in the VAD development world. This assay has shown that the MiniVAD is also superior at handling leukocytes. Upon further investigation into the activation profile of these microparticles, the CD11b populations were not as enhanced as the other pumps suggesting that granulocyte handling is better by the MiniVAD. HLA-DR expression on the other hand was elevated significantly even after 120 mins in all the pumps which suggests an activating effect on the lymphocyte population – but again the MiniVAD proved better than the competitors.

Translating the *in vitro* microparticle assays to *in vivo* did have some limitations. *In vitro* assays show the worst-case scenario as the blood tested has no oxygens/nutrients, there is no removal of waste products or damaged cells, and the blood volume passes through the pump more frequently than would be the case physiologically. The body clears circulating microparticles through recognition of phosphatidylserine on the exposed membrane and uptake into macrophages (333) so detection of large numbers LMPs *in vivo* is unlikely. However, the same type of LMPs were detected therefore the assays were successfully translated from *in vitro* to *in vivo*. In terms of detecting adverse events, the designs of the MiniVAD implanted varied slightly in all sheep and they were only implanted for a short amount of time with the intention of not producing adverse events. Whilst thrombus was observed in some of the pumps, microparticle analysis did not appear to predict the event. Continuing to use these assays for future chronic *in vivo* and clinical trials with the final MiniVAD may change this through increasing sample size.

Finally, the investigation into pump thrombus provides new information on samples that have come directly from implanted animals/patients. These preliminary results described here begin to identify the steps of thrombus formation and how cells interact to propagate them depending on the effects the pump has on the thrombus. When looking at thrombus found in the MiniVAD *in vivo* pumps, it brings together the importance of designing a pump with a low blood damage profile to all cells, not just the red blood cells.

## Chapter 6      General discussion

The aims of this thesis were to measure the effects ventricular assist devices have on white blood cells and how this relates to the design. The thesis also aimed to persuade the blood-handling device community that leukocytes are as important, if not more than, red blood cells and platelets when developing a VAD. The results presented here reveal that material choice greatly influences leukocyte activation which becomes exacerbated under artificial shear stress. Leukocytes contribute to the formation of pump thrombus and these novel assays demonstrate that design can be altered early on *in vitro* to reduce this and other adverse events.

Leukocytes are important in the progression of cardiovascular disease and the associated complications (334). Despite this, it has not been translated to thorough research in blood-handling devices. Some VAD-related studies have measured monocyte tissue factor expression (290, 335), platelet-leukocyte aggregates (128, 137), leukocyte counts, and some activation markers (336) but this has been largely limited to *in vivo* testing when the device design is (usually) fixed.

With this gap in the research, it became the aim of this thesis to delve into the effect VADs have on leukocytes. To achieve this, the VAD was deconstructed into the two main components that are known to influence the blood: Biomaterials (Chapter 3); and shear stress (Chapter 4). In the final chapter, the MiniVAD, currently under development by Calon, was tested in a mock circulatory loop against competitor devices which are approved for use in clinic, the HeartMate II (HMII) and the HeartWare VAD (HVAD). All three devices are designed very differently, and it was this final study that culminated all the data together to show that research *in vitro* helps improve design.

## 6.1 Biomaterials

Choosing materials that are both mechanically sound and biocompatible is not an easy task. As research progresses, materials that were once thought biocompatible and suitable for implantation have been found to be toxic due to the limited research done before clinical use. A more recent example of this is the recall of 56000 patients implanted with metal-on-metal hip replacements due to the risk of bone and muscle damage from wear-derived metal nanoparticles (337). The biomaterials used in this thesis were chosen by the Calon engineering team as examples of VAD-candidate materials that could be used or have already been used in VADs. Three materials were ceramics: silicon nitride (SiN); single-crystal sapphire (Sap); and zirconia-toughened alumina (ZTA). These materials are considered bearing candidates for their high strength, hardness, resistance to wear damage, and oxidation resistance (212, 213, 338) and have already been used in blood-handling devices (122, 188). However, the biocompatibility testing of these ceramics has been limited to osteoblasts for their use as joint or dental implants (189, 190). The metal material of choice was the most common biomaterials used for VAD bodies, the TiAl6V4 titanium alloy (Ti), known for its resistance against fatigue, corrosion, and commonly accepted biocompatible material (173, 186). The final material of choice was a coating over stainless steel. Coatings have been suggested as a solution to using materials with poor biocompatibility and diamond-like carbon (DLC) was used for this purpose for its deemed biocompatibility and desirable mechanical characteristics (191-193).

These biomaterials were incubated with whole blood using a simple model of balancing the discs on beads in a petri dish. This allowed maximum surface area of the biomaterial to be covered by blood for the 2h incubation time. The use of whole blood allowed an assessment of the effect these materials had on all components such as platelets, red blood cells, and proteins as well as leukocytes in a more biologically relevant environment (176). The model allowed a rapid, robust early stage evaluation of biomaterials of interest before progression to more complex studies with complex, costly rigs. In this study, Ti caused a significant decrease in platelet count, but had no measurable effect on platelet activation, aggregation, nor erythrocytes and leukocytes. This correlated with research on blood flow over TiAl6V4 wire under shear stress ( $100 \text{ s}^{-1}$ ) which did not significantly increase platelet activation nor platelet-

neutrophil/platelet-monocyte aggregates (209). Cytokine release was also not affected by Ti in this study, yet high levels of TNF $\alpha$  have been quoted in the literature and a decreased production of TNF $\alpha$  by monocytes stimulated with LPS (210, 211). However, those studies were conducted using isolated leukocytes, whereas our work correlates better with the *in vivo* implantation of Ti into rats which showed low levels of TNF $\alpha$ , IL-1 $\beta$  and IL-1 $\alpha$  (183). The ceramic materials had previously only been tested in terms of bone growth and tissue implantation (189, 214) therefore their testing in blood is novel and relevant. Monocytes were found to be most affected cell type by with a significant decrease in numbers (SiN and ZTA), and activation through L-selectin shedding (Sap and ZTA). All the ceramic materials showed a decrease in platelet count. It was supposed that these cells were adhering to the disc and some evidence of this was observed with the confocal microscopy of the discs. Monocytes, with their expression of tissue factor, and platelets contribute to thrombus (331, 339) making these materials potentially prone to thrombus formation, particularly when used as bearings in a high shear area. This has already been observed in the HeartMate II which has a single-crystal alumina ruby bearing (87, 191). Finally, DLC has been shown to rapidly adsorb albumin and inhibits fibrinogen adsorption so has been deemed biocompatible through reducing platelet adhesion, activation, and clotting time (191, 193). DLC did have comparable clotting times to the negative control in our study, yet there was a significant decrease in monocyte count and shedding of L-selectin by monocytes indicating a similar profile to that of ceramics. In the literature, this is not a surprising phenomenon as DLC has been shown to slightly increase monocyte adhesion (217).

The simple model developed in this thesis for assessing biomaterials suggested that monocytes were the type of leukocyte that was most affected – even in biomaterials classically considered biocompatible. The simplicity of the model is both a positive and negative in terms of VAD development. Whilst it allowed rapid measurements of cellular activation, the continued contact of blood with the biomaterial does not replicate the residence time in VADs (milliseconds) and is in the absence of shear stress. Despite this, it presented results that could be refined and moved forward to the next chapter on shear stress.



## 6.2 Shear stress

Shear stress is the force acting between adjacent layers (called laminae) under flow. The velocity, pressure, and other flow properties dictate this force and blood is naturally subjected to physiological shear stresses of 1 – 4 Pa in arteries (229), and 0.1-0.5 Pa in large veins (230). Shear stress in VADs is considerably higher than physiological levels and is causative of haemolysis (259), platelet activation (81), leukocyte damage (239), and degradation of vWF (260). To investigate the effect shear stress has on leukocytes in particular, two models were used: ovine venepuncture blood circulated in the CentriMag at different operating conditions; and the biomaterial discs used previously attached to a rheometer. The CentriMag allowed us to observe shear stress on its own due to the loop being made almost exclusively of polymers. After this, the rheometer model allowed the inclusion shear stress on the VAD-candidate materials to loosely mimic VAD conditions.

For the CentriMag study, three operating conditions were chosen per information from the computational-fluid dynamics engineer (CFD) and were *low flow*, *standard*, and *high speed*. The *high speed* condition significantly increased haemolysis levels and decreased platelet counts as normally characterised by high shear (81, 263). Leukocytes were assessed via haematology and microparticle formation showing a decrease in the granulocyte and monocyte counts correlating with an increase in CD45<sup>+</sup> LMPs in the *high speed* condition. Interestingly, when looking at the activation profile of these LMPs through CD11B and HLA-DR expression, the operating conditions differentially affected this. CD11B<sup>Bright</sup> populations were highest in the *high speed* condition reflecting the decrease in granulocyte and monocyte count where CD11B is expressed. This was not the case in LMPs expressing HLA-DR where the highest number of this population was observed in the *standard* operating condition, followed by *low flow*, then *high speed*. As lymphocytes express HLA-DR, this could be very important when considering the adaptive immunity changes observed in VAD patients (101, 125).

Whilst the CentriMag study gave interesting information on the effect shear has on leukocytes, VAD-related materials are absent. To rectify this, the VAD-candidate biomaterials were attached to a rheometer and blood subjected to both shear ( $1000 \text{ s}^{-1}$ ) and non-shear for 5 min. Under these conditions, leukocyte counts, activation

(CD11b upregulation and CD62L shedding), death, microparticle formation, and function (ROS production and phagocytosis) were assessed. Blood sheared on the Sap surface showed a decrease total leukocyte and neutrophil count and the monocyte count was decreased in the sheared Ti samples. These decreases were not related to CD45<sup>+</sup> LMP formation as there was no increase in comparison to the baseline in any samples. Shearing on Sap and Ti surfaces did show shedding of L-selectin from neutrophils whereas monocytes shed L-selectin regardless of biomaterial type or application of shear. In correlation with the literature and the findings in the Biomaterial chapter, DLC showed an upregulation of CD11B<sup>Bright</sup> expression when sheared indicating monocyte adhesion (217).

Functionally, there was no increase in total ROS production in any samples, but there were some interesting observations with regards to phagocytic ability. Neutrophils that had been in contact with DLC, Ti, and the Pel with and without shear showed a decreased immediate phagocytic response to pathogen which was resolved with longer incubation with the *E. Coli* bioparticles. Once again, the blood that had been sheared on Sap had an altered leukocyte response in that even after a long incubation with the pathogen, the neutrophils still had a reduced phagocytic response. Further to this, there was a complete abrogation of the LPS-stimulated MIF response after shearing on Ti whilst the IL-1 $\alpha$  response remained intact. MIF is involved in cell-mediated immunity and is considered an inflammatory cytokine that regulates macrophage function (274). Lack of MIF might contribute to an immunosuppression environment. Many pathogens, trauma, burns, and major surgery can cause acute immunosuppression leading to a diminished capability of responding to infection (277). The combination of major surgery and implantation of a VAD that is largely composed of titanium alloy could potentially increase patient susceptibility to infection.

Introducing shear stress to these materials offered further evidence that Sap and Ti may not be an entirely biocompatible material in that there is evidence of monocyte activation, neutrophil activation under shear, and a reduction in normal leukocyte function. This is very problematic for VAD patients who are prone to infection due to the driveline opening on the body. An inability to clear infection due to an inhibitory effect caused by components of the VAD could lead to sepsis and death. The limitations of this model included the maximum shear obtainable being 1000 s<sup>-1</sup> and a much longer residence time than that experienced in the VAD. However, the results

from this model have progressed the knowledge on how leukocytes subjected to shear on these materials are affected and can act as preliminary data for the Calon shear rig.

## 6.1 Ventricular assist device testing

An assessment of the individual components enabled a prediction as to how when biomaterials and shear stress come together, in the form of a VAD, leukocytes may be affected. It was shown in the biomaterial work that ceramic materials SiN, Sap and ZTA activated monocytes. With the addition of shear stress, Sap activated neutrophils whilst also attenuating their normal function. The MiniVAD has gone through many design changes during development, but what has stayed constant is that it is a passive magnetically levitated (maglev) centrifugal pump with titanium alloy body and ceramic bearings (diamond and zirconia). The competitor devices are quite different; the HVAD is a centrifugal pump combining hydrodynamic and maglev but with a different style rotor and parts made from zirconia (340), whereas the HMII is an axial flow pump with ceramic bearings (ruby) (187). The shear stresses present in these devices also vary due to running speed, residence time, static areas, and the size of the gaps inside the pumps.

During the benchmarking study, the MiniVAD performed admirably through exhibiting low haemolysis, low platelet activation, and comparatively low levels of leukocyte microparticle formation. Whilst this is excellent, the competitor devices received were not in brand new condition nor operated with the manufacturer's tools which introduces a large bias. The HVAD and HMII have been in clinic since the mid-2000's after successfully completing clinical trials (341, 342). Had these devices performed as such in this study, they would never have been accepted. In comparison, the MiniVAD was two to three-fold worse than the CentriMag in all assays. The CentriMag is the 'gold-standard' as it has a low blood damage profile, so the relatively small difference between it and the MiniVAD is promising.

The benchmarking study offered an opportunity to study leukocyte microparticle formation and activation status for the first time *in vitro*. CD45<sup>+</sup> LMPs increased with time in all pumps, but where the HMII was worst in haemolysis and platelet activation, the HVAD generated more LMPs. It is yet unknown as to how LMP generation is affected by device design, but it would suggest that the design of the HVAD negatively impacts leukocytes. Many papers claim that infections are not due to the pump, but there is very little evidence to support that claim and therefore the increase in LMPs by the HVAD may be responsible for the high infection rates (35% in HVAD (343)

vs. 23% in HMII (344)). The activation status on the other hand retained the trend of HMII having the highest levels. CD11B<sup>Bright</sup>HLA-DR<sup>-</sup> and CD11B<sup>Bright</sup>HLA-DR<sup>+</sup> LMPs were highest in the HMII which correlated with the *in vivo* study by Woolley et al., where MAC-1 expression was significantly higher in the HMII than the HVAD (127). This would suggest that neutrophils become activated when in contact with the shear stress and biomaterials exerted by the HMII more so than the other devices and produce LMPs with upregulated adhesion receptors which could contribute to thrombus (345). The CD11B<sup>Dull</sup>HLA-DR<sup>+</sup> LMPs were hypothesised to be lymphocyte-derived despite not expressing the MM1A T cell antigen. These types of LMPs were elevated early on during testing in all pumps, including the CentriMag, suggestive that the mere act of artificial circulation encourages leukocyte activation. Very little is known about how current VADs affect the cells of the adaptive immune system, so the benchmarking study goes some way to providing evidence for continuous-flow devices.

Embarking on the preclinical study of MiniVAD implantation in sheep allowed the progression of these assays in a novel, more relevant environment. The implantation occurring in continental Europe raised the problem of how to analyse blood samples as the site did not have the means to use our assays. This logistical issue was resolved in Chapter 2 through the testing of the Streck Cell Preservative™, a liquid preservative that maintains cellular antigen expression of biological samples for flow cytometry up to 7 days (346). This preservative had never been tested in bovine and ovine species so it was necessary to conduct a study to observe whether the leukocytes could be preserved well enough for analysis from taking the blood to arriving in the lab 2 – 3 days later. Through haematology and flow cytometry using CyTRAK Orange, preservation of leukocytes in bovine and ovine was possible for 7 days, with ‘splitting’ of the granulocyte population observed in the day 4 samples. Surprisingly, Streck Cell Preservative worked better in bovine/ovine than in the human samples. This is potentially due to the species neutrophil to lymphocyte ratio difference in that the more abundant human neutrophils are susceptible to differing fixation time of granules which alters their FSC/SSC and therefore cannot be ‘seen’ by haematology analysers (146, 159). Additionally, there is a higher abundance of lymphocytes in animal populations (157) which aids better preservation due to the lack of granules.

The main purpose of developing the *in vitro* leukocyte assays was to translate them to preclinical studies and eventually clinically. Blood taken from the implanted sheep was preserved using the Cyto-Chex BCT and in tubes containing just the Streck Cell Preservative (SCP). The use of these variations of Streck was to compare efficacy of preservation between what is used in the lab (SCP) and what is more user-friendly for preclinical studies (Cyto-Chex BCT). The Cyto-Chex tubes unfortunately arrived in poor condition with many samples partially clotted leading to the decision that any LMP analysis from these would be compromised. The SCP tubes were supposed to be a more accurate representation in the presence of LMPs over time in the sheep. However, there was no significant change in the number of CD45<sup>+</sup> LMPs when compared to pre-op levels and the activation status (CD11B/HLA-DR) did not give a clear indication of change. There are several reasons for this: different MiniVAD designs in each sheep; short time-frame; the aim of the study not to form adverse events; and the initial health of the sheep (without heart failure). One interesting comparison between *in vitro* venepuncture sheep blood and the *in vivo* implanted sheep was the absence of the CD11B<sup>Bright</sup>HLADR<sup>+</sup> positive population observed *in vitro*. Whether this is significant or not remains to be elucidated in further studies and may be caused by the preservation process (319). The increase in leukocyte microparticles has been documented in VAD patients and MCS (295, 308, 309) so continuing to use these assays in future studies may yet provide valuable insight.

The final aim of this thesis was to investigate the composition of the thrombus found in VADs. The explanted MiniVADs' from the acute non-GLP study did contain varying degrees of thrombus in different areas of the pump. The eighth pump had three thrombus build-ups; on top of the rotor, the outflow, and the outlet bearing. These samples were paraffin-embedded, sliced, and stained using the Carstairs method and fluorescently stained with CyTRAK Orange. The staining revealed that what would normally be classified as either a 'red' or a 'white' clot was far more complex in its structure. For instance, the 'red' clot found on top of the rotor showed areas of platelets and collagen formation which may have formed on the rotor (an area of high shear) and then trapped red blood cells when the pump was switched off for explant. This was also noticeable in the outflow sample which had more organised platelet/collagen/fibrin structure which may have been building on the titanium alloy surface (326) during use and covered by red blood cells when turned off. The

fluorescent staining also showed, perhaps for the first time, the presence of leukocytes in ‘red’ and ‘white’ clots in varying densities. Fewer leukocytes were present in the ‘red’ clot confirming that red clots are artefacts of low/no flow and the lack of a mature matrix. The ‘white’ clot on the other hand develops in areas of high shear which leads to platelet activation and aggregation (301). This would allow the recruitment of leukocytes to the area and building of the thrombus through the exposure of tissue-factor (330), hence why the ‘white’ clot had a denser population of leukocytes.

The thrombus is the first adverse event we can create *in vivo* which offers an opportunity to examine these more thoroughly than they have been before. The stains used will be modified and adapted as Calon continues to move the MiniVAD towards use in clinic and will aim to provide greater detail on how thrombus forms, and how to prevent it through design modifications. Creation of thrombus *in vitro* is difficult to achieve but it is possible (299).

## 6.2 Limitations

### *6.2.1 Enabling Technologies*

The DNA dyes work in the enabling technologies chapter had a study design flaw. The voltage thresholds for the forward- versus side-scatter (FSC/SSC) plot were dependent on counting bead type used. Ideally, the protocols for each bead should have been identical for comparison, however, due to the size of the beads, it was necessary to adjust the voltage threshold to fit both the beads and cells onto the FSC/SSC plot.

### *6.2.2 Biomaterials: Foreign surface interactions*

Complete sterilisation of the biomaterials before use and in between donors would have given more confidence that there was no contamination that could have influenced results. Ethylene oxide sterilisation would have been the desired method but was deemed too costly and inaccessible.

The disc size for this study was a limitation as they were needed for the rheometry study. The model could have been improved to include biomaterial pieces that were smaller but had a higher surface area (e.g. several cubes in a well of a 6-well plate).

### *6.2.3 Shear stress cell activation and damage*

The rheometer model limited the gap size, residence time, and shear stress that could be applied to the blood. This meant that the results are only an estimate of what may happen in VADs to leukocytes. Ideally, a shear device would be made that could adjust gap size, residence time, shear stress, biomaterial type, and surface finish.

### *6.2.4 VADs: From bench to bedside*

A common limitation during all mock circulatory loop testing was the availability of species-specific antibodies. There is no platelet lineage marker that is not affected by activation for bovine/ovine, nor a granulocyte antibody for ovine. Access to these antibodies would have helped eradicate platelet contamination from the microparticle assays and confirm lineage of CD11b<sup>bright</sup> MPs.



In terms of the post-explant devices used (HMII and HVAD), the cleanliness and operation of them could have worsened blood damage compared to new, sterile versions.

## 6.3 Future work

This thesis has demonstrated the potential monitoring leukocytes during VAD testing has on improving design but there are still many opportunities to extend the scope of this work. This section presents ideas as to what could be achieved in the future.

### *6.3.1 Heart failure, CPB, and paediatric blood*

Readily available healthy, adult human blood was used to develop the models for measuring the effects biomaterials and shear stress have on leukocytes. Whilst this is useful, the target patient group for VAD therapy suffer from an inflammatory disease where leukocytes are already active. It is hypothesised that leukocytes from the blood of these patients may behave differently towards biomaterials and under shear stress. Development of VADs suitable for children is also desirable and paediatric leukocytes may also react differently to that of adults. Ethics for acquiring blood from CPB and heart failure patients at the time of writing are in progress.

### *6.3.2 LVAD patient blood*

Building on from 6.3.1, it would also be useful to use blood from LVAD patients under 'normal' conditions, and during infection or pump thrombosis. This type of blood would help validate the assays developed in this thesis for use as diagnostic tools and to build a better understanding of inflammation during LVAD support.

### *6.3.3 Antibody development*

Characterisation of leukocyte-derived microparticles (LMPs) to determine parentage would prove useful in understanding how certain types of LMPs might behave and cause adverse events. This thesis has gone some way to doing this through using granulocyte, monocyte, T and B cell antibody markers for bovine blood. This was not possible to fully translate to the pre-clinical sheep study as, to the authors knowledge, as granulocyte or T cell antibodies for sheep do not exist. Production of a sheep granulocyte antibody suitable for incorporation into the flow cytometry LMP panel would prove useful.

#### 6.3.4 *Creating thrombus in vitro*

Thrombus is a problematic adverse event as it can lead to pump blockage which requires further surgery or replacement and can lead to death if left untreated. Understanding how thrombus forms in VADs would benefit design and to accomplish this *in vitro* might reduce the requirement for high numbers of animals during pre-clinical trials. As Hastings et al. demonstrated, it is possible to create thrombus in mock circulatory loops. Using their method and adapting it for use in the MiniVAD and competitor pumps would be an important step towards reducing adverse events long before implantation.

#### 6.3.5 *Clinical trials*

Within the next few years, Calon anticipates that the MiniVAD will be in clinical trials. Translating the assays developed in this thesis from bench to bedside would be a step towards validation and incorporation into standards. Using these assays in patients would also provide data which could be correlated with that found *in vitro* and in pre-clinical trials. Specifically, the CD45<sup>+</sup> MPs assay would be the most useful to incorporate into future clinical trials as these are related to infection and thrombosis. Expanding this assay to include lineage markers would also be beneficial in the attempt to identify biomarkers for these complications.

## 6.4 Conclusion

The work within this thesis provides novel evidence that leukocytes are reactive to VADs and should be monitored from the very beginning of development. The biomaterials work has shown that single-crystal sapphire activates monocytes and neutrophils with and without shear leading to the suspicion that its use, as well as other similar ceramics, in VADs may be causative of thrombus build-up. When shearing on these biomaterials, even at a low shear rate, all affect the leukocytes in some manner whether it be through activation (L-selectin decrease on sheared Ti), adhesion (CD11b increase in sheared DLC), or decreased functionality (attenuated phagocytosis in all). This knowledge is being applied to what happens to the MiniVAD as it goes through preclinical studies to work out how thrombus forms and how it can be prevented. Further research into this with more sophisticated models such as a shear rig with interchangeable biomaterial parts would shed more light on how leukocytes are affected by the components that make up a VAD.

Overall, the MiniVAD has performed excellently throughout *in vitro* testing with the benchmarking study revealing it to be almost as good at blood handling as the CentriMag, and far superior to competitor devices. The assays and models used throughout this work can be used to monitor leukocytes throughout the MiniVAD's progression to clinical trials, as well as research involving blood from paediatric, heart failure, and CPB patients. Acknowledging and accepting leukocytes as necessary to monitor during VAD development may, in time, make common adverse complications a rarer event in patients.

## Chapter 7 Bibliography

1. Flindt R. Heart, Circulation. *Amazing Numbers In Biology*. 1st ed: Springer-Verlag Berlin Heidelberg; 2006. p. 65-71.
2. Kirkpatrick JN, Wieselthaler G, Strueber M, St John Sutton MG, Rame JE. Ventricular assist devices for treatment of acute heart failure and chronic heart failure. *Heart*. 2015.
3. McMurray JJ, Adamopoulos S, Anker SD, Auricchio A, Bohm M, Dickstein K, et al. ESC guidelines for the diagnosis and treatment of acute and chronic heart failure 2012: The Task Force for the Diagnosis and Treatment of Acute and Chronic Heart Failure 2012 of the European Society of Cardiology. Developed in collaboration with the Heart Failure Association (HFA) of the ESC. *Eur J Heart Fail*. 2012;14(8):803-69.
4. Cleland JG, Swedberg K, Follath F, Komajda M, Cohen-Solal A, Aguilar JC, et al. The EuroHeart Failure survey programme-- a survey on the quality of care among patients with heart failure in Europe. Part 1: patient characteristics and diagnosis. *Eur Heart J*. 2003;24(5):442-63.
5. Tendera M. Epidemiology, treatment, and guidelines for the treatment of heart failure in Europe. *European Heart Journal Supplements*. 2005;7(suppl J):J5-J9.
6. Sharma K, Kass DA. Heart Failure With Preserved Ejection Fraction. Mechanisms, Clinical Features, and Therapies. 2014;115(1):79-96.
7. Roger VL. The Heart Failure Epidemic. *International Journal of Environmental Research and Public Health*. 2010;7(4):1807-30.
8. Ponikowski P. 2016 ESC Guidelines for the diagnosis and treatment of acute and chronic heart failure: The Task Force for the diagnosis and treatment of acute and chronic heart failure of the European Society of Cardiology (ESC). Developed with the special contribution of the Heart Failure Association (HFA) of the ESC. *Eur J Heart Fail*. 2016.
9. Thunberg CA, Gaitan BD, Arabia FA, Cole DJ, Grigore AM. Ventricular Assist Devices Today and Tomorrow. *J Cardiothorac Vasc Anesth*. 2010;24(4):656-80.

10. Briasoulis A, Androulakis E, Christophides T, Tousoulis D. The role of inflammation and cell death in the pathogenesis, progression and treatment of heart failure. *Heart failure reviews*. 2016;21(2):169-76.
11. Mill JG, Stefanon I, dos Santos L, Baldo MP. Remodeling in the ischemic heart: the stepwise progression for heart failure. *Brazilian journal of medical and biological research = Revista brasileira de pesquisas medicas e biologicas / Sociedade Brasileira de Biofisica* [et al]. 2011;44(9):890-8.
12. Frangogiannis NG. The immune system and the remodeling infarcted heart: cell biological insights and therapeutic opportunities. *Journal of cardiovascular pharmacology*. 2014;63(3):185-95.
13. Cotton JM, Kearney MT, Shah AM. Nitric oxide and myocardial function in heart failure: friend or foe? *Heart*. 2002;88(6):564-6.
14. Elahi MM, Naseem KM, Matata BM. Nitric oxide in blood. The nitrosative-oxidative disequilibrium hypothesis on the pathogenesis of cardiovascular disease. *The FEBS journal*. 2007;274(4):906-23.
15. Gullestad L, Ueland T, Vinge LE, Finsen A, Yndestad A, Aukrust P. Inflammatory cytokines in heart failure: mediators and markers. *Cardiology*. 2012;122(1):23-35.
16. Association TCCotNYH. *Nomenclature and Criteria for Diagnosis of Disease of the Heart and Great Vessels*. 9th ed. Boston, Mass: Little, Brown & Co.; 1994.
17. Hunt SA, Baker DW, Chin MH, Cinquegrani MP, Feldmanmd AM, Francis GS, et al. ACC/AHA Guidelines for the Evaluation and Management of Chronic Heart Failure in the Adult: Executive Summary A Report of the American College of Cardiology/American Heart Association Task Force on Practice Guidelines (Committee to Revise the 1995 Guidelines for the Evaluation and Management of Heart Failure). *Circulation*. 2001;104(24):2996-3007.
18. Stevenson LW, Couper G. On the fledgling field of mechanical circulatory support. *J Am Coll Cardiol*. 2007;50(8):748-51.
19. Jessup M, Brozena S. Heart failure. *N Engl J Med*. 2003;348(20):2007-18.

20. Costanzo MR, Mills RM, Wynne J. Characteristics of "Stage D" heart failure: insights from the Acute Decompensated Heart Failure National Registry Longitudinal Module (ADHERE LM). *American heart journal*. 2008;155(2):339-47.
21. Stevenson LW, Pagani FD, Young JB, Jessup M, Miller L, Kormos RL, et al. INTERMACS profiles of advanced heart failure: the current picture. *J Heart Lung Transplant*. 2009;28(6):535-41.
22. McMurray. The current cost of heart failure to the National Health Service in the UK. *European Journal of Heart Failure*. 2002;4(3):361-71.
23. Yamasaki N, Kitaoka H, Matsumura Y, Furuno T, Nishinaga M, Doi Y. Heart failure in the elderly. *Internal medicine (Tokyo, Japan)*. 2003;42(5):383-8.
24. Brown RC, A. L. Reducing the cost of heart failure while improving quality of life. *British Journal of Cardiology*. 2013;20:45-6.
25. Hayes HM, Dembo LG, Larbalestier R, O'Driscoll G. Management options to treat gastrointestinal bleeding in patients supported on rotary left ventricular assist devices: a single-center experience. *Artif Organs*. 2010;34(9):703-6.
26. DiBardino DJ. The history and development of cardiac transplantation. *Tex Heart Inst J*. 1999;26(3):198-205.
27. Hogg R, Mehew J, Collett D. Annual Report on Cardiothoracic Transplantation. National Health Service: Blood and Transplant; 2016.
28. John R, Liao K. Orthotopic Heart Transplantation. *Operative Techniques in Thoracic and Cardiovascular Surgery*. 2010;15(2):138-46.
29. Newcomb AE, Esmore DS, Rosenfeldt FL, Richardson M, Marasco SF. Heterotopic heart transplantation: an expanding role in the twenty-first century? *Ann Thorac Surg*. 2004;78(4):1345-50; discussion 50-1.
30. AHA. Heart Disease and Stroke Statistics - 2011 Update. *Circulation*. 2011;123:e000-e.
31. Lund LH, Edwards LB, Kucheryavaya AY, Benden C, Christie JD, Dipchand AI, et al. The registry of the International Society for Heart and Lung Transplantation: thirty-first official adult heart transplant report--2014; focus theme: retransplantation. *J Heart Lung Transplant*. 2014;33(10):996-1008.

32. BHF. Heart Transplant 2015 [Available from: <https://www.bhf.org.uk/heart-health/treatments/heart-transplant>].
33. Mancini D, Lietz K. Selection of cardiac transplantation candidates in 2010. *Circulation*. 2010;122(2):173-83.
34. Givertz MM. Cardiology patient pages: ventricular assist devices: important information for patients and families. *Circulation*. 2011;124(12):e305-11.
35. Slaughter MS, Giridharan GA, Tamez D, LaRose J, Sobieski MA, Sherwood L, et al. Transapical miniaturized ventricular assist device: design and initial testing. *J Thorac Cardiovasc Surg*. 2011;142(3):668-74.
36. Schulman AR, Martens TP, Christos PJ, Russo MJ, Comas GM, Cheema FH, et al. Comparisons of infection complications between continuous flow and pulsatile flow left ventricular assist devices. *J Thorac Cardiovasc Surg*. 2007;133(3):841-2.
37. Slaughter MS, Pagani FD, Rogers JG, Miller LW, Sun B, Russell SD, et al. Clinical management of continuous-flow left ventricular assist devices in advanced heart failure. *The Journal of Heart and Lung Transplantation*. 2010;29(4, Supplement):S1-S39.
38. Fukamachi K. Current Status of Artificial Heart (Assist/Replacement) Development in the United States. *Artif Organs*. 2013;37(8):675-6.
39. Hoshi H, Shinshi T, Takatani S. Third-generation blood pumps with mechanical noncontact magnetic bearings. *Artif Organs*. 2006;30(5):324-38.
40. Zipes DP, Libby P, Bonow RO, Mann DL, Tomaselli GF. Braunwald's Heart Disease E-book: A Textbook of Cardiovascular Medicine. 11th ed: Elsevier Health Sciences; 2018.
41. Arnold WS, Bourque K. The engineer and the clinician: understanding the work output and troubleshooting of the HeartMate II rotary flow pump. *J Thorac Cardiovasc Surg*. 2013;145(1):32-6.
42. Matsumiya G, Saitoh S, Sawa Y. Extracorporeal assist circulation for heart failure. *Circulation journal : official journal of the Japanese Circulation Society*. 2009;73 Suppl A:A42-7.



43. Thoratec. Thoratec CentriMag 2017 [Available from: <http://www.thoratec.com/medical-professionals/vad-product-information/thoratec-centrimag.aspx>].
44. Abiomed. Impella 2017 [Available from: <http://www.abiomed.com/impella/impella-25>].
45. Miller PE, Solomon MA, McAreavey D. Advanced Percutaneous Mechanical Circulatory Support Devices for Cardiogenic Shock. Critical care medicine. 2017.
46. Maquet. Rotaflow centrifugal pump 2017 [Available from: <https://www.maquet.com/int/products/rotaflow-centrifugal-pump/>].
47. Kashiwa K, Nishimura T, Saito A, Kubo H, Fukaya A, Tamai H, et al. Left heart bypass support with the Rotaflow Centrifugal Pump(R) as a bridge to decision and recovery in an adult. J Artif Organs. 2012;15(2):207-10.
48. CardiacAssist. Devices: TandemHeart 2017 [Available from: <http://www.texasheart.org/Research/Devices/tandemheart.cfm>].
49. Terumo. How it works: DuraHeart 2 2017 [Available from: <http://terumoheart.net/us/index.php/medical-professionals/how-it-works>].
50. ReliantHeart. The Next Generation LVAD HeartAssist5(R) 2017 [Available from: <http://reliantheart.com/new-heart-assist-5/the-next-generation-lvad/>].
51. Noon GP. Development of an Axial Flow Left Ventricular Assist Device (LVAD) from Inception to Clinical Application. 2006.
52. Wieselthaler GM, Schima H, Lassnigg AM, Dworschak M, Pacher R, Grimm M, et al. Lessons learned from the first clinical implants of the DeBakey ventricular assist device axial pump: a single center report. Ann Thorac Surg. 2001;71(90030):S139-43.
53. Thoratec. HeartMate II - Image Library (Europe) 2017 [Available from: <http://www.thoratec.com/about-us/media-room/library.aspx>].
54. SJM. HeartMate III 2017 [Available from: <https://www.sjmglobal.com/en-int/professionals/featured-products/heart-failure-management/mechanical-circulatory-support/left-ventricular-assist-device/heartmate-3-left-ventricular-assist-system/details#tab>].

55. HeartWare. Resources: HVAD 2017 [Available from: <https://www.heartware.com/resources>].
56. Tuzun E, Roberts K, Cohn WE, Sargin M, Gemmato CJ, Radovancevic B, et al. In vivo evaluation of investigation the HeartWare centrifugal ventricular assist device. *Tex Heart Inst J*. 2007;34(4):406-11.
57. Jarvik. Products: Jarvik 2000 2017 [Available from: <http://www.jarvikheart.com/products/>].
58. Macris MP, Parnis SM, Frazier OH, Fuqua JM, Jr, Jarvik RK. Development of an Implantable Ventricular Assist System. *Ann Thorac Surg*. 1997;63(2):367-70.
59. Mehta A, Hoffbrand V. Haemostasis. 2014. In: *Haematology at a Glance* [Internet]. Wiley Blackwell.
60. Mehta A, Hoffbrand V. Part 1: Basic physiology and practice. *Haematology at a Glance*. 4th ed: John Wiley & Sons; 2003. p. 136.
61. Shemin D, Rittenberg D. The life span of the human red blood cell. *The Journal of biological chemistry*. 1946;166(2):627-36.
62. Hattangadi SM, Wong P, Zhang L, Flygare J, Lodish HF. From stem cell to red cell: regulation of erythropoiesis at multiple levels by multiple proteins, RNAs, and chromatin modifications. *Blood*. 2011;118(24):6258.
63. Chan CH, Pieper IL, Hambly R, Radley G, Jones A, Friedmann Y, et al. The CentriMag centrifugal blood pump as a benchmark for in vitro testing of hemocompatibility in implantable ventricular assist devices. *Artif Organs*. 2015;39(2):93-101.
64. Bennett M, Horton S, Thuys C, Augustin S, Rosenberg M, Brizard C. Pump-induced haemolysis: a comparison of short-term ventricular assist devices. *Perfusion-UK*. 2004;19(2):107-11.
65. Kolaczkowska E, Kubes P. Neutrophil recruitment and function in health and inflammation. *Nature reviews Immunology*. 2013;13(3):159-75.
66. Fuchs TA, Abed U, Goosmann C, Hurwitz R, Schulze I, Wahn V, et al. Novel cell death program leads to neutrophil extracellular traps. *The Journal of Cell Biology*. 2007;176(2):231-41.

67. Hannigan BM, Moore CBT, Quinn DG. Components of the immune system. *Immunology*. 2nd ed. Oxon: Scion Publishing Ltd.; 2009.
68. Vivier E, Raulet DH, Moretta A, Caligiuri MA, Zitvogel L, Lanier LL, et al. Innate or Adaptive Immunity? The Example of Natural Killer Cells. *Science*. 2011;331(6013):44.
69. Janeway CA, Travers P, Walport M, Shlomchik MJ. Basic Concepts in Immunology. *Janeway's Immunobiology*. 7th ed. New York, USA: Garland Science; 2001.
70. Hayday AC, Spencer J. Barrier immunity. *Seminars in immunology*. 2009;21(3):99-100.
71. Hannigan BM, Moore CBT, Quinn DG. The innate immune response. *Immunology*. 2nd ed. Oxon: Scion Publishing Ltd.; 2009.
72. Dunkelberger JR, Song WC. Complement and its role in innate and adaptive immune responses. *Cell research*. 2010;20(1):34-50.
73. Janeway CA, Travers P, Walport M, Shlomchik MJ. The Adaptive Immune Response. *Janeway's Immunobiology*. 7th ed. New York, USA: Garland Science; 2001.
74. Hannigan BM, Moore CBT, Quinn DG. Antigen acquisition and presentation. *Immunology*. 2nd ed: Scion Publishing Ltd.; 2009.
75. Hannigan BM, Moore CBT, Quinn DG. Generation of adaptive immune responses. *Immunology*. 2nd ed. Oxon: Scion Publishing Ltd.; 2009.
76. Hannigan BM, Moore CBT, Quinn DG. Regulation of the adaptive immune response. *Immunology*. 2nd ed: Scion Publishing Ltd.; 2009.
77. Yip J, Shen Y, Berndt MC, Andrews RK. Primary platelet adhesion receptors. *IUBMB life*. 2005;57(2):103-8.
78. Vogler EA, Siedlecki CA. Contact activation of blood-plasma coagulation. *biomaterials* 2009;30:1857-69.
79. Holbrook AM, Pereira JA, Labiris R, McDonald H, Douketis JD, Crowther M, et al. Systematic overview of warfarin and its drug and food interactions. *Archives of internal medicine*. 2005;165(10):1095-106.

80. Thiruvankatarajan V, Pruett A, Adhikary SD. Coagulation testing in the perioperative period. *Indian Journal of Anaesthesia*. 2014;58(5):565-72.
81. Sheriff J, Bluestein D, Girdhar G, Jesty J. High-Shear Stress Sensitizes Platelets to Subsequent Low-Shear Conditions. *Annals of Biomedical Engineering*. 2010;38(4):1442-50.
82. Zhang J, Gellman B, Koert A, Dasse KA, Gilbert RJ, Griffith BP, et al. Computational and experimental evaluation of the fluid dynamics and hemocompatibility of the CentriMag blood pump. *Artif Organs*. 2006;30(3):168-77.
83. Linneweber J, Dohmen PM, Kerzschner U, Affeld K, Nosé Y, Konertz W. The Effect of Surface Roughness on Activation of the Coagulation System and Platelet Adhesion in Rotary Blood Pumps. *Artif Organs*. 2007;31(5):345-51.
84. John R, Kamdar F, Liao K, Colvin-Adams M, Miller L, Joyce L, et al. Low thromboembolic risk for patients with the Heartmate II left ventricular assist device. *The Journal of Thoracic and Cardiovascular Surgery*. 2008;136(5):1318-23.
85. Blitz A. Pump thrombosis—A riddle wrapped in a mystery inside an enigma. *Annals of Cardiothoracic Surgery*. 2014;3(5):450-71.
86. Goldstein DJ, John R, Salerno C, Silvestry S, Moazami N, Horstmanshof D, et al. Algorithm for the diagnosis and management of suspected pump thrombus. *J Heart Lung Transplant*. 2013;32(7):667-70.
87. Mokadam NA, Andrus S, Ungerleider A. Thrombus formation in a HeartMate II. *European Journal of Cardio-Thoracic Surgery*. 2011;39(3):414.
88. Pagani FD, Miller LW, Russell SD. Extended mechanical circulatory support with a continuous-flow rotary left ventricular assist device. *J Am Coll Cardiol*. 2009;54.
89. Slaughter MS, Rogers JG, Milano CA, Russell SD, Conte JV, Feldman D, et al. Advanced Heart Failure Treated with Continuous-Flow Left Ventricular Assist Device. *New England Journal of Medicine*. 2009;361(23):2241-51.
90. Aaronson KD, Slaughter MS, Miller LW, McGee EC, Cotts WG, Acker MA, et al. Use of an intrapericardial, continuous-flow, centrifugal pump in patients awaiting heart transplantation. *Circulation*. 2012;125(25):3191-200.

91. Lahpor J, Khaghani A, Hetzer R, Pavie A, Friedrich I, Sander K, et al. European results with a continuous-flow ventricular assist device for advanced heart-failure patients. *Eur J Cardiothorac Surg*. 2010;37(2):357-61.
92. Kirklin JK, Naftel DC, Kormos RL, Pagani FD, Myers SL, Stevenson LW, et al. Interagency Registry for Mechanically Assisted Circulatory Support (INTERMACS) analysis of pump thrombosis in the HeartMate II left ventricular assist device. *J Heart Lung Transplant*. 2014;33(1):12-22.
93. Uriel N, Han J, Morrison KA, Nahumi N, Yuzefpolskaya M, Garan AR, et al. Device thrombosis in HeartMate II continuous-flow left ventricular assist devices: a multifactorial phenomenon. *J Heart Lung Transplant*. 2014;33(1):51-9.
94. Wang JX, Lee EH, Bonde P. Over 400% Increase in LVAD Thrombosis Reported to the FDA's Manufacturer and User Facility Device Experience (MAUDE) Database from 2010 to 2012. *The Journal of Heart and Lung Transplantation*. 2014;33(4):S9-S10.
95. Krabatsch T, Netuka I, Schmitto JD, Zimpfer D, Garbade J, Rao V, et al. Heartmate 3 fully magnetically levitated left ventricular assist device for the treatment of advanced heart failure –1 year results from the Ce mark trial. *Journal of cardiothoracic surgery*. 2017;12(1):23.
96. Holman WL, Rayburn BK, McGiffin DC, Foley BA, Benza RL, Bourge RC, et al. Infection in ventricular assist devices: prevention and treatment. *The Annals of thoracic surgery*. 2003;75(6):S48-S57.
97. Simon D, Fischer S, Grossman A, Downer C, Hota B, Heroux A, et al. Left Ventricular Assist Device—Related Infection: Treatment and Outcome. *Clinical Infectious Diseases*. 2005;40(8):1108-15.
98. Holman WL, Park SJ, Long JW, Weinberg A, Gupta L, Tierney AR, et al. Infection in permanent circulatory support: Experience from the REMATCH trial. *The Journal of Heart and Lung Transplantation*. 2004;23(12):1359-65.
99. Chinn R, Dembitsky W, Eaton L, Chillcott S, Stahovich M, Rasmusson B, et al. Multicenter experience: prevention and management of left ventricular assist device infections. *Asaio J*. 2005;51(4):461-70.

100. Iversen PO, Woldbaek PR, Christensen G. Reduced immune responses to an aseptic inflammation in mice with congestive heart failure. *European journal of haematology*. 2005;75(2):156-63.
101. Ankersmit HJ, Tugulea S, Spanier T, Weinberg AD, Artrip JH, Burke EM, et al. Activation-induced T-cell death and immune dysfunction after implantation of left-ventricular assist device. *Lancet*. 1999;354(9178):550-5.
102. Kirsch M, Boval B, Damy T, Ghendouz S, Vermes E, Loisanche D, et al. Importance of monocyte deactivation in determining early outcome after ventricular assist device implantation. *The International journal of artificial organs*. 2012;35(3):169-76.
103. Enciso JS. Mechanical Circulatory Support: Current Status and Future Directions. *Progress in Cardiovascular Disease*. 2016;58(4):444-54.
104. Stocksclaeder M, Schneppenheim R, Budde U. Update on von Willebrand factor multimers: focus on high molecular-weight multimers and their role in hemostasis. *Blood coagulation & fibrinolysis : an international journal in haemostasis and thrombosis*. 2014;25(3):206-16.
105. Nascimbene A, Neelamegham S, Frazier OH, Moake JL, Dong JF. Acquired von Willebrand syndrome associated with left ventricular assist device. *Blood*. 2016;127(25):3133-41.
106. Bartoli CR, Kang J, Restle DJ, Zhang DM, Shabahang C, Acker MA, et al. Inhibition of ADAMTS-13 by Doxycycline Reduces von Willebrand Factor Degradation During Supraphysiological Shear Stress. *JACC Heart Failure*. 2015;3(11):860-9.
107. Tan H, Chen H, Xu C, Ge Z, Gao Y, Fang J, et al. Role of vascular endothelial growth factor in angiodysplasia: an interventional study with thalidomide. *Journal of Gastroenterology and Hepatology*. 2012;27(6):1094-101.
108. Hayes HM, Dembo LG, Larbalestier R, O'Driscoll G. Management Options to Treat Gastrointestinal Bleeding in Patients Supported on Rotary Left Ventricular Assist Devices:A Single-Center Experience. *Artif Organs*. 2010;34(9):703-6.
109. Dang NC, Topkara VK, Mercado M, Kay J, Kruger KH, Aboodi MS, et al. Right Heart Failure After Left Ventricular Assist Device Implantation in Patients With

Chronic Congestive Heart Failure. *The Journal of heart and lung transplantation : the official publication of the International Society for Heart Transplantation*. 2006;25(1):1-6.

110. Lampert BC, Teuteberg JJ. Right ventricular failure after left ventricular assist devices. *J Heart Lung Transplant*. 2015;34(9):1123-30.

111. Jorde UP, Uriel N, Nahumi N, Bejar D, Gonzalez-Costello J, Thomas SS, et al. Prevalence, Significance, and Management of Aortic Insufficiency in Continuous Flow Left Ventricular Assist Device Recipients. *Circulation: Heart Failure*. 2014;7(2):310.

112. Goldstein DJ. Worldwide Experience With the MicroMed DeBakey Ventricular Assist Device® as a Bridge to Transplantation. *Circulation*. 2003;108(10 suppl 1):II-272-II-7.

113. Rothenburger M, Wilhelm MJ, Hammel D, Schmidt C, Tjan TDT, Böcker D, et al. Treatment of Thrombus Formation Associated With the MicroMed DeBakey VAD Using Recombinant Tissue Plasminogen Activator. *Circulation*. 2002;106(12 suppl 1):I-189-I-92.

114. Malehsa D, Meyer AL, Bara C, Struber M. Acquired von Willebrand syndrome after exchange of the HeartMate XVE to the HeartMate II ventricular assist device. *Eur J Cardiothorac Surg*. 2009;35(6):1091-3.

115. Demirozu ZT, Radovancevic R, Hochman LF, Gregoric ID, Letsou GV, Kar B, et al. Arteriovenous malformation and gastrointestinal bleeding in patients with the HeartMate II left ventricular assist device. *The Journal of Heart and Lung Transplantation*. 2011;30(8):849-53.

116. Bhamidipati CM, Ailawadi G, Bergin J, Kern JA. Early thrombus in a HeartMate II left ventricular assist device: A potential cause of hemolysis and diagnostic dilemma. *The Journal of Thoracic and Cardiovascular Surgery*. 2010;140(1):e7-e8.

117. Meyer AL, Kuehn C, Weidemann J, Malehsa D, Bara C, Fischer S, et al. Thrombus formation in a HeartMate II left ventricular assist device. *J Thorac Cardiovasc Surg*. 2008;135(1):203-4.

118. Clarke T, Sherman D. HeartWare device had 9.2 percent thrombosis rate in trial. Reuters2011.
119. Nainggolan L. Change in anticoagulation reduces thrombi in HeartWare trials theheartorg [Internet]. 2011 12/10/2011.
120. Letsou GV, Shah N, Gregoric ID, Myers TJ, Delgado R, Frazier OH. Gastrointestinal bleeding from arteriovenous malformations in patients supported by the Jarvik 2000 axial-flow left ventricular assist device. *The Journal of Heart and Lung Transplantation*. 2005;24(1):105-9.
121. Dembitsky WP, Schmitto JD, Pya Y, editors. *The HeartMate III: From Design to Trial*. ISRBP; 2015 28th September 2015; Dubrovnik, Croatia.
122. Slaughter MS, Giridharan GA, Tamez D, LaRose J, Sobieski MA, Sherwood L, et al. Transapical miniaturized ventricular assist device: Design and initial testing. *The Journal of thoracic and cardiovascular surgery*. 2011;142(3):10.1016/j.jtcvs.2011.01.011.
123. Vandenberghe S, Segers P, Meyns B, Verdonck P. Hydrodynamic characterisation of ventricular assist devices. *The International journal of artificial organs*. 2001;24(7):470-7.
124. Johnson Jr CA, Wearden PD, Kocyildirim E, Maul TM, Woolley JR, Ye S-H, et al. Platelet Activation in Ovines Undergoing Sham Surgery or Implant of the Second Generation PediaFlow Pediatric Ventricular Assist Device. *Artif Organs*. 2011;35(6):602-13.
125. Ankersmit HJ, Edwards NM, Schuster M, John R, Kocher A, Rose EA, et al. Quantitative changes in T-cell populations after left ventricular assist device implantation: relationship to T-cell apoptosis and soluble CD95. *Circulation*. 1999;100(19 Suppl):II211-5.
126. Diehl P, Aleker M, Helbing T, Sossong V, Beyersdorf F, Olschewski M, et al. Enhanced microparticles in ventricular assist device patients predict platelet, leukocyte and endothelial cell activation. *Interact Cardiovasc Thorac Surg*. 2010;11(2):133-7.
127. Woolley JR, Teuteberg JJ, Bermudez CA, Bhamra JK, Lockard KL, Kormos RL, et al. Temporal leukocyte numbers and granulocyte activation in pulsatile and rotary ventricular assist device patients. *Artif Organs*. 2014;38(6):447-55.



128. Radovancevic R, Matijevic N, Bracey AW, Radovancevic B, Elayda M, Gregoric ID, et al. Increased leukocyte-platelet interactions during circulatory support with left ventricular assist devices. *ASAIO journal (American Society for Artificial Internal Organs : 1992)*. 2009;55(5):459-64.
129. Klovaite J, Gustafsson F, Mortensen SA, Sander K, Nielsen LB. Severely impaired von Willebrand factor-dependent platelet aggregation in patients with a continuous-flow left ventricular assist device (HeartMate II). *J Am Coll Cardiol*. 2009;53(23):2162-7.
130. Sobieski MA, Giridharan GA, Ising M, Koenig SC, Slaughter MS. Blood trauma testing of CentriMag and RotaFlow centrifugal flow devices: a pilot study. *Artif Organs*. 2012;36(8):677-82.
131. Chan CH, Hilton A, Foster G, Hawkins KM, Badiei N, Thornton CA. The evaluation of leukocytes in response to the in vitro testing of ventricular assist devices. *Artif Organs*. 2013;37(9):793-801.
132. Pieper IL, Friedmann Y, Jones A, Thornton C. Evaluation of Four Veterinary Hematology Analyzers for Bovine and Ovine Blood Counts for In Vitro Testing of Medical Devices. *Artif Organs*. 2016.
133. Robinson JP. Flow Cytometry. In: Wnek GE, Bowlin GL, editors. *Encyclopedia of Biomaterials*: Marcel Decker Inc.; 2004. p. 630-40.
134. Sopp P, Howard CJ. Cross-reactivity of monoclonal antibodies to defined human leucocyte differentiation antigens with bovine cells. *Vet Immunol Immunopathol*. 1997;56(1-2):11-25.
135. Sopp P, Redknap L, Howard C. Cross-reactivity of human leucocyte differentiation antigen monoclonal antibodies on porcine cells. *Vet Immunol Immunopathol*. 1998;60(3-4):403-8.
136. Johnson CA, Jr., Snyder TA, Woolley JR, Wagner WR. Flow cytometric assays for quantifying activated ovine platelets. *Artif Organs*. 2008;32(2):136-45.
137. Baker LC, Davis WC, Autieri J, Watach MJ, Yamazaki K, Litwak P, et al. Flow cytometric assays to detect platelet activation and aggregation in device-implanted calves. *J Biomed Mater Res*. 1998;41(2):312-21.

138. Brando B, Barnett D, Janossy G, Mandy F, Autran B, Rothe G, et al. Cytofluorometric methods for assessing absolute numbers of cell subsets in blood. European Working Group on Clinical Cell Analysis. *Cytometry*. 2000;42(6):327-46.
139. Shenkin M, Babu R, Maiese R. Accurate assessment of cell count and viability with a flow cytometer. *Cytometry Part B, Clinical cytometry*. 2007;72(5):427-32.
140. Edward R, Dimmick I. Compensation-free dead cell exclusion: multi-beam excitation of the far-red DNA binding viability dye DRAQ7.(TECH2P. 873). *The Journal of Immunology*. 2014;192(1 Supplement):135.4-.4.
141. Wlodkowic D, Akagi J, Dobrucki J, Errington R, Smith PJ, Takeda K, et al. Kinetic viability assays using DRAQ7 probe. *Current protocols in cytometry*. 2013;Chapter 9:Unit 9.41.
142. Edward R. Use of DNA-specific anthraquinone dyes to directly reveal cytoplasmic and nuclear boundaries in live and fixed cells. *Molecules and cells*. 2009;27(4):391-6.
143. Turac G, Hindley CJ, Thomas R, Davis JA, Deleidi M, Gasser T, et al. Combined flow cytometric analysis of surface and intracellular antigens reveals surface molecule markers of human neurogenesis. *PloS one*. 2013;8(6):e68519.
144. Warrino DE, DeGennaro LJ, Hanson M, Swindells S, Pirruccello SJ, Ryan WL. Stabilization of white blood cells and immunologic markers for extended analysis using flow cytometry. *Journal of immunological methods*. 2005;305(2):107-19.
145. Schumacher A. Effect of ex vivo storage and Cyto-Chex on the expression of P-selectin glycoprotein ligand-1 (PSGL-1) on human peripheral leukocytes. *Journal of immunological methods*. 2007;323(1):24-30.
146. Canonico B, Betti M, Luchetti F, Battistelli M, Falcieri E, Ferri P, et al. Flow cytometric profiles, biomolecular and morphological aspects of transfixed leukocytes and red cells. *Cytometry Part B, Clinical cytometry*. 2010;78(4):267-78.
147. Ng AA, Lee BT, Teo TS, Poidinger M, Connolly JE. Optimal cellular preservation for high dimensional flow cytometric analysis of multicentre trials. *Journal of immunological methods*. 2012;385(1-2):79-89.
148. Cian F, Guzera M, Frost S, Van Poucke S, Comazzi S, Archer J. Stability of immunophenotypic lymphoid markers in fixed canine peripheral blood for flow

cytometric analysis. *Veterinary clinical pathology / American Society for Veterinary Clinical Pathology*. 2014;43(1):101-8.

149. Davis C, Wu X, Li W, Fan H, Reddy M. Stability of immunophenotypic markers in fixed peripheral blood for extended analysis using flow cytometry. *Journal of immunological methods*. 2011;363(2):158-65.

150. Ruaux CG, Williams DA. The effect of ex vivo refrigerated storage and cell preservation solution (Cyto-Chex II) on CD11b expression and oxidative burst activity of dog neutrophils. *Vet Immunol Immunopathol*. 2000;74(1-2):59-69.

151. Saxton JM, Pockley AG. Effect of ex vivo storage on human peripheral blood neutrophil expression of CD11b and the stabilizing effects of Cyto-Chex. *Journal of immunological methods*. 1998;214(1-2):11-7.

152. ASTM. F1841-97: Standard Practice for Assessment of Hemolysis in Continuous Flow Blood Pumps. 2013.

153. Altin JG, Sloan EK. The role of CD45 and CD45-associated molecules in T cell activation. *Immunology and cell biology*. 1997;75(5):430-45.

154. Garraud O, Cognasse F. Are Platelets Cells? And if Yes, are They Immune Cells? *Frontiers in immunology*. 2015;6:70.

155. Borner MM, Schneider E, Pirnia F, Sartor O, Trepel JB, Myers CE. The detergent Triton X-100 induces a death pattern in human carcinoma cell lines that resembles cytotoxic lymphocyte-induced apoptosis. *FEBS letters*. 1994;353(2):129-32.

156. Chan C, Pieper IL, Robinson CR, Friedmann Y, Kanamarlapudi V, Thornton CA. Shear Stress-Induced Total Blood Trauma in Multiple Species. *Artif Organs*. 2017.

157. Jones ML, Allison RW. Evaluation of the ruminant complete blood cell count. *Veterinary Clinics of North America: Food Animal Practice*. 2007;23(3):377-402.

158. Kruger P, Saffarzadeh M, Weber ANR, Rieber N, Radsak M, von Bernuth H, et al. Neutrophils: Between Host Defence, Immune Modulation, and Tissue Injury. *PLoS pathogens*. 2015;11(3):e1004651.

159. Canonico B, Zamai L, Burattini S, Granger V, Mannello F, Gobbi P, et al. Evaluation of leukocyte stabilisation in TransFix-treated blood samples by flow cytometry and transmission electron microscopy. *Journal of immunological methods*. 2004;295(1-2):67-78.
160. Pieper IL, Radley G, Chan CHH, Friedmann Y, Foster G, Thornton CA. Quantification methods for human and large animal leukocytes using DNA dyes by flow cytometry. *Cytometry Part A*. 2016:565-74.
161. Vert M, Doi Y, Hellwich K-H, Hess M, Hodge P, Kubisa P, et al. Terminology for biorelated polymers and applications (IUPAC Recommendations 2012). *Pure and Applied Chemistry*. 2012;84(2):377-410.
162. Manivasagam G. Biomedical Implants: Corrosion and its Prevention - A Review. *Recent Patents on Corrosion Science*. 2010.
163. Bobbio A. The first endosseous alloplastic implant in the history of man. *Bulletin of the Historical Dentology*. 1972;20:1-6.
164. Crubezy E, Murail P, Girard L, Bernadou JP. False teeth of the Roman world. *Nature*. 1998;391(6662):29.
165. Buchanan G. Vesico-Vaginal Fistula, operated on by Dr. Bozeman with his Button Suture. *The New Orleans Medical and Surgical Journal*. 1859;16:115.
166. Ratner BD. History of Biomaterials. *Biomaterials Science: An Introduction to Materials in Medicine*. 3rd ed: Academic Press; 2012.
167. Apple DJ, Sims J. Harold Ridley and the invention of the intraocular lens. *Survey of ophthalmology*. 1996;40(4):279-92.
168. Peitzman SJ. Chronic Dialysis and Dialysis Doctors in the United States: A Nephrologist-Historian's Perspective. *Seminars in Dialysis*. 2001;14(3):200-8.
169. Liotta D. Early Clinical Application of Assisted Circulation. *Tex Heart Inst J*. 2002;29(3):229-30.
170. Ramsden JJ, Allen DM, Stephenson DJ, Alcock JR, Peggs GN, Fuller G, et al. The Design and Manufacture of Biomedical Surfaces. *CIRP Annals - Manufacturing Technology*. 2007;56(2):687-711.

171. Dietschweiler C, Sander, M., . Protein Adsorption at Solid Surfaces. Zurich: Swiss Federal Institute of Technology; 2008.
172. Serro AP. Principle of Protein Adsorption. Centro de Quimica Estrutural 2015.
173. Bakir M. Haemocompatibility of titanium and its alloys. J of biomat app. 2012;27(1):3-15.
174. Eriksson C, Nygren H. Adhesion receptors of polymorphonuclear granulocytes on titanium in contact with whole blood. J Lab Clin Med. 2001;137(1):56-63.
175. Yahyapour N, Eriksson C, Malmberg P, Nygren H. Thrombin, kallikrein and complement C5b-9 adsorption on hydrophilic and hydrophobic titanium and glass after short time exposure to whole blood. Biomaterials. 2004;25(16):3171-6.
176. Anderson JM, Rodriguez A, Chang DT. Foreign body reaction to biomaterials. Seminars in immunology. 2008;20(2):86-100.
177. Rabe M, Verdes D, Seeger S. Understanding protein adsorption phenomena at solid surfaces. Advances in Colloid and Interface Science. 2011;162(1–2):87-106.
178. Zadei TN, McIntire LV, Farrell DH, Thiagarajan P. Adhesion of Platelets to Surface-Bound Fibrinogen Under Flow. Blood. 1996.
179. Rainger GE, Chimen M, Harrison MJ, Yates CM, Harrison P, Watson SP, et al. The role of platelets in the recruitment of leukocytes during vascular disease. Platelets. 2015;26(6):507-20.
180. Schuster M, Kocher A, Lietz K, Ankersmit J, John R, Edwards N, et al. Induction of CD40 ligand expression in human T cells by biomaterials derived from left ventricular assist device surface. Transplantation proceedings. 2001;33(1-2):1960-1.
181. Gorbet MB, Sefton MV. Biomaterial-associated thrombosis: roles of coagulation factors, complement, platelets and leukocytes. Biomaterials. 2004;25(26):5681-703.
182. Gorbet MB, Yeo EL, Sefton MV. Flow cytometric study of in vitro neutrophil activation by biomaterials. J Biomed Mater Res. 1999;44(3):289-97.

183. Suska F, Esposito M, Gretzer C, Kalltorp M, Tengvall P, Thomsen P. IL-1alpha, IL-1beta and TNF-alpha secretion during in vivo/ex vivo cellular interactions with titanium and copper. *Biomaterials*. 2003;24(3):461-8.
184. Schutte RJ, Parisi-Amon A, Reichert WM. Cytokine profiling using monocytes/macrophages cultured on common biomaterials with a range of surface chemistries. *Journal of biomedical materials research Part A*. 2009;88(1):128-39.
185. Shive MS, Salloum ML, Anderson JM. Shear stress-induced apoptosis of adherent neutrophils: a mechanism for persistence of cardiovascular device infections. *Proceedings of the National Academy of Sciences of the United States of America*. 2000;97(12):6710-5.
186. Ufukerbulut D, Lazoglu I. Biomaterials for improving the blood and tissue compatibility of total artificial hearts (TAH) and ventricular assist devices (VAD). *Biomaterials for Artificial Organs*2010. p. 207.
187. Griffith BP, Kormos RL, Borovetz HS, Litwak K, Antaki JF, Poirier VL, et al. HeartMate II left ventricular assist system: from concept to first clinical use. *Ann Thorac Surg*. 2001;71(90030):S116-20.
188. Palanzo DA, El-Banayasy A, Stephenson E, Brehm C, Kunselman A, Pae WE. Comparison of Hemolysis Between CentriMag and RotaFlow Rotary Blood Pumps During Extracorporeal Membrane Oxygenation. *Artif Organs*. 2013;37(9):E162-6.
189. Hisbergues M, Vendeville S, Vendeville P. Zirconia: Established facts and perspectives for a biomaterial in dental implantology. *Journal of biomedical materials research Part B, Applied biomaterials*. 2009;88(2):519-29.
190. Parthasarathy KS, Cheng YC, McAllister JP, 2nd, Shen Y, Li J, Deren K, et al. Biocompatibilities of sapphire and borosilicate glass as cortical neuroprostheses. *Magnetic resonance imaging*. 2007;25(9):1333-40.
191. Fedel M, Motta A, Maniglio D, Migliaresi C. Surface properties and blood compatibility of commercially available diamond-like carbon coatings for cardiovascular devices. *Journal of biomedical materials research Part B, Applied biomaterials*. 2009;90(1):338-49.
192. Dearnaley G, Arps JH. Biomedical applications of diamond-like carbon (DLC) coatings: A review. *Surface and Coatings Technology*. 2005;200(7):2518-24.

193. Nurdin N, Francois P, Mugnier Y, Krumeich J, Moret M, Aronsson BO, et al. Haemocompatibility evaluation of DLC- and SiC-coated surfaces. *European cells & materials*. 2003;5:17-26; discussion -8.
194. Han V, Serrano K, Devine D. A comparative study of common techniques used to measure haemolysis in stored red cell concentrates. *Vox Sang*. 2010;98(2):116-23.
195. Frelinger AL, 3rd, Grace RF, Gerrits AJ, Berny-Lang MA, Brown T, Carmichael SL, et al. Platelet function tests, independent of platelet count, are associated with bleeding severity in ITP. *Blood*. 2015;126(7):873-9.
196. Redlich H, Vickers J, Losche W, Heptinstall S, Kehrel B, Spangenberg P. Formation of platelet-leukocyte conjugates in whole blood. *Platelets*. 1997;8(6):419-25.
197. Gorbet MB, Sefton MV. Endotoxin: the uninvited guest. *Biomaterials*. 2005;26(34):6811-7.
198. ASTM. F1841-97: Standard Practice for Assessment of Hemolysis in Continuous Flow Blood Pumps. 2005.
199. Bahl N, Winarsih I, Tucker-Kellogg L, Ding JL. Extracellular haemoglobin upregulates and binds to tissue factor on macrophages: implications for coagulation and oxidative stress. *Thrombosis and haemostasis*. 2014;111(1):67-78.
200. Long AT, Kenne E, Jung R, Fuchs TA, Renne T. Contact system revisited: an interface between inflammation, coagulation, and innate immunity. *J Thromb Haemost*. 2015.
201. Butenas S, Mann KG. Blood coagulation. *Biochemistry Biokhimiia*. 2002;67(1):3-12.
202. Falanga A, Marchetti M, Vignoli A, Balducci D, Barbui T. Leukocyte-platelet interaction in patients with essential thrombocythemia and polycythemia vera. *Experimental hematology*. 2005;33(5):523-30.
203. Chang DT, Colton E, Matsuda T, Anderson JM. Lymphocyte adhesion and interactions with biomaterial adherent macrophages and foreign body giant cells. *Journal of biomedical materials research Part A*. 2009;91(4):1210-20.

204. Smalley DM, Ley K. L-selectin: mechanisms and physiological significance of ectodomain cleavage. *Journal of cellular and molecular medicine*. 2005;9(2):255-66.
205. Migeotte I, Communi D, Parmentier M. Formyl peptide receptors: a promiscuous subfamily of G protein-coupled receptors controlling immune responses. *Cytokine & growth factor reviews*. 2006;17(6):501-19.
206. Gane P, Fain O, Mansour I, Roquin H, Rouger P. Expression of CD11b (Leu15) antigen on CD3+, CD4+, CD8+, CD16+ peripheral lymphocytes. Estimation of CD3+8+11b+ and CD3+4-8-11b+ T-cell subsets using a single laser flow cytometer. *Scandinavian journal of immunology*. 1992;36(3):395-404.
207. Frank RD, Dresbach H, Thelen H, Sieberth HG. Glutardialdehyde induced fluorescence technique (GIFT): a new method for the imaging of platelet adhesion on biomaterials. *J Biomed Mater Res*. 2000;52(2):374-81.
208. ISO. Biological evaluation of medical devices - part 4: Selection of tests for interactions with blood 10993-4:2009. 2010.
209. Chang X, Gorbet M. The effect of shear on in vitro platelet and leukocyte material-induced activation. *Journal of biomaterials applications*. 2013;28(3):407-15.
210. Martinesi M, Bruni S, Stio M, Treves C, Borgioli F. In vitro interaction between surface-treated Ti-6Al-4V titanium alloy and human peripheral blood mononuclear cells. *J Biomed Mater Res Part A*. 2005;74A(2):197-207.
211. Gretzer C, Gisselalt K, Liljensten E, Ryden L, Thomsen P. Adhesion, apoptosis and cytokine release of human mononuclear cells cultured on degradable poly(urethane urea), polystyrene and titanium in vitro. *Biomaterials*. 2003;24(17):2843-52.
212. Capello WN, D'Antonio JA, Feinberg JR, Manley MT. Alternative Bearing Surfaces: Alumina Ceramic Bearings for Total Hip Arthroplasty. *Bioceramics and Alternative Bearings in Joint Arthroplasty*. Darmstadt: Steinkopff; 2005. p. 87-94.
213. Christel PS. Biocompatibility of surgical-grade dense polycrystalline alumina. *Clinical orthopaedics and related research*. 1992(282):10-8.
214. Kue R, Sohrabi A, Nagle D, Frondoza C, Hungerford D. Enhanced proliferation and osteocalcin production by human osteoblast-like MG63 cells on silicon nitride ceramic discs. *Biomaterials*. 1999;20(13):1195-201.



215. Takami Y, Nakazawa T, Makinouchi K, Glueck J, Nose Y. Biocompatibility of alumina ceramic and polyethylene as materials for pivot bearings of a centrifugal blood pump. *J Biomed Mater Res.* 1997;36(3):381-6.
216. Takami Y, Yamane S, Makinouchi K, Otsuka G, Glueck J, Benkowski R, et al. Protein adsorption onto ceramic surfaces. *J Biomed Mater Res.* 1998;40(1):24-30.
217. Linder S, Pinkowski W, Aepfelbacher M. Adhesion, cytoskeletal architecture and activation status of primary human macrophages on a diamond-like carbon coated surface. *Biomaterials.* 2002;23(3):767-73.
218. Santos EDD, Luqueta G, Rajasekaran R, Santos TBd, Doria ACOC, Radi PA, et al. Macrophages adhesion rate on Ti-6Al-4V substrates: polishing and DLC coating effects. *Research on Biomedical Engineering.* 2016;32:144-52.
219. Dion I, Roques X, Baquey H, Baudet E, Basse Cathalinat B, More N. Hemocompatibility of Diamond-Like Carbon Coating. *Bio-medical materials and engineering.* 1993;3(1):51-5.
220. Damas JK, Gullestad L, Ueland T, Solum NO, Simonsen S, Froland SS, et al. CXC-chemokines, a new group of cytokines in congestive heart failure--possible role of platelets and monocytes. *Cardiovasc Res.* 2000;45(2):428-36.
221. Gurbel PA, Gattis WA, Fuzaylov SF, Gaulden L, Hasselblad V, Serebruany VL, et al. Evaluation of platelets in heart failure: Is platelet activity related to etiology, functional class, or clinical outcomes? *American heart journal.* 2002;143(6):1068-75.
222. Braune S, Gross M, Walter M, Zhou S, Dietze S, Rutschow S, et al. Adhesion and activation of platelets from subjects with coronary artery disease and apparently healthy individuals on biomaterials. *Journal of biomedical materials research Part B, Applied biomaterials.* 2016;104(1):210-7.
223. Wilkes JO. *Introduction to Fluid Mechanics. Fluid Mechanics for Chemical Engineers with Microfluidics and CFD.* 2nd ed: Prentice Hall; 2005.
224. Amaral F, Egger C, Steinseifer U, Schmitz-Rode T. Differences Between Blood and a Newtonian Fluid on the Performance of a Hydrodynamic Bearing for Rotary Blood Pumps. *Artif Organs.* 2013;37(9):786-92.

225. Schaschke C. Laminar flow and lubrication. *Fluid Mechanics: Worked Examples for Engineers*. Rugby, Warwickshire, UK: Institution of Chemical Engineers; 2005. p. 61.
226. Pope SB. The nature of turbulent flows. *Turbulent Flow*: Cambridge University Press; 2000.
227. Watts T. Comparative effect of haemodynamic variables and rheological properties of the blood on the margination and adhesion of leukocytes and platelets. University of Birmingham  
University of Birmingham; 2010.
228. Lu D, Kassab GS. Role of shear stress and stretch in vascular mechanobiology. *Journal of the Royal Society Interface*. 2011;8(63):1379-85.
229. Resnick N, Yahav H, Shay-Salit A, Shushy M, Schubert S, Zilberman LC, et al. Fluid shear stress and the vascular endothelium: for better and for worse. *Progress in biophysics and molecular biology*. 2003;81(3):177-99.
230. Fitts MK, Pike DB, Anderson K, Shiu Y-T. Hemodynamic Shear Stress and Endothelial Dysfunction in Hemodialysis Access. *The open urology & nephrology journal*. 2014;7(Suppl 1 M5):33-44.
231. Wynn R, Will A. Haemolytic anemia. *Current Paediatrics*. 1996;6(1):62-6.
232. Olsen DB. The history of continuous-flow blood pumps. *Artif Organs*. 2000;24(6):401-4.
233. Arora D, Behr M, Pasquali M. A tensor-based measure for estimating blood damage. *Artif Organs*. 2004;28(11):1002-15.
234. Bartoli CR, Restle DJ, Zhang DM, Acker MA, Atluri P. Pathologic von Willebrand factor degradation with a left ventricular assist device occurs via two distinct mechanisms: mechanical demolition and enzymatic cleavage. *J Thorac Cardiovasc Surg*. 2015;149(1):281-9.
235. Proudfoot AG, Davidson SJ, Strueber M. State of the art: Von willebrand factor disruption and continuous flow circulatory devices. *The Journal of Heart and Lung Transplantation*. 2017.

236. Malehsa D, Meyer AL, Bara C, Struber M. Acquired von Willebrand syndrome after exchange of the HeartMate XVE to the HeartMate II ventricular assist device. *Eur J Cardiothorac Surg.* 2009;35(6):1091-3.
237. Wurzinger LJ, Opitz R, Blasberg P, Schmid-Schonbein H. Platelet and coagulation parameters following millisecond exposure to laminar shear stress. *Thrombosis and haemostasis.* 1985;54(2):381-6.
238. Kroll MH, Hellums JD, McIntire LV, Schafer AI, Moake JL. Platelets and shear stress. *Blood.* 1996;88(5):1525-41.
239. Dewitz TS, Hung TC, Martin RR, McIntire LV. Mechanical trauma in leukocytes. *J Lab Clin Med.* 1977;90(4):728-36.
240. Dewitz TS, McIntire LV, Martin RR, Sybers HD. Enzyme release and morphological changes in leukocytes induced by mechanical trauma. *Blood cells.* 1979;5(3):499-512.
241. Takami Y, Yamane S, Makinouchi K, Glueck J, Nose Y. Mechanical white blood cell damage in rotary blood pumps. *Artif Organs.* 1997;21(2):138-42.
242. Moazzam F, DeLano FA, Zweifach BW, Schmid-Schönbein GW. The leukocyte response to fluid stress. *Proceedings of the National Academy of Sciences of the United States of America.* 1997;94(10):5338-43.
243. Fukuda S, Yasu T, Predescu DN, Schmid-Schönbein GW. Mechanisms for regulation of fluid shear stress response in circulating leukocytes. *Circulation research.* 2000;86(1):e13-e8.
244. Chittur KK, McIntire LV, Rich RR. Shear stress effects on human T cell function. *Biotechnology Progress.* 1988;4(2):89-96.
245. De Somer F, Foubert L, Vanackere M, Dujardin D, Delanghe J, Van Nooten G. Impact of oxygenator design on hemolysis, shear stress, and white blood cell and platelet counts. *J Cardiothorac Vasc Anesth.* 1996;10(7):884-9.
246. Gu YJ, Boonstra PW, Graaff R, Rijnsburger AA, Mungroop H, van Oeveren W. Pressure Drop, Shear Stress, and Activation of Leukocytes During Cardiopulmonary Bypass: A Comparison Between Hollow Fiber and Flat Sheet Membrane Oxygenators. *Artif Organs.* 2000;24(1):43-8.

247. Fontana F, Ballestri M, Makomi C, Morandi R, Cappelli G. Hemorheologic alterations in peritoneal dialysis. *Clinical hemorheology and microcirculation*. 2017;65(2):175-83.
248. Reinhart WH, Cagienard F, Schulzki T, Venzin RM. The passage of a hemodialysis filter affects hemorheology, red cell shape, and platelet aggregation. *Clinical hemorheology and microcirculation*. 2014;57(1):49-62.
249. ASTM. F1830-97: Standard Practice for Selection of Blood for in vitro Evaluation of Blood Pumps. 2013.
250. Griebel PJ, Entrican G, Rocchi M, Beskorwayne T, Davis WC. Cross-reactivity of mAbs to human CD antigens with sheep leukocytes. *Vet Immunol Immunopathol*. 2007;119(1):115-22.
251. Lowe DM, Bangani N, Mehta MR, Lang DM, Rossi AG, Wilkinson KA, et al. A novel assay of antimycobacterial activity and phagocytosis by human neutrophils. *Tuberculosis (Edinburgh, Scotland)*. 2013;93(2):167-78.
252. Burger D, Schock S, Thompson CS, Montezano AC, Hakim AM, Touyz RM. Microparticles: biomarkers and beyond. *Clinical science*. 2013;124(7):423-41.
253. VanWijk MJ, VanBavel E, Sturk A, Nieuwland R. Microparticles in cardiovascular diseases. *Cardiovascular Research*. 2003;59(2):277-87.
254. Angelillo-Scherrer A. Leukocyte-derived microparticles in vascular homeostasis. *Circulation Research*. 2012;110(2):356-69.
255. Distler JH, Huber LC, Gay S, Distler O, Pisetsky DS. Microparticles as mediators of cellular cross-talk in inflammatory disease. *Autoimmunity*. 2006;39(8):683-90.
256. Kotsougiani D, Pioch M, Prior B, Heppert V, Hänsch GM, Wagner C. Activation of T Lymphocytes in Response to Persistent Bacterial Infection: Induction of CD11b and of Toll-Like Receptors on T Cells. *International Journal of Inflammation*. 2010;2010:10.
257. Reinisch W, Lichtenberger C, Steger G, Tillinger W, Scheiner O, Gangl A, et al. Donor dependent, interferon- $\gamma$  induced HLA-DR expression on human neutrophils in vivo. *Clinical & Experimental Immunology*. 2003;133(3):476-84.

258. Janeway CA, Travers P, Walport M, Shlomchik MJ. *Innate Immunity. Janeway's Immunobiology*. 7th ed. New York, USA: Garland Science; 2001.
259. Ding J, Niu S, Chen Z, Zhang T, Griffith BP, Wu ZJ. Shear-Induced Hemolysis: Species Differences. *Artif Organs*. 2015;39(9):795-802.
260. Chan CH, Pieper IL, Fleming S, Friedmann Y, Foster G, Hawkins K, et al. The effect of shear stress on the size, structure, and function of human von Willebrand factor. *Artif Organs*. 2014;38(9):741-50.
261. Zhang JT, Gellman B, Koert A, Dasse KA, Gilbert RJ, Griffith BP, et al. Computational and experimental evaluation of the fluid dynamics and hemocompatibility of the CentriMag blood pump. *Artif Organs*. 2006;30(3):168-77.
262. Fraser K. Mechanical Stress Induced Blood Trauma. In: Becker SM, Kuznetsov AV, editors. *Heat transfer and fluid flow in biological processes*. USA: Elsevier; 2015. p. 305-33.
263. Holme PA, Ørvim U, Hamers MJ, Solum NO, Brosstad FR, Barstad RM, et al. Shear-induced platelet activation and platelet microparticle formation at blood flow conditions as in arteries with a severe stenosis. *Arteriosclerosis, thrombosis, and vascular biology*. 1997;17(4):646-53.
264. Pluskota E, Woody NM, Szpak D, Ballantyne CM, Soloviev DA, Simon DI, et al. Expression, activation, and function of integrin  $\alpha$ M $\beta$ 2 (Mac-1) on neutrophil-derived microparticles. *Blood*. 2008;112(6):2327-35.
265. Miguet L, Pacaud K, Felden C, Hugel B, Martinez MC, Freyssinet JM, et al. Proteomic analysis of malignant lymphocyte membrane microparticles using double ionization coverage optimization. *Proteomics*. 2006;6(1):153-71.
266. Hambly RJ. *The thrombogenicity of candidate materials for an implantable ventricular assist device*: Swansea University; 2016.
267. Lee D, Schultz JB, Knauf PA, King MR. Mechanical shedding of L-selectin from the neutrophil surface during rolling on sialyl Lewis x under flow. *The Journal of biological chemistry*. 2007;282(7):4812-20.
268. Fukuda S, Schmid-Schonbein GW. Regulation of CD18 expression on neutrophils in response to fluid shear stress. *Proceedings of the National Academy of Sciences of the United States of America*. 2003;100(23):13152-7.

269. Carter J, Hristova K, Harasaki H, Smith WA. Short exposure time sensitivity of white cells to shear stress. *ASAIO journal (American Society for Artificial Internal Organs : 1992)*. 2003;49(6):687-91.
270. Cunningham KS, Gotlieb AI. The role of shear stress in the pathogenesis of atherosclerosis. *Laboratory investigation; a journal of technical methods and pathology*. 2004;85(1):9-23.
271. Damsgaard CT, Lauritzen L, Calder PC, Kjær TMR, Frøkiær H. Whole-blood culture is a valid low-cost method to measure monocytic cytokines — A comparison of cytokine production in cultures of human whole-blood, mononuclear cells and monocytes. *Journal of immunological methods*. 2009;340(2):95-101.
272. Brodbeck WG, Voskerician G, Ziats NP, Nakayama Y, Matsuda T, Anderson JM. In vivo leukocyte cytokine mRNA responses to biomaterials are dependent on surface chemistry. *Journal of biomedical materials research Part A*. 2003;64(2):320-9.
273. Cohen HC, Joyce EJ, Kao WJ. Biomaterials selectively modulate interactions between human blood-derived polymorphonuclear leukocytes and monocytes. *The American journal of pathology*. 2013;182(6):2180-90.
274. Calandra T, Roger T. Macrophage migration inhibitory factor: a regulator of innate immunity. *Nature reviews Immunology*. 2003;3(10):791-800.
275. Calandra T, Bernhagen J, Mitchell RA, Bucala R. The macrophage is an important and previously unrecognized source of macrophage migration inhibitory factor. *The Journal of experimental medicine*. 1994;179(6):1895-902.
276. Bernhagen J, Calandra T, Mitchell RA, Martin SB, Tracey KJ, Voelter W, et al. MIF is a pituitary-derived cytokine that potentiates lethal endotoxaemia. *Nature*. 1993;365(6448):756-9.
277. Janeway CA, Travers P, Walport M, Shlomchik MJ. *Failures of Host Defense Mechanisms*. *Janeway's Immunobiology*. 7th ed. New York, USA: Garland Science; 2001.
278. Foster G. *The Design of a Miniturised Implantable Blood Pump*: Swansea; 2013.
279. Rother RP, Bell L, Hillmen P, Gladwin MT. The clinical sequelae of intravascular hemolysis and extracellular plasma hemoglobin: A novel mechanism of

human disease. JAMA : the journal of the American Medical Association. 2005;293(13):1653-62.

280. Wu Y, Zhu L, Luo Y. Design and Hemocompatibility Analysis of a Double-Suction Injection Suspension Blood Pump Using Computational Fluid Dynamics Methods. *Artif Organs*. 2017.

281. Snyder TA, Watach MJ, Litwak KN, Wagner WR. Platelet activation, aggregation, and life span in calves implanted with axial flow ventricular assist devices. *The Annals of thoracic surgery*. 2002;73(6):1933-8.

282. Johnson CA, Jr., Shankarraman V, Wearden PD, Kocyildirim E, Maul TM, Marks JD, et al. Platelet activation after implantation of the Levitronix PediVAS in the ovine model. *ASAIO journal (American Society for Artificial Internal Organs : 1992)*. 2011;57(6):516-21.

283. Johnson CA, Jr., Wearden PD, Kocyildirim E, Maul TM, Woolley JR, Ye SH, et al. Platelet activation in ovines undergoing sham surgery or implant of the second generation PediaFlow pediatric ventricular assist device. *Artif Organs*. 2011;35(6):602-13.

284. Sacristan C, Escobedo CR, Bojalil R, Izaguirre RA, Cortina E, Aranda A, et al. In vivo assessment of hemocompatibility of a ventricular assist device in healthy swine. *Archivos de cardiologia de Mexico*. 2010;80(2):67-76.

285. Wei X, Li T, Li S, Son HS, Sanchez PG, Niu S, et al. Pre-clinical evaluation of the infant Jarvik 2000 heart in a neonate piglet model. *J Heart Lung Transplant*. 2013;32(1):112-9.

286. Snyder TA, Watach MJ, Litwak KN, Wagner WR. Platelet activation, aggregation, and life span in calves implanted with axial flow ventricular assist devices. *Ann Thorac Surg*. 2002;73(6):1933-8.

287. Wearden PD, Morell VO, Keller BB, Webber SA, Borovetz HS, Badylak SF, et al. The PediaFlow pediatric ventricular assist device. *Seminars in thoracic and cardiovascular surgery Pediatric cardiac surgery annual*. 2006:92-8.

288. Johnson CA, Jr., Vandenberghe S, Daly AR, Woolley JR, Snyder ST, Verkaik JE, et al. Biocompatibility assessment of the first generation PediaFlow pediatric ventricular assist device. *Artif Organs*. 2011;35(1):9-21.

289. Chen H, Zhou J, Sun H, Tang Y, Zhang Y, Liu G, et al. Short-term in vivo preclinical biocompatibility evaluation of FW-II axial blood pump in a sheep model. *ASAIO journal (American Society for Artificial Internal Organs : 1992)*. 2011;57(3):177-82.
290. Snyder TA, Litwak KN, Tsukui H, Akimoto T, Kihara S, Yamazaki K, et al. Leukocyte-platelet aggregates and monocyte tissue factor expression in bovines implanted with ventricular assist devices. *Artif Organs*. 2007;31(2):126-31.
291. Chittester B. *Medical Device Clinical Trials - How DO They Compare with Drug Trials?* : MasterControl Inc.; 2014.
292. Khazanie P, Rogers JG. Patient Selection for Left Ventricular Assist Devices. *Congestive Heart Failure*. 2011;17(5):227-34.
293. Caruso R, Botta L, Verde A, Milazzo F, Vecchi I, Trivella MG, et al. Relationship between pre-implant interleukin-6 levels, inflammatory response, and early outcome in patients supported by left ventricular assist device: a prospective study. *PloS one*. 2014;9(3):e90802.
294. Caruso R, Trunfio S, Milazzo F, Campolo J, De Maria R, Colombo T, et al. Early expression of pro- and anti-inflammatory cytokines in left ventricular assist device recipients with multiple organ failure syndrome. *ASAIO journal (American Society for Artificial Internal Organs : 1992)*. 2010;56(4):313-8.
295. Ivak P, Pitha J, Netuka I. Circulating microparticles as a predictor of vascular properties in patients on mechanical circulatory support; hype or hope? *Physiological research*. 2016.
296. Schuster M, Kocher A, John R, Hoffman M, Ankersmit J, Lietz K, et al. B-cell activation and allosensitization after left ventricular assist device implantation is due to T-cell activation and CD40 ligand expression. *Human immunology*. 2002;63(3):211-20.
297. Badiei N, Sowedan AM, Curtis DJ, Brown MR, Lawrence MJ, Campbell AI, et al. Effects of unidirectional flow shear stresses on the formation, fractal microstructure and rigidity of incipient whole blood clots and fibrin gels. *Clinical hemorheology and microcirculation*. 2015;60(4):451-64.



298. Mosaad AA, Elbagory AR, Khalid AM, Waters WR, Tibary A, Hamilton MJ, et al. Identification of monoclonal antibody reagents for use in the study of the immune response to infectious agents in camel and water buffalo. *J Camel Practice Res.* 2006;13(2):91-101.
299. Hastings SM, Deshpande SR, Wagoner S, Maher K, Ku DN. Thrombosis in centrifugal pumps: location and composition in clinical and in vitro circuits. *The International journal of artificial organs.* 2016;39(4):200-4.
300. Carstairs KC. The identification of platelets and platelet antigens in histological sections. *The Journal of pathology and bacteriology.* 1965;90(1):225-31.
301. Casa LDC, Ku DN. Thrombus Formation at High Shear Rate. *Annual review of biomedical engineering.* 2017.
302. Cadroy Y, Horbett TA, Hanson SR. Discrimination between platelet-mediated and coagulation-mediated mechanisms in a model of complex thrombus formation in vivo. *J Lab Clin Med.* 1989;113(4):436-48.
303. Miller LW, Pagani FD, Russell SD, John R, Boyle AJ, Aaronson KD, et al. Use of a Continuous-Flow Device in Patients Awaiting Heart Transplantation. *New England Journal of Medicine.* 2007;357(9):885-96.
304. Moazami N, Fukamachi K, Kobayashi M, Smedira NG, Hoercher KJ, Massiello A, et al. Axial and centrifugal continuous-flow rotary pumps: a translation from pump mechanics to clinical practice. *J Heart Lung Transplant.* 2013;32(1):1-11.
305. Singhal R, Annarapu GK, Pandey A, Chawla S, Ojha A, Gupta A, et al. Hemoglobin interaction with GP1b $\alpha$  induces platelet activation and apoptosis: a novel mechanism associated with intravascular hemolysis. *Haematologica.* 2015;100(12):1526-33.
306. Chiu WC, Girdhar G, Xenos M, Alemu Y, Soares JS, Einav S, et al. Thromboresistance Comparison of the HeartMate II Ventricular Assist Device (VAD) with the Device Thrombogenicity Emulation (DTE)-Optimized HeartAssist 5 VAD. *Journal of biomechanical engineering.* 2013.
307. Chiu W-C, Slepian MJ, Bluestein D. Thrombus Formation Patterns in the HeartMate II VAD-Clinical Observations Can Be Predicted by Numerical

Simulations. *ASAIO journal* (American Society for Artificial Internal Organs : 1992). 2014;60(2):237-40.

308. Diehl P, Aleker M, Helbing T, Sossong V, Beyersdorf F, Olschewski M, et al. Enhanced microparticles in ventricular assist device patients predict platelet, leukocyte and endothelial cell activation. *Interactive cardiovascular and thoracic surgery*. 2010;11(2):133-7.

309. Nascimbene A, Hernandez R, George JK, Parker A, Bergeron AL, Pradhan S, et al. Association between cell-derived microparticles and adverse events in patients with nonpulsatile left ventricular assist devices. *J Heart Lung Transplant*. 2014;33(5):470-7.

310. Burger D, Kwart DG, Montezano AC, Read NC, Kennedy CR, Thompson CS, et al. Microparticles induce cell cycle arrest through redox-sensitive processes in endothelial cells: implications in vascular senescence. *Journal of the American Heart Association*. 2012;1(3):e001842.

311. Ueno A, Murasaki K, Hagiwara N, Kasanuki H. Increases in circulating T lymphocytes expressing HLA-DR and CD40 ligand in patients with dilated cardiomyopathy. *Heart and vessels*. 2007;22(5):316-21.

312. Kornek M, Popov Y, Libermann TA, Afdhal NH, Schuppan D. Human T cell microparticles circulate in blood of hepatitis patients and induce fibrolytic activation of hepatic stellate cells. *Hepatology* (Baltimore, Md). 2011;53(1):230-42.

313. Kimball PM, Flattery M, McDougan F, Kasirajan V. Cellular immunity impaired among patients on left ventricular assist device for 6 months. *Ann Thorac Surg*. 2008;85(5):1656-61.

314. Kimball P, Flattery M, Kasirajan V. T-cell response to staphylococcal enterotoxin B is reduced among heart failure patients on ventricular device support. *Transplantation proceedings*. 2006;38(10):3695-6.

315. Mondal NK, Sobieski MA, Pham SM, Griffith BP, Koenig SC, Slaughter MS, et al. Infection, Oxidative Stress and Changes in Circulating Regulatory T cells of Heart Failure Patients Supported by Continuous-Flow Ventricular Assist Devices. *Asaio J*. 2017;63(2):128-33.

316. Mitchell M, Lin K, King M. Fluid Shear Stress Increases Neutrophil Activation via Platelet-Activating Factor. *Biophys J*. 2014;106(10):2243-53.
317. Valignat MP, Theodoly O, Gucciardi A, Hogg N, Lellouch A. T Lymphocytes Orient against the Direction of Fluid Flow during LFA-1-Mediated Migration. *Biophys J*. 2013;104(2):322-31.
318. Riley LK, Rupert J. Evaluation of Patients with Leukocytosis. *American family physician*. 2015;92(11):1004-11.
319. Schimenti KJ, Jacobberger JW. Fixation of Mammalian Cells for Flow Cytometric Evaluation of DNA Content and Nuclear Immunofluorescence. *Cytometry*. 1992;13(1).
320. Merli GJ. Pathophysiology of venous thrombosis, thrombophilia, and the diagnosis of deep vein thrombosis-pulmonary embolism in the elderly. *Clin Geriatr Med*. 2006;22:75-92.
321. Jerjes-Sanchez C. Venous and arterial thrombosis: a continuous spectrum of the same disease? *Eur Heart J*. 2005;26:3-4.
322. Lip GY, Blann AD. Thrombogenesis and fibrinolysis in acute coronary syndromes. Important facets of a prothrombotic or hypercoagulable state? *J Am Coll Cardiol*. 2000;36(7):2044-6.
323. Turpie AG, Chin BSP, Lip GY. Venous thromboembolism: pathophysiology, clinical features, and prevention. *Br Med J*. 2002;325:887-90.
324. Mackman N. Triggers, targets and treatments for thrombosis. *Nature*. 2008;451(7181):914-8.
325. Turpie AG, Esmon C. Venous and arterial thrombosis - pathogenesis and the rationale for anticoagulation. *Thrombosis and haemostasis*. 2011;105:586-96.
326. Walkowiak-Przybylo M, Klimek L, Okroj W, Jakubowski W, Chwilka M, Czajka A, et al. Adhesion, activation, and aggregation of blood platelets and biofilm formation on the surfaces of titanium alloys Ti6Al4V and Ti6Al7Nb. *Journal of biomedical materials research Part A*. 2012;100(3):768-75.

327. Fuchs TA, Brill A, Duerschmied D, Schatzberg D, Monestier M, Myers DD, et al. Extracellular DNA traps promote thrombosis. *Proceedings of the National Academy of Sciences*. 2010;107(36):15880-5.
328. Brill A, Fuchs T, Savchenko A, Thomas G, Martinod K, De Meyer S, et al. Neutrophil extracellular traps promote deep vein thrombosis in mice. *Journal of Thrombosis and Haemostasis*. 2012;10(1):136-44.
329. Lindemann S, Tolley ND, Dixon DA, McIntyre TM, Prescott SM, Zimmerman GA, et al. Activated platelets mediate inflammatory signaling by regulated interleukin 1beta synthesis. *J Cell Biol*. 2001;154(3):485-90.
330. Swystun LL, Liaw PC. The role of leukocytes in thrombosis. 2016;128(6):753-62.
331. von Brühl M-L, Stark K, Steinhart A, Chandraratne S, Konrad I, Lorenz M, et al. Monocytes, neutrophils, and platelets cooperate to initiate and propagate venous thrombosis in mice in vivo. *The Journal of experimental medicine*. 2012;209(4):819-35.
332. Owens AP, Mackman N. Microparticles in hemostasis and thrombosis. *Circulation research*. 2011;108(10):1284-97.
333. Hargett LA, Bauer NN. On the origin of microparticles: From “platelet dust” to mediators of intercellular communication. *Pulmonary Circulation*. 2013;3(2):329-40.
334. Swirski FK, Nahrendorf M. Leukocyte behavior in atherosclerosis, myocardial infarction, and heart failure. *Science (New York, NY)*. 2013;339(6116):161-6.
335. Wilhelm CR, Ristich J, Kormos RL, Wagner WR. Monocyte tissue factor expression and ongoing complement generation in ventricular assist device patients. *Ann Thorac Surg*. 1998;65(4):1071-6.
336. Woolley JR, Teuteberg JJ, Bermudez CA, Bhamra JK, Lockard KL, Kormos RL, et al. Temporal Leukocyte Numbers and Granulocyte Activation in Pulsatile and Rotary Ventricular Assist Device Patients. *Artif Organs*. 2013;38(6):447-55.
337. Devlin H. 'Metal-on-metal' hip implant patients recalled for tests over toxicity fears: *Guardian News and Media Ltd.*; 2017 [Available from:

<https://www.theguardian.com/science/2017/jun/29/metal-on-metal-hip-implant-patients-recalled-for-tests-over-toxicity-fears>.

338. Bocanegra-Bernal MH, Matovic B. Mechanical properties of silicon nitride-based ceramics and its use in structural applications at high temperatures. *Materials Science and Engineering: A*. 2010;527(6):1314-38.

339. Shantsila E, Lip GY. The role of monocytes in thrombotic disorders. Insights from tissue factor, monocyte-platelet aggregates and novel mechanisms. *Thrombosis and haemostasis*. 2009;102(5):916-24.

340. Cao H, Lancisi DM. Rotary blood pump with ceramic members. *Google Patents*; 2008.

341. John R. Current axial-flow devices--the HeartMate II and Jarvik 2000 left ventricular assist devices. *Semin Thorac Cardiovasc Surg*. 2008;20(3):264-72.

342. Dell'Aquila AM, Schneider SR, Schlarb D. Initial clinical experience with the HeartWare left ventricular assist system: a single-center report. *Ann Thorac Surg*. 2013;95.

343. Wu L, Weng YG, Dong NG, Krabatsch T, Stepanenko A, Hennig E, et al. Outcomes of HeartWare Ventricular Assist System support in 141 patients: a single-centre experience. *Eur J Cardiothorac Surg*. 2013;44(1):139-45.

344. Konarik M, Szarszoi O, Netuka I, Maly J, Pirk J, Urban M. Infectious complications in patients with ventricular assist device HeartMate II. *Journal of cardiothoracic surgery*. 2013;8(Suppl 1):P74-P.

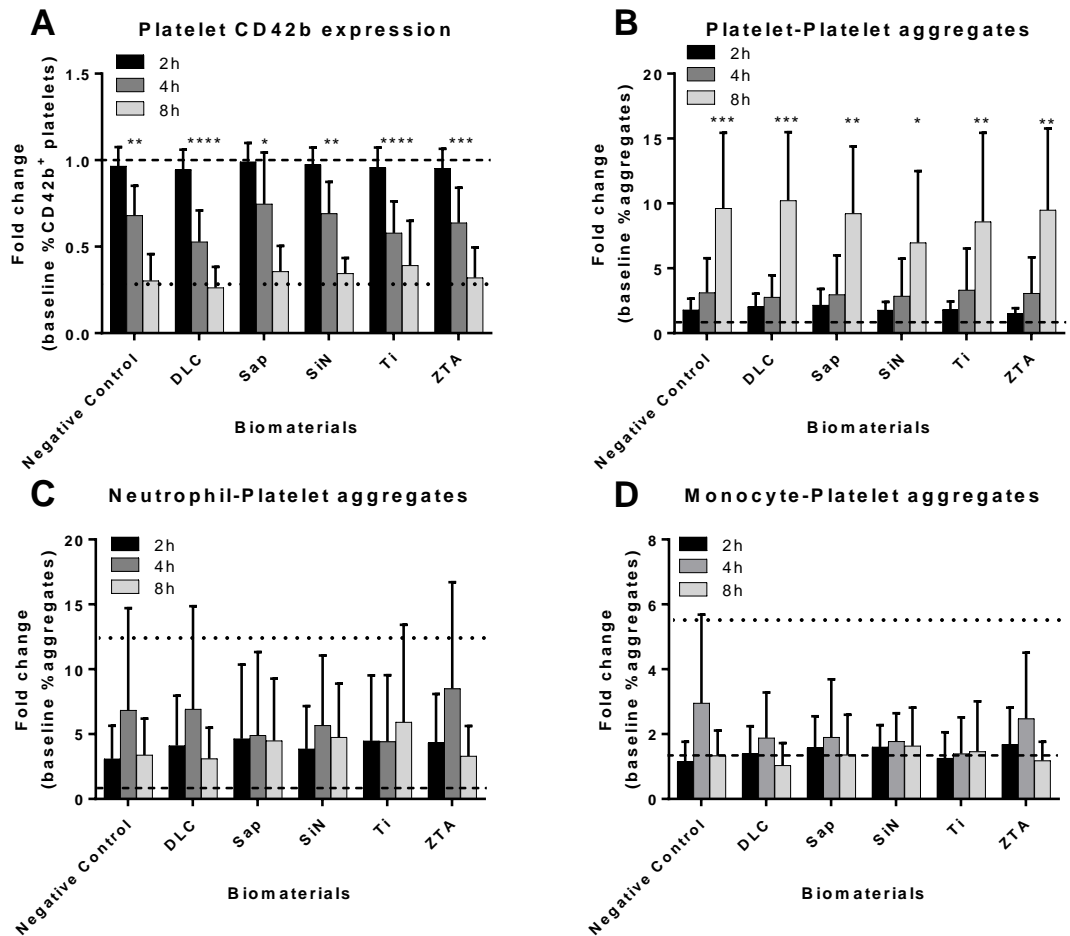
345. Faille D, Frere C, Cuisset T, Quilici J, Moro PJ, Morange PE, et al. CD11b+ leukocyte microparticles are associated with high-risk angiographic lesions and recurrent cardiovascular events in acute coronary syndromes. *Journal of Thrombosis and Haemostasis*. 2011;9(9):1870-3.

346. Inc. S. Streck Cell Preservative Stabilization Reagent 2017 [Available from: <https://www.streck.com/collection/streck-cell-preservative/>].

# Chapter 8 Appendix

## 8.1 Supplementary figures

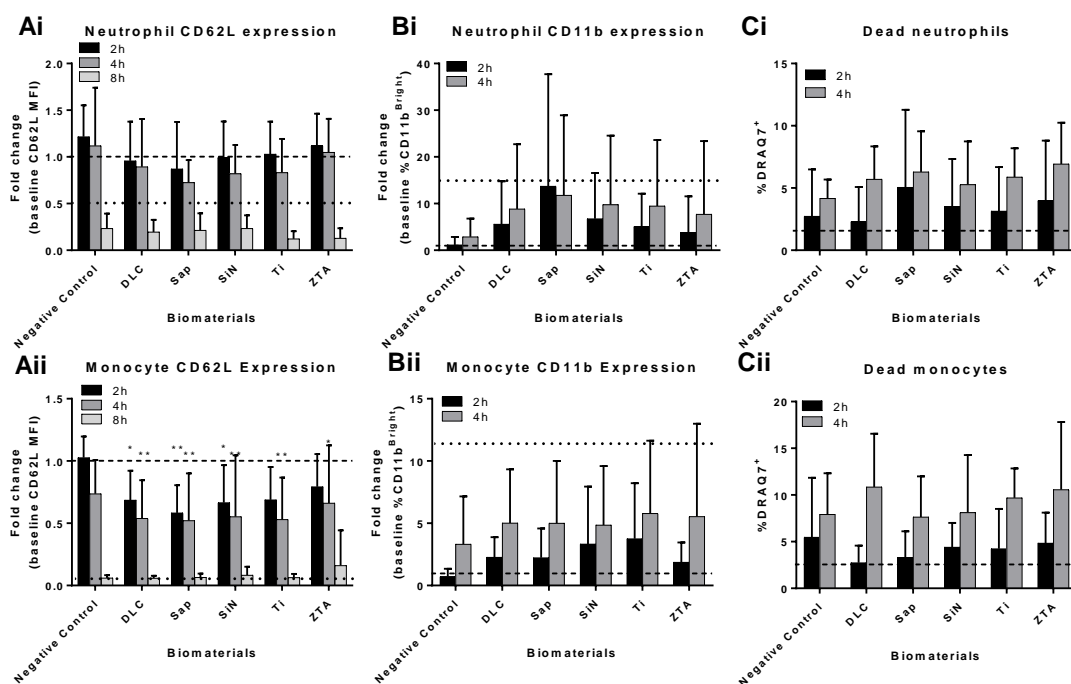
### 8.1.1 Time-course data



**Figure 8.1: Time-course data for platelet activation, platelet aggregation, and leukocyte-platelet aggregation**

Whole heparinised blood was exposed to each of the biomaterials - diamond-like carbon coated stainless steel (DLC), single-crystal sapphire (Sap), silicon nitride (SiN), titanium alloy (Ti), and zirconia toughened alumina (ZTA). **A**) Platelet CD42b expression at 2, 4 and 8 hours shown as percentage of baseline expression at time 0 (n = 6); **B**) Platelet-platelet aggregates determined through forward vs side-scatter characteristics at 2, 4 and 8 hours as a percentage and compared to baseline at time to give a fold change (n = 5). **C & D**) Neutrophil-platelet and monocyte-platelet aggregates determined as CD15+/CD41+ and CD14+/CD41+ events, respectively at

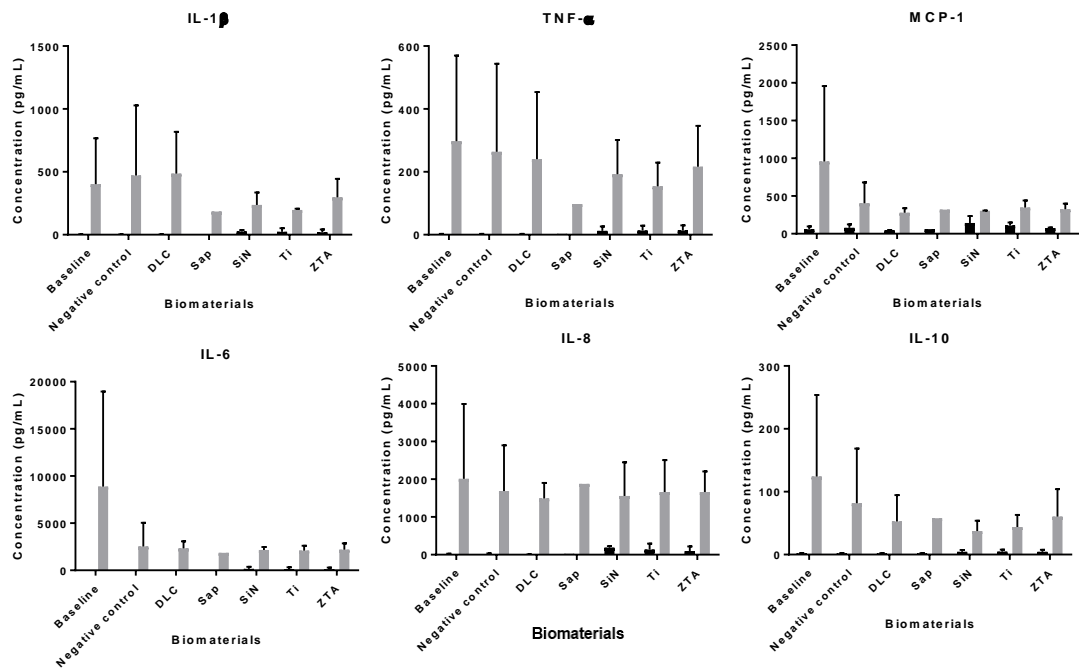
2, 4 and 8 hours as a percentage and compared to baseline at time to give a fold change (n = 5); \* p ≤ 0.05, \*\* p ≤ 0.01, \*\*\* p ≤ 0.001, \*\*\*\* p ≤ 0.0001



**Figure 8.2: Time-course data for CD62L expression, CD11b expression, and death**

Whole heparinised blood was exposed to each of the biomaterials - diamond-like carbon coated stainless steel (DLC), single-crystal sapphire (Sap), silicon nitride (SiN), titanium alloy (Ti), and zirconia toughened alumina (ZTA) - for 2, 4 and 8 hours. Samples were then stained with CD62L, CD11b, CD15, CD14, and DRAQ7. Leukocyte activation was investigated by: **A)** change in median fluorescent intensity (MFI) of CD62L on **i)** CD15+ neutrophils (n = 8) and **ii)** CD14+ monocytes (n = 8); **B)** change in percentage of CD11b+ cells on **i)** CD15+ neutrophils and **ii)** CD14+ monocytes (n = 6); **C)** percentage of non-viable **i)** CD15+ neutrophils and **ii)** CD14+ monocytes cells as determined by DRAQ7 (n = 5). All were compared to the time 0 baseline (dashed line) as a fold change (\* p ≤ 0.05, \*\* p ≤ 0.01). LPS positive control shown as dotted line.

### 8.1.2 Human inflammatory multiplex panel

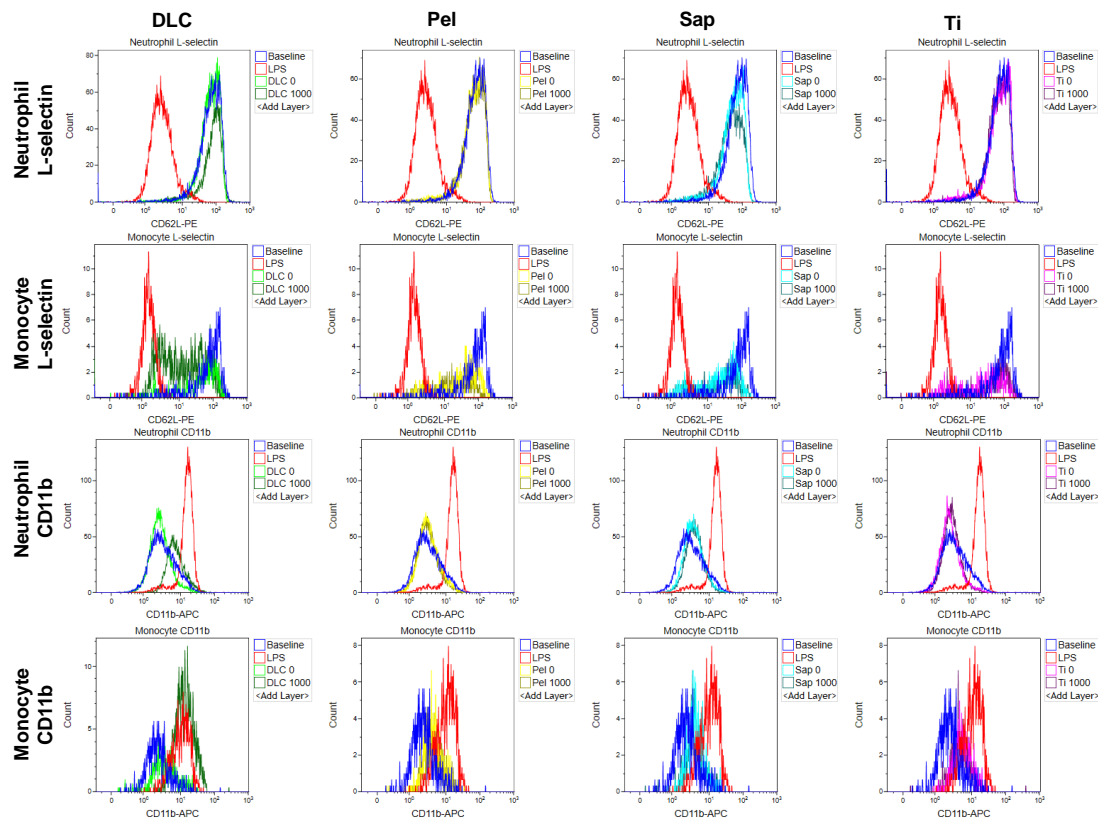


**Figure 8.3: Cytokine expression in cell culture supernatants measured using the LEGENDplex kit**

Levels of inflammatory cytokines (interleukin 1 beta: IL-1 $\beta$ , tumour necrosis factor alpha: TNF $\alpha$ , monocyte chemoattractant protein-1: CCL2/MCP-1, interleukin 6: IL-6, interleukin 8: CXCL8/IL-8, and interleukin 10: IL-10) were measured in cell-free supernatants (grey = unstimulated; black = stimulated with 10 ng/mL LPS) from blood exposed to each of the biomaterials - diamond-like carbon coated stainless steel (DLC), single-crystal sapphire (Sap), silicon nitride (SiN), titanium alloy (Ti), and zirconia toughened alumina (ZTA) - using LEGENDplex Human Inflammatory Panel (BioLegend) on the Navios Flow Cytometer (Beckman Coulter) according to the manufacturer's instructions and data analysed in the LEGENDplex v7 software.



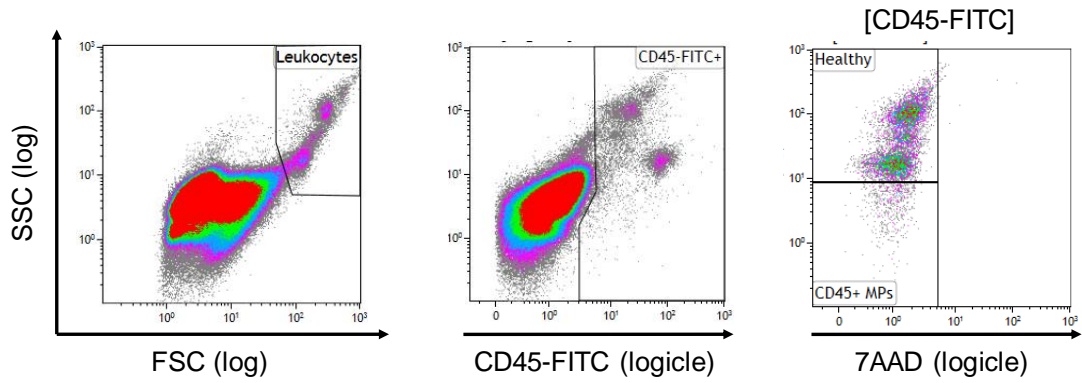
### 8.1.3 Leukocyte activation in response to biomaterials and shear



**Figure 8.4: Leukocyte activation in response to biomaterials and shear**

Human whole blood was placed between biomaterial discs - diamond-like carbon coated stainless steel (green = DLC), peltier (yellow = Pel), single-crystal sapphire (turquoise = Sap), and titanium alloy (purple = Ti) - attached onto a rheometer. Shear stress ( $1000 \text{ s}^{-1}$ ) or no shear stress ( $0 \text{ s}^{-1}$ ) was applied for 5 min. Leukocyte activation was measured as change in median fluorescence intensity (MFI) of CD62L and CD11b on neutrophils ( $\text{CD}15^+$ ) and monocytes ( $\text{CD}14^+$ ). Baseline (dark blue) and LPS (red) samples are shown as controls.

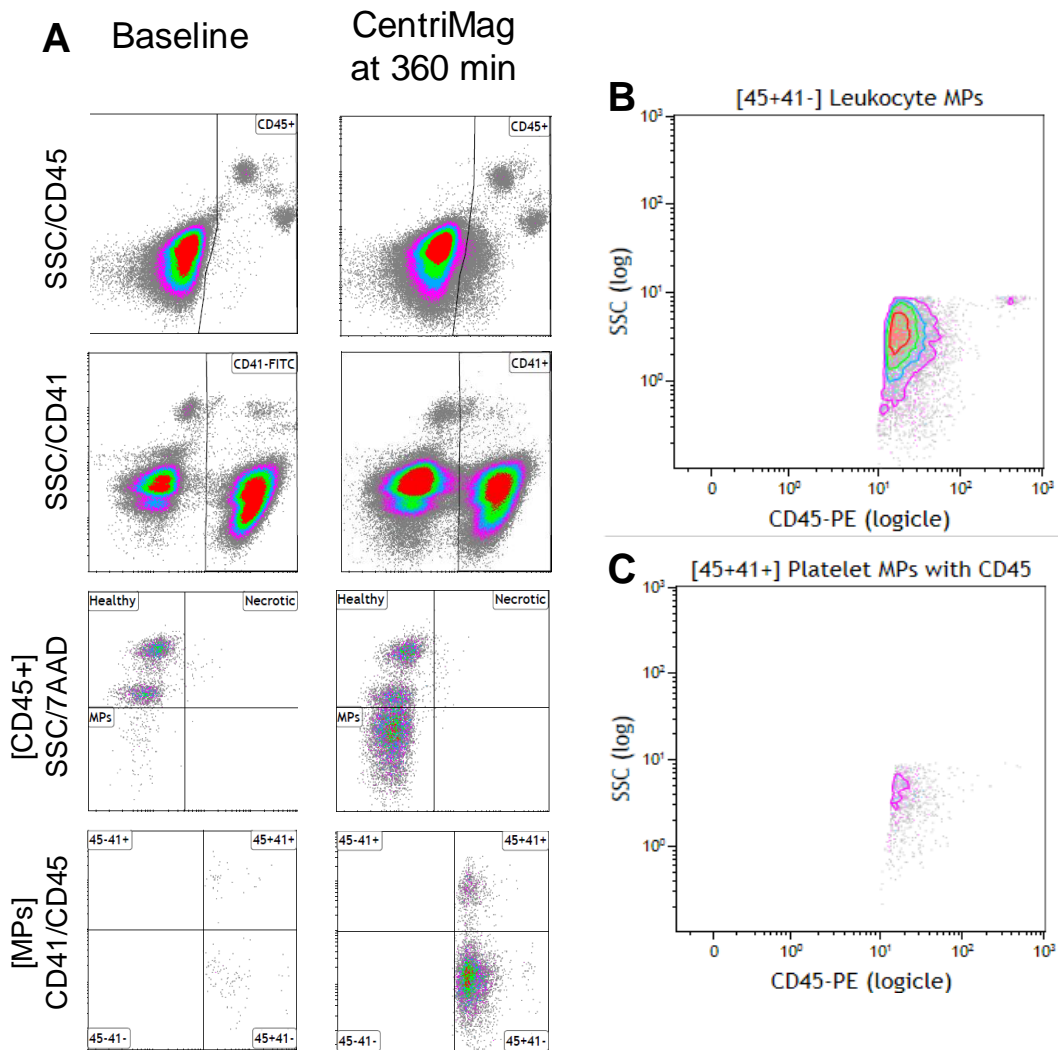
### 8.1.4 Leukocyte microparticles gating strategy



**Figure 8.5: Gating strategy for leukocyte microparticles**

Human blood stained with CD45-PE and 7AAD then acquired for 60 secs on the Navios flow cytometer. CD45<sup>+</sup> events were displayed on SSC vs 7AAD plot to display healthy, necrotic and leukocyte microparticles (CD45<sup>+</sup> MPs).

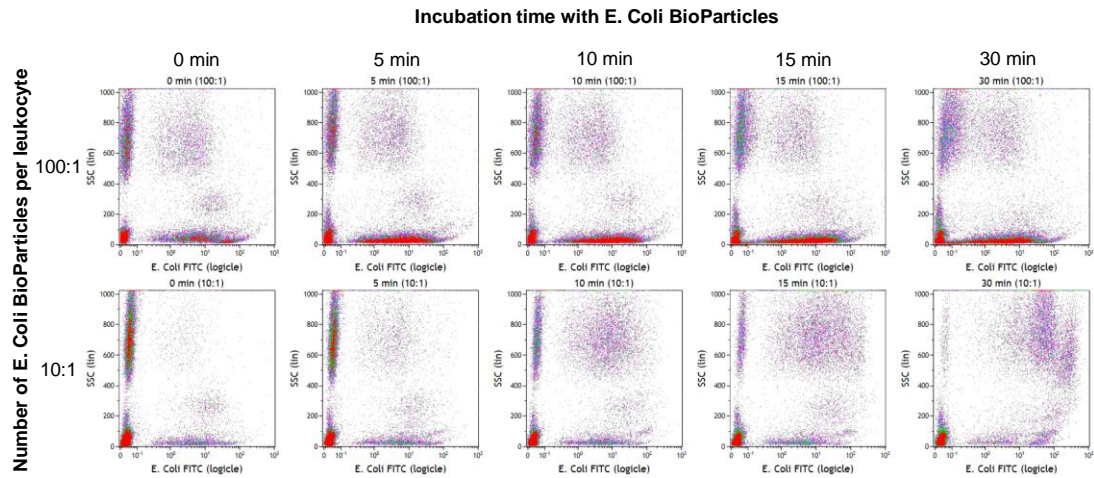
### 8.1.5 Microparticle differentiation



**Figure 8.6: Differentiating leukocyte-derived and platelet-derived microparticles**

Human blood from polycythaemic patients was circulated through the CentriMag for 360 min. Blood samples including the baseline (time 0) sample were stained with CD45, CD41, and 7AAD. CD45+ events were displayed on a SSC/7AAD plot to gate microparticles (**A**, MPs). These MPs were gated on CD41/CD45 to show leukocyte-derived MPs (CD45+ LMPs) or platelet-derived MPs (CD41+ PMPs). The location of these LMPs/PMPs were displayed on a SSC/CD45 plot (**B** & **C**).

### 8.1.6 Optimisation of phagocytosis assay



**Figure 8.7: Optimisation of phagocytosis assay**

Baseline blood was incubated in a +37°C shaking water-bath with fluorescent *E. coli* bioparticles (100 per leukocyte or 10 per leukocyte) for 0, 5, 10, 15 and 30 min. Phagocytosis was stopped through the addition of cytochalasin D and two washes with ice-cold PBS. Red blood cells were lysed, then samples were washed with ice cold PBS containing trypan blue to quench the bioparticles on the cell surface.

## 8.2 Publications and conferences

### 8.2.1 Publications

1. Pieper, I. L., Radley, G., & Thornton, C. A., (2018). “Multidimensional Flow Cytometry for Testing of Blood-Handling Medical Devices” IN “Multidimensional Flow Cytometry Techniques for Novel Highly Informative Assays”. *InTech Open* (chapter being processed for publishing)
2. Radley, G., Pieper, I. L., & Thornton, C. A., (2017). “The Effect of Ventricular Assist Device-Associated Biomaterials on Human Blood Leukocytes”. *Journal of Biomedical Materials Research Part B* (epub ahead of print)
3. Pieper, I. L., Radley, G., Christen, A., Ali, S., Bodger, O. & Thornton, C. A. (2017) “Ovine leukocyte microparticles generated by the CentriMag ventricular assist device in vitro”. *Artificial Organs* (epub ahead of print)
4. Pieper, I. L., Radley, G., Chan, C. H. H., Friedmann, Y., Foster, G. & Thornton, C. A., (2016). “Quantification methods for human and large animal leukocytes using DNA dyes by flow cytometry”. *Cytometry Part A* **89** (6): 565-74
5. Chan, C. H. H., Pieper, I. L., Hambly, R., Radley, G., Jones, A., Friedmann, Y., Hawkins, K. M., Westaby, S., Foster, G. & Thornton, C. A., (2015). “The CentriMag Centrifugal Blood Pump as a Benchmark for In Vitro Testing of Hemocompatibility in Implantable Ventricular Assist Devices”. *Artificial Organs* **39** (2): 93-101

### 8.2.2 *Conference posters*

1. International Society on Thrombosis and Haemostasis (2018) – Characterisation of thrombus in VADs
2. European Society of Cardiology: Heart Failure (2016) – The effect of shear stress on leukocytes at a biomaterial interface
3. European Society of Artificial Organs (2015) - Biomaterial-induced leukocyte activation in reference to ventricular assist devices

### 8.2.3 *Conference presentations*

1. European Society of Artificial Organs (2017) – Assessment of leukocyte functionality in contact with a foreign surface under shear stress
2. European Society of Artificial Organs (2016) – The impact of artificial shear stress on leukocytes at a biomaterial interface
3. European Society of Cardiology: Heart Failure (2015) – The impact of ventricular assist device biomaterials on leukocyte activation
4. International Society for Rotary Blood Pumps (2015) – Biocompatibility of ventricular assist device materials